Fatigue Load Model Safety

Verifying Reliability for Reinforced Concrete Railway Structures

J. R. Houtenbos

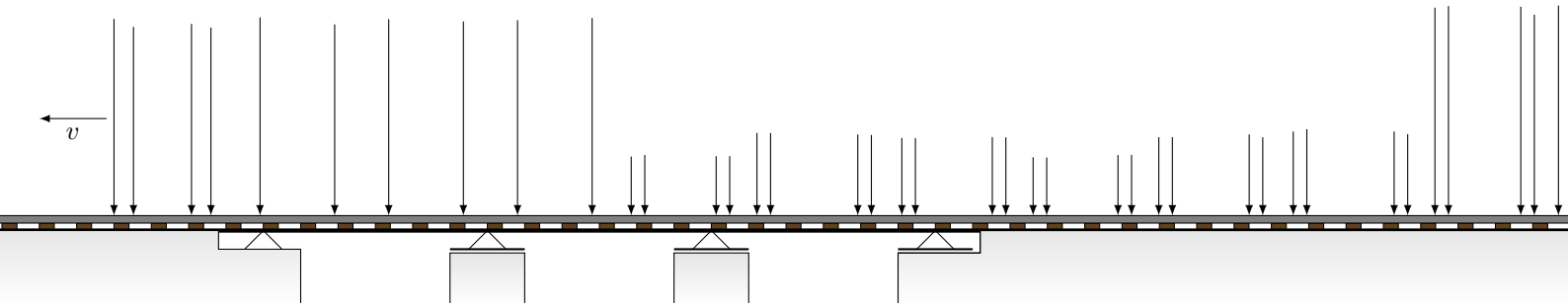

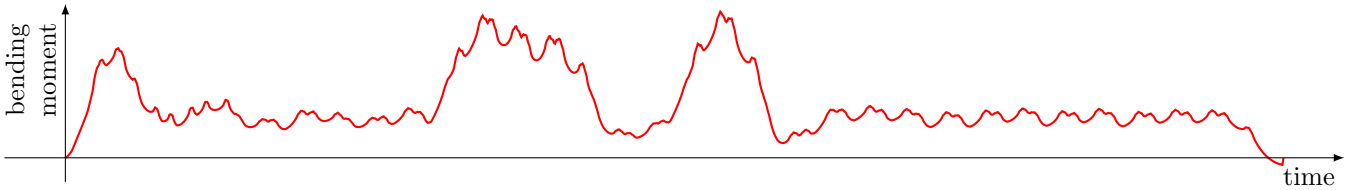

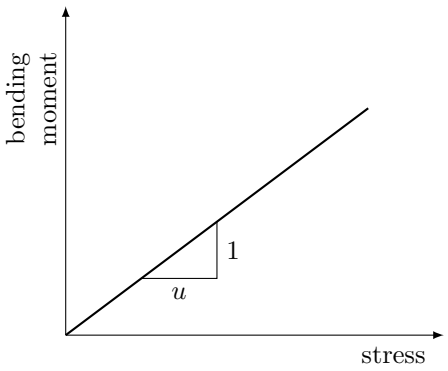

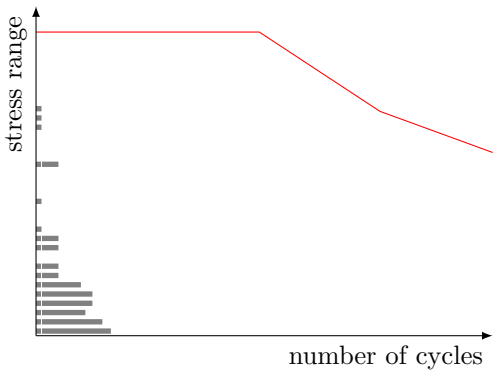

TU Delft

Movares
adviseurs & ingenieurs

Cover: part of a measured train (100th train of detector 111 traffic), represented by its axle load magnitudes and distances. The structure corresponds to scheme 5, with a span of 30 m, and is displayed to scale. Furthermore, a time-signal of the mid-span bending moment (starting right: 1st span), resulting from the entire passage, is displayed. Using a fictive reinforced concrete section, the signal is transformed into a spectrum using rainflow counting, the result from which can be seen in the last figure (both axes on logarithmic scale).

Fatigue Load Model Safety: Verifying Reliability for Reinforced Concrete Railway Structures
Joost Ruben Houtenbos

Fatigue Load Model Safety

Verifying Reliability for Reinforced Concrete Railway Structures

J. R. Houtenbos

in partial fulfillment of the requirements for the degree of

Master of Science
in Civil Engineering

at the Delft University of Technology,

to be defended publicly on Wednesday April 20, 2016 at 2:00 PM.

Student number:	4172728	
Thesis Committee:	prof. dr. ir. **D. A. Hordijk**	TU Delft
	dr. ir. **C. B. M. Blom**	Gemeente Rotterdam
	prof. dr. ir. **R. P. B. J. Dollevoet**	TU Delft
	ir. **T. W. Groeneweg**	Movares
	prof. dr. ir. **J. Maljaars**	TNO

Abstract

It was unclear what level of reliability was provided by appliance of the Eurocode load models for fatigue due to train loads, meaning that it might be insufficient. Therefore, it was investigated what the provided reliability is, compared to what is should be. Within this report, the focus is solely on fatigue induced by bending moments on reinforced concrete sections.

Determination of reliabilities is done by creating a fictitious design, exactly satisfying the Eurocode. Then, this design is used as input for a probabilistic analysis, where the load models are replaced by measured traffic, and other uncertainties were quantified. The target reliability for the fatigue limit state proved to be vague in the Eurocode. However, the target reliability for ultimate limit states can be adopted as an upper bound, which was used in this report.

The reliability was shown to be below this target, caused by, among others, a partial factor which is equal to 1 for fatigue loads according to the Eurocode. The idea was that variations in loads will converge due to the vast number of appliances. However, here it is argued that correlations between variations, which systematically affect each load its effect, invalidate this assumption. Also, reliabilities were shown to depend heavily on the span lengths (remarkably lower for spans of 1-10 m). It was demonstrated that such behavior results by lack of variety in the load model axle distances and loads, compared to measured traffic.

Recommendations are, apart from further research, to increase the partial factor for fatigue loading. Also, a novel load model should be created with comparable variation in axle distances and loads as measured traffic.

Keywords: *fatigue*, *load model*, *railway structures*, *reinforced concrete*, *reinforcement steel*, *probabilistic design*, *reliability*, *partial factor*.

Samenvatting

Het was onduidelijk welk betrouwbaarheidsniveau geboden wordt door toepassing van de Eurocode belastingmodellen voor vermoeiing door treinbelastingen, wat betekent dat dit onvoldoende zou kunnen zijn. Daarom is onderzocht wat de geboden betrouwbaarheid is en is deze vergeleken met wat het zou moeten zijn. De focus ligt in dit rapport enkel op vermoeiing veroorzaakt door buigende momenten op gewapend betonnen constructies.

Het bepalen van de betrouwbaarheden is gedaan door het maken van een fictief ontwerp, dat precies voldoet aan de Eurocode. Dit ontwerp is vervolgens gebruikt als invoer voor een probabilistische analyse waarin de belastingmodellen vervangen zijn door gemeten verkeer en overige onzekerheden gekwantificeerd zijn. De doelbetrouwbaarheid voor de grenstoestand vermoeiing bleek slechts vaag aangegeven te zijn in de normen. Er is beredeneerd dat de doelbetrouwbaarheid voor uiterste grenstoestanden gebruikt kan worden als bovengrens, wat dan ook gedaan is binnen dit rapport.

Het is aangetoond dat de betrouwbaarheid onder deze doelwaarde ligt, wat veroorzaakt wordt door, onder andere, een partiële factor gelijk aan 1, zoals voorgeschreven in de Eurocode. Het idee hierachter was dat variaties in belastingen zullen convergeren door het grote aantal verschillende belastingen. In dit rapport wordt echter geredeneerd dat correlaties tussen variaties deze aanname tegenspreken, omdat deze stelselmatig het effect door elke belasting aantasten. Daarnaast is gebleken dat de betrouwbaarheid erg afhankelijk is van de overspanningslengte (opvallend lager voor overspanningen van 1-10 m). Het is gedemonstreerd dat dit gedrag voortkomt uit een gebrek aan variatie in as-afstanden en aslasten in de belastingmodellen, vergeleken met het gemeten verkeer.

Aanbevelingen zijn, naast verder onderzoek, om de partiële factor voor vermoeiingsbelastingen te verhogen. Daarnaast zou een nieuw belastingmodel gemaakt moeten worden met vergelijkbare variatie in as-afstanden en aslasten als het gemeten verkeer.

Trefwoorden: *vermoeiing*, *belastingmodel*, *spoorconstructies*, *gewapend beton*, *wapeningsstaal*, *probabilistisch ontwerp*, *betrouwbaarheid*, *partiële factor*.

Preface

Writing this thesis was an endeavor I entered without much knowledge on the subject of fatigue. It was especially this aspect which made it a very special experience during which I learned a lot, and I feel as if this has enabled me to form and share my own vision on the subject. I am grateful for the support and encouragement of the people close to me, which has enabled me to complete this thesis.

I would like to thank the members of the Committee: Dick Hordijk, Kees Blom, Rolf Dollevoet, Tom Groeneweg, and Johan Maljaars, for their invaluable input. Their criticism, enthusiasm, and encouragement were of great help.

Ricardo Rail has generously provided the traffic measurement data used for this investigation, for which I am very grateful. I would like to thank Edward de Jong and Erik Jansen, both working at Ricardo Rail, for their efforts of supplying the data to me, and for taking the time to explain exactly what was handed over. Then there was a site-visit to the Lingebrug, set up by Ruud van Bezooijen, which was much appreciated.

Furthermore, I am grateful to Arend Kremer for initiating this research topic and for helping me on my way.

Finally, I would like to thank Movares for providing the resources used for creating this thesis.

Joost Ruben Houtenbos
March 30, 2016

Contents

Abbreviations

cdf	Cumulative distribution function
CoV	Coefficient of variation
DAF	Dynamic amplification factor
EVT	Extreme value theory
FORM	First order reliability method
GPD	Generalized Pareto distribution
KDE	Kernel density estimate
pdf	Probability density function
PoD	Probability of detection
PoT	Peak-over-threshold

Nomenclature

C_0	initial investment
C_f	failure costs
C_i	inspection costs
C_r	repair costs
C_t	total costs
$\bar{s}$	measure of fatigue resistance concrete
β_{cc}	coefficient for the concrete strength at first load application
$\boldsymbol{\sigma}_t$	time signal for stress
ΔD_i	incremental normalized damage from cycle i
ΔK	stress intensity at the crack tip
Δ	critical damage number
$\Delta\sigma$	stress cycle magnitude
$\Delta\sigma_e$	equivalent stress cycle magnitude
$\Delta\sigma_{FLM}$	fatigue load model stress range
ϵ_c	concrete strain
η_σ	multiplication factor for the stress cycle intensity
η_N	multiplication factor for the stress cycle count
γ_{Ff}	partial safety factor for fatigue loading
γ_{Mf}	partial safety factor for fatigue strength
$\hat{\beta}_\pm$	sensitivity index for the reliability
$\hat{\Phi}$	uncertainty in dynamic amplification
$\hat{F}$	measurement error load
$\hat{v}$	measurement error velocity
λ	equivalent damage factor
$\lambda_{\text{calibration}}$	factor for adjustment based on calibration
λ_i	bandwidth-parameter which depends of the local variability of measurement i
$\mathbf{e}_t$	time signal for effect
$\mathbf{H}$	set of historical loads
$\mathbf{M}$	set of model loads
$\mathcal{I}(\bullet)$	influence operator
$\mathcal{R}(\bullet)$	rainflow operator
Φ	dynamic equivalence factor
$\propto$	proportional to
σ	standard deviation
σ_c	stress in concrete
σ_s	stress in steel
$\sigma_{cd,max,i}$	maximum stress in cycle i
$\sigma_{cd,min,i}$	minimum stress in cycle i
$\sum \mathcal{D}(\bullet)$	cumulative damage operator
θ_S	model uncertainty factor
ξ_{ext}	extrapolation factor

ζ_{perm}	ratio of permanent stress over design concrete stress
A_{crack}	crack growth proportionality factor
a_{crack}	size of the crack
A_s	reinforcement area
$c_{i,j}$	influence factor relating the i'th effects and the j'th action
$c_{v,X}$	coefficient of variation corresponding to X
D	normalized cumulative fatigue damage or 'damage number'
d	effective section depth
E_c	modulus of elasticity, concrete
E_i	i'th effect
E_s	modulus of elasticity, steel
$E_{cd,max,i}$	maximum relative stress level in cycle i
$E_{cd,min,i}$	minimum relative stress level in cycle i
F_j	j'th action
$f_{cd,fat}$	concrete design fatigue strength
f_{cd}	concrete design compression strength
f_{ck}	concrete characteristic compression strength
$f_{X,Y}(x,y)$	bivariate probability density function
g	limit state function
h	bandwidth-parameter which depends on the variability of the entire dataset
$I_{[\text{condition}]}$	indicator-function, equal to 1 if the condition is true, and to 0 if false
$K(x,y)$	bivariate kernel function
L	reliability
L_Φ	governing length for dynamic amplification factor
M	applied bending moment
m	fatigue exponent
M_e	mean excess function
N	number of cycles
n	number of samples
N^*	measure of fatigue resistance reinforcement
N_c	force in concrete
N_e	equivalent number of cycles
N_i	number of allowed cycles of type i
n_i	number of applied cycles of type i
N_s	force in steel
P_F	probability of failure
R	resistance to failure
r	threshold-level
R_i	stress ratio corresponding to cycle i
S	load or 'solicitation'
s	coefficient to take into account the cement class
s_x	sample standard deviation
$s_{max,i}$	maximum relative stress level in cycle i
$s_{min,i}$	minimum relative stress level in cycle i
t	age of the concrete in days
u	proportionality between generalized forces and stresses
v	maximum allowed train speed
W	section modulus
x_c	concrete compressive zone height
Z	safety margin
$\sim$	distributed according to the following distribution
$\text{SE}_{\bar{x}}$	standard error of the mean

1 | Introduction

The Eurocode program, initiated in 1975, has been fully operational for a few years now at the time of writing. While the program fulfills its goals regarding the elimination of technical obstacles and the harmonization of technical specifications, there have been doubts concerning parts of the content since its start (which is only natural considering the concessions which are inherently brought by a harmonization program).

Recently, doubts have been expressed to the author by the Dutch railway infrastructure manager, ProRail, regarding the load model for fatigue on railway bridges (EN 1991–2). As a load model, this should provide a fair representation of the expected reality, while providing a sufficiently large safety margin, in order to arrive at a desired reliability level. Measured values (addressed further in this report) in the Dutch railway network, however, were said to indicate that the load model for fatigue might not provide such a margin, and is even exceeded on a regular basis.

1.1 Problem description

The Eurocode in its current form provides a load model for fatigue on bridges and other parts of the railway infrastructure. This load model is based on a cumulative tonnage, i.e. the summed weight of all vehicles passing over a single rail per year, of 25×10^6 tonnes per year. However, measurements have been said to reveal that this might be a gross underestimation for some parts of the Dutch railway network, leading to designs which do not meet the required reliability. It is then also unclear what the actual reliability of structures complying with the Eurocode equals. This suggests vagueness, which is a problem in itself because the safety might be less than thought.

Problem statement: The model for fatigue loading on railway bridges, as laid out in EN 1991–2, might not represent reality in a safe and thus sufficient manner. This implies that the reliability requirement which is deemed fulfilled by design and verification according to the Eurocodes, is not met by using the aforementioned load model.

1.2 Objective

The primary goal of this endeavor is to determine the reliability provided by the current code, and whether this is *sufficient* or not. Therefore it is clear that insight is to be acquired in both the provided and the required reliability. Based on the problem statement and the objective, a research question was formed:

> "Is the requirement regarding reliability, as stated in the Eurocode, proven by applying the load model for fatigue on concrete railway structures, as laid out in NEN–EN 1991–2?"

To this extent, the following sub-questions are to be answered:

1. "What level of reliability is **required** by the current code?"
2. "What level of reliability is **provided** by the current code?"

1.3 Method & Scope

The goal of this thesis is to show the reliability, provided by design using the Eurocode verification methodology for reinforced concrete structures. For this, measured trains are used as a representation of loading on structures. These traffic records will be used to establish the reliability level of the current code. Altering the current load model is however not done within this study. The load model's reliability which is to be shown, however, might initiate such activities in future research.

The scope of this project is mainly on the load model for fatigue loading on railway bridges (and other appropriate structures) in the Dutch railway network. However, to determine the reliability, it is of critical importance to include the strength-side of the problem as well. At the start of this project, ProRail expressed specific interest towards fatigue in concrete structures due to possible fatigue damage (to concrete) at the 'Lingebrug', connecting Tricht and Geldermalsen. Actual information regarding possible fatigue damages is, however, not yet available but under investigation within ProRail. These suspicions have also formed the incentive to investigate the current load model for fatigue. This specific interest in concrete structures has formed the reason to base the calibration (meant here as comparison, thus not including subsequent adjustment) on the resistance models for (reinforced) concrete. During a site visit within this investigation (see figure 1.1), however, no damages were spotted at the bridge.

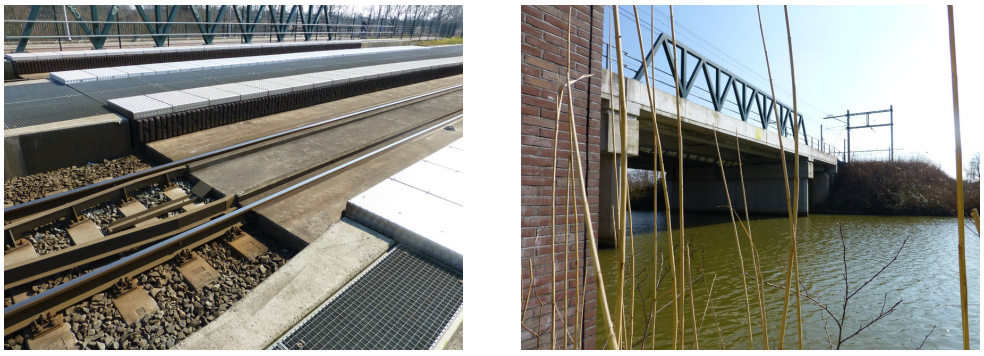

(a) (b)

Figure 1.1: Lingebrug near Tricht as seen during site visit. (a) Bridge deck; (b) Side view;

1.4 Outline

In this report, one will first find an introduction to fatigue (chapter 2), explaining some basics regarding the phenomenon and an overview of rules used for design according to the Eurocode. The target reliability, together with the background concerning this aspect, is included as a single chapter, i.e. chapter 3.

The following two chapters, 4 and 5, are dedicated to the analysis of provided reliabilities. In chapter 6, these reliabilities are compared to the required value and the reasons for discrepancies are demonstrated. Note that the background of probabilistic calculation methods, as far as required for comprehending the steps taken in this thesis, is explained briefly in appendix A.

2 | Background Information

In the early 1800s, fatigue was first recognized as a problem when European investigators observed the failure of bridge and railroad components (American Society for Materials, 2008, p. 243). The study of failures caused by, among others, heavy duty railway locomotives, led to a preliminary understanding during the industrial revolution. In 1837 it was Albert who published the first article on the novel subject, describing for the first time the correlation between fluctuating loads and the durability of metal (Bath & Patibandla, 2011).

2.1 The fatigue phenomenon

Fatigue is a process of degradation, where cumulative damage is done through subsequent loading and unloading cycles. This is defined by Steel Construction Institute (1993) as:

> "*The mechanism whereby cracks grow in a structure.*"

where the American Society for Testing and Materials handles a more extensive definition (American Society for Materials, 1985), which seems to be more appropriate given that fluctuating compressive stresses can also lead to fatigue:

> "*Fatigue — the process of progressive localised permanent structural change occurring in a material subjected to conditions that produce fluctuating stresses and strains at some point or points and that may culminate in cracks or complete fracture after a sufficient number of fluctuations.*"

Progressive implies that failure occurs through accumulated damage over a period of time. This means that the mechanism which led to failure operates during the structure's life-time. The fact that fatigue damage affects small parts of the structure, as opposed to the entire structure at once, is contained in the word *localized*.

The danger lies in the way in which fatigue failure unfolds. During the use of a structure, damage is accumulated through the repetitive application of loads. These are loads which produce stresses well below the point of yielding. A conventional stress analysis might thus rate the structure as *safe*, because a single application of the load would not lead to failure, but through accumulated damage the structure might fail (Roylance, 2001). A well-known example of fatigue failure is the Comet Jet Airliner (Bath & Patibandla, 2011).

2.1.1 Designing for fatigue

When preparing a design it is important to check whether the material will fatigue given the way it is loaded, and to which extent. Resistance to fatigue can be created by keeping the stresses sufficiently low, which leads to the question what 'sufficiently low' entails.

The general consensus is that the number of load cycles that a material can withstand depends upon the magnitude of the cycle, or the *stress range* (also the absolute stress levels when concrete is concerned). This is displayed in a S-N diagram, in which the stress range $\Delta\sigma$ (generally denoted with 'S') is plotted against the number of cycles N which can be withstood at that stress range. For low stress ranges the number of cycles is generally found to be orders of magnitude larger than at high stress ranges. This is why the S-N curves are plotted on logarithmic scales (Roylance, 2001). Commonly, simplified S-N diagrams are used, with linear proportionality on a double logarithmic scale. This implies an expression in the form of

$$N = \frac{C}{\Delta\sigma^m} \tag{2.1}$$

where

N = number of cycles
C = constant in S-N formulation
$\Delta\sigma$ = stress cycle magnitude
m = fatigue exponent

from which the linearity can be shown by taking the logarithm of both sides:

$$\log N = \log C - m \log \Delta\sigma \tag{2.2}$$

Equation 2.2 shows that the S-N diagrams can be plotted as straight lines on double-logarithmic paper (see figure 2.1).

For metals and composites, the generally accepted theory is the that there are three distinguishable phases in fatigue cracking (in some literature only the first two are mentioned):

1. crack initiation;
2. propagation of one dominant crack;
3. final fracture.

The fatigue life is determined as the sum of the duration of phases 1 and 2. During the second phase, the *growth rate* of cracks can be approximately described using Paris' law, which states (Paris & Erdogan, 1963):

$$\frac{da_{\text{crack}}}{dN} = A_{\text{crack}} \Delta K^m \tag{2.3}$$

where

a_{crack} = size of the crack
ΔK = $K_{max} - K_{min}$, the stress intensity at the crack tip
A_{crack} = crack growth proportionality factor

Equation 2.3 is used for an approach known as 'fracture mechanics'. It implies that the cracks grow at a rate proportional to the local intensity of the stress cycles, raised to a power m (generally in the order of 3–9).

The pragmatic approach which is frequently used for fatigue calculations is the theory of *damage accumulation*. This theory states that each application of loading affects a structural element, and results in a permanent effect which is named 'damage' (not to be confused with failure, rather some equivalence to remaining life). The

accumulation of this damage is then studied, where failure is assumed to occur at the attainment of a specific value, generally 1. The accumulation of damage is most often assumed to occur in a linear fashion. This principle is formulated in Palmgren-Miner's law (Miner, 1945):

$$D = \sum_{i=1}^{k} \Delta D_i = \sum_{i=1}^{k} \frac{n_i}{N_i} \tag{2.4}$$

where

D = normalized cumulative fatigue damage ($0 \leq D < 1$ corresponds to survival and $D \geq 1$ to failure), also called '**damage number**'
ΔD_i = incremental normalized damage from band i
n_i = number of applied cycles in band i
N_i = number of allowed cycles in band i

Cumulative fatigue damage is thus formed through repetitive loading, where each load is assumed to contribute to the total damage through an incremental damage. Such incremental damages are determined using the aforementioned S-N curves. Starting from a single cycle with known stress range, $\Delta\sigma_i$, the number of cycles which can be sustained is read from the S-N curve. The result is denoted with N_i. One cycle of this magnitude then causes a damage increment of $1/N_i$ according to equation 2.1.1. In doing so for all cycles, and adding all damage increments, the cumulative fatigue damage D is calculated. Real world loading will generally consist of cycles with varying magnitudes. These can thus be combined using Miner's rule.

According to Roylance (2001), Miner's law should be viewed skeptically. Some effects which influence the strength are ignored, which is why the essential physics of the fatigue process are not captured in an accurate manner. It is however widely employed in fatigue calculations, and can lead to sufficient reliability provided that it is correctly calibrated (which is essentially accomplished through the S-N curve).

2.1.2 Fatigue in steel

Because of the large differences in fatigue strength related to different details and their geometry, a number of strength models had to be developed to represent this variety. NEN-EN 1993-1-9 (CEN, 2005c) provides S-N curves for different detail categories with corresponding fatigue strengths. This is expressed using the parameter $\Delta\sigma_C$ (reference strength), which is defined as the stress range which leads to failure for $N = 2 \times 10^6$ cycles.

The exponent m from equation 2.2 is taken as a constant for each detail category, while it varies for different regions of cycles (thus being responsible for the shape of the curve). Five example S-N curves, each corresponding to a different detail category, have been reproduced using the parameters given in the Eurocode, shown in figure 2.1.

For normal stresses, the slope (or 'fatigue exponent', denoted with m) for variable amplitude stress cycles is given as (NEN-EN 1993-1-9 art. 7.1(2), CEN, 2005c):

$$m = \begin{cases} 3 & \text{for } N \leq 5 \times 10^6 \\ 5 & \text{for } 5 \times 10^6 < N \leq 1 \times 10^8 \\ \infty & \text{for } 1 \times 10^8 < N \end{cases} \tag{2.5}$$

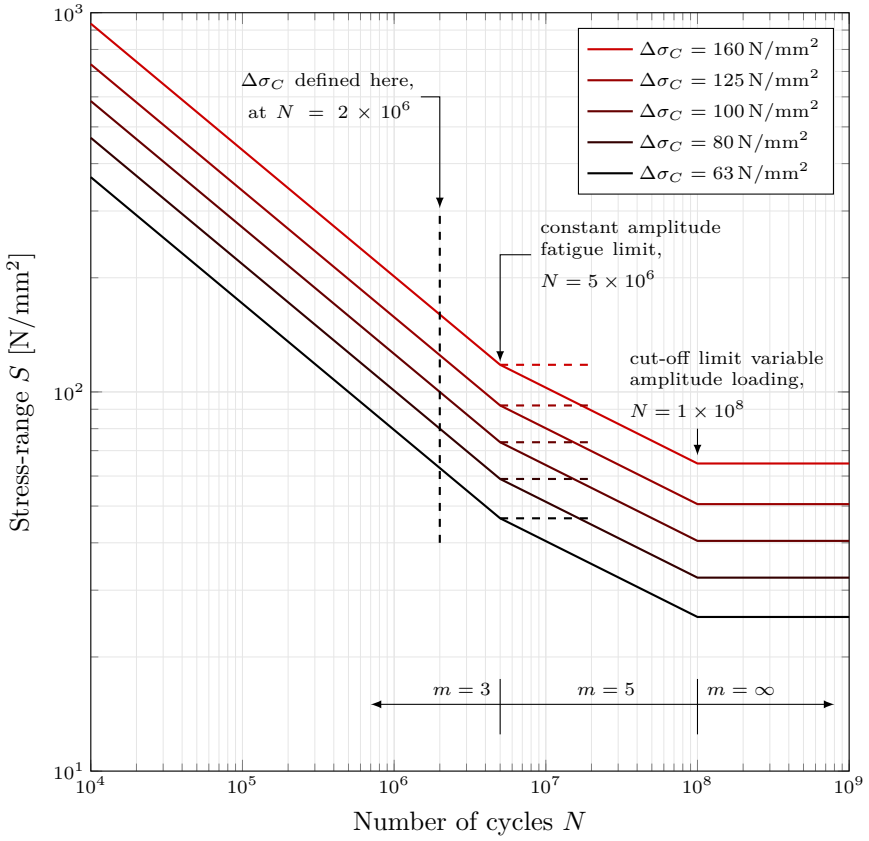

Figure 2.1: S-N curves for normal stresses in steel, given for five detail categories (expressed as $\Delta\sigma_C$). Based on NEN-EN 1993-1-9 (CEN, 2005c).

In the case of constant amplitude loading, the *cut-off limit* for fatigue may be taken at 5×10^6 cycles, as indicated with dashed segments in figure 2.1. Using this information, combined with the definition of $\Delta\sigma_C$, the S-N curves are fully defined. When the detail is subjected to shear stresses, the value for m is equal to 5 for the entire range above the cut-off limit.

The verification of fatigue resistance in steel does not take into account the mean stress level. This is because it implicitly contains the assumption that steel in the vicinity of a weld has residual stresses of a magnitude comparable to that of the yield stress. For non-welded details, the Eurocode allows a reduction of the compression part of the cycle to 60 % of its original value.

2.1.3 Fatigue in reinforced concrete

Although it is commonly thought that no fatigue collapses of concrete structures have ever been observed, there are a number of documented cases where fatigue has resulted in damage. Also, one case where concrete compressive fatigue led to collapse was documented. Seventeen case studies of damage were presented by CEB (1988), which cover bridges, pavement and slabs, prestressed concrete, machine foundations, and pile driving. The most relevant cases are summarized below (CEB, 1988) (numbering corresponds to cited source, other cases can be found in appendix B):

2. Japanese bridge decks: there have been numerous reports of fatigue failures in reinforced concrete bridge decks. The result is spalling of the concrete covering

the bottom layer of reinforcement, as well as damage to the running surfaces, which were associated with punching failure. Note that there were no cases of failing reinforcement, only the concrete was affected. Repetition of shear and torsional effects were suggested to reduce the fatigue strength by about 50 %.

4. Bridge decks in Holland: several bridge decks, supported by frames of steel beams, have been replaced because of their bad condition. This was due to the formation of many small cracks, which led to complete disintegration of the concrete. The damage was highly localized, and coincided with wheel tracks. The reinforcing steel was undamaged, which led to the conclusion of fatiguing concrete.

6. Bridge over Tarnaforsen, Sweden: vertical cracks and inclined shear cracks have been observed in the bridge. The main cause was identified as repetitive overloading by timber trucks, with one exceptionally heavy truck signifying the start of fatigue cracking problems.

10. Factory floor slab, United Kingdom: a prestressed factory floor slab, consisting of three adjacent parts which were connected by a single top-layer, lost all serviceability due to fatigue (cracking and deflections). The repeated passing of forklifts was identified as the cause. This caused the joints between prestressed elements to degrade, in turn reducing the spreading of loads over the elements. This reduced spread made matters even worse.

14. Footing at Skutskarsverken, Sweden: a machine hit its footing with great force, approximately 100 times per minute. Also, resonance was part of the excitation. Cracks were observed after 6 years of use, or 70×10^6 cycles. These cracks were said to gradually increase in width.

As a last addition, a quote from CEB (1988) is included: "*In most cases it is unlikely that fatigue can be isolated as the sole reason for deterioration*".

In all literature, only one example of collapse due to concrete fatigue in compression was found. The case at hand (see Van der Veen and Den Uijl, 2015) describes failure of a concrete wind turbine, which had a wall thickness of 90 mm instead of the nominal 150 mm. Although it is noted that the shaft should not have passed quality control, it did anyway, resulting in collapse (see figure 2.2). It is stated explicitly that this was due to concrete fatigue in compression. As with fatigue in

Figure 2.2: Concrete wind turbine after collapse due to concrete compressive fatigue (Van der Veen and Den Uijl, 2015).

steel, the resistance provided by reinforced concrete can also be given by characteristic

S-N relationships (see sections 2.1.3.1 and 2.1.3.2). Notion must be made, that the behavior of reinforced concrete, as this is a composite material, is dictated by the behavior of both its components, which will therefore both be discussed. Note that, in this report, prestressing steel is not treated.

2.1.3.1 Reinforcement steel

An extensive overview regarding the fatigue strength, behavior, and testing of reinforcement steel was given by Tilly (1979). Different types of bars, e.g. plain or deformed, are compared on their fatigue behavior. It is found that plain bars outperform other types on fatigue, while their bonding properties are reduced. This is said to be due to stress concentrations which are introduced by e.g. ribs on bars, especially at intersecting rib patterns (CEB, 1988). More interestingly, it was found that manufacturer's markings on the reinforcement bars reduce fatigue life by about 50 % on account of the same principle.

Looking at the different types of fatigue life testing of steel reinforcement bars, two clear methods can be distinguished (Tilly, 1979):

- Axial testing: it is difficult to attach the specimen in such a way that large stress concentrations near the attachment points are avoided. Also, slight misalignment of the testing equipment and the bar can introduce secondary stresses, which cloud the results.
- Bending testing: these are usually performed on concrete beams with a single reinforcement bar. The main advantage that is brought by this type of testing, is that it also includes the interaction effects of reinforced concrete as a composite material (e.g. bond between the reinforcement steel and the concrete).

Considering factors that influence the actual fatigue life of the material itself, in general five aspects are listed (Tilly, 1979):

- Type of steel: the fatigue life is affected by the chemical composition of the steel. Steel strengths higher than 420 $\mathrm{N/mm^2}$ only deliver a small increase in the resistance to fatigue.
- Geometry and size of the bars: this is partly expressed by the *size effect*, which entails that the fatigue strength decreases with increasing sizes. Reasons for this are also known. The first and most trivial is the increased likelihood of defects in the material, from which a crack may initiate. This also implies increased scatter in smaller samples. Another reason which is given, is that smaller diameter steel can be worked more effectively, resulting in a more uniform product with a higher fatigue strength.
- Nature of the loading cycle: in reinforcement, also there are less residual stresses than in other structural steel (assuming structural steel is welded while reinforcement is not). This implies that the mean stress might have a more pronounced effect in reinforced concrete than in (welded) steel details. It is found, that for increasing mean stresses, the fatigue life decreases.
- Welding: welding of the reinforcement may also lower the strength (reductions up to 50 % were found for tack welded stirrups at 1 - 5 $\times 10^6$ cycles), although results obtained through axial testing are reported to be very conservative, and may be unnecessarily preventing the use welding.
- Presence of corrosion: corrosion and fatigue damage can interact, meaning that the total result is larger than the superposition of individual effects.

The working in itself can also affect the quality. This is achieved through the rolls used to work the steel. It is found that the best results are produced using worn rolls. Defects in the rolls can also affect the steel in a considerable manner, as reported in *Fatigue of Concrete Structures* (CEB, 1988):

> "*Samples from a* 32 mm *diameter bar having a gross defect due to a chipped mill roll failed at* 2.5 *million cycles when tested at a stress range of* 225 $\mathrm{N/mm^2}$ *whereas a sound bar tested at this stress was unbroken after* 300 *million cycles.*"

The Eurocode prescribes S-N relations for reinforcement, which differ slightly from those for structural steel, as covered in section 2.1.2. The first difference is that no stresses above the design yield stress are permitted whatsoever, which is in line with design conditions for ultimate strength limit states. The slope of the relations, or actually the fatigue exponents, varies for different conditions. This is also the case for the transitional point, denoted as N^*. A schematic representation of the curve is given in figure 2.3 while the accompanying parameters are presented in table 2.1.

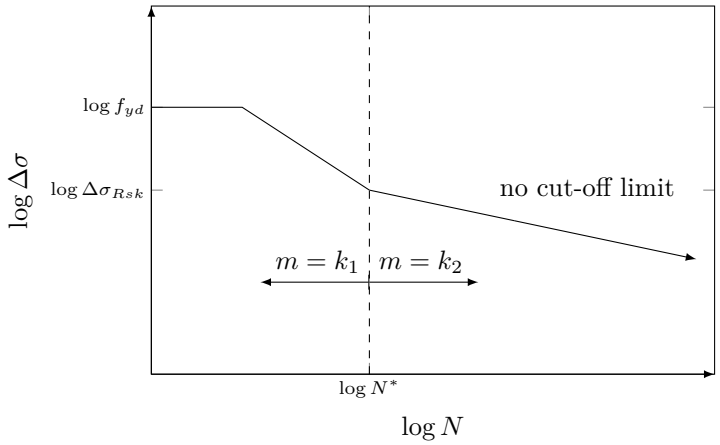

Figure 2.3: S-N curve for reinforcement steel. Based on NEN-EN 1992-2 (CEN, 2005b). Note that for bent bars, a reduction factor for the fatigue strength is given in the Eurocode.

reinforcement type	N^*	fatigue exponents		$\Delta\sigma_{Rsk}$
		k_1	k_2	@$N = N^*$
straight and bent bars	10^6	5	9	162.5 $\mathrm{N/mm^2}$
welded reinforcement	10^7	3	5	58.5 $\mathrm{N/mm^2}$
connections	10^7	3	5	35 $\mathrm{N/mm^2}$

Table 2.1: Parameters for reinforcement S-N curves. Based on NEN-EN 1992-2 (CEN, 2005b).

2.1.3.2 Concrete

As opposed to fatigue in steel, the relative position of the stress cycle in the stress-domain, as indicated by the cycle's mean stress, plays a crucial role in the fatigue verification of concrete. This has resulted in more complex S-N relations, because more information is included. The mean stress and amplitude, equivalent to the minimum and maximum of the cycle, are included via a ratio of minimum and maximum stress, denoted with R.

Note that the Dutch National Annex provides alternative (less conservative, for an extensive comparison see Lantsoght, 2014) formulations for the S-N curves in the

domain up to 10^6 cycles, than the basic Eurocode. The National Annex to NEN-EN 1992-2 provides the following expressions (CEN, 2005b):

$$\log N_i = \frac{6}{1 - 0.57\,k_1\left(1 - \frac{f_{ck}}{250}\right)} \frac{1 - E_{cd,max,i}}{\sqrt{1 - R_i}} \qquad \text{for } N_i \leq 10^6 \tag{2.6}$$

$$\log N_i = 14\,\frac{1 - E_{cd,max,i}}{\sqrt{1 - R_i}} \qquad \text{for } N_i > 10^6 \tag{2.7}$$

$$R_i = \frac{E_{cd,min,i}}{E_{cd,max,i}} \tag{2.8}$$

$$E_{cd,min,i} = \frac{\sigma_{cd,min,i}}{f_{cd}\left(0.9 + \frac{\log N_i}{60}\right)} \qquad \text{for } N_i \leq 10^6 \tag{2.9}$$

$$E_{cd,min,i} = \frac{\sigma_{cd,min,i}}{f_{cd,fat}} \qquad \text{for } N_i > 10^6 \tag{2.10}$$

$$E_{cd,max,i} = \frac{\sigma_{cd,max,i}}{f_{cd}\left(0.9 + \frac{\log N_i}{60}\right)} \qquad \text{for } N_i \leq 10^6 \tag{2.11}$$

$$E_{cd,max,i} = \frac{\sigma_{cd,max,i}}{f_{cd,fat}} \qquad \text{for } N_i > 10^6 \tag{2.12}$$

where

R_i = stress ratio corresponding to cycle i
$E_{cd,min,i}$ = minimum relative stress level in cycle i
$E_{cd,max,i}$ = maximum relative stress level in cycle i
$\sigma_{cd,min,i}$ = minimum stress in cycle i
$\sigma_{cd,max,i}$ = maximum stress in cycle i
$f_{cd,fat}$ = concrete design fatigue strength

Here, the design strength for concrete subjected to fatigue is given by

$$f_{cd,fat} = k_1\,\beta_{cc}(t_0)\,f_{cd}\left(1 - \frac{f_{ck}}{250}\right) \tag{2.13}$$

$$\beta_{cc}(t) = \exp\left(s\left(1 - \left(\frac{28}{t}\right)^{\frac{1}{2}}\right)\right)\,\alpha_{cc} \tag{2.14}$$

$$f_{cd} = \frac{f_{ck}}{\gamma_{c,fat}} \tag{2.15}$$

$$s = \begin{cases} 0.20 & \text{for cement class R} \\ 0.25 & \text{for cement class N} \\ 0.38 & \text{for cement class S} \end{cases} \tag{2.16}$$

where

f_{cd} = concrete design compression strength
f_{ck} = concrete characteristic compression strength
$\beta_{cc}(t)$ = coefficient for the concrete strength at first load application
s = coefficient to take into account the cement class (Rapid/Normal/Slow)
t = age of the concrete in days

According to the Dutch National Annex, the coefficients k_1 and α_{cc} shall be taken equal to one, which probably results in the best correspondence to test results. The term $E_{cd,max,i}$ in equation 2.6 depends on $\log N_i$ in the domain of $N_i \leq 10^6$. Therefore, the equation does not provide a closed solution straight ahead. It is however possible to write it in explicit form for both $\log N_i$ as for $E_{cd,max,i}$. For the following, the notion of a *relative maximum and minimum stress level* is introduced, similar to Lantsoght (2014):

$$s_{max,i} = \frac{\sigma_{cd,max,i}}{f_{cd}} \tag{2.17}$$

$$s_{min,i} = \frac{\sigma_{cd,min,i}}{f_{cd}} \tag{2.18}$$

so that

$$R_i = \frac{E_{cd,min,i}}{E_{cd,max,i}} = \frac{s_{min,i}}{s_{max,i}} \tag{2.19}$$

Now, an explicit expression for $\log N_i$ as a function of s_{max} can be derived, granted that either s_{min} or R is fixed, by solving a quadratic equation. This results in

$$\log N_i = \frac{C}{2\sqrt{1-R}} - 27 + \sqrt{\left(27 - \frac{C}{2\sqrt{1-R_i}}\right)^2 - \frac{60\,C\,(s_{max,i} - 0.9)}{\sqrt{1-R_i}}} \tag{2.20}$$

with

$$C = \frac{6}{1 - 0.57\,k_1\left(1 - \frac{f_{ck}}{250}\right)} \tag{2.21}$$

Although the expression for the domain $N > 10^6$ is already given in explicit form, it still needs an alteration before the S-N curve can be plotted in a convenient manner. The term $E_{cd,max,i}$ can be substituted by

$$E_{cd,max,i} = \frac{\sigma_{cd,max,i}}{f_{cd,fat}} = \frac{\sigma_{cd,max,i}}{f_{cd}} \frac{f_{cd}}{f_{cd,fat}} = s_{max,i} \frac{f_{cd}}{f_{cd,fat}} \tag{2.22}$$

With this substitution it is clear how the two parts of the curve can be plotted with s_{max} as the ordinate. Plots for three stress ratios ($R = \{0; 0.4; 0.8\}$) and three concrete strength classes (C40; C80; C120) are given in figure 2.4. Note that these have been plotted for $t = 28$ days, resulting in $\beta_{cc} = 1$.

It is clear from the plots that, especially for increasing R, the curve is interrupted at $N = 10^6$ cycles. It is not clear why this is the case, as logic argues against the notion that the resistance, expressed as the number of cycles, remains constant for a (in case of large R) significant portion of the stress-domain. Actually, this is believed to be the result of some mistake. Lantsoght did propose changes for a continuous curve, which will be adopted later on in this work (discussed in chapter 5). However, this somewhat reduces the compatibility with the current Eurocode.

The fatigue resistance at one cycle, thus for $\log N = 0$, is equal to $0.9\,f_{cd}$ for all cases. While this may seem odd at first, it should be realized that when dealing with the fatigue limit state, the partial factor for fatigue is used, which is equal to 1.35 for concrete. For the ultimate limit state, this partial factor is 1.50, and the ratio of these partial factors is precisely 0.9. Therefore, when dealing with actual stresses instead of relative levels, the maximum stress which can be sustained for a single cycle, corresponds to the design compressive strength corresponding to ultimate limit

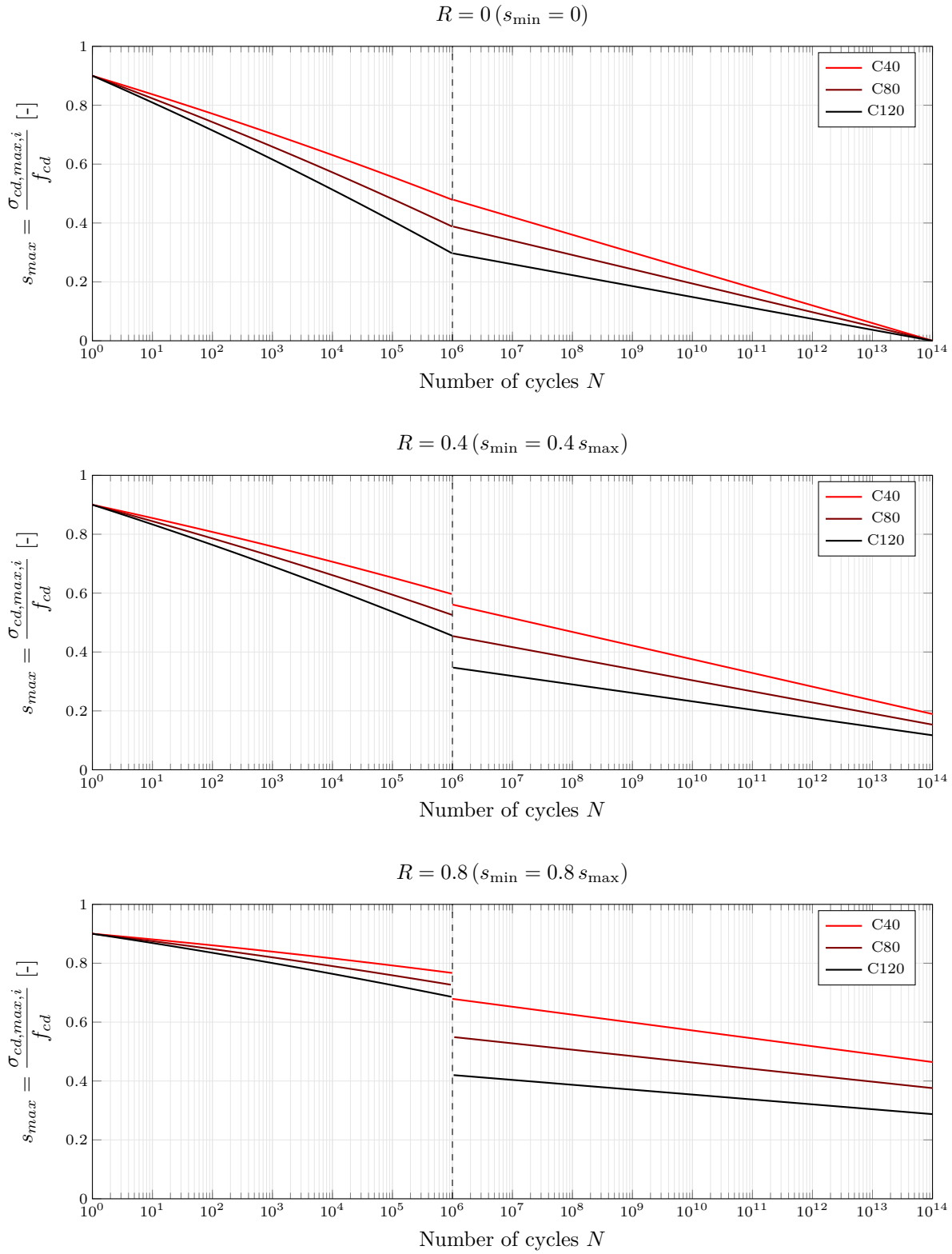

Figure 2.4: S-N curves for normal stresses in concrete, as a function of s_{max} for a given stress ratio R. Based on NEN-EN 1992-2 (CEN, 2005b).

states. In the author's opinion, such measures are quite unclear, and might therefore lead to confusion or mistakes.

Another interesting observation is that the line segments are fairly straight, while the stress is plotted at linear scale instead of logarithmic as was the case with the S-N curves for steel (compare to figure 2.1).

2.1.3.3 Composite behavior of reinforced concrete

The relations given in the previous sections may be accurate for reinforcement and plain concrete, but this does not necessarily validate them for the composite in which these components are mainly used. Regarding bending fatigue, it was found that:

> "*The fatigue damage process can be summarized as follows. After first cracking the fatigue loading causes progressive deterioration of the bond between the reinforcement and the concrete adjacent to the crack. Larger crack widths and a smaller contribution of the concrete in tension between the cracks result in larger deflections. Failure normally occurs due to bar fatigue fracture; another failure mechanism is spalling of concrete in the compression zone. However, even over-reinforced beams (i.e. concrete compression failure under static loading) fail due to reinforcement fracture when subjected to fatigue loading. Due to the strain redistribution under compression, in most cases the concrete of a reinforced concrete member does not fail under bending stresses.*" — Plos et al., 2007

Acting on the notion that local failure of concrete in compressive fatigue may lead to redistribution, it is imaginable that such a redistribution of compressive forces may alter the tensile counterpart. This interaction may be of great importance, and may even explain the way in which reinforced concrete elements generally fail in testing, being fracturing of reinforcement.

If some reinforced concrete section, with reinforcement near the bottom fibers, is loaded intensively with repetitive nature, this in turn causes the concrete near the top fibers to lose part of its stiffness, leading to a decrease in stresses for equal strain. This loss of stiffness is believed to be due to the formation of cracks on a microscopic level (Plos et al., 2007). In order to retain equilibrium of horizontal forces in the cross-section, the strains should increase (where it is assumed that the load is unaltered). Also, the internal lever arm is affected. The concrete near the top acts only partly, causing the resultant equivalent compressive force to shift downwards into the section (the effective section height is reduced). This shift of the compressive force leads to an increased aggressiveness of the reinforcement's loading, and therefore intensifies the accumulation of fatigue damage. When failure now occurs, it will be due to the fracture of reinforcement, while it is actually induced by concrete compressive failure. This is accompanied by concrete which is, while partially fatigued, able to redistribute loads internally because of the relatively larger area. This theory was also partially suggested in Plos et al. (2007).

What is also of interest, is that, if the stiffness of the concrete decreases with repetitive loading, failure in terms of stresses may actually never occur. It would thus be better practice to speak of strain instead. In the Eurocode, the prescription of the linear elastic calculation model circumvents this issue by not taking into account any decrease in stiffness. Therefore, it is equivalent to verifying the resistance to fatigue using the strain.

As a concluding remark it is added that the failure mechanism of reinforced concrete in fatigue, under presupposition of the above, is caused by a progressive degeneration of both its components. Designing for fatigue failure should reflect such mechanisms,

which it currently seems not to (at least explicitly). For the sake of this thesis, and because the above is just a theory, the load models shall be calibrated using the Eurocode's current damage models (or actually those proposed for the new national annex, discussed in chapter 5), without incorporating interaction between concrete and reinforcement.

As far as the reliability is concerned, the fatigue limit state is compared to that of ultimate strength. Because of the progressive deterioration, the strength (capacity) of the material is decreased. Therefore, the resistance in the ultimate strength limit state is decreased as well. If failure occurs, it is thus a combination of progressive deterioration and the occurrence of a somewhat severe load, and the final mechanism will be identical to failure in the ultimate strength limit state. Elaborating on this idea, it may even be concluded that both limit states cannot be separated, and should therefore be captured in a single limit state. This also implies that the reliability should be equal for both limit states, and that the ultimate strength limit state might be more time-dependent than generally accounted for. More on this will be discussed in chapter 3.

2.1.4 Fatigue verification à la Eurocode

This section is focused primarily on the verification procedure for fatigue effects on railway bridges as adopted by the Eurocodes. There are two procedures specified in the code, namely:

1. simplified method, i.e. the λ-*method*;
2. cumulative damage method.

Both methods will be discussed in the remainder of this section.

2.1.4.1 Simplified method

The simplified method consists of one straightforward check that needs to be satisfied. Although the method is explained slightly different in the codes for steel and concrete, it is essentially the same. According to the codes, NEN-EN 1992-2 (CEN, 2005b) and NEN-EN 1993-2 (CEN, 2006), the requirement is given in the form of (presented here for structural steel)

$$\gamma_{Ff}\,\lambda\,\Phi\,\Delta\sigma_{FLM} \;\leq\; \frac{\Delta\sigma_c}{\gamma_{Mf}} \tag{2.23}$$

where

γ_{Ff} = partial safety factor for fatigue loading (section 3.2)
λ = equivalent damage factor, defined in eq. 2.24
Φ = dynamic equivalence factor (section 2.1.4.3)
$\Delta\sigma_{FLM}$ = fatigue load model stress range
$\Delta\sigma_c$ = reference fatigue strength, depending on the detail category. For its definition, see figure 2.1
γ_{Mf} = partial safety factor for fatigue strength

The equivalent damage factor λ is used to transform the spectrum of traffic loads into one single, equivalent, stress range at $N = 2 \times 10^6$ cycles. It is defined as:

$$\lambda = \lambda_1\,\lambda_2\,\lambda_3\,\lambda_4 \tag{2.24}$$

where

λ_1 = factor which takes into account the influence of the span lengths, i.e. the relevant influence line for the detail

λ_2 = factor which takes into account the (yearly) traffic volume

λ_3 = factor which takes into account the design life

λ_4 = factor which takes into account the influence of loading on multiple tracks

Each of the λ's is defined by expressions which relate to the reference circumstances which were used for calibration of $\Delta\sigma_{FLM}$. These consist of a traffic volume of 25×10^6 tonnes per year per track, and a design life of 100 years. The proportionality of these λ's with respect to different conditions is given through the fatigue exponent m. Because this exponent differs for varying stress ranges, and materials, the results are different for e.g. reinforcement steel. Stress ranges resulting from real traffic are generally in the range below the constant amplitude fatigue limit, that is, in the region of $m = 5$ in figure 2.1 (thus for structural steel) (Jacob & Kretz, 1996). This exponent therefore is used to calculate the tabulated values for λ_2 and λ_3 in NEN-EN 1993-2. Further description of the model is not relevant and thus omitted.

For concrete in compression this model differs, but the Dutch national annex to NEN-EN 1992-2 states that Miner's sum should be used for concrete, implying that the use of simplified models is not permitted. Miner's sum, used in conjunction with the *cumulative damage method*, will be elucidated in section 2.1.4.2.

2.1.4.2 Cumulative damage method

The method of cumulative damage is based directly on the actual traffic that is expected to pass a bridge. The method basically consists of six consecutive steps:

1. Specification of a representative *traffic mix*.
2. Structural analysis, which in principle should include dynamic effects.
3. For each passing train the relevant stress at the considered detail should be determined as a function of the vehicle's position as it crosses the bridge, resulting in a *stress history*.
4. The stress histories corresponding to all passages are converted to a spectrum of cycles, using either the *rainflow* method (see chapter E) or the *reservoir* cycle counting method. This yields the total expected *stress spectrum* (description of all occurring stress ranges) for the detail under consideration.
5. The spectrum of stresses is generally divided into bands and for each band the number of cycles to failure is determined from the S-N curve belonging to the detail (see chapter 2).
6. Using the Palmgren-Miner assumption (eq. 2.1.1), the damage number is determined which finalizes the verification. This should be less than one to pass.

From the above it may be clear that this approach is much more cumbersome. It can therefore be said that it is generally time-efficient to start by applying the simplified model to identify which details might be susceptible to fatigue failure during the design life. These details can then be further optimized using the cumulative damage method, which is expected to yield a more accurate load effect, because the transformation from a spectrum to a single load application will most likely be at the expense of some of the accuracy.

In order to apply the cumulative damage method, it is required to have a specification of expected traffic, i.e. a load or vehicle model. In the Eurocode, three different traffic mixes are specified, corresponding to standard, heavy, and light traffic. These mixes

correspond to certain types of usage, being predominantly passengers of freight, or a mixture. All three traffic mixes are based on an annual cumulative tonnage of 25 million tonnes per track. The way these mixes are specified is via reference trains. A mix is then composed of frequencies of reference trains passing. The reference trains can be found in chapter J. The three mixes are discussed below.

Standard traffic mix (EC1) According to NEN-EN 1991-2 Appendix D, the standard traffic mix is composed of reference trains 1-8. Its composition is according to table 2.2.

train type	nr. per day	train mass [t]	traffic volume $[10 \times 10^6$ ton/year]
1	12	663	2.90
2	12	530	2.32
3	5	940	1.72
4	5	510	0.93
5	7	2160	5.52
6	12	1431	6.27
7	8	1035	3.02
8	6	1035	2.27
	67		24.95

Table 2.2: Composition of the standard traffic mix (NEN-EN 1991-2 App. D, CEN, 2002b)

Heavy traffic mix (EC2) The heavy traffic mix is composed of reference trains 5, 6, 11, and 12. Its composition is according to table 2.3.

train type	nr. per day	train mass [t]	traffic volume $[10 \times 10^6$ ton/year]
5	6	2160	4.73
6	13	1431	6.79
11	16	1135	6.63
12	16	1135	6.63
	51		24.78

Table 2.3: Composition of the heavy traffic mix (NEN-EN 1991-2 App. D, CEN, 2002b)

Light traffic mix (EC3) The light traffic mix is composed of reference trains 1, 2, 5, and 9. Its composition is according to table 2.4.

The abbreviations 'EC1', 'EC2', and 'EC3' are used in the rest of this report. Although the cumulative annual tonnages are equal, there are large differences in occurring axle loads and the number of passages, which can be observed in figure 2.5.

This is the only specification which is supplied. There is no method supplied for correction of these traffic mixes to the actual location, neither is it clear whether these are trains which can actually be expected (frequent loads) or design situations which are calibrated to provide some reliability (an approach which is comparable to the λ-method). Also, zero information is provided on how to apply the model to multiple tracks.

train type	nr. per day	train mass [t]	traffic volume $[10 \times 10^6$ ton/year]
1	10	663	2.40
2	5	530	1.00
5	2	2160	1.40
9	190	296	20.50
	207		25.30

Table 2.4: Composition of the light traffic mix (NEN-EN 1991-2 App. D, CEN, 2002b)

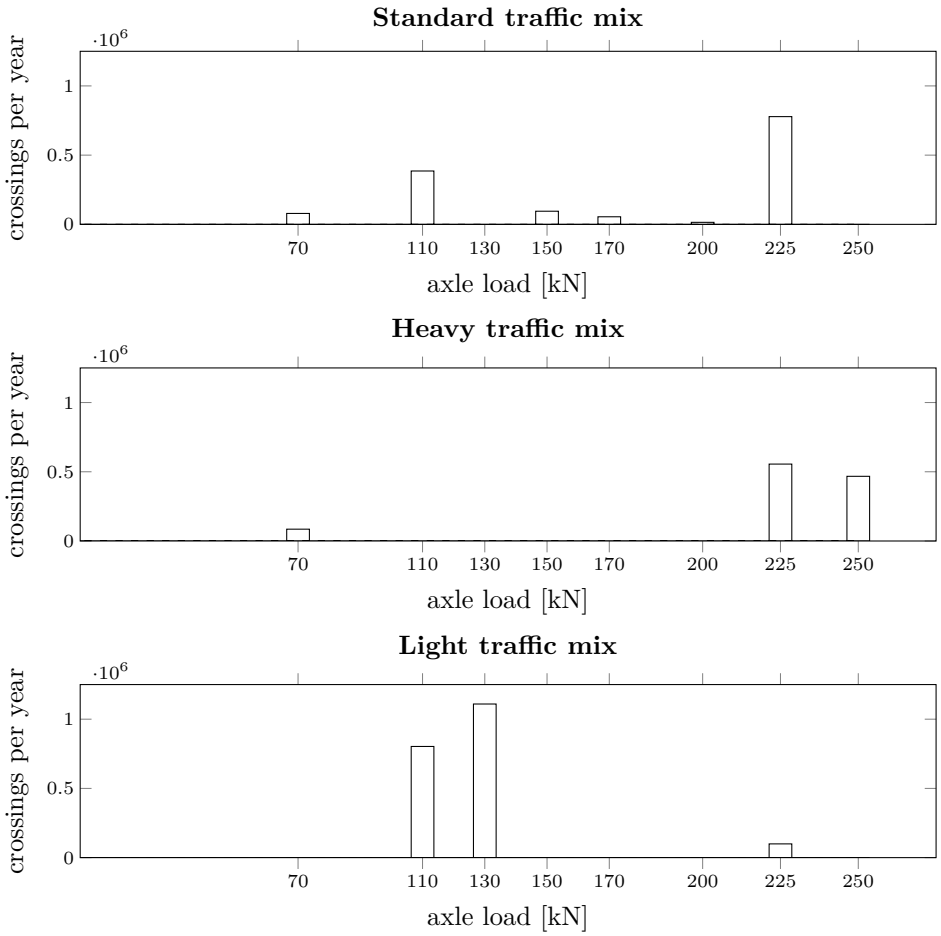

Figure 2.5: Eurocode traffic mixes expressed in yearly crossings per track as a function of the axle loads (based on NEN-EN 1991-2, CEN, 2002b)

2.1.4.3 Dynamic effects

As mentioned in equation 2.23, the dynamic factor Φ plays a role in the fatigue verification. Excitation of a structural system can lead to dynamic effects such as vibrations, which lead to varying stresses, i.e. stress cycles. When these are of significant intensity, their contribution to the fatigue damage can be relevant. Also, this is to take into account the effects of deviations in the roundness of the train's wheels, which lead to impact on top of static forces.

These dynamic effects should be evaluated using a model which fully captures the time-dependent behavior. In the Eurocode there is, however, an expression for the dynamic amplification factor Φ. This deviates from the regular dynamic amplification factor (DAF), which is only applicable to ultimate limit state (ultimate strength) conditions and thus contains some factor of safety. It is noted that appliance of this factor would lead to unnecessarily high equivalent loads on the bridge for **fatigue**. Therefore a reduced factor is proposed, namely (NEN-EN 1991-2, CEN, 2002b):

$$\Phi = 1 + {}^1/_2\,(\phi' + {}^1/_2\,\phi'') \tag{2.25}$$

$$\phi' = \frac{K}{1 - K + K^4} \tag{2.26}$$

$$\phi'' = 0.56 \exp\left(-\frac{L_\Phi^2}{100}\right) \tag{2.27}$$

with

$$K = \begin{cases} \dfrac{v}{160} & \text{for } L \leq 20\,\text{m} \\ \dfrac{v}{47.16\,L_\Phi^{0.408}} & \text{for } L > 20\,\text{m} \end{cases} \tag{2.28}$$

where

v = maximum allowed train speed [m/s]

L_Φ = governing length for dynamic amplification factor [m], according to table 6.2 of NEN-EN 1992-1

As this study is focused on the load model, the dynamic factor and its background are outside of the project's scope. However, the dynamic amplification factor will, in this report, be used to include the train's velocity into calculations.

2.2 Measurements

The data used in this thesis was provided by Ricardo Rail (formerly known as Lloyd's Register Rail). The measurements correspond to four locations, for all tracks at these sites. These sites are:

- Voorschoten – 4 tracks (detectors 11, 12, 18, 19);
- Tricht – 2 tracks (detectors 111, 114);
- Schiedam – 2 tracks (detectors 163, 164);
- Zeist – 2 tracks (detectors 363, 364).

More information can be found in chapter C. In this aforementioned chapter, apart from providing some extra information on the measurement systems and locations, exploratory analyses were done to asses the frequency distribution of axle loads vs. their magnitudes, the average tonnage vs. time, and the average axle loads vs. time. Using these results, it was possible to assess whether 4 years of data provided insight into some trend in time, which was shown not to be the case.

2.3 Preliminary deterministic comparison

With the availability of measurements, the urge to compare these to the Eurocode traffic mixes arises. However, there are differences in

- the **magnitude** of axle loads;
- the **number of crossings** by each axle load;
- the **distances** between axles.

Therefore, it is not immediately clear which criterion should be used to compare. Another important difference between measured loads and the Eurocode traffic mixes, is that the latter is defined as a 'characteristic value', and therefore corresponds to a value that includes an implicit safety margin. In an effort to compare the loads anyway, their magnitudes are compared, including frequencies of occurrence (see figure 2.6). It has to be emphasized again that **the Eurocode load models represent characteristic values, i.e. a certain safety margin is expected to be included**.

Observing these figures, it must be concluded that, in a 'deterministic sense' (without any of the uncertainties included), the characteristic Eurocode traffic mixes seem to cover the measured traffic reasonably well, and even seem quite conservative. There are some axle loads which exceed the maximum of 25 tonnes which is present in the Eurocode traffic mixes, which are therefore not covered. However, these occur in small numbers. Annual cumulative tonnages were also determined (see chapter C). These were shown never to exceed the 25 million tonnes which are prescribed in the Eurocode.

From such a 'deterministic comparison', one may conclude that the Eurocode traffic mixes are safe enough, and can therefore be used to verify structures in order to provide enough reliability. However, as will be demonstrated in the remainder of this thesis, this is not the case.

2.4 Conclusions

- Fatigue was identified as progressive and localized structural change, resulting from repetitive loading. This structural change was named 'cumulative fatigue damage'.
- Miner's sum can be used to calculate this fatigue damage, which is expressed using the 'damage number'. It is applicable to (reinforcement) steel and concrete, among other materials.
- A material's resistance to repetitive loading is expressed in a S-N curve. For each change in stress (a cycle), such a curve provides the number of permissible changes (cycles). This is used as input for Miner's sum, in order to calculate a damage number.
- It has been argued that, for a reinforced concrete section, fatigue degradation of the concrete in compression can lead to increased aggressiveness of stress fluctuations in the reinforcement. This may contribute to an explanation to why reinforced concrete sections generally fail due to reinforcement bar fracture.
- Two procedures for fatigue verification which are prescribed in the Eurocode have been explained. These are the simplified method (or λ-method) and the elaborate cumulative damage method.

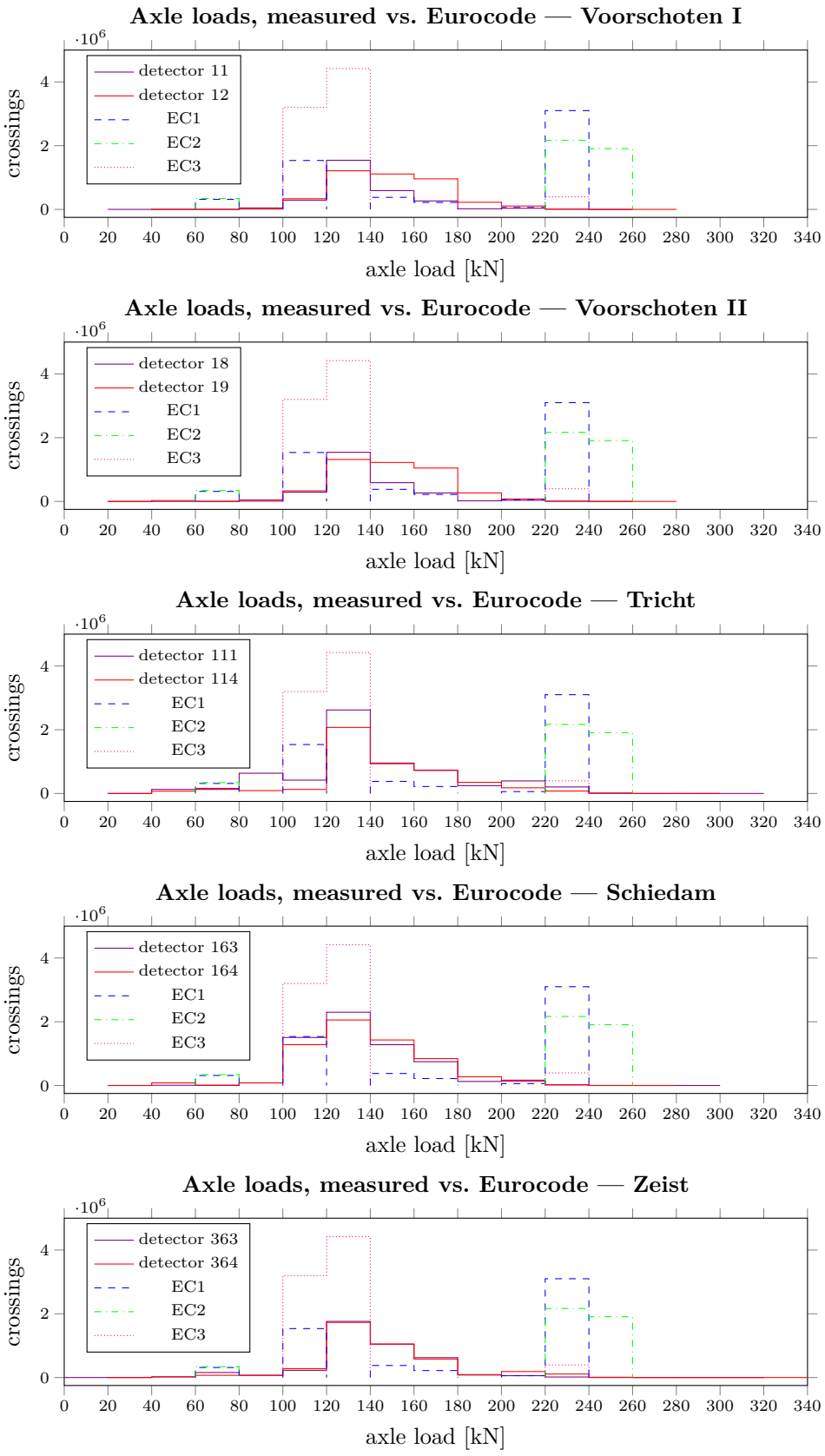

Figure 2.6: Deterministic comparison of measured axle loads to Eurocode traffic mixes. All figures correspond to 3.98 years, which is the time of measurement.

- Dynamic effects which accompany the passages of trains were discussed, and a factor to take these into account has been presented.
- Data corresponding to 4 locations (10 tracks) was provided by Ricardo Rail. The locations are: Voorschoten, Tricht, Schiedam, and Zeist.
- Comparison of the Eurocode traffic mixes with the measured traffic shows that the traffic mixes seem quite conservative. Also, the annual cumulative tonnages were determined. In all cases, these were lower than 25×10^6 tonnes, which is prescribed in the Eurocode. It should be noted that the traffic mixes are 'characteristic values', and therefore are assumed to include some sort of safety margin, or represent an upper bound of some sort.

Furthermore, no information regarding the background of the Eurocode load models for fatigue could be obtained. Even if this was available, demonstrating a certain reliability level given some traffic records at that time, this would not imply this reliability for the current situation, as traffic probably evolved. Therefore, this reliability level will be determined in the remainder of this report; a process in which the theoretical background covered in this chapter will be used intensively. There was also no information on comparing different sets of loads, so a strategy for this will have to be developed.

Regarding the target level: this was skipped in this chapter of background information. Its background and aspects are treated in the next chapter as a whole.

3 | Target Reliability Level

> *"When it first became evident — which was not very long ago — that a small stress, sufficiently repeated, was able to cause a failure, the designer based his calculations on the simple rule that the stress should be well below the endurance limit, i.e. the stress below which it is known that an infinite number of stress cycles can be borne. It seemed to hazardous to allow stresses giving a finite life."* — Weibull, 1949

In his report, Weibull then continues by discussing the fact that, under the influence of increasing economical demands, this has led to the actual question of relating the load and the life. Because both the loads and the life are subject to uncertainties, and can thus only be described by their statistical distributions, the notion of a *safety level* is introduced. Essential now for the verification and calibration of load models, is the question:

> "What level of safety is sufficient?"

Given a structure and failure mode, the level of reliability of the structure which is found to be acceptable is denoted as the **target reliability**. Several factors influence this, among which:

- the consequences of exceeding the target reliability (including loss of human life);
- the required costs for improving the safety;
- the structure's design life;
- the discount rate (interest);
- by law, a lower bound safety level which is to be respected when human life is involved in the decision;
- the ductility of a structure, i.e. to which extent it warns prior to failure.

The target reliability should theoretically be derived using an economic optimization (respecting the lower bound reliability level when human life is involved), where the minimized quantity is the expectance of total costs, in the form of (based on Leon and Pérez, 2000):

$$E\left[C_t\right] = E\left[C_0\right] + E\left[C_f\right] + E\left[C_i\right] + E\left[C_r\right] \tag{3.1}$$

where

C_t = total costs
C_0 = initial investment
C_f = failure costs
C_i = inspection costs
C_r = repair costs

The expected failure costs are a result of the failure probability and the associated consequences. As the initial investment costs influence the resistance, and thus the expected costs from failure (cumulative risk), an optimum can be found from equation 3.1. In this way, it is always economically justified to increase the reliability for as long as the costs of doing so are outweighed by the descrease of risk (benefits).

The problem with such an approach is that it requires significant assumptions to be made for uncertain aspects. These can be of tremendous influence for the results. Therefore, for this project and its scope, it seems more appropriate to use reasoning in obtaining a target reliability level for fatigue.

3.1 Inspections during service life

In order to determine an optimal reliability for fatigue limit states, first the expected process is considered. By now it is clear that fatigue is a cumulative process, where damage is done through repeated loading. Each applied load is expected not to cause failure by itself, and will generally be far below the material's static, let alone dynamic, capacity. Therefore time is needed before the fatigue limit state is reached, which can be a positive characteristic from a design point of view.

During this time, it might be possible to monitor the process of cumulative damage by inspections. Consider a certain repair threshold, which can for instance be set to a remaining capacity of twice the expected damage during the next inspection interval. Given that measurements are done correctly and all damage can be spotted, one could now determine the failure probability for a given location using the knowledge that damages are repaired when exceeding the repair threshold. Uncertainties in the fatigue loading will be, among other things, in the extrapolation in time, so by calculating for an inspection interval rather than for the life time, the uncertainties and therefore the failure probability may be greatly reduced. It can thus be concluded that inspection and repair can significantly improve the reliability of a structure susceptible to fatigue loading, provided that these are possible.

Designing structures to withstand fatigue loading over their service life without the need for inspection is deemed uneconomical (Baker & Descamps, 1999). It is more economic to use planned periodic inspections combined with a small probability of failure. Using such an approach also has the added benefit of enabling the detection of design and fabrication errors (Tammer & Kaminski, 2013).

The cumulative nature of fatigue loading can only be employed for improvement of the reliability, if there are techniques for the actual detection of fatigue damage. In other words, the overall reliability, given a certain inspection, maintenance, and repair program, will only benefit to the degree in which this inspection is effective.

3.1.1 Fatigue detection in steel

The detection of fatigue damage to steel structures is supposed to be 'relatively easy', of course when granted that the inspected detail is accessible. Cracks in the steel can be visible during inspection, and when the intervals between inspections are limited, detection is generally thought to be possible before structural failure occurs.

The limitation of the intervals between inspections should be based on the expected crack growth in this interval. The reliability of detection, i.e. the probability that, given a crack or defect, this will be detected during an inspection, can be described by so called *PoD*-curves (probability of detection curves). These curves relate the size of the defect to the probability of detection, belonging to a certain detection method.

However, the problem with fatigue cracks is their behavior during the fatigue life. Given the initiation of a crack, the growth will start out small. This can be explained by the fact that the remaining cross sectional area is still near its initial size. From Paris's law (equation 2.3) it is known that the crack growth is proportional to ΔK^m. As ΔK is a measure of the stress intensity, i.e. the magnitude of the stress cycle (or strain, if plastic behavior is concerned), this will increase for a decreasing cross section. The relevant part is its influence on the crack growth. It can be observed that the crack will grow at an increasing rate. As the probability of detection is linked to the crack size, this will also increase with time. The inverse is also true: because the crack will remain small until nearing failure, the probability that it will be detected before failure is relatively small until the final stage of fatigue life. However, such an approach could very well work in practice.

3.1.2 Fatigue detection in reinforced concrete

The detection of fatigue damage in concrete, also in reinforcement and prestressing steels, is difficult compared to steel structures. This is of course result of the fact that the surface of the concrete does not give sufficient information regarding the state of fatigue damage of the underlying steel.

Although the detection is difficult, techniques have been developed to inspect the steel through the concrete cover. These techniques make use of *acoustic emmission* (AE) or magnetic fields (Motavalli, Havranek, & Saqan, 2011). Acoustic emission is appropriate for continuous monitoring, while inspections can be done by magnetizing the reinforcement. The resulting magnetic field can then be *read*, showing discontinuities and flaws which may indicate fatigue damage. Methods like this have, however, never been used by ProRail. Also, it is not clear what the minimum size of detectable defects is.

The aforementioned techniques are however not available for fatigue inspection of concrete. According to CEB (1988), the "*fatigue cracks in concrete have no identifiable surface topography unlike fatigue cracks in steel*". Therefore it is reported to be extremely difficult to inspect the concrete for fatigue cracks (which is not facilitated by the concrete's characteristic property to crack).

3.2 Reliability in the codes

The Eurocode bases its verifications on the theory of 'limit states'. A limit state is defined as "*a demarcation between desired and adverse states of the structure*" (Vrouwenvelder, 1996). Furthermore, two main types of limit states can be distinguished, namely ultimate limit states and serviceability limit states. Ultimate limit states concern the collapse of a structural system or part of it, while serviceability limit states are related to the usefulness of the structure. However, as will be discussed in the this section, fatigue is not clearly classified as either.

In the Eurocode, the differentiation in target reliability is based on the consequences of failure. For this, three classes, the so called *consequence classes*, are defined (table 3.1). These classes are linked to a minimum required reliability level, which also depends on the relevant *limit state* and its severity and reversibility. For example,

consequence class	description	examples of buildings and civil engineering works
CC3	High consequence for loss of human life, *or* economic, social or environmental consequences very great	Grandstands, public buildings where consequences of failure are high (e.g. a concert hall)
CC2	Medium consequence for loss of human life, economic, social or environmental consequences considerable	Residential and office buildings, public buildings where consequences of failure are medium (e.g. an office building)
CC1	Low consequence for loss of human life, *and* economic, social or environmental consequences small or negligible	Agricultural buildings where people do not normally enter (e.g. storage buildings), greenhouses

Table 3.1: Consequence classes as defined in EN 1990 table B1 (CEN, 2002a)

for an ultimate limit state, the β-values for a design period of 50 years[1] for CC3, CC2 and CC1 are, 4.3, 3.8 and 3.3 respectively. Furthermore, differentiation is present depending on the type of limit state, i.e. ultimate, fatigue, or serviceability. For CC2 the values are given in table 3.2. Clearly, the value for fatigue limit states is defined

limit state	target reliability index	
	1 year	50 years
ultimate	4.7	3.8
fatigue		1.5 – 3.8
serviceability (irreversible)	2.9	1.5

Table 3.2: Target values for the reliability indices β related to structural elements in RC2 (corresponds to CC2) (CEN, 2002a)

as *in between* the target values for the ultimate and the irreversible serviceability limit states.

The Probabilistic Modeling Code (PMC) uses a more elaborate approach. While the Eurocode solely uses the consequences (also damage tolerance and inspectability in case of structural steel and aluminum), the PMC also differentiates by taking into account the costs for improving the safety (table 3.3). This allows for an economically more sound decision regarding the target reliability.

relative cost of safety measure	minor consequences of failure	moderate consequences of failure	large consequences of failure
large	$\beta = 3.1$ ($P_F \approx 10^{-3}$)	$\beta = 3.3$ ($P_F \approx 5 \times 10^{-4}$)	$\beta = 3.7$ ($P_F \approx 10^{-4}$)
normal	$\beta = 3.7$ ($P_F \approx 10^{-4}$)	$\beta = 4.2$ ($P_F \approx 10^{-5}$)	$\beta = 4.4$ ($P_F \approx 5 \times 10^{-6}$)
small	$\beta = 4.2$ ($p_f \approx 10^{-5}$)	$\beta = 4.4$ ($p_f \approx 5{\times}10^{-6}$)	$\beta = 4.7$ ($p_f \approx 10^{-6}$)

Table 3.3: Tentative target reliability indices β (and associated target failure rates) related to one year reference period and ultimate limit states (Joint Committee on Structural Safety, 2000a).

The above information is mainly general, and not specific to the fatigue limit state. Regarding the latter, one has to consult the material-specific guidelines (i.e. EN1992

[1] In the context of the Eurocode, '50 years' should be read as 'design service life'.

– EN1999). Upon investigation it has become clear that the approaches followed in these parts of the code are far from harmonized. To show this, a comparison is made using the Eurocode's standard format for simplified fatigue verification:

$$\Delta\sigma_{FLM}\,\gamma_{Ff} \leq \frac{\Delta\sigma_c}{\gamma_{Mf}} \tag{3.2}$$

See section 2.1.4 for an explanation of the symbols used. The first code to be examined is NEN-EN 1992-1 (CEN, 2005a), giving rules related to concrete design. It is stated that the partial factor for fatigue loading, $\gamma_{F,fat}$ (equivalent to γ_{Ff} in eq. 3.2), shall be taken equal to 1. The partial factors for the resistance (γ_{Mf}) are given in table 3.4.

concrete	$\gamma_{c,fat} = 1.50\,;\,1.35$
reinforcing steel	$\gamma_{s,fat} = 1.15\,;\,1.15$
prestressing steel	$\gamma_{s,fat} = 1.15\,;\,1.15$

Table 3.4: Partial factor for fatigue resistance ($\gamma_{c,fat}$ and $\gamma_{s,fat}$) according to NEN-EN 1992-1 (CEN, 2005a). The former is the recommended value, while the latter is prescribed in the Dutch National Annex.

A similar approach if followed in the code for steel structures. NEN-EN 1993-1-9 (CEN, 2005c) also states that the partial factor for fatigue loads shall be taken equal to 1. There is however some differentiation in the partial factors, depending on the consequences of failure and the assessment method. Regarding the latter, the code specifies two methods:

- Damage-tolerant method: this method is to be used for details which are accessible to inspections, maintenance and repair. This approach is thus a combination of fairly low partial factors with inspections during the life time to prevent failure.
- Safe-life method: for inaccessible details a different approach should be followed. Because cracks will not be detected, the margin of safety is increased by applying larger partial factors on the fatigue strength.

Furthermore, the level of redundancy is expressed through the *consequences of failure*. Details for which the consequences of their failure remain limited to local failure only, can be said to have minor consequences. It would therefore not be economical to increase their resistance. The partial factors as adopted by the code are given in table 3.5.

assessment method	consequences of failure	
	small	large
damage-tolerant	1.00	1.15
safe-life	1.15	1.35

Table 3.5: Partial factor for fatigue resistance (γ_{Mf}) according to NEN-EN 1993-1-9 (CEN, 2005c)

Yet another approach is followed in the code for aluminum structures. Here the partial factor for the material shall be taken from the range of 1 to 1.3, depending on the consequence class, accessibility, and design method. The partial factor on the loading in this code depends on the load model itself, more specific: on the confidence limits used for the load model:

> *"The confidence limit to be used for the intensity of the design load spectrum should be based on the mean predicted value plus k_F standard deviations. The confidence limit to be used for the number of cycles in the design load spectrum should be based on the mean predicted values plus k_N standard deviations."* — CEN, 2007

It is stated that the partial factor for the loading may be taken equal to 1 if the load models from NEN-EN 1991 are applied, thus implying that these models are based on $k_F = k_N = 2$. The numerical values for the partial factor are stated in table 3.6.

k_F	γ_{Ff}	
	$k_N = 0$	$k_N = 2$
0	1.5	1.4
1	1.3	1.2
2	1.1	1.0

Table 3.6: Partial factor for fatigue loading (γ_{Ff}) according to NEN-EN 1999-1-3 (CEN, 2007)

From the aforementioned models, it is clear that there are significant discrepancies in the treatment of fatigue reliability between different parts of the Eurocode. In all mentioned standards, compatibility with the load models supplied in NEN-EN 1991 is assumed, although the reliability is treated differently. Using the same load model for fatigue loading on railway bridges, the partial factors for the load and resistance differ considerably among the referenced codes. The code for aluminum is the unique in the sense that it describes a methodology for defining a partial factor for fatigue loads that takes into account the confidence limits. Overall, it is not clear whether these methods result in the same reliability.

Another difference is elucidated by Maljaars, Luki, and Soetens (2013). Apart from noticing the discrepancies in the partial factors adopted by the Eurocode-range, it is also stated that the codes for aluminum and steel use a different approach with regard to the stress which is to be used in the verifications (principal stress vs. combined stress). It is however stated that "*in most practical cases either direct or shear stress dominates so that there is no difference between the two methods*" (Maljaars et al., 2013).

3.3 Proposed methodology

It is clear that the problem entails multiple facets and is thus not easily captured. There is no such thing definable as 'the target probability of failure for fatigue', because this probability depends on aspects which vary per case.

As a reference, the Eurocode's classification of the fatigue limit state as a range between serviceability and and ultimate limit states seems appropriate. One may argue that the consequences of failure show large variations depending on the specific component and situation. Regarding railway infrastructure, generally categorized in CC3 (see table 3.1) with a design life of 100 years, it can be concluded that the consequences of **global failure** are large and that society is willing to invest significantly in their avoidance.

The resistance at a given time can be seen as the remaining *safety margin* on the damage number (see chapter 2), i.e. the difference between the accumulated damage and the resistance. The result is an increasing probability of failure as time progresses, which increases risk. With ultimate strength limit states, given a constant distribution of loads and assuming negligible degradation, the risk is constant throughout the

service life. Because the probability of failure increases with the service life when fatigue is concerned, it is extra important to have sufficient reliability in the final years of service to comply with the lower bound associated with the involvement of human life.

It is not within the scope of this project to fully derive the optimal probability of failure for fatigue limit states. This decision should, as mentioned before, be based on an economical optimization which includes the financial means society is willing to provide for a decrease in the expectation of loss of human life and structural damages. Therefore this is also a political decision, as opposed to an engineering decision. For the sake of this research however, some target value should be chosen for comparison with the provided reliability.

For fatigue limit states, the remaining failure probability (after taking into account the redundancy) should be thought of as the combination of a probability of the load exceeding the capacity and the effect of inspections. This can also be viewed differently: the level of inspection and the detection method influences the overall reliability. In the Eurocodes on metals (excluding reinforcement steel) this effect is taken into account in the partial factor for the resistance. Higher quality of inspection and maintenance, and also the *inspectability* (the degree in which the detail is accessible), results in a lower partial safety factor, granted that inspections are possible.

Focusing on reinforced concrete, where detection of fatigue damage is deemed (next to) impossible, and consequences can be as severe as collapse similar to failure due to a single ultimate loading, the target reliability is chosen. Without the availability of further information, the target reliability index is taken from the Eurocode's prescription for ultimate limit states, which seems appropriate. For CC3 this equals $\beta_{target} = 4.3$ and the corresponding probability of failure is $P_{F;target} = 10^{-5}$. This decision is supported by CEB (1988), where it is stated that:

> "*The design of a structure under static loading has to ensure among others that during lifetime of the structure the probability of failure is smaller than a given value P_F. Concerning safety the design of a structure under fatigue loading has to be treated in the same manner, because fatigue loading can also lead to a failure of the structure, i.e. fatigue must be handled here as an ultimate limit state.*" — (CEB, 1988)

An accompanying target reliability of 4.16 was also given for situations corresponding to 'increased safety' and a design life of 100 years, which clearly is in line with the value of 4.3 as given in the current Eurocodes. Future differentiation in target reliability levels with respect to conditions of inspectability and detectability of fatigue in (reinforced) concrete may however allow lower reliabilities for some components.

3.4 Conclusions

- Regarding reliability in fatigue verification and design, the Eurocode is not harmonized throughout the different parts. Several methods are currently prescribed in a mixed sense, and it is hard to believe that these methods result in optimized reliabilities.

- The actual target reliability should be based on an economical optimization with lower bound, and is not solely an engineering decision. Because such an optimization is mainly based on assumptions combined with political debate, it was omitted in this study.

- For the fatigue limit state of reinforced concrete, the target reliability for ultimate limit states corresponding to consequence class 3 is adopted for this work, i.e. $\beta_{target} = 4.3$ ($P_{F;target} = 10^{-5}$) corresponding to the design life. Future differentiation in target reliability levels with respect to conditions of inspectability and detectability of fatigue in (reinforced) concrete may however allow lower reliabilities for some components.

4 | Load Model Calibration

The only set of trains (i.e. loads) which results in the exact damage number for each structure is the real loading sequence (represented by measurements, in this case). This implies that every other set of trains, differing from this set, results in a non-exact load effect on most structures. Therefore, load models should be calibrated to provide sufficient reliability irrespective of which design case is concerned. Using the results from calibration, load models can be adjusted in order to comply with demands. Important to note is that 'calibration' is, at least in this thesis, defined as '**comparing** what is provided to what is required', and therefore **does not include adjustments**.

4.1 Load and vehicle models

The main reason for using load or vehicle models, is that it would be far too cumbersome to require every structure to be checked using the real measured data-set, as this, in case of fatigue verification, contains quite a large number of (unique) trains, and future changes are unknown. Equivalently, verification of the ultimate strength would require checking the resistance using a large array of vehicles which may cross the structure in its design life, to see which one causes the maximum load effect, which is not very practical. As explained in section 2.1.4, the Eurocode contains two verification models for fatigue:

- The elaborate vehicle model, composed of 12 trains with frequencies of occurrence.
- The simpler λ-method, where the verification is linked to the load model for ultimate strength.

The first model can be seen as a *vehicle model*, based on the correspondence of its components to real trains. The vehicle model's trains are specified using actual axle distances, axle loads, and velocities. When comparing such an elaborate model to the simpler λ-method, the differences are clear. The latter uses LM71[1] as its load model, and therewith calculated the stresses which correspond to a fictitious 2×10^6 load repetitions during the design life ($\Delta\sigma_{FLM}$ in chapter 2).

The simplified method shows very little correspondence to the real loading (i.e. actual trains), and is therefore to be adjusted for different boundary conditions when applied (hence the name λ-*method*, where the λ's are used for adjusting). This complicates the verification, which clearly is not very transparent. Therefore, in the author's opinion, the elaborate vehicle model is to be preferred for verification. Advantages are the transparent relation between the vehicle model and the resulting *load effect*, as well as the broader field of application (because of its resemblance to the real loading, at least containing the passing of vehicles resembling real railway traffic). A general note on these approaches is:

[1] Fairly straightforward load model used for verification of other limit states than fatigue.

- The simplified method results in a convenient design calculation. The calibration of the load model, however, is very sensitive to the type of structure and its dimensions. This increases the likelihood of mistakes or use of the model outside of its limits of application.
- The elaborate method is easier to calibrate because larger parts of the calculation remain undetermined in the model, in other words: the load model is less specific. It therefore results in a more difficult and time-consuming design calculation. It does however add to the designer's insight in the fatigue behavior of the structure and is therefore to be preferred. Also, the odds of application of the model to an exception regarding the cases aimed at for calibration are more favorable.

For the remainder of this report, 'load model' will be used to denote the elaborate vehicle model for fatigue verification, which is the main subject of this thesis.

4.2 Calibration methodology

To calibrate a vehicle model for fatigue, basically a comparison is made between two sets of trains. The central question is, however, in which way this is possible. First an overview of the available information[2] is given in table 4.1.

Eurocode vehicle model	measured trains
• deterministic in nature • consists of: 1. axle loads 2. axle distances 3. velocities 4. frequencies	• probabilistic in nature, i.e. *uncertain* • consists of: 1. axle loads 2. axle distances 3. velocities

Table 4.1: Available data for the calibration.

From this is may be concluded that comparing the Eurocode model to measured trains is not a straightforward task. One cannot simply draw conclusions based on the differences in magnitude of axle loads, or the system of axle distances, because it is not clear what their influence on the load effect is: the damage number in case of fatigue. In other words: there is no clear criterion of sets of trains to use for comparison. Furthermore, the uncertainties in the measurements are to be included in the calibration.

In comparing the load model and the measured trains, it was chosen to compare based on damage numbers, which is also the focus of the Eurocode's verification method. In case of e.g. ultimate strength limit state checks, the load effect scales linearly with respect to the magnitude of the load(s). When calculating the resulting damage number from passing trains however, this is far from linear due to the number of non-linear steps which form the transformation from a set of trains to the resulting damage number, among which the S-N curves. Distinguishable steps in the transition from loading history to a damage number are (already stated in section 2.1.4.2, although less detailed and in a different context):

1. Calculate the generalized forces from the passing of traffic. This results in a *signal* for the generalized force (or: effect) under consideration, as a function

[2] Here the Eurocode vehicle model corresponds to the 'elaborate method'.

of pseudo-time. This is done using influence lines, see appendix E, where it is demonstrated in which way the influence line affects the result. It is therefore important to include in the calibration procedure. Also, in this step the axle loads are converted to dynamic loads by multiplication with the dynamic factor which was treated in section 2.1.4.3.

2. The generalized forces need to be translated to stresses in the cross-section of interest, i.e. for which the limit state function is set up. This procedure results in the stress-signal.

3. The stress-signal is reduced to its extrema, because for the fatigue analysis only the minima and maxima are of importance. The result is a set of turning points of the stress-signal.

4. The cycles are counted using an appropriate algorithm (in this thesis: rainflow counting, see appendix E). In doing so, time and thus frequency information is lost. In the Eurocode verification it is assumed that this information does not influence the damage number. By counting the cycles, a table of cycle amplitudes, means, and counts is obtained.

5. For each cycle the damage number increment is calculated. For this the S-N relation is used, yielding the number of permissible cycles at a certain stress level. According to Miner's rule, the damage increment caused by this cycle is equal to the fraction of applied cycles over permissible cycles.

6. Finally, the damage number is obtained by summing up all damage increments.

From the above it may be clear that the damage number, resulting from a loading history, is linked to the loading by significant nonlinearity with respect to characteristics of the input. Therefore it is very difficult to predict the influence of changes in the loading's characteristics on the resulting damage number. It is noted that the λ-method gives even less insight, because the connection to actual repetitive loading is completely lost when designing a structure to resist fatigue loading.

4.3 Fictitious cross-section

In section 4.2, the steps taken to determine the damage number from a set of trains passing over a structure were briefly stated. In step 2, the signal of generalized forces was used to determine the signal for stress-fluctuations using a cross-section. In this thesis, the assumption of linear elasticity is used to justify replacement of the aforementioned step by a linear transformation. For this, the entire signal of the generalized force is multiplied by some factor, from now on denoted with 'u', representing some fictitious cross-section, to obtain the stress-signal.

To perform a generally applicable calibration, it is best to limit the dependence of the calibration on characteristics of a structure to a minimum. Now, in case of a linear proportionality between generalized forces and stresses, u thus not being a function of the cycle's mean or amplitude, it is not required to have information regarding the cross-section which is checked. If u is taken as non-constant, however, cross-sectional knowledge is a prerequisite. This is caused by the fact that u would then be a non-linear characteristic, which is defined by the cross-sectional properties. The assumption of linear proportionality is further explored in this section.

For bending moments in steel structures this linearity is fairly straightforward (in the linear elastic range, i.e. when yielding of the steel does not occur). The stress, due to a bending moment on the section, is obtained from

$$\sigma_s = \frac{M}{W} \tag{4.1}$$

where

σ_s = stress in steel
M = applied bending moment
W = section modulus (elastic)

Therefrom it is clear that the stress is proportional to the applied bending moment on the section, as the section's modulus is generally assumed constant. For concrete sections this is also approximately true, under a few assumptions. First of all, as seen in the section 2.1.3.2, the S-N curves for concrete all result in a capacity of $\sigma_{c,max} = 0.9\, f_{cd}$ at one cycle. Therefore, each cycle which causes stresses above this level, leads to failure by definition. This in turn allows the conclusion that the domain of interest with regard to the concrete compressive stresses is limited to $[0 \;\; 0.9\, f_{cd}]$.

The bending moments in the elastic domain can be withstood by the section according to the strain distribution in figure 4.1. Note that the domain for σ_c is elastic, so the

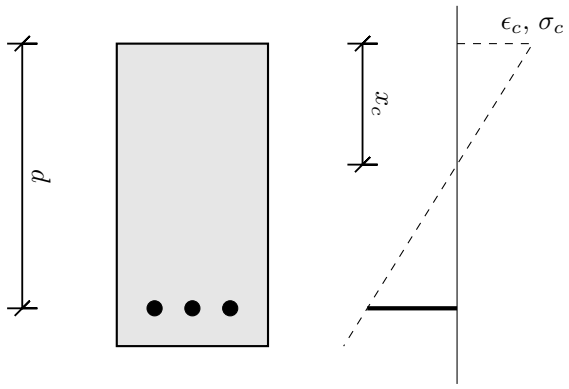

Figure 4.1: Elastic concrete strain distribution

design strength will not be reached in the compression zone. The forces acting in the cross-section can be expressed as:

$$N_c = \frac{1}{2}\, x_c\, \sigma_c\, b \tag{4.2}$$

$$N_s = \frac{(d - x_c)}{x_c}\, \epsilon_c\, E_s\, A_s = \frac{(d - x_c)\, \sigma_c\, E_s\, A_s}{x_c\, E_c} \tag{4.3}$$

where

N_c = force in concrete (compression)
N_s = force in reinforcement (tension)
x_c = concrete compressive zone height
σ_c = stress in concrete
b = section width
d = effective section depth
ϵ_c = concrete strain
A_s = reinforcement area
E_s = modulus of elasticity, steel
E_c = modulus of elasticity, concrete

From the condition of horizontal force-equilibrium in the section, the height of the compression zone can be determined:

$$N_c = N_s \tag{4.4}$$

$$x_c = \frac{E_s\, A_s}{E_c\, b} \left(\sqrt{1 + \frac{2\, b\, d\, E_c}{E_s\, A_s}} - 1 \right) \tag{4.5}$$

from which it is clear that the height of the compression zone is independent of the stress in the concrete. From this it is concluded that the compression zone height is constant, under the assumption that the steel does not yield before the concrete reaches 90 % of its compression strength. This raises the question whether this assumption is reasonable.

Generally, the reinforcement will yield before the concrete reaches its ultimate strength (which nullifies the above assumption). Only for very high reinforcement ratio's this is not the case , which are purposely avoided by a maximum reinforcement ratio based on ductility. Because the force in the reinforcement reaches its definite maximum when yielding occurs (assuming bi-linear behavior without strain-hardening), the only way for the moment capacity to increase further is by an increase of the internal lever arm. This increase can be achieved, by decreasing the height of the compression zone until the maximum concrete strength is reached. This would then result in the maximum moment capacity.

Before the point of yielding, the capacity increases by increasing the internal forces. Beyond yielding, the only mechanism available for this is increasing of the internal lever arm, resulting in a smaller increase of the moment capacity relative to an increase in concrete compressive stresses (sudden change in slope in figure 4.2).

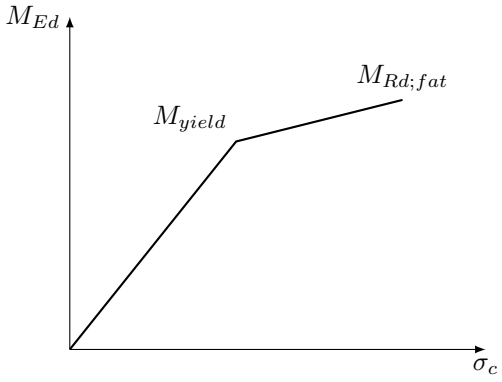

Figure 4.2: Bi-linear characteristic relation between the bending moment and the corresponding compression in the concrete.

If the reinforcement ratio is large enough, the maximum moment in figure 4.2 occurs prior to yielding of the reinforcement. The characteristic is then straight to $M_{Rd;fat}$ in the figure, implying a perfectly linear (or elastic) relation. Unloading would follow the same characteristic, when elasticity is assumed. This is not the case for the bi-linear characteristic. If the applied moment is larger than the capacity at which yielding occurs, the reinforcement will deform permanently, resulting in plastic strain. Unloading will then, more or less, follow a straight characteristic. This behavior is portrayed in figure 4.3, and is known as *hysteresis*. This means that the previous states (history) influence subsequent states and behavior.

New loadings then follow the path of unloading, and form a new path only if they surpass the preceding maximum bending moment. From this it can be concluded

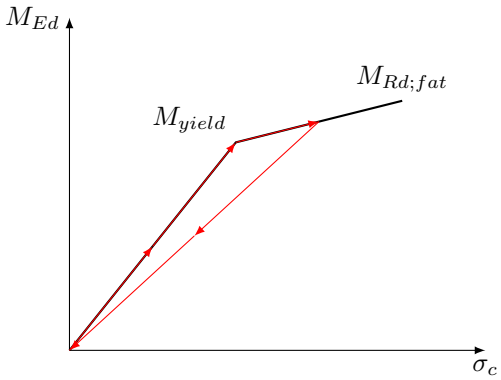

Figure 4.3: Unloading after surpassing the moment at which yielding of the reinforcement occurs.

that the characteristic relation will be linear up until the maximum moment which has occurred to the current time. Assuming a linear relation over the entire domain can therefore also be explained as assuming that the largest load occurs first, setting the behavior for the rest of the loads to linear.

According to the Eurocode, fatigue verifications should be based on cracked concrete and linear elastic material behavior. Therefore, reaching plasticity in details which are prone to fatigue is not within the limits of the code. Also, yielding of the reinforcement would lead to direct failure based on the S-N curves for reinforcement. As this calibration is based on the rules in the Eurocode, this assumption will be followed. Please note that in calibrations performed prior to this work, this linear assumption has also been used (without the authors going into further detail regarding its justification). See for instance Zilch and Bagayoko (1997). The main advantage is, as the bi-linear characteristic is a function of the reinforcement ratio, this ratio should then be included as a calibration variable. This would lead to a larger variety of cases. Also the incorporation of the hysteresis in the calibration would add significant complication without addition of a large benefit.

But, there is more. As explained in Zilch and Bagayoko (1997), the characteristic is nonlinear for sections where normal forces are applied (e.g. prestressing). It is then slightly curved. In the aforementioned work, this effect is neglected, and the characteristic is assumed as perfectly linear, because differences are said to be small (Zilch & Bagayoko, 1997). This strategy will therefore also be adopted here.

4.3.1 Permanent stresses

Permanent stresses are important for the damage when fatigue damage in concrete is calculated. This is due to the fact that the S-N curves depend on the stress ratio R, which cannot be separated from the presence of permanent stresses. These should therefore be incorporated in the calibration as a variable, because their influence on the results cannot be neglected. For this purpose a stress ratio is introduced, in which the permanent stress (due to permanent actions, including but not limited to prestressing) are expressed relatively to the concrete's design resistance in compression:

$$\zeta_{\text{perm}} = \frac{\sigma_{c,\text{perm}}}{f_{cd,fat}} \tag{4.6}$$

where

ζ_{perm} = permanent concrete stress as fraction of design strength
$\sigma_{c,\text{perm}}$ = permanent concrete stress

Using the permanent stress, the minimum and maximum stress ratios (relative to the design fatigue strength) can be written as:

$$E_{cd,min,i} = \frac{u_c\,\sigma_{c,min,i} + \sigma_{c,\text{perm}}}{f_{cd,fat}} = \frac{u_c\,\sigma_{c,min,i}}{f_{cd,fat}} + \zeta_{\text{perm}} \geq 0 \tag{4.7}$$

$$E_{cd,max,i} = \frac{u_c\,\sigma_{c,max,i} + \sigma_{c,\text{perm}}}{f_{cd,fat}} = \frac{u_c\,\sigma_{c,max,i}}{f_{cd,fat}} + \zeta_{\text{perm}} \geq 0 \tag{4.8}$$

With this, the stress ratio becomes

$$R_i = \frac{E_{cd,min;i}}{E_{cd,max;i}} = \frac{\dfrac{u_c\,\sigma_{c,min,i}}{f_{cd,fat}} + \zeta_{perm}}{\dfrac{u_c\,\sigma_{c,max,i}}{f_{cd,fat}} + \zeta_{perm}} \geq 0 \tag{4.9}$$

where it is very convenient that only the concrete design compressive strength, which was already a variable for the calibration because of its influence on the S-N curves, remains in the stress ratio. With inclusion of the above, the stress amplitude in the steel and in the concrete can be obtained from (Zilch & Bagayoko, 1997):

$$\Delta\sigma_s = u_s\,\Delta M \tag{4.10}$$

$$\sigma_c \approx u_c\,M + \zeta_{\text{perm}}\,f_{cd,fat} \geq 0 \tag{4.11}$$

where

u_s = proportionality between bending moments on a section and resulting stresses, steel
u_c = proportionality between bending moments on a section and resulting stresses, concrete

The above relations are used exclusively, because the focus is on fatigue effects caused by bending moments in the remainder of this report.

4.4 Enforcing the limit state

When comparing load models, it is of critical importance to do this upon attainment of the limit state. This is a direct consequence of the non-linearity of the S-N relations. Starting from a set of stress cycles (a spectrum), damage increments are calculated for every cycle, and their magnitude is derived from these S-N relations. Now, consider that the entire spectrum of cycles is scaled in magnitude by some arbitrary scaling factor. This will result in a change in damage (see also chapter D). The change in resulting damage numbers will not be linearly proportional to the scaling factor, as is to be expected for a non-linear stress-to-damage relation. Rather, the scaling in damage depends on the shape of the spectrum. With the 'shape' of the spectrum, reference is made to a histogram of stress cycle magnitudes.

Interestingly, this suggests that two spectra with different shapes will compare differently in terms of damage for a varying scaling factor, even when an equal scaling factor is applied to both. This is demonstrated in figure 4.4, where two example spectra are displayed (upper and lower graph). Consider that u, which is included in the spectra already (because they are stresses), is multiplied by an alteration factor η_u. Both spectra will shift upward over distance $\log \eta_u$, as displayed in the figure.

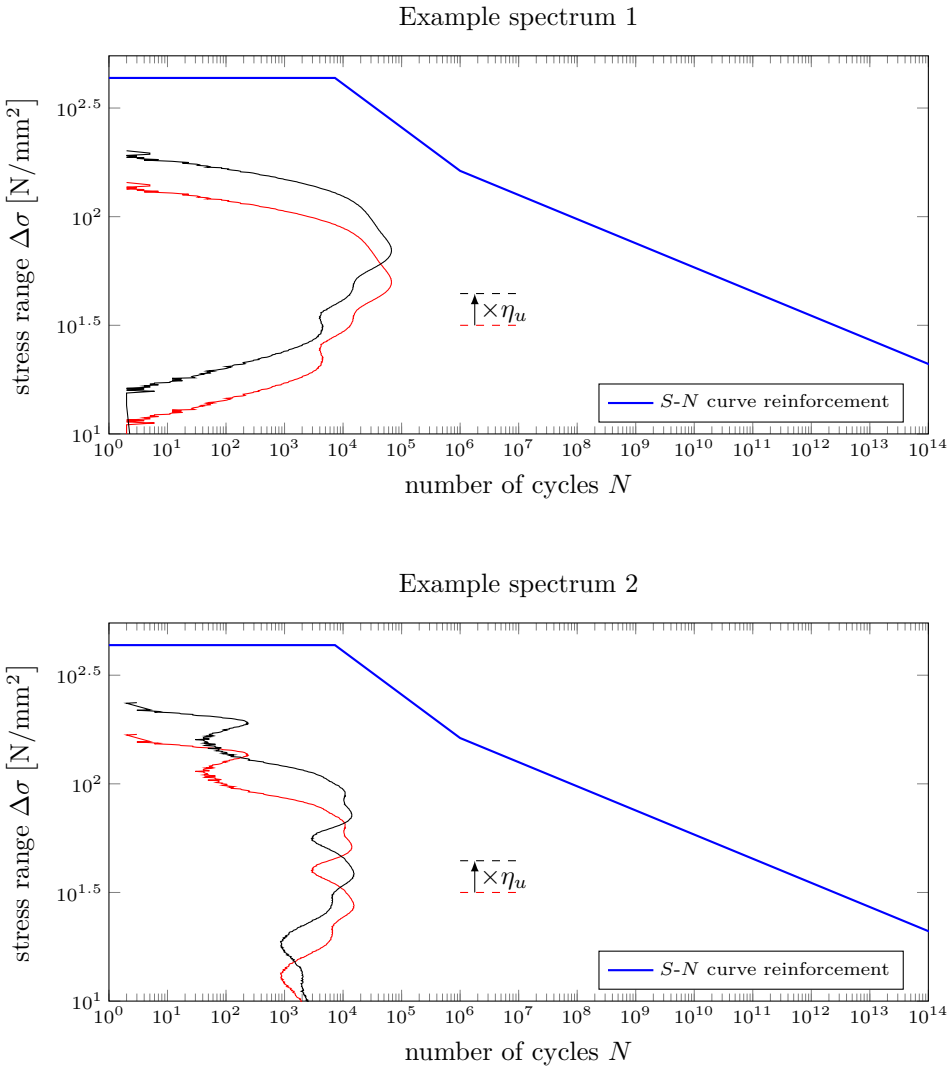

Figure 4.4: Effect of altering u: consider in which way the cumulative damage will change.

Now, due to the non-linear S-N curve, the resulting shift in damage will not be proportional to η_u. In case of a S-N curve as in figure 4.4, the non-constant fatigue exponent (slope) causes significant differences in terms of changes in damage numbers, when comparing two different spectra.

Because calibration basically consists of a comparison, it is required to determine the (uniquely defined) scaling factor at which the calibration is to be performed. The value of this scaling factor follows from reversal of the Eurocode's verification procedure. If one were to design a structure to resist fatigue loading, then the maximum allowable damage number would be equal to unity, corresponding to a unity check for the fatigue limit state of 1. Because of this design criterion, it follows that the unique scaling factor for both spectra, required for calibration, is obtained from attainment of the limit state by appliance of the Eurocode vehicle model (one of the mixes). A higher scaling factor would imply an *unsafe* structure, and a lower scaling factor a *safe* structure (following the limit state methodology). This value for u therefore corresponds to a critical section, thus being capable of exactly withstanding the loads.

This concept can be generalized by defining one of the spectra as a *reference* or *design spectrum*. This reference spectrum defines the boundary condition required for the calibration. This will be used extensively in formulating the different possibilities for calibration in the remainder of this chapter.

4.5 Types of calibration

Using the concepts presented so far, three different calibration types can be distinguished. Strictly speaking, two of these implicitly include adjustment after calibration. Each of methods is discussed, after which an overview is presented.

4.5.1 Deterministic calibration

The deterministic calibration procedure is an extended adaptation of the procedure presented by Zilch and Bagayoko (1997). In this work the calibration of the Eurocode λ-method for different structural types is explained. The general idea will be explained, instead of elucidating all details. For this, it was chosen to introduce some *operators*. These operators are printed in a different $\mathcal{F}$ont.

The general idea is to take two traffic mixes, one of which is a load model. For both, the damage number is determined, therefore calibrating on this basis. From this, it is straightforward to adjust either the measured traffic or the load model in order for both traffic mixes to match in damage number. To stay in line with the aforementioned work, it is chosen to use the set of measured trains as reference, thereby defining the load model as non-reference.

The first step is to determine a signal for the effect of interest. This is done by simulating the passing of measured trains over a certain structure, which is fully represented by its influence line, see appendix E. This step will be symbolized using the *influence*-operator, $\mathcal{I}(\bullet)$. It also encompasses the distillation of *turning points* from the signal, i.e. the extrema which are the input for the rainflow-counting algorithm. Given the measured loading history, denoted by $\mathbf{H}$, the signal for the effect of interest ($\mathbf{e}_t$) is obtained via the influence operator:

$$\mathbf{e}_t = \mathcal{I}(\mathbf{H}) \tag{4.12}$$

The signal of the fluctuating stress is determined using the linear transformation which was explained in section 4.3 (for concrete in compression, also tension peaks are set to zero, according to the assumption of cracked concrete):

$$\boldsymbol{\sigma}_t = u\,\mathbf{e}_t = u\,\mathcal{I}(\mathbf{H}) \tag{4.13}$$

Subsequently, the stress-signal is passed to the *rainflow*-operator ($\mathcal{R}(\bullet)$) which extracts the half-cycles (see appendix E):

$$\mathbf{R} = \mathcal{R}\left(\boldsymbol{\sigma}_t\right) = \mathcal{R}\left(u\,\mathcal{I}\left(\mathbf{H}\right)\right) \tag{4.14}$$

Here the time-dependence is lost, and the result is a rainflow-matrix or spectrum which consists of, for each cycle, its mean, amplitude, and count. From this the *damage-number*-operator $\sum \mathcal{D}(\bullet)$ is employed to determine the damage number using the relevant S-N relations.

$$D = \sum \mathcal{D}\left(\mathbf{R}\right) = \sum \mathcal{D}\left(\mathcal{R}\left(u\,\mathcal{I}\left(\mathbf{H}\right)\right)\right) \tag{4.15}$$

To obtain the value for u corresponding to the limit state of interest, the damage number should be equal to 1, as discussed earlier in this chapter. Effectively, the task of finding this value u, which is denoted as u_{limit}, can be solved by an optimization-algorithm[3]. To this extent the problem is formulated as:

$$\text{minimize} \left\{ \left| 1 - \sum \mathcal{D}\left(\mathcal{R}\left(u\,\mathcal{I}\left(\mathbf{H}\right)\right)\right) \right| \right\} \text{ for } u \;\rightarrow\; u_{\text{limit}} = u \tag{4.16}$$

Note that the calibration is done by assuming that the history which is used as input, is a history of measured train data (the load model could also be used as reference traffic mix). The symbol $\mathbf{M}$ will be used to denote the load model (traffic mix). Using the previously obtained u_{limit}, the damage from the load model is determined. Calibration (with implicit adjustment) is then performed by equating the results in terms of damage for the same fictitious cross-section (which is contained in u_{limit}):

$$\lambda_{\text{calibration}} = \frac{\sum \mathcal{D}\left(\mathcal{R}\left(u_{\text{limit}}\,\mathcal{I}\left(\mathbf{H}\right)\right)\right)}{\sum \mathcal{D}\left(\mathcal{R}\left(u_{\text{limit}}\,\mathcal{I}\left(\mathbf{M}\right)\right)\right)} = \frac{1}{\sum \mathcal{D}\left(\mathcal{R}\left(u_{\text{limit}}\,\mathcal{I}\left(\mathbf{M}\right)\right)\right)} \tag{4.17}$$

In this way, the calibration factor $\lambda_{\text{calibration}}$ is formulated in the domain of the damage number, and can be applied as a magnification factor for the load model train frequencies because of the damage number's linear proportionality to the number of load cycles (see chapter D). Another possibility is to formulate a calibration factor in the stress-domain. This is done by obtaining the values for u_{limit} for both $\mathbf{H}$ and $\mathbf{M}$. Effectively this is achieved by solving equation 4.16 subsequently using $\mathbf{H}$ and $\mathbf{M}$. The quotient of these limit values (which both represent a proportionality of stresses) yields the calibration factor in the stress-domain.

4.5.2 Probabilistic calibration

With 'probabilistic calibration', it is meant that the load model and the measured traffic are compared using a probabilistic criterion, in this case: the probability of failure (equivalently: reliability index). Such a probability of failure should be interpreted as the probability that a component fails in fatigue, given that it has been designed to withstand the load model, and it is being loaded by the measured trains.

For the formation of a probabilistic calibration procedure, some changes to the deterministic procedure are required. By definition a probabilistic analysis includes variations in, or uncertainties of, its components and variables. For the procedure, the main interest is on the uncertainties in the measured loading, the determination of damage numbers, and the material's resistance. Also, because the measurements span a limited time frame, extrapolation to the design life is required (see appendix G). This also introduces uncertainties. Below, two procedures with different goals and results will be explained.

[3] The value of u for which the damage equals 1 is uniquely defined for S-N curves where the allowable stress decreases for increasing N, which is the case for all known relations. Problems may arise with 'jumps' as in the S-N curves for concrete in compression, and also for horizontal branches such as with the reinforcement yield stress or the fatigue limit for structural steel.

4.5.2.1 Measured loads as reference

Consider the following scenario: one has a measured traffic history and a load model, but the latter needs adjustment to provide the desired level of safety. Then the first step would be to calibrate (i.e. analyze the current failure probability which results), after which the load model can be adjusted to provide the desired level. The process to do so, is formulated in terms of an implementation using Monte Carlo simulation (see appendix A). Alternatively, it could be formulated using other techniques as well, however this formulation allows for better visualization and thus insight.

The set of measurements $\mathbf{H}$, representing the true loading, can vary depending on, for example, the period which was measured. Therefore, it is clear that a different formulation is needed which incorporates this aspect. For this, first the set $\mathbf{H}$ is thought to consists of multiple possibilities denoted by $\mathbf{H}_1, \mathbf{H}_2, \ldots, \mathbf{H}_n$, which could represent the expected loading in reality. These could for example be the results of extrapolation of a shorter set to the design life.

Because of the non-linear operations in the verification procedure, it is required to work with these histories through the same process as in the deterministic case. Cause for this, is that the outcome in terms of damage number can not be predicted based on alterations (caused by variations or uncertainties) of input. First, for each history the influence-operator yields the stress-signals:

$$\mathbf{E} = \begin{bmatrix} \mathbf{e}_{t,1} \\ \mathbf{e}_{t,2} \\ \vdots \\ \mathbf{e}_{t,n} \end{bmatrix} = \begin{bmatrix} \mathcal{I}(\mathbf{H}_1) \\ \mathcal{I}(\mathbf{H}_2) \\ \vdots \\ \mathcal{I}(\mathbf{H}_n) \end{bmatrix} \tag{4.18}$$

where different rows represent Monte Carlo iterations (n iterations in total). Transformation to stresses is done using **one single value for u for all loading histories**[4], because this formulation focuses on a single cross-section, which is loaded, with a certain probability, by each history. From this, the damage numbers are calculated via the rainflow-counting algorithm and subsequent summation of damage fractions:

$$\mathbf{D} = \begin{bmatrix} D_1 \\ D_2 \\ \vdots \\ D_n \end{bmatrix} = \sum \mathcal{D}(\mathcal{R}(\mathbf{E})) = \begin{bmatrix} \sum \mathcal{D}(\mathcal{R}(u\mathcal{I}(\mathbf{H}_1))) \\ \sum \mathcal{D}(\mathcal{R}(u\mathcal{I}(\mathbf{H}_2))) \\ \vdots \\ \sum \mathcal{D}(\mathcal{R}(u\mathcal{I}(\mathbf{H}_n))) \end{bmatrix} \tag{4.19}$$

The damage number is determined through the use of a probabilistic resistance model which allows for variations in the S-N curve (will be discussed in chapter 5). In the deterministic case, it was sufficient to enforce the condition that the damage should be equal to one. For the probabilistic case this is more complicated, as it should now include a certain probability of failure. First, an assumption is required for the allowable damage number of the (unknown) section. This quantity will be symbolized by Δ. The limit state function, and an array of its realizations (i.e. outcomes), can then be written as:

$$\mathbf{z} = \boldsymbol{\Delta} - \mathbf{D} = \begin{bmatrix} \Delta_1 - \sum \mathcal{D}(\mathcal{R}(u\mathcal{I}(\mathbf{H}_1))) \\ \Delta_2 - \sum \mathcal{D}(\mathcal{R}(u\mathcal{I}(\mathbf{H}_2))) \\ \vdots \\ \Delta_n - \sum \mathcal{D}(\mathcal{R}(u\mathcal{I}(\mathbf{H}_n))) \end{bmatrix} \tag{4.20}$$

[4] Uncertainties in the cross sectional properties wuld lead to a unique value for u drawn from a common probability distribution.

For each iteration in equation 4.20 it is determined whether the structure fails or survives using:

$z_i \leq 0$ failure

$z_i > 0$ survival

Here, $\mathbf{z}$ represents the vector of safety margins. The goal is to obtain a value for u using which the failure probability resulting from equation 4.20 equals the target value, $P_{F;\text{target}}$. This is done through iteration for u, solving the following optimization-problem:

$$\text{minimize } \{|P_F - P_{F;\text{target}}|\} \text{ for } u \rightarrow u_{\text{limit}} = u \tag{4.21}$$

where P_F is approximated using equation 4.20 and the conditions for z_i (ratio of failures over total number of iterations, see appendix A).

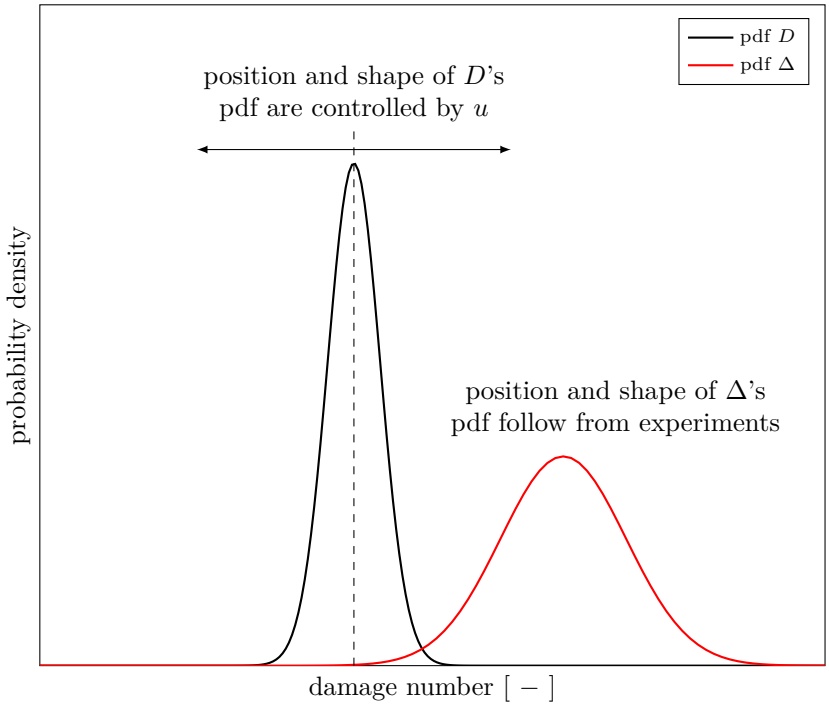

Figure 4.5: Visualization of the probabilistic calibration and optimization, used to obtain u_{limit}.

Important is to understand that u determines the magnitude of stress ranges, and that this magnitude influences the damage number in a nonlinear manner. Therefore, the position and shape of **D**'s pdf, displayed in terms of the damage number, are a direct consequence of u. Hence, the impact of uncertainties in the measured loading also depends on u.

Obtaining u_{limit} from this process is a very significant step to solving the problem at hand. This is where the target value for the probability of failure is included to steer the results. To find the calibration-factor (for adjustment), the damage number resulting from application of the **load model** should be set equal to unity (or any design criterion one might prefer):

$$\lambda_{\text{calibration}} = \frac{1}{\sum \mathcal{D}\left(\mathcal{R}\left(u_{\text{limit}}\, \mathcal{I}\left(\mathbf{M}\right)\right)\right)} \tag{4.22}$$

where u_{limit} ensures that the target failure probability is met using measured traffic. This may not be directly clear, therefore consider the following statement:

> "If we design the structure to result in a damage number of 1 using the load model, then this is equivalent to the real loading producing a distribution of damage numbers which corresponds to a failure probability equal to the target value."

The *equivalence* in the statement above is enforced by using the same value for u_{limit}.

4.5.2.2 Load model as reference

Using the presented procedures it is also possible to determine the reliability which is provided by the current fatigue loading model, i.e. exactly what is pursued in this thesis. Start from the assumption that a section is designed exactly to withstand the load effect caused by the load model (thus being a design based on the Eurocode, with unity check equal to 1 for the fatigue limit state, or, equivalently, a damage number of 1). This assumption is an essential step in load model calibration, because limit states in the Eurocode contain a safety margin, introduced by partial factors (details are discussed in chapter 5).

The condition of exact attainment of the limit state is enforced by determining u_{limit} for a section which is loaded by the Eurocode load model, where the safety format using partial factors is included in this determination. Basically, u_{limit} is obtained using the procedure for deterministic calibration, only now by applying the load model with safety margin:

$$\text{minimize} \left\{ \left| 1 - \sum \mathcal{D}\left(\mathcal{R}\left(u\,\mathcal{I}\left(\mathbf{M}\right)\right)\right) \right| \right\} \text{ for } u \;\rightarrow\; u_{\text{limit}} = u \tag{4.23}$$

Using the resulting value for u, again denoted as u_{limit}, the damage done by the set of possible loading histories $\mathbf{H} = \mathbf{H}_1, \mathbf{H}_2, \ldots, \mathbf{H}_n$ is used to determine the actual failure probability given the measured loading. For this, the limit state function is formulated as follows (in terms of Monte Carlo iterations):

$$\mathbf{z} = \mathbf{\Delta} - \mathbf{D} = \begin{bmatrix} \Delta_1 - \sum \mathcal{D}\left(\mathcal{R}\left(u_{\text{limit}}\,\mathcal{I}\left(\mathbf{H}_1\right)\right)\right) \\ \Delta_2 - \sum \mathcal{D}\left(\mathcal{R}\left(u_{\text{limit}}\,\mathcal{I}\left(\mathbf{H}_2\right)\right)\right) \\ \vdots \\ \Delta_n - \sum \mathcal{D}\left(\mathcal{R}\left(u_{\text{limit}}\,\mathcal{I}\left(\mathbf{H}_n\right)\right)\right) \end{bmatrix} \tag{4.24}$$

$z_i \leq 0$ failure
$z_i > 0$ survival

Notice that in equation 4.24, the obtained value for u_{limit} is put in directly and remains fixed. Therefore, no iterative solving of the limit state function is required. Equation 4.24 finally results in the probability of failure, and thus the reliability, provided by the Eurocode's current load model and safety format. The section is designed to withstand the Eurocode load model, with exact attainment of the deterministic limit state (unity check), and it is loaded by measured traffic.

4.5.3 Overview

An overview of calibration methods is presented in table 4.2. Note that a 'boundary condition' should of course be interpreted as fixed. In the remainder of this report, only the third method will be applied. Therefore, 'calibration' should from here on be interpreted as 'calibration using the third method', resulting in a failure probability which can be compared (calibrated) to a desired or reference value. The load models will thus not be adjusted.

#	method	boundary condition(s)	result (output)
1	deterministic	either the load model or the measured traffic as reference traffic	adjustment factor for non-reference traffic to result in an equal damage number
2	probabilistic	measured loads and target failure probability	adjustment factor for the load model to meet the desired failure probability given measured traffic
3	probabilistic	measured loads and load model	failure probability given a design based on the load model, loaded by measured traffic

Table 4.2: Different types of calibration.

4.6 Conclusions

- It is necessary to calibrate fatigue load models, because in transforming from measured loading to load models, information is lost. Therefore the load model should be adjusted to comply with measured traffic.
- It has been shown that the fluctuations in generalized forces can be translated into fluctuations in stresses, using a linear relationship.
- The variations in the measured loading have to be incorporated into the calibration procedure, alongside other sources of uncertainties and variations. Basically, this is used to determine (or alternatively, to set) the reliability corresponding to the unity check, as per the Eurocode's format.
- The procedure for both deterministic and probabilistic calibration has been formulated and explained. This is done by simulating the fatigue limit state, and using this limit state situation to compare the damage numbers resulting from different load models.

5 | Probabilistic Analysis

Probabilistic analyses are done to take into account uncertainties and variation, or, in other words: to take into account the things we do not know in a quantitative way. This allows for making designs subject to uncertainties in an objective manner. In this chapter, the format of the probabilistic analyses used in this thesis is first laid out, followed by a quantification of uncertainties in the various components of this analysis' format. Also, deterministic variables which are of interest are discussed. The theoretical background of probabilistic analysis is briefly described in appendix A.

5.1 Methodology for comparison

Verifications in the Eurocode are based on *design*-values for loads and resistance. Considering the uncertainties in both the loads and resistance, these design-values are obtained by including a margin of safety. In the Eurocode it was chosen to include this margin trough the use of partial factors, which quantify the uncertainty and the importance, of both loads and resistances in the verification. This is known as a semi-probabilistic approach, or level I probabilistic calculation (see also appendix A).

For the full probabilistic analysis, it is important to know the safety margin which is provided by appliance of the Eurocode's partial factors. Basically, these are directly responsible for the provided safety, and thus failure probability. In the Eurocode, two partial factors are generally included for each verification, which are set-up as follows (CEN, 2002a):

- partial factor for load effects (γ_F):
  - uncertainties in the representative values of load effects;
  - uncertainties in the modeling of loads and load effects;
- partial factor for resistance (γ_M):
  - uncertainties introduced in modeling the structural resistance;
  - uncertainties in material properties.

This grouping of partial factors is done to simplify analysis (by limiting the number of partial factors that have to be applied). In figure 5.1, the Eurocode verification procedure for fatigue (left column) is compared to a full probabilistic analysis (right column). As described in chapter 4, a design which exactly satisfies the limit state is simulated, without knowing the actual cross-section, through the use of a proportionality between generalized forces and stress (denoted with u). The limit-value for u, u_{limit}, is determined by equalizing the design strength and resistance (unity check for the fatigue limit state equal to 1). In the context of the Eurocode, this means that, using the design values for loads and resistance, a damage number of 1 is found.

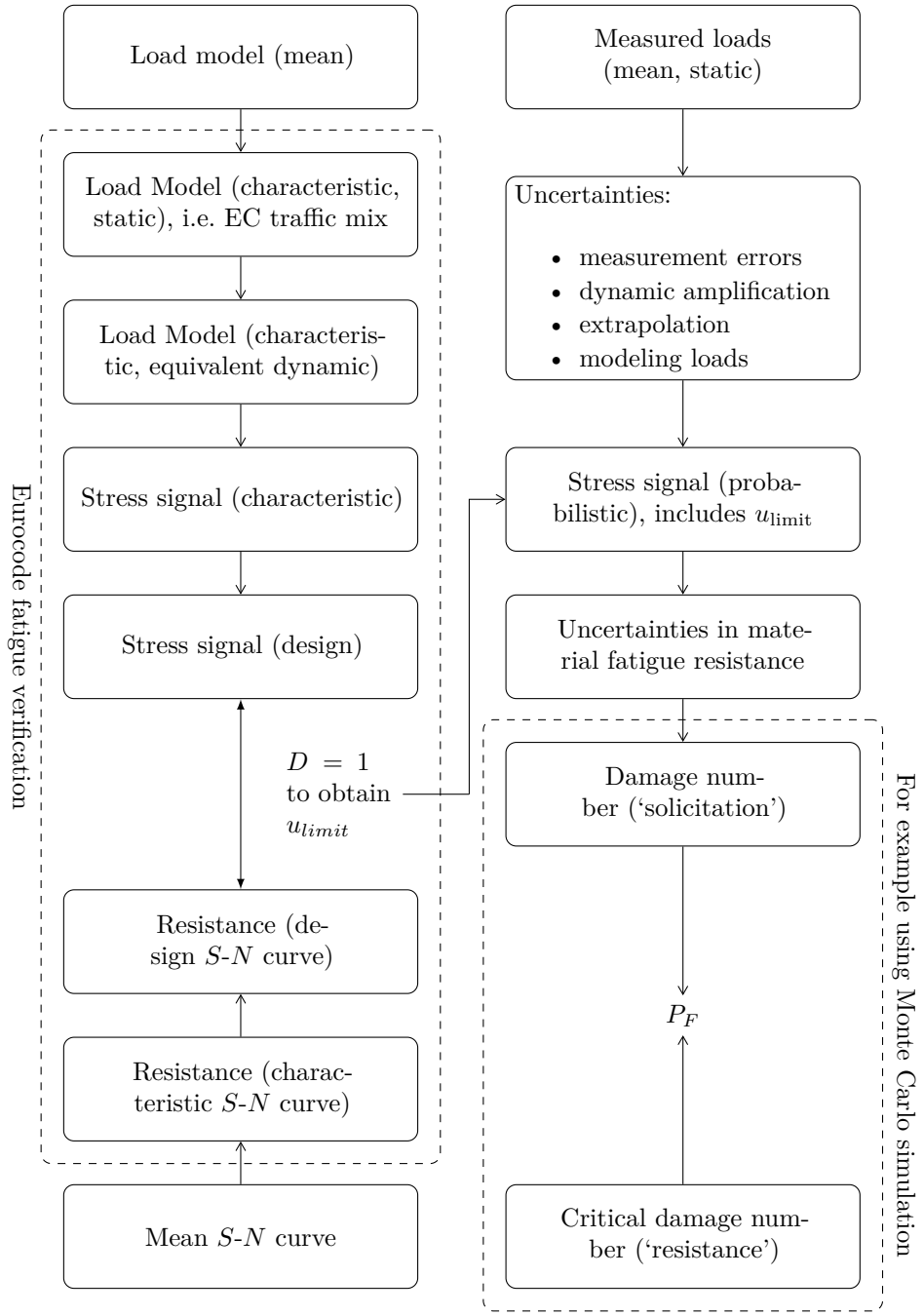

Figure 5.1: Process of fatigue verification, semi-probabilistic vs. fully probabilistic.

5.2 Probabilistic calibration variables

For the level III analysis, it is required to obtain knowledge regarding the variations and uncertainties which are present in the fatigue limit state and its verification. The items of interest have been included in figure 5.1. Each of these items will be discussed in this chapter, of which an overview is given in table 5.1. Note that, from here on, the investigation of reliability focuses on reinforced concrete, as opposed to structural steel.

uncertainties regarding:	addressed in:
measurement errors	section 5.2.1
dynamic amplification	section 5.2.2
extrapolation	section 5.2.3 and appendix G
dimensional uncertainties	section 5.2.4
load effect modeling	section 5.2.5
fatigue resistance (concrete)	section 5.2.6
fatigue resistance (reinforcement)	section 5.2.7
critical damage number	section 5.2.8

Table 5.1: Overview of uncertainties and variations which were used in this thesis.

5.2.1 Measurement errors

As measurements will never be fully accurate, it is generally required to take uncertainties into account. For the Quo Vadis weigh-in-motion system, target values were set with regards to the accuracy. For the quantities of interest for this work, namely axle loads and velocities, the target values were provided by Ricardo Rail. It was noted that the system is more accurate than these targets in reality, however, in the absence of further information, these values will be used.

5.2.1.1 Axle load

It is prescribed that measurements should be normally distributed around the mean value at the level of an entire train. For axle loads, the following is requested:

> "*The measurement on the level of the axle must, within the speed interval* 30 *to at least* 150 km/h *and independent of type or composition,* 95 % *of the weight measurements be presented with an accuracy better than* ±12 %."

For individual axles, the normal distribution will be adopted as well. The parameters are determined using the standard normal quantiles (in this case, $|q_{2.5\%}| = 1.96$):

$$\mu_{\hat{F}} = 1, \sigma_{\hat{F}} = c_{v,\hat{F}} = \frac{0.12}{1.96} = 0.0612 \tag{5.1}$$

where $\hat{F}$ is used as a multiplication factor for measured axle loads. It is assumed that measurement errors are fully independent.

5.2.1.2 Velocity

The target accuracy for measured velocities was also supplied:

> "*The train speed shall be measured with an accuracy better than* ±5 km/h *and be presented with a resolution of* 1 km/h."

No further information is provided about the probability distribution for these deviations. The lack of bounds, as opposed to the axle load measurements, suggests an absolute interval. Therefore a normal distribution seems inappropriate with its infinite support. Rather, it was chosen to model the measurement error on the velocities using a triangular distribution, as this is bounded. The choice for triangular in particular, rather than for example uniform, is based on the assumption that the system is most likely to produce an unbiased measurement. With this, the distribution parameters are taken equal to:

$$a = \frac{-5}{3.6}\ \text{m/s}, b = 0, c = \frac{5}{3.6}\ \text{m/s} \tag{5.2}$$

where a, b, c, are the lower bound, center, and upper bound, respectively. Using this distribution, a value is determined which is to be **added** to the train's speed. Again, these errors are assumed uncorrelated.

As time is not a variable in the measurements, velocities and axle distances are related directly. This implies that, theoretically, a deviation between actual and measured velocity, results in a variation in axle distances. These are, however, not taken into account in this thesis. This choice is based on the capabilities of the measurement system to identify trains, after which it can correct the measured axle distances with known values for the identified train type. It is however not clear to which extent this method is employed.

5.2.2 Dynamic amplification

Information on the variations in the dynamic behavior of loads was found to be scarce. James (2003) argues, in his dissertation, that the value for the dynamic amplification factor Φ corresponding to ultimate strength limit states, as given in the Eurocode, represents the 95 % quantile. The coefficient of variation is calculated backwards through the assumption of a normal distribution with the standard normal quantiles as:

$$\mu_\Phi = \frac{\Phi_{0.95}}{1 + k\, c_{v;\Phi}} \tag{5.3}$$

One more assumption is required: the mean is still unknown. For this, the argument is that the dynamic amplification factor for fatigue loading represents a mean value. Using this assumptions James' work was performed. It is, of course, easy to find critique for this approach, as both the assumption of a normal distribution and the quantiles corresponding to both the amplification factors are not necessarily justified. However, as said before, information is scarcely available and therefore such approaches are required.

Some extra information was obtained from a master's thesis on the subject of dynamic effects on railway bridges. Rylander (2006) simulated the dynamic excitation induced by passing trains. It is based on solving the Frýba model (a specific solution of the standard equation of motion for Euler-Bernoulli bending). In his work, Rylander distinguishes three different dynamic amplification factors, i.e. (related to the passage of a train):

1. DAF1 is defined at the position of maximum static moment. The dynamic moment at the time when the train is in this position, is divided by the static moment.

2. DAF2 is defined the other way around. The maximum dynamic moment is divided by the static moment at this time.

3. DAF3 is different, in the sense that it is not fixed to a time specifically. Rather, it is the fractional of the maximum dynamic moment during the passage and the maximum static moment, also during the passage.

It is noted that DAF3 is the factor which is of importance for engineers. His next step was to assume probability distributions for the various components which influence the dynamic amplification: the axle load, velocity, bending stiffness, first natural frequency, and the amount of damping. From this, via a Monte Carlo simulation, the empirical distributions of the dynamic amplification factor were generated. Normal and lognormal distributions were fitted to the results, and fits compared using their mean square distance.

For the current study, however, where axle loads and velocities are known, although with errors on measurements, it would be erroneous to use such distributions directly. This would imply taking into account uncertainties in the axle loads and velocity twice. Now, consider the Frýba-equation (Frýba, 2001; Gillet, 2010):

$$EI\,\frac{\partial^4 y(x,t)}{\partial x^4} + m_b\,\frac{\partial^2 y(x,t)}{\partial t^2} + 2\,m_b\,\omega_d\,\frac{\partial y(x,t)}{\partial t} = \sum_{k=1}^{n} \epsilon_k(t)\,\delta(x - x_k)\,F_k \qquad (5.4)$$

The right hand side of equation 5.4, representing the excitation, suggests that the response is linearly proportional to the applied axle load(s) F_k. As the same is true for the static bending moment, the variations in axle loads are not expected to present themselves in the dynamic amplification factor.

The function $\epsilon_k(t)$ is composed of two Heaviside-functions. In this way it is equal to 1 during presence of the k'th axle on the beam, and 0 for all other t. Through the velocity of the train and its axle distances, this term results in the time-component for the load. Resonance may occur when the right hand side frequency resembles one of the natural frequencies with corresponding mode (obtained from solving the left hand side for zero excitation). Obviously, a proportionality to the speed cannot be obtained so easily as with the axle loads. More information would be required, for instance the bending stiffness which is necessary to solve equation 5.4 in order to obtain the natural frequencies of the structure. So, due to nonlinearities in the system, influences from different components in Rylander's work can not be quantified separately, making it, unfortunately, very hard to apply in practical situations.

In a search for more information on the subject, another source was identified. In this identified report, recommendations are made for statistical distributions using which the dynamic amplification can be modeled in a reliability-based analysis. The accuracy of these claims are, however, questioned, as the only source mentioned is "*recent studies*", which is not very convincing in the author's opinion. In absence of better sources, the information was considered anyway. The recommendation is to use a lognormal distribution for the dynamic amplification factor, which is said to produce the most accurate results for both bending moments and displacement (MAINLINE, 2013). The mean value ranges from 1.0 for speeds lower than 150 km/h to 1.25 for 250 km/h. The coefficient of variation is said to be "*independent of both train speed and train loading and the values range from* 20 *to* 25 %"(MAINLINE, 2013).

In other literature the focus was explicitly on steel railway bridges, and thus clearly not suited for application in the remainder of this work. Also, it is unclear to which extent the considered sources include both the effects of resonance and impact, as for instance Rylander seems to consider only the former. James's approach, based on the Eurocode, does in principle include both. However, justification for this method is weak. The advice given by MAINLINE (2013), when observing figure 5.2, seems

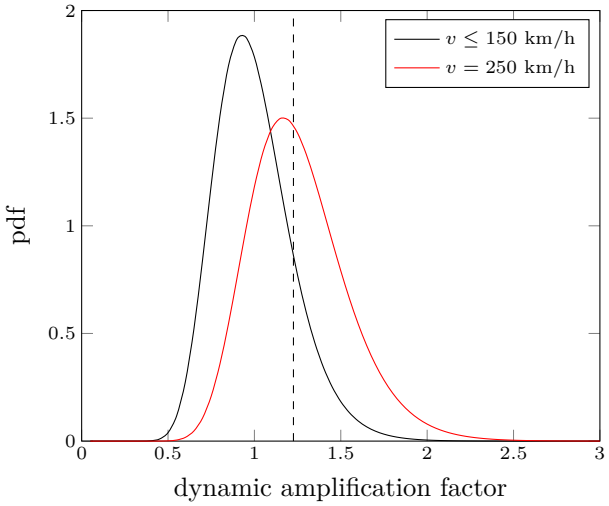

Figure 5.2: Distributions of the dynamic amplification factor according to MAINLINE (2013), with a coefficient of variation equal to 0.225. The dashed line represents the dynamic amplification factor according to the Eurocode (section 2.1.4.3) for $v = 150\,\mathrm{km/h}$ and $L_\Phi = 10\,\mathrm{m}$.

rather pessimistic, with very large amplification factors occurring quite frequently. Certainly for the main structure, as opposed to local elements, this is deemed too large.

In the end a decision has to be made. Based on the information presented here, it is concluded that the dynamic amplification is subject to significant variability. As an average value, it is seems that the Eurocode dynamic amplification factor for real trains, as presented in section 2.1.4.3, is usable. It also seems the best estimate available for the correlation between structural effects from resonance and impact versus span length and train velocity. It will be assumed that the dynamic amplification factor follows a lognormal distribution, where the value obtained from the Eurocode methodology represents the mean. The coefficient of variation will then be taken equal to 0.1, a value which seems to capture most variations on the level of an axle.

The dynamic amplification factor will be applied per axle (passage), and is assumed to be uncorrelated between passages. In a more detailed analysis, one may want to investigate the dynamic amplifications and the correlation within and between passages. For instance, if the stiffness deviates from the assumed value, the eigenfrequencies and modes are influenced, leading to variations in dynamic amplification which are systematic, and thus somehow correlated. For this analysis, however, such effects are not taken into account because information is lacking.

5.2.3 Extrapolation

In this work, the term 'extrapolation' is used for the activity in which one tries to gain insight into loads which can be expected in the future, based on measured traffic loads. Extrapolation should provide an answer to the question: "Which loads can be expected in the future, and should thus be incorporated into the design of structures?". In chapter 3, it was stated that railway bridges are designed for 100 years. Therefore, it is important to gain insight into the loads which can be expected during such a 100 year period. Clearly, these may differ from those loads which were observed. Also, the interest is not solely on one single extrapolated set of loads or

load effects, but rather on some description of all possible sets of loads or load effects which may occur, each with a probability of occurrence.

When dealing with extrapolation, it is the author's opinion that two facets should be considered thoroughly: the **importance**, and the **uncertainties**. The focus of extrapolation should only be on those parts that are important for the results, as well as subject to significant uncertainties. If one of these conditions is not met, then extrapolation might not be an essential step in an analysis. It is, however, in the judgment of these facets that difficulties present themselves. There is no *right* or *wrong*, in which extrapolation distinguishes itself from other engineering questions. This characteristic is beautifully expressed by Scholz:

> *"Ultimately, the extrapolation step is one of good faith and not statistical in nature."* (Scholz, n.d.)

Extrapolation in itself consists of two components: trends in traffic, and statistical extrapolation from the measured time to the desired service life of the structure. Trends in axle weights include for instance the increasing detail to which the transportation of freight is planned, leading to a shift in the ratio of loaded to unloaded trains. In this work, trends could not be assessed due to the lack of information. Due to the fact that, for instance, historical annual cumulative tonnages do not provide any insight into resulting damage numbers, such trends cannot be assessed without the availability of detailed historical traffic records of sufficient length.

The statistical extrapolation is an entirely different source of load increases. It is based on the notion that, due to the fact that measuring time is generally limited, not all loads can be measured. Therefore, there is no reason to believe that extrapolation of a measured set of trains should not include different (and possibly more severe) loads than the ones which are measured. The word 'extrapolation' will be used to denote this form of extrapolation in the remainder of this work.

Some deem it sufficient to simply scale the loads history or histories to the service life. With this, it is assumed that the limited measurements contain the main body of the loading, and that this is the important part for the verification. The tail of the distribution is found to be important by others. Events in this tail do not occur frequently (therefore it is called a 'tail'), and it can be assumed that this tail would fill in as the measured time is increased. Also, some designers note that the high stress events influence the service lifetime significantly and should therefore be taken into account (Sutherland & Veers, 1995). For fatigue loads on railway structures, this aspect is treated in appendix F.1. Here, it was concluded that, for a reference case and considering concrete, about 1 % of the traffic is responsible for practically the entire damage number (about 80 percent). Also, the type of trains which are responsible were assessed. For this same reference case, practically all damage is done by freight trains (> 99 %). For reinforcement, the damage is done by a larger portion of traffic, although still rather small (1 % of traffic is responsible for 50 % of damage).

In appendix 4, it is explained that the different characteristics which surround fatigue loads (magnitude of axle loads, their frequency, and their distances), make that there is no clear single criterion to compare them. It was decided to use the load effect, being the damage number. When extrapolating fatigue loads, the difficulty is precisely in this number of characteristics, namely: which characteristic(s) should be extrapolated, and to which extent. When it comes to the extrapolation of fatigue loading magnitudes, a number of methods were identified in literature:

1. extrapolation of traffic, i.e. extrapolation 'on the level of traffic' as opposed to the other methods;

2. time-extrapolation using extreme value theory, in this case the 'peak over threshold' method;
3. spectrum fitting, both uni- and bivariate;
4. extrapolation of the damage number (increments).

Each of these methods was first discussed in chapter G. From this, a choice was presented (time-extrapolation using extreme value theory) which is compared to another technique for verification (spectrum fitting of rainflow matrices). For the elaboration of the above, please refer to chapter G, from which the following conclusions were drawn:

- Two methods, time-extrapolation using extreme value theory and the bivariate spectrum fitting using kernel density estimation, have been implemented and demonstrated. Comparison has shown that the kernel density estimate (KDE) results in a larger spread in damage numbers than the peak-over-threshold method. Notably, the maximum amplitudes were obtained by appliance of the KDE method. It was argued that the latter is fundamentally more powerful because it allows variations in the entire spectrum, although differences in damage numbers were mainly attributed to differing extrapolations of the largest load cycles. Also, the kernel density estimate involves estimating the kernel width, which turned out to be both essential and somewhat subjective.
- Variations in damage, obtained by the extrapolation of the load histories were negligibly small. Therefore it was decided to omit this entire step in subsequent analysis, as this saves a considerable amount of time while maintaining practically all accuracy in determining the damage numbers.
- Variations in the number of cycles have been quantified. The main source of uncertainties was shown to be in the determination of the mean value (statistical uncertainty). It was demonstrated that, whatever the mean number of cycles per time unit, the total number of cycles will converge with negligible variations. For this mean value, standard errors were determined. Furthermore, the assumption has been made to use an average coefficient of variation obtained for traffic from all detectors (0.01) over the reference structure, for all future analyses, regardless of the exact structure or detector. These uncertainties are normally distributed.

The most interesting conclusions, however, might be the resulting variations in damage numbers obtained from the extrapolation. It has been shown that these are very small, even negligible, and therefore it seems that 4 years of measurements seems enough to draw conclusions about design life fatigue loading. At least, the measurements have converged, thereby not implying an expected occurrence of much larger loads. Also, even more useful than determination of expected variability through extrapolation, may be the *feeling* one gains for the data, yielding the confidence required to proceed with results of extrapolation methods such as those described in this thesis.

Now that the extrapolation in time has been discussed, the results still need implementation in the analysis. It was shown that extrapolation of magnitudes did not result in effects of any significance. The uncertainty in determining the mean number of cycles was identified as the only factor which has some distinguishable influence on the overall damage number, although small. It was also shown that this is normally distributed.

Using the knowledge that the measured load histories (with exception of traffic records, or 'detectors', 11 and 14, but these will not be used for the calibration) correspond to a time-frame of 3.98 years, the mean number of cycles expected in 100 years is

100/3.98 times larger than the number of cycles in the measured time frame. The coefficient of variation was determined to be 0.01 and equal for all detectors (at least for the detectors which will be used for the calibration). The standard deviation can thus be determined as $0.01 \times 100/3.98$. From this follows the distribution for time-extrapolation:

$$\xi_{\text{ext}} \sim N\left(\frac{100}{3.98}, \frac{0.01 \times 100}{3.98}\right) = N(25.126, 0.2513) \tag{5.5}$$

This extrapolation factor will be applied directly on the damage number, thus in the damage-domain. Justification for this crude approach is that a long period is concerned, during which the number of cycles is large. Alternatively, one could draw this many of random cycles, for instance, and find out that the law or large numbers leads to minimal differences with the method used in this thesis. Direct application to the damage is allowed due to the proportionality of damage to the number of cycles, as shown in appendix D.

5.2.4 Dimensional uncertainties

Dimensional uncertainties are deviations of dimensions from their nominal values. Technically, these introduce uncertainty into the transition from generalized forces (bending moments in this thesis) to stresses used for fatigue verification. In this work, it was decided to skip dimensional uncertainties for two reasons:

- Deviations are absolute in nature, and can therefore not be implemented into the analysis by using a fictitious cross-section, simply because this fictitious cross-section does not have any real dimensions. Therefore, it is impossible to add or subtract, for instance, deviations in section height. Future analyses using actual cross-sections would however produce more precise results by including dimensional uncertainties, especially for smaller sections.
- The deviations, as laid out in part 3 of the Probabilistic Model Code (Joint Committee on Structural Safety, 2000b), are quite small. The coefficient of variation for the effective height for instance, is in the order of 1 %. Cause for this notion is that civil engineering structures are generally quite bulky. Deviations in size do not seem to correlate with the structure's size (according to the Probabilistic Model Code, which advices to use probability distributions independent of the structure its dimensions), their relative importance decreases for increasing structural dimensions.

It is added that, would on want to include this quantitatively, it would entail imposing variations on the proportionality between generalized forces and local stress, u. In this way, all stresses in a single point are systematically smaller or larger than expected. However, as said before, this is not included in the current work.

5.2.5 Load effect modeling

For a cross-section, generalized forces are determined using models, which by definition are a simplification of reality. Therefore the results obtained using these models deviates from what is actually happening. To take deviations of this nature into account, a model factor is generally used in probabilistic analyses, which includes (Joint Committee on Structural Safety, 2000b):

- effects of a random nature, which are neglected in the models used for calculations.
- simplifications used in the mathematical relations (for example linear elastic calculations).

Because the Eurocode prescribes, for example, linear elastic calculations and finite element modeling for fatigue verifications, a sufficiently large margin of safety should be included to deal with modeling uncertainties introduced by these methods. These modeling uncertainties usually result from neglecting for instance 3D-effects, inhomogeneities, interactions, boundary effects, simplifications of connection behavior, imperfections and so on (Joint Committee on Structural Safety, 2000b).

The Probabilistic Modeling Code states some recommendations for practice. The accuracy of load effect calculations (meaning generalized forces in this context, not to be confused with damage numbers) depends on the *type* of calculation, distinguishing between bending moment, shear force, axial force, stresses in 2D-solids, stresses in 3D-solids, and also between frames and plates. Most relevant for this thesis are the model uncertainties related to bending moments in plates[1], being lognormally distributed with mean of 1 and standard deviation of 0.2 (Joint Committee on Structural Safety, 2000b). These are said to be based on a standard structural finite element model, which can be assumed for this type of calculations.

Generalized forces are determined through the use of an influence line and superposition. Therefore, in general, the obtained force will be the effect of multiple loads. In applying the factor for model uncertainties, it is implicitly assumed that the effects of all loads on the generalized force at the point of interest, are over- or underestimated by this factor, or in other words: that there is a modeling error in the influence line, with full correlation over the span.

The uncertainty in modeling the constant stresses (expressed using ζ_{perm}) is also assumed to be distributed according to the same distribution, as it would generally be determined using equal means. Therefore full correlation with the load effect from variable loads is assumed (conservative), as errors in for example the finite element model or its constraints are thought to be correlated between different load cases. Variations in determining the self-weight and prestressing forces were not included separately.

5.2.6 Fatigue resistance (concrete)

The background of the fatigue resistance model, in the form of S-N curves included in the Eurocode, could not be obtained. Furthermore, it was learned that the curves according to the Dutch national annex, which were shown to result in 'jumps' at 10^6 cycles, have no solid basis. Lantsoght (2014) compared a large number of measurements of concrete fatigue resistance in compression and even proposed an adaptation for the S-N curves found in the Eurocode. It is expected that the new version of the Dutch national annex will adopt this proposal, which forms the basis for adopting this proposal for this thesis.

5.2.6.1 Lantsoght's proposal

Interestingly for this thesis is that the background of the proposed curves is available, including statistics. First the resistance model proposed by Lantsoght (2014) will be laid out. There are actually two proposals: one for existing structures, the other for new structures. Here, the proposal for new structures is adopted. The fatigue resistance is based on the design value of the concrete compressive strength:

$$f_{cd,fat} = k_1 \, \beta_{cc}(t_0) \, f_{cd} \left(1 - \frac{f_{ck}}{400}\right) \tag{5.6}$$

[1] It is assumed that here actually *slabs* are meant instead of plates, i.e. loaded out-of-plane instead of in-plane.

The number of permissible cycles is then given as

$$N_i = 10^{\left(14 \frac{1 - E_{cd,max,i}}{\sqrt{1 - R_i}}\right)} \tag{5.7}$$

with (similar to chapter 2)

$$R_i = \frac{E_{cd,min,i}}{E_{cd,max,i}} \tag{5.8}$$

$$E_{cd,min,i} = \frac{\sigma_{cd,min,i}}{f_{cd,fat}} \tag{5.9}$$

$$E_{cd,max,i} = \frac{\sigma_{cd,max,i}}{f_{cd,fat}} \tag{5.10}$$

Comparison of the above resistance model with measurements, based on $k_1 = 1$ and $\gamma_{c,fat} = 1.5$, was expressed in the ratio of tested maximum permissible stress over predicted maximum permissible stress for a given number of cycles corresponding to the experiment:

$$\bar{s} = \frac{s_{max,\text{tested}}}{s_{max,\text{predicted}}} \tag{5.11}$$

The mean value of $\bar{s}$ was found to be 1.137 and the standard deviation equal to 0.086, although these values were found for the proposal for existing structures. The characteristic value[2], determined by subtracting 1.64 times the standard deviation from the mean, is equal to 0.996. From the comparison, also the value of $\bar{s}$ corresponding to a 5 % probability of non-exceedance was determined from the measurements directly (representing the empirical distribution instead of an assumed normal distribution). This resulted in a value of 1.003, which is almost equal to the value found using the normal approximation.

In figure 5.3 the normal and lognormal distributions corresponding to the mean and standard deviations obtained by Lantsoght (2014) are plotted. Clearly, differences are very small. The normal distribution results in a more conservative left tail, and was therefore chosen to model $\bar{s}$. It is assumed that the statistical parameters related to the proposal for new structures are approximately equal, because the proposals differ only slightly. The mean value of $\bar{s}$ will be taken as 1.137, with a standard deviation of 0.086 ($c_v = 0.076$) (which thus applies to the stress level).

5.2.6.2 Implementation

In the preceding section it was shown that the ratio of tested over predicted s_{max} can be modeled using a normal distribution:

$$\bar{s} = \frac{s_{max,\text{tested}}}{s_{max,\text{predicted}}} \sim N(1.137, 0.086) \tag{5.12}$$

where the predicted values are based on the proposed model by Lantsoght (2014). Assuming that the distribution obtained from these tests holds for the entire range of stresses and therefore also cycles, plus full correlation (which is justified by viewing

[2]This term was used by Lantsoght, but is actually inaccurate. Because this value is determined with inclusion of the partial factor $\gamma_{c,fat}$, it is actually a *design* value. Strangely, however, is that the variance in fatigue resistance was not considered in determining the partial factor, although this is fundamentally required.

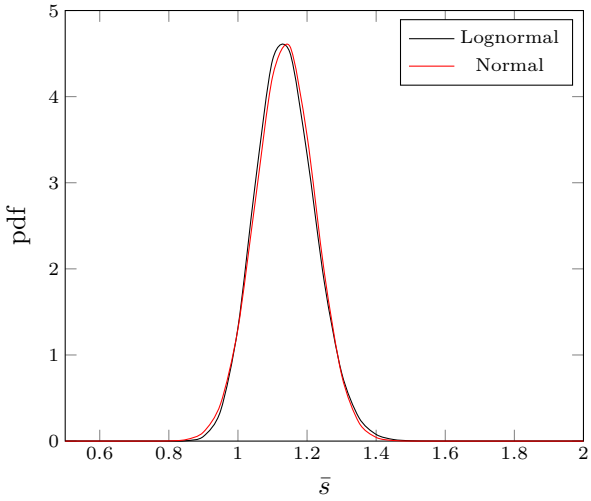

Figure 5.3: Approximations using a normal and lognormal distribution for $\bar{s}$.

'fatigue resistance' as somewhat of a range-independent material property), this can be used to describe the S-N curves in a stochastic manner. The shape and slope are thus controlled by the stochast $\bar{s}$. Because $s_{\max}$ represents a relative stress level, it was chosen to apply $\bar{s}$ directly on the relative stress level in the model proposed by Lantsoght:

$$N_i = 10^{\left(14 \frac{1 - \frac{E_{cd,max,i}}{\bar{s}}}{\sqrt{1 - R_i}}\right)} \tag{5.13}$$

This means that the S-N curve lies, on average, a factor 1.137 higher (mean value of $\bar{s}$) than the curve used for design, on top of the difference caused by the partial factor. Note that only $E_{cd,max,i}$ in the numerator is divided by $\bar{s}$, in order to preserve the shape of the S-N curve. This is allowed because only the relative stress is of importance, hence R is not affected (also used by Lantsoght). Furthermore it is important to use $\gamma_{c,fat} = 1.0$ for the probabilistic analysis. If not, the safety margin provided by the partial factor would not be incorporated.

5.2.7 Fatigue resistance (reinforcement)

The fatigue resistance of steel reinforcement bars is derived directly from test results. Data from two sources was used: Tilly (1984) and Helgason and Hanson (1974) (gained from Wight and MacGregor, 2012). The data was merged because it is based on equal test types and also shows good resemblance. From this, a S-N curve is fitted. A linear S-N relation on double logarithmic scale was assumed, therefore fitting a function of the form

$$\Delta\sigma_s = 10^{\left(A - \frac{1}{m} \log N\right)} \tag{5.14}$$

which results in best estimates $A = 3.506$ and $m = 5.179$.

Because it is customary to express the material's variability in terms of the number of stress changes, all data points were *projected* on the horizontal N-axis using the best estimate for the slope. In other words, the intercept with the horizontal axis,

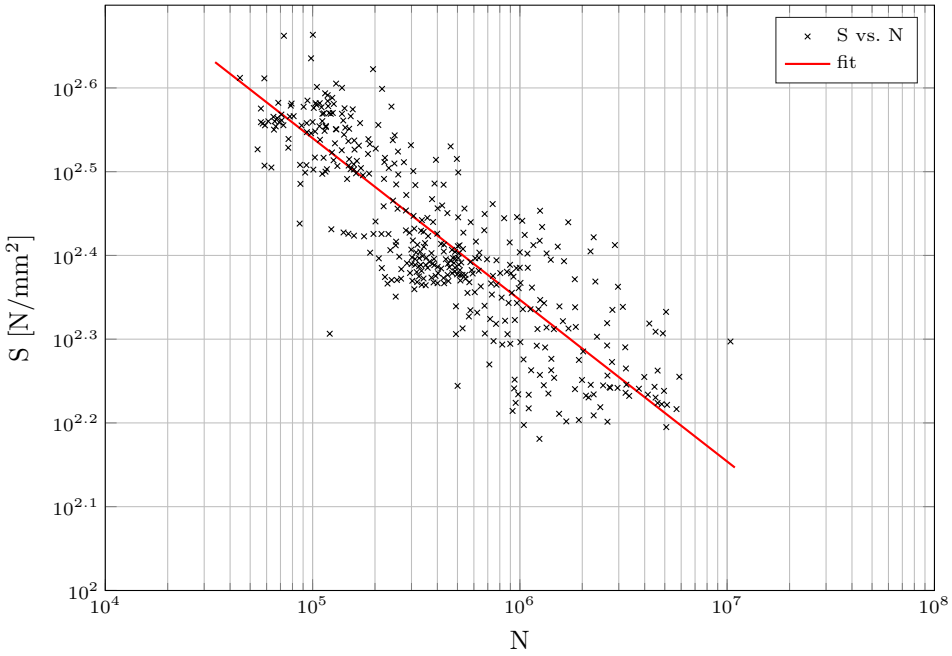

Figure 5.4: Data vs. fitted S-N relation.

denoted with C, is determined for each data point using

$$C_i = \log N_i + m \log \Delta\sigma_{s,i} \tag{5.15}$$

The result is an array of values for C, which is approximately normally distributed, see figure 5.5 (note that C is expressed in the logarithmic scale, therefore the life is actually lognormally distributed). Parameters for C's probability distribution are $\mu_C = 18.141$ and $\sigma_C = 0.2969$.

With appliance of the above model for resistance, full correlation in terms of number of cycles to failure is assumed between the upper and lower branch of the S-N curve (based on the approach followed in the Probabilistic Model Code, Joint Committee on Structural Safety, 2013). This is coupled with a stochast to model the damage number at failure (discussed in next section, i.e. section 5.2.8). This also implies that $\log N^*$ shares the same distribution as C, and with full correlation. Its mean value is derived from the Eurocode and the fit. Assuming the characteristic line lies two standard deviations from the mean, the mean of N^* should lie two standard deviations above the mean Eurocode value (where the standard deviation is taken from the fit): $\mu_{N^*} = 10^{(6+2\times0.2969)} \approx 10^{6.6}$.

From this, the stress range magnitude corresponding to μ_{N^*} is determined from the mean value of C and the slope:

$$\log \Delta\sigma_{Rs} = \frac{\log \mu_C - \log \mu_{N^*}}{k1} = \frac{18.141 - 6.6}{5.179} = 2.22 \tag{5.16}$$

which means that the stress range is equal to $169.2\,\mathrm{N/mm^2}$. This stress shall remain fixed, as the variations are expressed through its corresponding number of cycles, N^*.

The fatigue exponent for the lower magnitude cycles is based on the starting point of EN 1992:

$$k2 = 2\,k1 - 1 = 9.358 \tag{5.17}$$

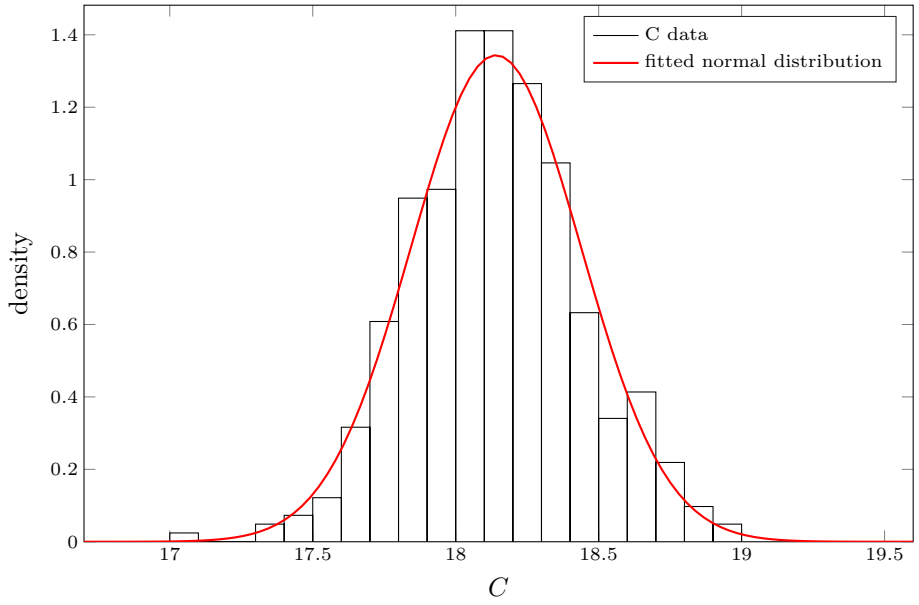

Figure 5.5: Data vs. fitted distribution for variability in number of stress changes.

With these parameters, the whole S-N curve is defined. As a short recap: the fatigue exponents $k1$ and $k2$ remain fixed, while the variations are expressed by shifting the S-N curve in the horizontal direction with full correlation (shape remains the same on double logarithmic scale). Finally, this approach is compared to the Eurocode S-N curve in figure 5.6, which shows the two correspond very well.

5.2.8 Critical damage number

Using the linear damage rule proposed by Palmgren and Miner, as described in chapter 2, the damage number at failure is assumed to be equal to unity. However, the actual damage number at which failure occurs is not set deterministically. Generally, the damage number at failure is denoted as 'critical damage number' (Δ).

Some effects which can influence the critical damage number have not been included in the analysis of concrete by Lantsoght (2014) and for the analysis of reinforcement in this work. These analyses were based on constant amplitude loading, and the size of the specimens does not necessarily validate the results for e.g. different dimensions.

For concrete, other factors which were identified as influential are (Naik, Singh, & Ye, 1993):

- rate of loading / loading frequency;
- rest periods;
- stress gradient;
- moisture conditions;
- curing conditions;
- air entrainment.

For reinforcement steel, there are also aspects which do not seem to be covered by the constant amplitude tests alone (effects of variable loading, size effect, corrosion,

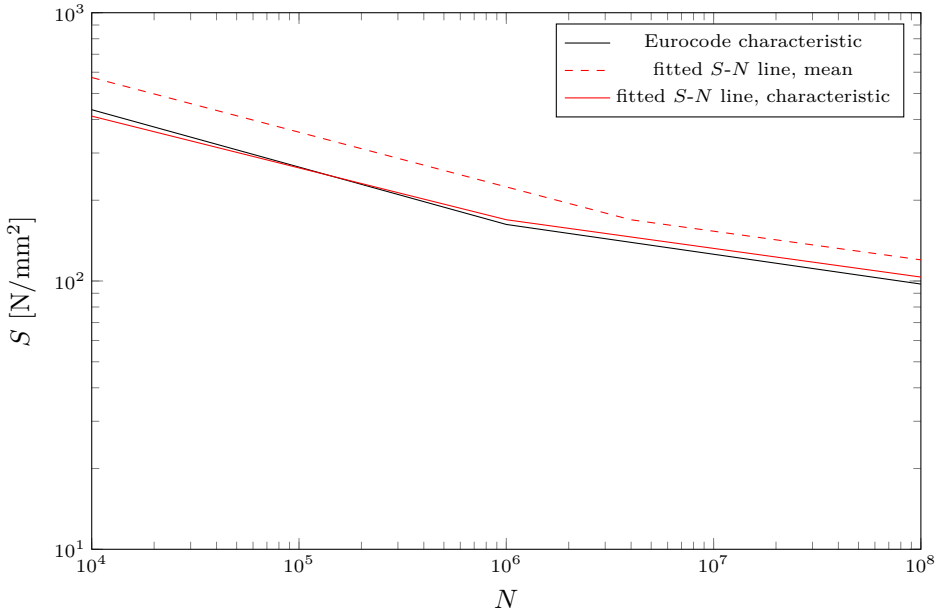

Figure 5.6: Comparison of Eurocode S-N curve with characteristic curve derived from fitting the data.

...). These are also included by allowing variations in the critical damage number.

A review of literature did result some guidance on the variability in critical damage. According to the Probabilistic Model Code (Joint Committee on Structural Safety, 2013), based on Wirsching (1984), the damage number at failure can be modeled using a lognormal distribution with unit mean and coefficient of variation equal to 0.3. This advice is given for steel, but no information could be obtained for concrete. Therefore it was chosen to apply this distribution for concrete as well.

5.3 Deterministic calibration variables

So far, it has become clear that there are a number of variables where upon the results of calibration analyses depend. Basically, 8 variables were identified, of which an overview is given in table 5.2.

calibration depends on:	addressed in:
static scheme	section 5.3.1
span length	section 5.3.1
cross-section	section 5.3.1
traffic history	section 5.3.2
Eurocode traffic mix	section 5.3.2
concrete class	section 5.3.3
ratio of permanent stresses	section 5.3.3
reinforcement S-N curve parameters	section 5.3.4

Table 5.2: Overview of calibration variables which were used in this thesis.

Also, for a given structure, multiple effects (i.e. generalized forces) can be of interest

(for example the longitudinal and transverse bending moment), as well as multiple locations where details could be situated (denoted as 'point of interest'). Because of this significant number there are numerous combinations which can be investigated. However, due to limited time (or: time-consuming analyses), only a subset of combinations will be treated.

5.3.1 Static schemes, cross-sections & span length

Differences in static schemes correspond to different influence lines, which dictate the results of a calibration procedure of this nature. This necessitates the use of various static schemes, each spanning multiple lengths. For this work, five static schemes were chosen, as displayed in figure 5.8 (the figure shows 7, which is due to the combinations with cross-sectional types). These can be combined with different cross-sectional shapes, which results in even more combinations. Cross-section which have been used in this work, are presented in figure 5.7.

The most simple cross-section is the 'slab', as used in the reference case throughout the appendices. This cross-section is included in the calibration, where for the slab-type always the longitudinal bending moment is calibrated. To study the transverse bending moments, it is of more interest to introduce a cross-sectional type with greater dependence on transverse rigidity. This is accomplished by including for instance a trough- or box-section, from which the former was chosen. Overall, the following schemes were selected for calibration (corresponds to figures 5.7 and 5.8):

Scheme 1 Cross-section: slab, single span, both ends fully restrained. The point of interest is the mid-span bending moment in longitudinal direction (sagging).

Scheme 2 Cross-section: slab, single span, both ends fully restrained. The point of interest is the longitudinal bending moment at the support (hogging).

Scheme 3 Cross-section: slab, single span, simply supported at both ends. The point of interest is the mid-span bending moment in longitudinal direction (sagging).

Scheme 4 Cross-section: slab, continuous on three supports, all hinges. The point of interest is the mid-span longitudinal bending moment in one of the spans (sagging). Note that this point is not loaded most severely, however, it has an interesting influence line due to loads on the adjacent span resulting in bending moments of opposite sign.

Scheme 5 Cross-section: slab, continuous on four supports, all hinges. The point of interest is the mid-span bending moment in one of the outer spans, where the longitudinal bending moment is investigated (sagging).

Scheme 6 Cross-section: trough, single span, both ends fully restrained. The point of interest is the mid-span bending moment in transverse direction (sagging or hogging, whichever was governing), which is observed between the tracks and the trough's edge.

Scheme 7 Cross-section: through, single span, simply supported at both ends. The point of interest is the mid-span bending moment in transverse direction (sagging or hogging, whichever was governing), which is, again, observed between the tracks and the trough's edge.

For cases with a slab cross-section, where the longitudinal bending moment is of interest, the span is of critical importance because of its interaction with axle distances. To study it's influence, a large number of spans were included, namely the set $L = \{1, 2, 3, 4, 5, 6, 7, 8, 9, 10, 12, 14, 16, 18, 20, 22, 24, 26, 28, 30, 35, 40, 45, 50\}$ m.

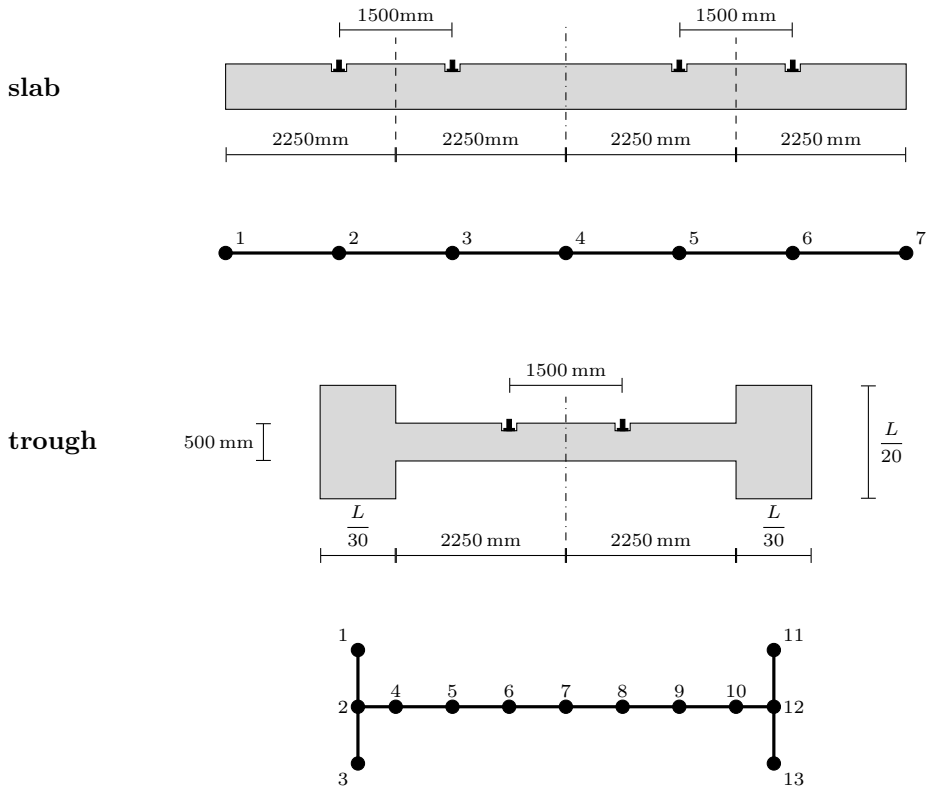

Figure 5.7: Cross-sections used in this thesis, with their finite element discretizations.

When the transverse bending moments are of interest, the span is of lesser importance. Therefore it is not required to calibrate for such a diversity of span lengths, so that the calibration is done for the set $L = \{5, 6, 7, 8, 9, 10, 12, 14, 16, 18, 20, 22, 24\}$ m.

5.3.2 Traffic

As explained in chapter 2, the Eurocode load model for fatigue consists of three different traffic mixes. For the calibration, measured traffic is compared to all three traffic mixes from the code. This also allows for the differences between load models to be assessed. In the remainder of this report, the traffic mixes will be represented using the numbers introduced in chapter 2:

- standard traffic mix (EC1);
- heavy traffic mix (EC2);
- light traffic mix (EC3).

The measured traffic which will be used for the calibration is limited to a selection of all available detectors, because not all seem relevant (see chapter 2). The traffic measured at detector 111 seems most damaging, but also detector 364 (highest axle load) and detector 164 (2nd highest cumulative annual tonnage) are interesting. Therefore, it was chosen to calibrate the Eurocode models with these three traffic records (detectors 111, 164, and 364).

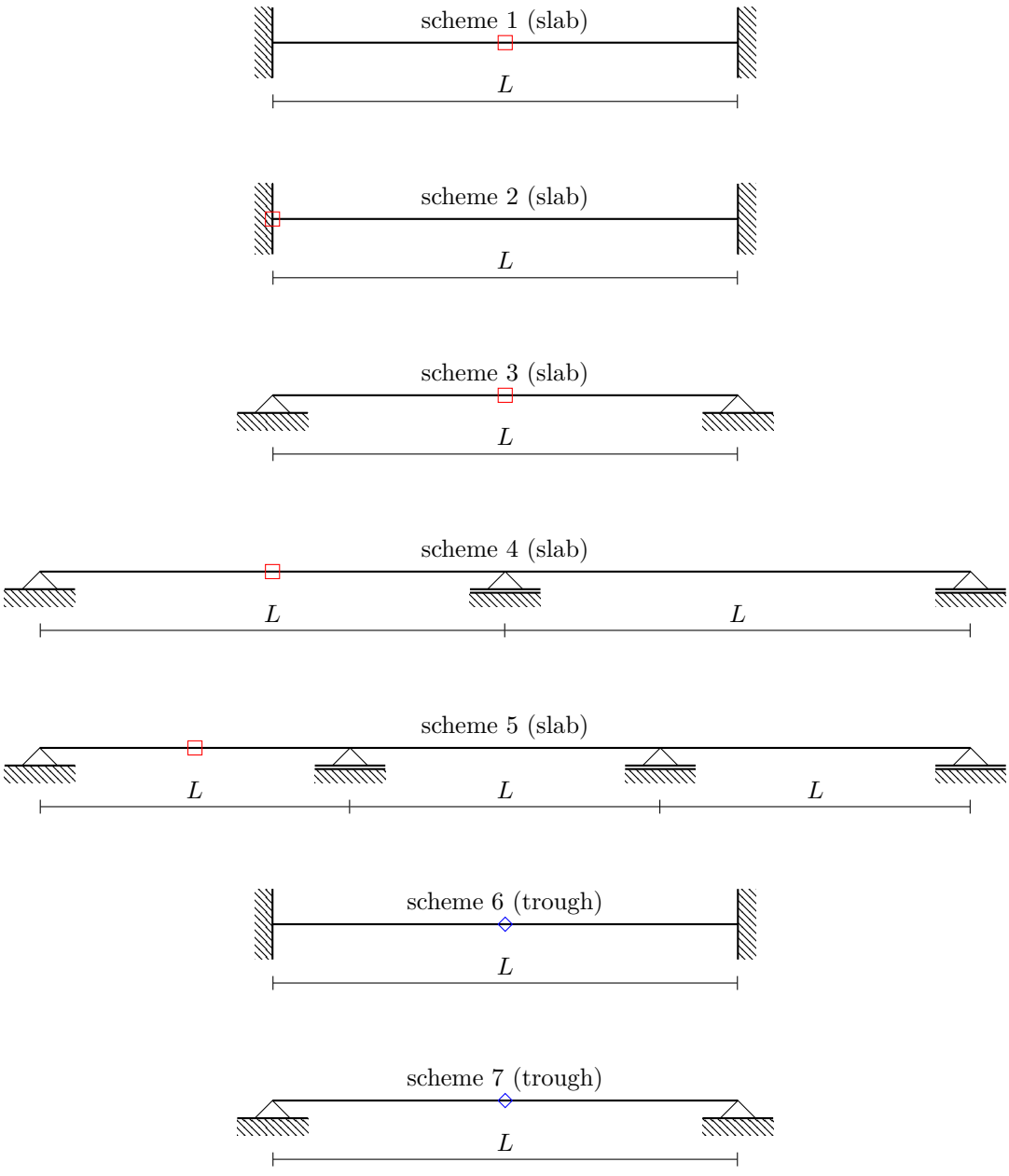

□ point of interest, longitudinal bending moment (cross-section: slab)

◇ point of interest, transverse bending moment (cross-section: trough)

Figure 5.8: Static schemes to be used for the calibration.

5.3.3 Concrete class & permanent stresses

In the model proposed by Lantsoght (2014), discussed in section 5.2.6, the critical number of cycles to failure is determined using a single equation for the entire range of stress ranges, as opposed to the current Eurocode model. It can be shown that the reliability resulting from appliance of this S-N formulation is **invariant to the concrete compressive strength**, and that it therefore is of non-importance to the calibration procedure. The permissible number of cycles is determined from

$$\log N_i = \frac{14\left(1 - \dfrac{\sigma_{c,max,i}}{f_{cd,fat}}\right)}{\sqrt{1-R_i}} \tag{5.18}$$

Substitution of the stresses per cycle, including the permanent part, yields the following equation:

$$\log N_i = 14\,\frac{1 - \left(\dfrac{u_c\left(\sigma_{mean,i} + \sigma_{amp,i}\right)}{f_{cd,fat}} + \zeta_{\text{perm}}\right)}{\sqrt{1 - \dfrac{\dfrac{u_c\left(\sigma_{mean,i} - \sigma_{amp,i}\right)}{f_{cd,fat}} + \zeta_{\text{perm}}}{\dfrac{u_c\left(\sigma_{mean,i} + \sigma_{amp,i}\right)}{f_{cd,fat}} + \zeta_{\text{perm}}}}} \tag{5.19}$$

From equation 5.19 it is clear that the concrete compressive fatigue design strength is only of influence in combination with the proportionality factor u_c. Therefore, in obtaining the value for u_{limit} corresponding to the limit state, the effect of the compressive strength will be fully compensated by the proportionality factor. In other words: the ratio $u_c / f_{cd,fat}$ remains constant for all $f_{cd,fat}$ **upon enforcement of the limit state**. This shows that the reliability is invariant to $f_{cd,fat}$. Of course a higher strength does allow for a higher u_c, thereby showing the benefit of using stronger concrete.

The ratio of permanent stresses over the design compressive strength is of influence though, as opposed to the concrete compressive strength itself. This is due to the fact that ζ_{perm} cannot be isolated in combination with u_c. Therefore it will be included in the calibration with three different values. For this, the set $\{0.3; 0.45; 0.6\}$ was chosen as to cover an interval of realistic options for most spans.

5.3.4 Reinforcement resistance parameters

The parameters which define the S-N curve for the reinforcement steel are of interest for the reliability calculation. Engineers within Movares stated that reinforcement in railway structures is practically never welded (which would reduce the fatigue resistance greatly). Therefore, in compliance with the Eurocode, the following parameters were chosen for the calibration:

$$\begin{aligned} \Delta\sigma_{Rsk} &= 162.5\,\text{N/mm}^2 \\ N^* &= 10^6\,\text{cycles} \\ k_1 &= 5 \\ k_2 &= 9 \end{aligned}$$

5.4 Limit State Formulation

Essential to determining the provided failure probability, is the formulation of a limit state function. The process which is captured in the limit state equation is described first, after which the equations are presented. The process is described using Monte Carlo analysis, so using iterations. During each iteration:

1. One single possible 100 year load is determined, based on 4 years of measurements corresponding to the location of interest. This extrapolation was carefully studied (see section 5.2.3 and appendix G), from which it was concluded that only uncertainties in the expected number of cycles need to be incorporated. It was concluded that an extrapolation factor can be applied directly and linearly on the damage number.

2. This 100 year load is passed over the structure using simulation, from which the stress-signal is obtained. This is done by determining the signal for the measured 4 years, and extrapolating this linearly. The uncertainties in this extrapolation are taken into account by use of a factor (stochast).

3. The signal is passed through rainflow counting, which yields a description of all cycles (amplitude and mean stress). Miner's law is applied to determine the damage number, in which uncertainties in material resistance are incorporated.

4. The resulting damage number is compared to a critical value, above which, by definition, the section fails in fatigue. If the obtained damage number is lower than the critical value, the section survives.

Each iteration results in a unique load and resistance, caused by the underlying probabilistic descriptions of each variable. The number of failures is counted, as well as the number of iterations. Dividing the number of iterations resulting in failure, by the total number of iterations, the failure frequency is determined, which is an estimator for the probability of failure.

The structure which is used, basically consists of an influence line corresponding to a point of interest, and a cross-section. Comparison with the Eurocode is done by, prior to starting the Monte Carlo analysis, determining the resistance which this cross-section provides to be exactly equal to what is solicited by the load model, based on the Eurocode verification procedure (and thus, by definition, in a deterministic sense).

For this work it was decided to compose separate limit state functions for concrete in compression and reinforcement steel. The form in which the limit state function is presented here, is not the classical '$R - S$' format. Instead, it should be interpreted as '$R/S - 1$', in which R and S are not strictly separable.

For the calibration of reliability, provided by design according to the Eurocode, when loaded by measured traffic, the reliability equations were formulated as follows:

$$Z = g\left(\Delta, \theta_s, \bar{s}, u, \mathbf{H}\right) = \frac{\Delta}{\xi_{\text{ext}} \sum \mathcal{D}(\theta_s, \bar{s}, \mathcal{R}(u\,\mathcal{I}(\mathbf{H}), \zeta_{\text{perm}}))} - 1 \tag{5.20}$$

with

$$u = u_{\text{limit}} \text{ based on } \sum \mathcal{D}\left(\mathcal{R}\left(u\,\mathcal{I}\left(\mathbf{M}\right), \zeta_{\text{perm}}\right)\right) = 1 \tag{5.21}$$

for concrete in compression, and

$$Z = g\left(\Delta, \theta_s, N^*, u, \mathbf{H}\right) = \frac{\Delta}{\xi_{\text{ext}} \sum \mathcal{D}(\theta_s, N^*, \mathcal{R}(u\,\mathcal{I}(\mathbf{H})))} - 1 \tag{5.22}$$

with

$$u = u_{\text{limit}} \text{ based on } \sum \mathcal{D}\left(\mathcal{R}\left(u\,\mathcal{I}\left(\mathbf{M}\right)\right)\right) = 1 \tag{5.23}$$

for reinforcement steel, where (repeated for completeness):

g = limit state function
Z = safety margin
Δ = critical damage number
ξ_{ext} = extrapolation factor
$\sum \mathcal{D}(\bullet)$ = damage number operator
θ_s = model uncertainty factor
$\bar{s}$ = strength uncertainty factor (concrete)
N^* = strength uncertainty factor (reinforcement)
u = proportionality between generalized forces and resulting stresses
$\mathbf{H}$ = traffic history from detector
u_{limit} = value of u for which the deterministic limit state is enforced
$\mathcal{I}(\bullet)$ = influence-operator, which transforms traffic into a signal using an influence line (thereby incorporating a structure)
$\mathbf{M}$ = traffic mix from the Eurocode
ζ_{perm} = ratio of permanent stresses over design compressive strength
$\mathcal{R}(\bullet)$ = *rainflow*-operator, divides a (stress) signal into separate (stress) cycles using the *rainflow cycle counting* algorithm

Furthermore, it follows from Z's definition as the safety margin that:

$Z > 0$ survival
$Z \leq 0$ failure

In equations 5.20 and 5.22, the stochasts are: Δ, ξ_{ext}, θ_s, $\bar{s}$, N^*, and therefore also Z. The signals which are determined from measured trains ($\mathbf{H}$), using the influence operator, also include uncertainties which are expressed using $\hat{F}$, $\hat{v}$, and $\hat{\Phi}$ (see sections 5.2.1 and 5.2.2).

The operators which are used in the limit state formulation were discussed in chapter 4, and more details were covered in the appendices. The distributions which are used to model the uncertainties and variations in the limit state function's parameters were determined in chapter 5. The reason to deviate from the regular $Z = R - S$ format, is that this format proved difficult to solve using an approximation technique instead of Monte Carlo (FORM, see appendix A). This was caused by the fact that the partial derivatives with respect to the variables differ greatly from each other, and also depend heavily on the point of linearization, which makes it impossible to reach convergence using this technique. This problem is mitigated using the formulation presented in equations 5.20 and 5.22. It is noted that the fundamental assumption which allows changing the limit state function, is the definition of the reliability index β, which is invariant to the formulation of the limit state function (again, see appendix A).

5.5 Conclusions

- The basics of code calibration were illustrated, and the background of partial factors was discussed. An overview of partial factors which were used in the deterministic analysis, to set the boundary conditions for the probabilistic analysis, is given in table 5.3. Stochastic variables have been discussed and distributions to model their uncertainties and variations were chosen, see table 5.4.

- Most difficult, and therefore proposed as a subject for further investigation, are these components:

  - dynamic amplification factor;
  - modeling uncertainties;
  - critical damage number.

  In chapter 6, their importance is assessed, from which a complete picture of important voids in current knowledge can be drawn.

- The sets of variables are combined in order to form combinations for which the calibration is to be performed. These combinations are displayed in figure 5.9. The overall number of calibrations, thus all cases, is equal to 3942 for concrete and 1314 for reinforcement.
- The reliability equation was formulated for both concrete under compression, as for reinforcement steel. This equation allows solving for the failure probability or the reliability index.

partial factor on	deterministic analysis	probabilistic analysis
fatigue loads	1.00	1.00
fatigue resistance concrete	1.50	1.00
fatigue resistance reinforcement	1.15	1.00

Table 5.3: Partial factors used in deterministic analysis. In the probabilistic analysis, all partial factors were, of course, set to unity.

stochastic variable	symbol	distribution	parameters	notes
measurement error load	$\hat{F}$	normal	$\mu_{\hat{F}} = 1$ $\sigma_{\hat{F}} = 0.0612$	multiplier for measured axle load, uncorrelated between axles
measurement error velocity	$\hat{v}$	triangular	$a_{\hat{v}} = -1.39$ $b_{\hat{v}} = 0$ $c_{\hat{v}} = 1.39$	added to measured velocity, uncorrelated between axles
uncertainty in dynamic amplification	$\hat{\Phi}$	lognormal	$\mu_{\hat{\Phi}} = 1$ $\sigma_{\hat{\Phi}} = 0.1$	multiplier for DAF according to the EC, uncorrelated between axles
dimensional uncertainties	u	-	-	skipped in current work, so u is kept at the deterministic value obtained by loading with one of the Eurocode traffic mixes
model uncertainties	θ_S	lognormal	$\mu_{\theta_S} = 1$ $\sigma_{\theta_S} = 0.2$	applied on the stresses with full correlation over the structure's life time
fatigue resistance (concrete)	$\bar{s}$	normal	$\mu_{\bar{s}} = 1.137$ $\sigma_{\bar{s}} = 0.086$	variations in permissible stress level, fully correlated between different stress levels (expressed as ratio)
fatigue resistance (reinforcement)	$\log N^*$	normal	$\mu_{\log N^*} = 6.6$ $\sigma_{\log N^*} = 0.297$	variations in number of permissible cycles, fully correlated over entire S-N curve
extrapolation factor	ξ_{ext}	normal	$\mu_{\xi_{\text{ext}}} = 25.126$ $\sigma_{\xi_{\text{ext}}} = 0.2513$	applied to damage number resulting from the passage of actual traffic, based on linear extrapolation (circa 25 times in time) with CoV 0.01
critical damage number	Δ	lognormal	$\mu_{\Delta} = 1$ $\sigma_{\Delta} = 0.3$	taken as equal for concrete and reinforcement

Table 5.4: Overview of probability distribution parameters for each stochastic variable.

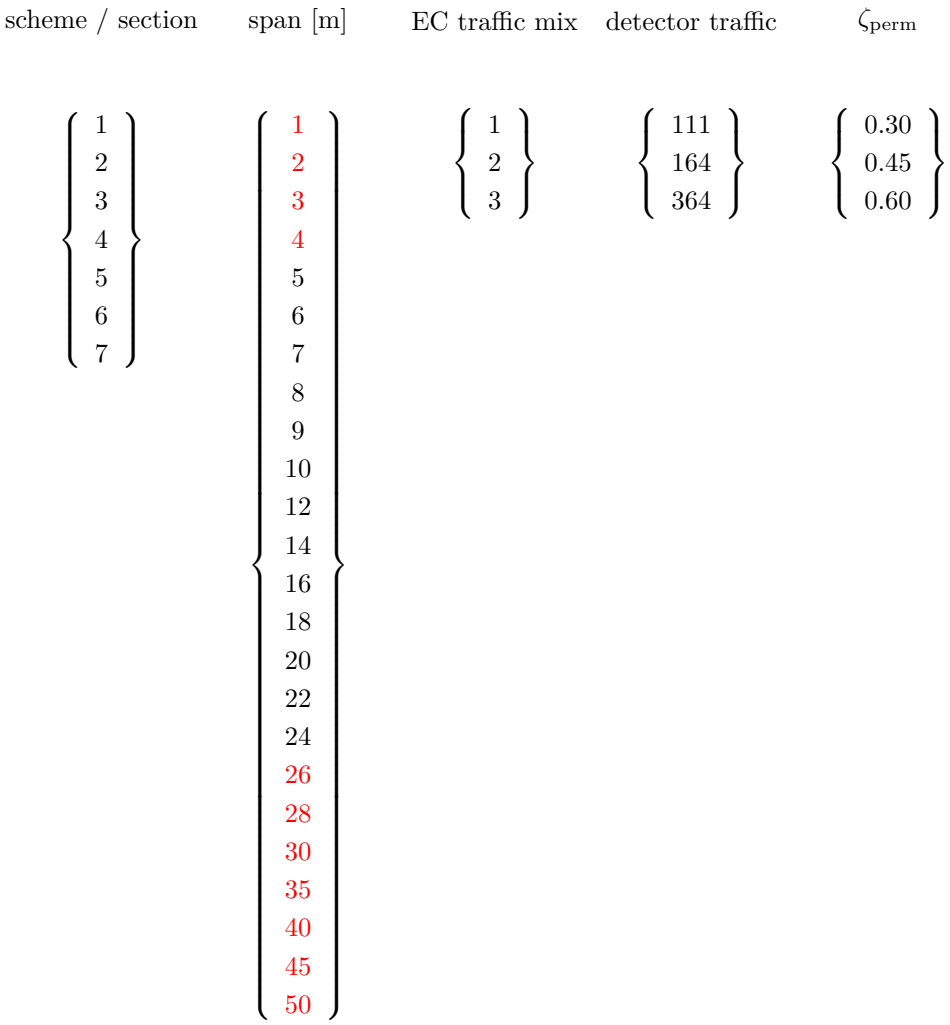

Figure 5.9: Combinations of variables for which the calibration is performed.

6 | Calibration Results

The results for all 5256 cases presented in the previous chapter have been obtained from an equal number of analyses. The reliability indices were exclusively determined using the procedure described in appendix H. Here, it is concluded that an approximation technique for obtaining the reliability is sufficiently accurate, and that the generation of a single signal for one analysis leads to satisfactory accuracy. The outcomes are plotted as a function of the span length, with the results for all three Eurocode traffic mixes and three permanent stress ratios combined in one graph. This allows for the results to be condensed to 21 graphs (7 structural schemes with traffic from three different locations). References to all figures are summarized in table 6.1 (all but one are placed in appendix I).

scheme	detector	results plotted in
1	111	figure 6.1
	164	figure I.1
	364	figure I.2
2	111	figure I.3
	164	figure I.4
	364	figure I.5
3	111	figure I.6
	164	figure I.7
	364	figure I.8
4	111	figure I.9
	164	figure I.10
	364	figure I.11
5	111	figure I.12
	164	figure I.13
	364	figure I.14
6	111	figure I.15
	164	figure I.16
	364	figure I.17
7	111	figure I.18
	164	figure I.19
	364	figure I.20

Table 6.1: Overview of calibration results, corresponding to all cases which were described in chapter 5.4.

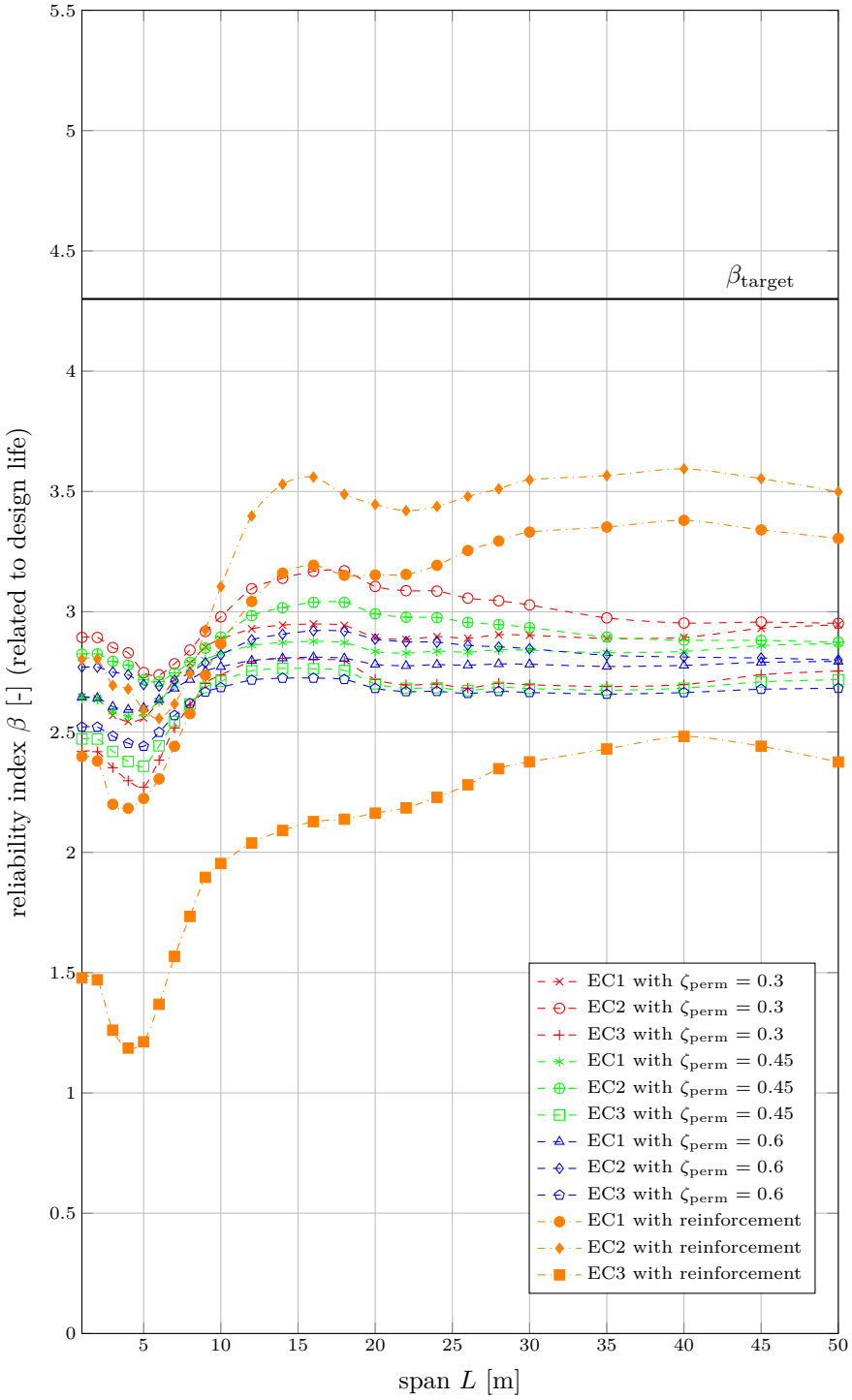

scheme	detector
1	111

Figure 6.1: SC1-ECX-111

6.1 Interpretation of results

One example from table 6.1 has been included in the main report and will be commented on. Figure 6.1 shows the resulting reliability indices for structures corresponding to scheme 1 (chapter 5.4), designed to withstand loading from all three Eurocode traffic mixes, while actually being loaded by traffic from detector 111. For cases regarding concrete in compression, three ratios of permanent stress have been included.

To interpret the results correctly, it is of vital importance to understand what these figures show. Each of the figures shows the resulting reliability indices for a number of different combinations of deterministic variables. For this, it was chosen to employ the span length as horizontal coordinate. In this way, these figures show the dependence of the reliability on the span length. Each point thus represents a unique case for which the reliability is calculated, resulting in a unique β.

Ideally, the reliability should be constant for each combination of parameters and traffic. However, it is allowed to be different for varying combinations of traffic records (detectors) and Eurocode traffic mixes. As each graph is constructed from a single record of measured traffic, combined with three Eurocode mixes, it should ideally show three horizontal lines (constant reliability). Here, it is implicitly assumed that concrete and reinforcement should be equally reliable. If not, there may be six horizontal lines, three for concrete and three for reinforcement. The absolute positions of these horizontal lines are, logically, also important. Ideally, these three lines should envelop the target reliability, showing that actual traffic can be categorized in between the load models (it will probably never be completely equal). It is noted that such an ideal picture is somewhat Utopic. Some variations will always be present, and the target reliability should also be interpreted as an approximate value. Therefore, small deviations are not deemed problematic, and even inherent to the accuracy of such analyses.

Observation of figure 6.1, taking into account the aforementioned remarks regarding the desired situation, leads to two conclusions:

- Compared to the target level ($\beta_{\text{target}} = 4.3$, see figure), the overall reliability level is too low (addressed in section 6.3).
- There are rather large variations in reliability for different sets of calibration variables (addressed in section 6.4).

Clearly, the reliability shows severe dependence on the calibration variables. Compared to reinforcement steel, the concrete shows little dependence, although the spread is still rather large. It is especially the reinforcement which shows very large variation with respect to the length of the span. Overall, there is a clear dip near 1-10 m spans. Examining the other cases, included in appendix I, a similar pattern is found. Note that, in principle, the reliability should also be invariant to the structural scheme (different schemes are included as different figures).

All cases (read: β's), which should ideally be equal, have been grouped. Because the spread in results is of interest, these sets are displayed as boxplots, see figure 6.2. This figure shows all of the calibration results in a very condensed manner. It is concluded that Eurocode traffic mix 3 clearly is not appropriate to use for design against the measured traffic from detectors 111, 164, and 364. This was of course to be expected (EC3 being the 'light traffic mix'), but it could not be concluded beforehand. The other two mixes perform similarly, EC2 outperforming EC1 slightly (again, as expected). In the remainder of this chapter, first a sensitivity analysis is presented, followed by an explanation of what causes the reliability to deviate from

the ideal situation explained in this section.

6.2 Sensitivity Analysis

In this section, a sensitivity analysis is conducted on the calculation method, or 'model', used for determining the reliability indices. Reasons for performing a sensitivity analysis as part of this thesis are: it is critical for model validation, and, it serves to guide further research. It can also be employed to help identify causes which result in varying reliabilities, as obtained in all calibration cases.

Normally, when using the first order reliability method (approximation technique as mentioned earlier in this chapter, and explained in appendix A) for the determinations of reliability, it would be logical to consider the α-factors as a measure for sensitivity of the system with respect to the variable of interest. However, in the practical implementation of the reliability calculation developed for this thesis, not all variables are included directly in the limit state function. As shown in section H.4, the variability in the signal has very little influence on the reliability, where it is noted that the signal includes the accuracy of measurements (both magnitude of axle loads as the velocity), and the dynamic amplification. In other words, the cumulative effect caused by differences in axle loads and dynamic amplification, converges over the design life of a structure[1]. Although of little importance for the spread between separately generated signals, the general principle of $E[X^n] \neq E[X]^n$ (explained in section 6.3) is expected to express differences in the parameters for the underlying distributions which are responsible for the creating of a random signal. It was therefore chosen to employ a method of sensitivity analysis which includes, besides the random variables used in the FORM calculation, also the influence of stochastic influences on the signal.

6.2.1 Method

The overall methodology which was chosen for this, is to vary each variable's distribution parameters, one by one, and observe the effect on the system. The distributions are all parametric, which allows for alteration of distributions through their underlying parameters. To include the effect of their magnitude *as is*, it was decided to alter them by a given percentage. Furthermore, to asses the non-linearity of the response, the parameters are altered to both greater and lesser magnitudes. In this way, three points are available for the response, theoretically capable of revealing convex or concave behavior.

Another possible method would be to add uncertainties in parameters one by one. However, due to the non-linear nature of the analyses, this would not provide a proper picture of sensitivities with respect to the parameters when the design situation is concerned.

An overview of cases for which the sensitivity analysis was done, each characterized by a single altered parameter, is presented in table 6.2. The plus-values (p_i^+) are calculated as the parameter value $+10\,\%$, while the minus-values (p_i^-) correspond to $-10\,\%$ (both for concrete and reinforcement).

The accuracy of the velocity measurement is an exception between, as first of all: it is added to the measured velocity, and therefore alterations are independent of the measured value itself. Also, because the bias is zero, adding or subtracting percentages will not alter the value. Effectively, this parameter ($b_{\hat{v}}$, see chapter 5) is skipped in the sensitivity analysis, which was accepted for this analysis. Note that a different parameter alteration could be thought of, but this would skew the comparison, that

[1] Of course their mean values are still of great importance.

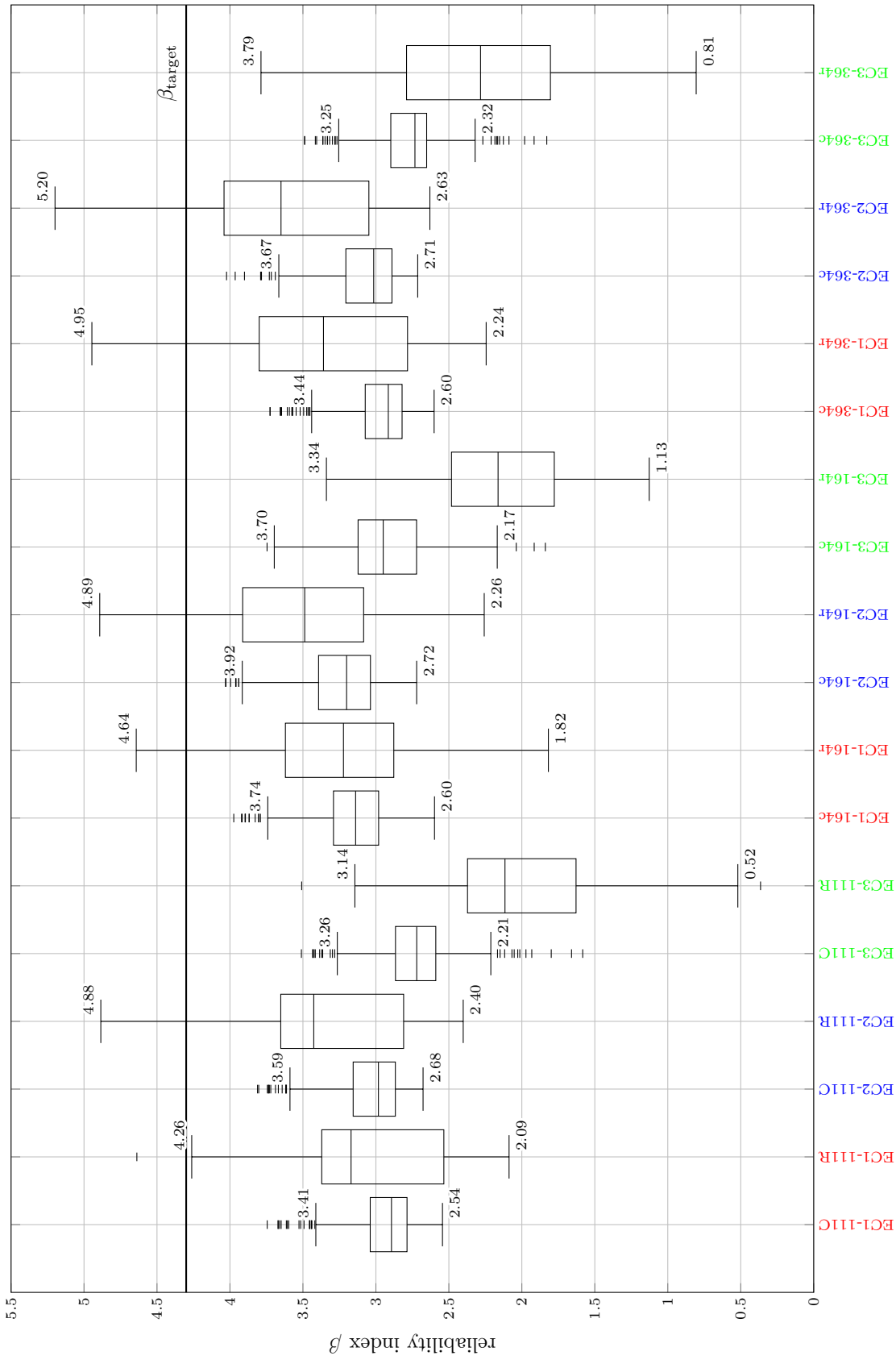

Figure 6.2: Overview of calibration results. Label-format is 'Eurocode traffic mix - detector - concrete/reinforcement'. Results from all structural schemes are combined, for concrete also those for differing values of ζ_{perm}. Convention for outliers: exceeding 1.5 times the inter-quartile-range from the upper or lower quartile.

variable	symbol	parameter	p_i^-	p_i	p_i^+
measurement error velocity	$\hat{v}$	$a_{\hat{v}}$	-1.251	-1.390	-1.529
		$b_{\hat{v}}$	0.000	0.000	0.000
		$c_{\hat{v}}$	1.251	1.390	1.529
measurement error load	$\hat{F}$	$\mu_{\hat{F}}$	0.900	1.000	1.100
		$\sigma_{\hat{F}}$	0.056	0.062	0.069
dynamic amplification	$\hat{\Phi}$	$\mu_{\hat{\Phi}}$	0.900	1.000	1.100
		$\sigma_{\hat{\Phi}}$	0.090	0.100	0.110
extrapolation factor	ξ_{ext}	$\mu_{\xi_{\text{ext}}}$	22.61	25.13	27.64
		$\sigma_{\xi_{\text{ext}}}$	0.452	0.503	0.553
model uncertainties	θ_S	μ_{θ_S}	0.900	1.000	1.100
		σ_{θ_S}	0.180	0.200	0.220
variability in strength (concrete)	$\bar{s}$	$\mu_{\bar{s}}$	1.023	1.137	1.251
		$\sigma_{\bar{s}}$	0.077	0.086	0.095
variability in strength (reinforcement)	$\log N^*$	$\mu_{\log N^*}$	5.94	6.60	7.26
		$\sigma_{\log N^*}$	.267	0.297	0.327
critical damage	Δ	μ_Δ	0.900	1.000	1.100
		σ_Δ	0.180	0.200	0.220

Table 6.2: Overview of parameter-alterations for the sensitivity analysis.

is, the relative sensitivity, and is therefore omitted. The other parameters, $a_{\hat{v}}$ and $c_{\hat{v}}$, which characterize the accuracy of measurements in terms of spread, are kept equal in terms of absolute magnitude. This means that the distribution is always symmetric, or $a_{\hat{v}} = -c_{\hat{v}}$.

To express the results, being the deviations in resulting reliability, relative differences were determined using:

$$\hat{\beta}_{\pm} = \left\langle \frac{\boldsymbol{\beta}_{\pm} - \boldsymbol{\beta}_0}{\boldsymbol{\beta}_0} \right\rangle \tag{6.1}$$

where

$\hat{\beta}_{\pm}$ = sensitivity index for the reliability, for positive or negative (+ or −) alterations respectively

$\boldsymbol{\beta}_{\pm}$ = vector of reliability indices for all spans, obtained using altered parameters (either + or −)

$\boldsymbol{\beta}_0$ = vector of reliability indices for all spans, obtained using original parameters

and the angled brackets symbolize taking the mean value. Division of the vectors in equation 6.1 is performed element-wise, resulting in a vector that is of equals size. It is of the elements in this vector, that the mean value is determined.

6.2.2 Model sensitivity

Results from the sensitivity analysis for concrete are given in figure 6.3 and in figure 6.4 for reinforcement. It is emphasized that, because the alterations were chosen as percentages of the original values, the magnitude of parameters is included in the results. In other words, altering two parameters with equal function, although different in magnitude, would result in different relative reliabilities, because and only because the original values of these parameters differ. For the overall reliability though, this gives insight into each parameters influence, both relative as absolute.

The sensitivity analysis was performed for a set of spans, the same as in the main analyses. This was done in order to find out whether the sensitivity of the reliability to parameters varies with the span. It was expected to do so, mainly because of the influence operator, which includes summation. This means that, as the span increases, and thus allows for a larger number of simultaneous axles to be present, variations of individual axle loads will be somewhat dampened. Such behavior was observed, although differences were rather small, order of magnitude 10% of $\hat{\beta}_{\pm}$ (over the entire range of spans). Therefore, it was decided not to include graphs of the effects on reliability as a function of the span. Instead, all values were grouped and $\hat{\beta}_{\pm}$ was defined.

Clearly, the uncertainties in stresses outweigh the influence of parameters in the damage domain by an order of magnitude. In itself, this is not a surprise. It is more of a confirmation of what was already expected. Interestingly, the damage number domain was treated proportional to time. Following along this path of thought, and considering that the reliability only influenced to a minor extent by parameters in the damage domain, the conclusion can be drawn that the same can be said for time.

The results of the sensitivity analysis can be used to estimate the effects of parameter variations, without having to do the entire analysis again. For instance, if one would obtain new information regarding the dynamic amplification factor Φ, the effect of this information on the reliability can be estimated directly, without the need to perform analyses all over again.

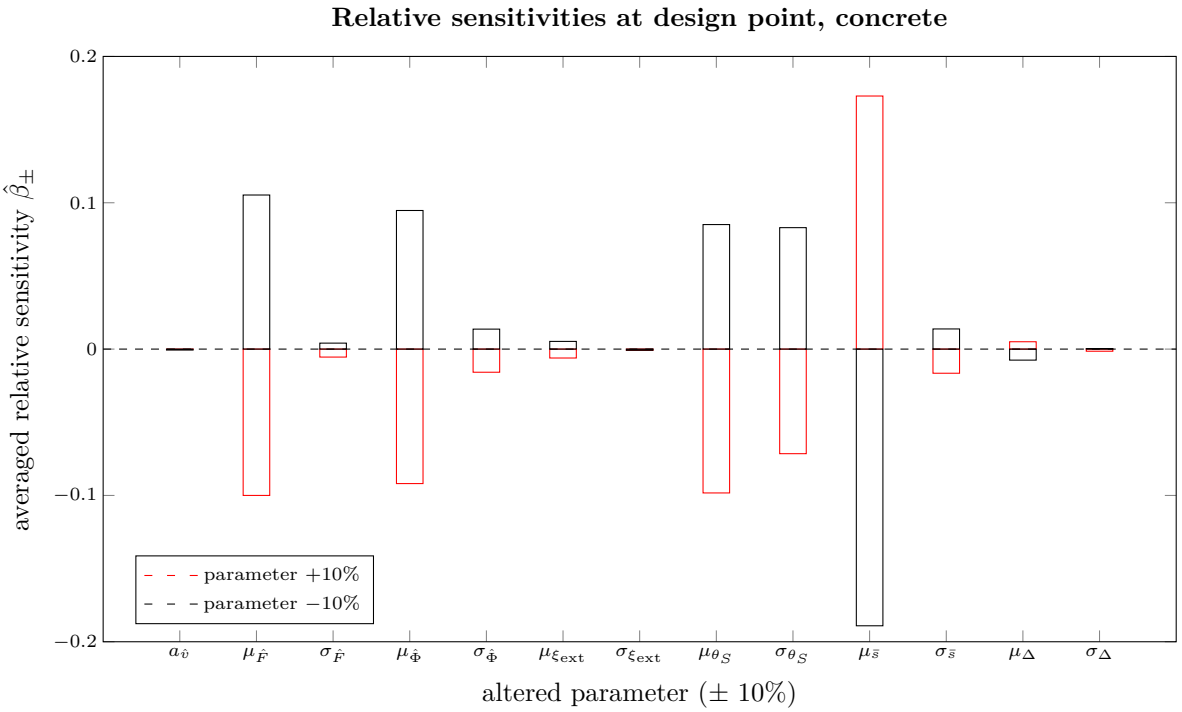

Figure 6.3: Results of the sensitivity analysis using parameter alterations (concrete).

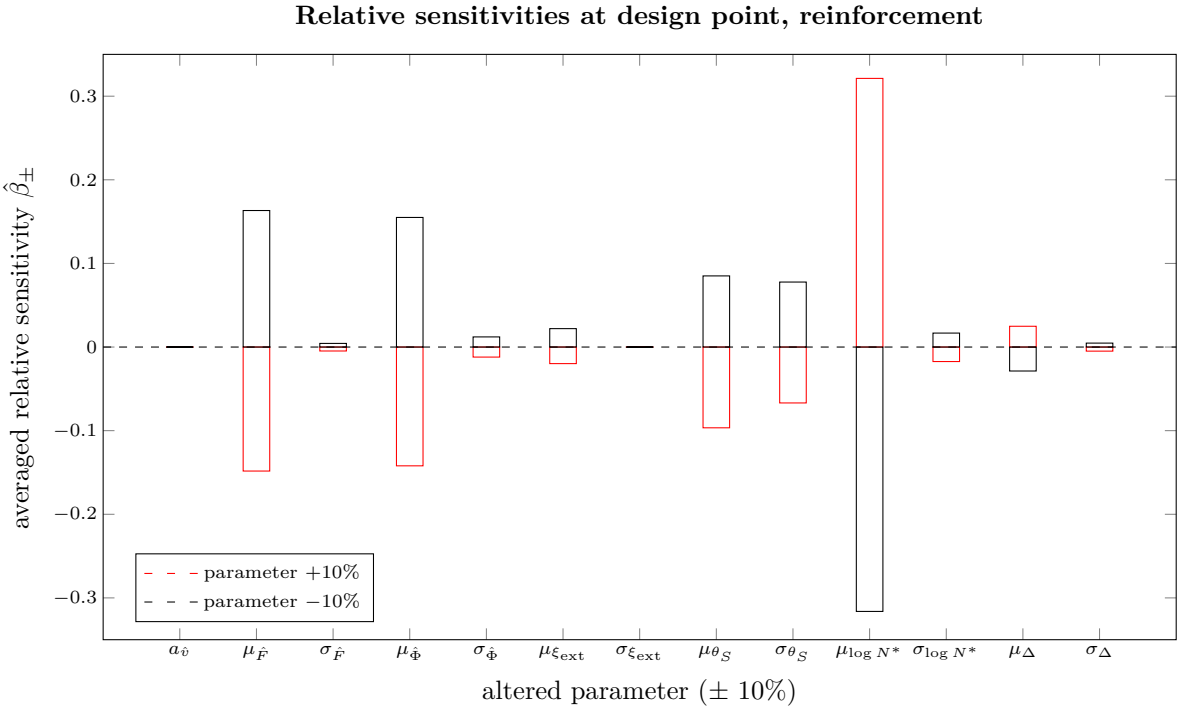

Figure 6.4: Results of the sensitivity analysis using parameter alterations (reinforcement).

It is also helpful in directing future research, as it reveals if there are e.g. quick wins. In chapter 5 it was stated that some aspects were covered by little usable information, being:

- dynamic amplification factor;
- modeling uncertainties;
- critical damage number (both concrete and reinforcement).

The critical damage number was shown not to influence the reliability in a significant extent, especially not when concrete is of interest. This means that the first two items from the aforementioned list are important to investigate in future endeavors.

Focusing on the dynamic amplification factor: effectively, the Eurocode's value was used as a mean for this, motivated by a lack of better information. Therefore, this should be investigated thoroughly, also to gain insight into the correlations between or within passages. A similar argument is given for the investigation of model uncertainties. Here, full correlation over the service life was assumed, as would be the result of errors made in determining the influence line. Clearly, this results in significant dependence of the reliability to the standard deviation of model uncertainties. Therefore, the reliability could benefit greatly from new information on these aspects.

6.3 Global deviation

As a first step, the overall difference between the reliabilities (in an average sense) and the target level is addressed. Employing the results from the sensitivity analysis, and focusing on three components of the load which all work in the stress domain (measurement uncertainties, dynamic amplification, and model uncertainties), the following is noted:

- Regarding the measurement uncertainties and dynamic amplification: the uncertainty was applied per axle. This means that a unique factor is drawn from a distribution, for each axle which passes the structure. As many axles pass the structure during its (simulated) design life, such uncertainties converge to a stable mean level (law of large numbers). In the Eurocode, this is most probably used as an argument for setting the partial factor for fatigue loading equal to unity. It is noted that, from a citation in CEB (1988) based on a document which could not be obtained (*Agreements for Fatigue Design*, Coordination Group for Eurocodes, 1988), the partial factor for fatigue loading may be taken equal to 1 based on the notion that any distribution function for loads would converge to its expected value.
- The modeling uncertainties are implemented using a different method. A high level of correlation in modeling uncertainties is to be expected, for example when a mistake is made in creating an influence line, which is subsequently used for an entire analysis. This results in systematic deviations which do not converge over the design life of the structure. It could already be concluded from the sensitivity analysis that this influences the reliability to a great extent.

It is especially this argument of correlation between uncertainties over the structure its life, that falsifies the Eurocode assumption of convergence. Expanding this idea, **it is concluded that the partial factor for fatigue loading being equal to unity in the Eurocode, is not justified at all**[2]. This would only apply for uncorrelated

[2]It could be that the characteristic load model is defined in such a way that it provides a sufficient margin of safety. However, it is assumed here that a characteristic load model preferably corresponds to the actual loads which can for instance be measured, in this case the traffic records.

uncertainties over the life of such a structure.

Even when all uncertainties would be uncorrelated, a partial factor of 1 may not necessarily result in sufficient reliability. Take for instance a normal distribution with mean value of 1 and a coefficient of variation larger than zero. Imagine that this can be used to model the uncertainties in stresses. As the interest is on the damage number, which partially is a result of the stresses, these assumed uncertainties will present themselves in the damage number as well. Because the S-N curves used for determining the damage number are quite non-linear with fatigue exponent far greater than 1, all uncertainties above 1 (the mean of the assumed distribution) are amplified. Below this level, these are decreased, but with a smaller impact on the overall result. This implies that the expected value is increased, in general: $E[X^m] \neq E[X]^m$ provided that $m \neq 1$. For m larger than 1, as with these fatigue calculations, the expectation is increased. So, **even when the variations have dampened out in time, the non-linearity of the stress-damage relation still leads to an increased average damage number, caused by these variations**.

A final remark regarding the global deviations is that further research is required for the model uncertainties and their correlations. Also, dimensional uncertainties, which were neglected in this thesis, result in systematic differences between calculated and actual stresses. These should therefore be implemented in future analyses. The same conclusion can be drawn for dynamic amplification. These depend on characteristics of the structure, and that it is quite hard to model dynamic behavior correctly, let alone to replace it by some factor. Therefore, it is probably also prone to significant variations. More problematic is that these characteristics of the structure will also induce correlation between passages, which can be fatal for the reliability. Therefore, further research is also indispensable for the dynamic amplifications, and especially their correlation between passages.

6.4 Origin of span-dependence

In this section, the mechanisms which cause differences in reliability for variations in parameters (especially the length of the span) are analyzed. Overall, two mechanisms will be illustrated:

- differences in traffic;
- non-linearity of the S-N curves.

6.4.1 Differences in traffic

First, the most trivial source of span-dependent reliability is investigated, namely the differences in traffic. Central throughout this report, was the notion that one can not just compare sets of trains due to their array of characteristics. Therefore, it was decided to compare based on the load effect, namely the damage number. In this section, differences between traffic are assessed in a direct manner by comparison of their limit values for the proportionality-factor u (see chapter 4). This is similar in meaning to comparing based on damage number, however it aids clearer interpretation of the differences (because the damage number amplifies such differences severely). A solid marker for the aggressiveness of measured traffic, compared to the load model, therefore seems to be the ratio of u_{limit}-values (ratio of stress-levels which exactly result in attainment of the limit state for both the Eurocode traffic mix and the measured traffic). In formulae (both for detector 111 traffic and the EC1 traffic mix,

both for reinforcement):

$$\sum \mathcal{D}\left(\mathcal{R}\left(u\,\mathcal{I}\left(\mathbf{H}_{\mathrm{D111}}\right)\right)\right) = 1 \qquad \rightarrow u_{\mathrm{limit,D111}} \tag{6.2}$$

$$\sum \mathcal{D}\left(\mathcal{R}\left(u\,\mathcal{I}\left(\mathbf{M}_{\mathrm{EC1}}\right)\right)\right) = 1 \qquad \rightarrow u_{\mathrm{limit,EC1}} \tag{6.3}$$

using which the ratio of limit-values is expressed as

$$\bar{u} = \frac{u_{\mathrm{limit,D111}}}{u_{\mathrm{limit,EC1}}} \tag{6.4}$$

Results should be interpreted as follows: higher aggressiveness of traffic results in a lower u_{limit}. Therefore, the lower $\bar{u}$, the more aggressive the detector traffic is compared to the Eurocode load model. The values of $\bar{u}$ have been plotted in figure 6.5. Note that the signal for detector traffic was determined using uncertainties in measurements and dynamic amplification.

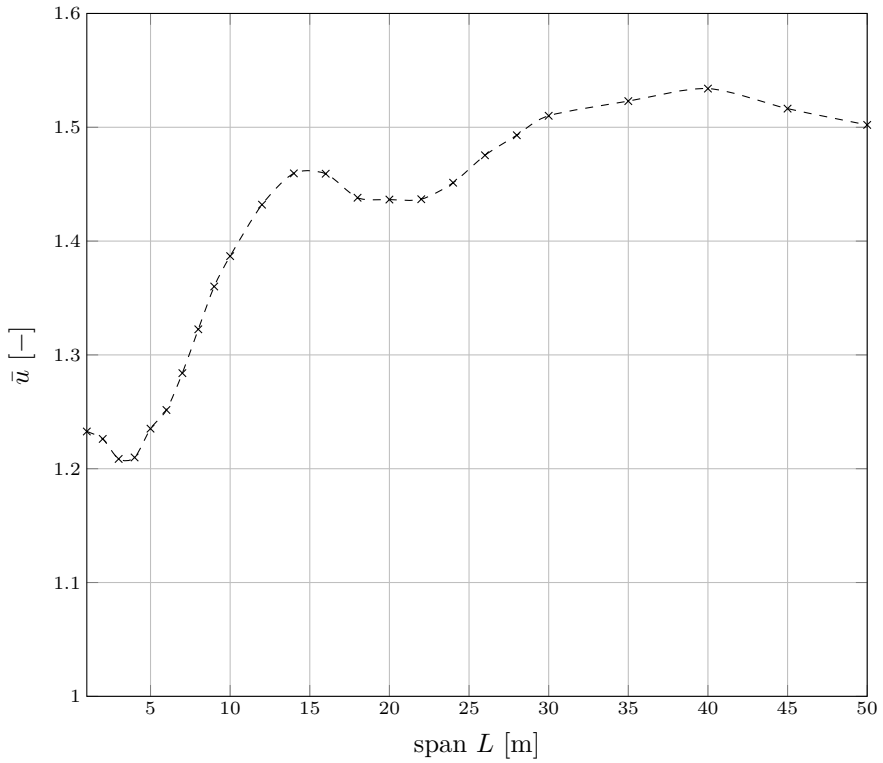

Figure 6.5: Ratio of limit values for u (Eurocode over measured traffic). Reinforcement, scheme 1, detector 111 traffic and Eurocode traffic mix 1.

Comparing the dependency of $\bar{u}$ with respect to the span length, it may be clear that the shape resembles that of the resulting reliability index quite precisely (compare with figure 6.1, EC1 for reinforcement). Therefore, **it can be concluded that the main source of non-constant reliability originates from differences between the measured traffic and the load model traffic**. Further investigation was clearly appropriate.

The focus was especially at the apparent dip for 1-10 m spans (for this structural scheme). Axle distances of the Eurocode traffic mixes and the measurements were compared, but no clear reason for this dip could be found. Therefore, the stress-signals resulting from the passage of particular axle systems were generated. When

analyzing the results, something stood out: some specific span lengths seem to result in a phenomenon which closely resembles interference between signal components. Cycles will not only change in magnitude, more importantly and somewhat surprising, cycles disappear for these 'critical interference lengths'. The effects is best explained by an example featuring two (unit) axle loads at a distance a, passing over a simply supported beam with span L.

The focus is on the ratio of a/L, which is varied accordingly (see figure 6.6, left column). For large ratio's, being large distances between axle loads relative to the span length, the structure is loaded by each axle consecutively. This result in two full load cycles, each following the influence line. However, when a/L becomes smaller than 1, interaction between these signals arises, in this work denoted as '**interference**'. Considering this particular example, the result is a decreasing level of unloading in between cycles, and therefore a decreased effect. Now, when a/L attains a value of exactly $1/2$, the cycle in between completely disappears. Important to realize is that the stress **changes** are of interest. For this latter value of a over L, the complete vanishing of cycles, effectively means that the bridge experiences a load effect equal to that of a single axle passing. Therefore, this ratio is denoted as the 'critical ratio for destructive interference'.

Repeating this procedure for three equally spaced axles (see figure 6.6, middle column), interestingly, the same behavior is observed. Upon attainment of the critical ratio, the destructive interference now causes two cycles to vanish, leaving only a single stress change. The load effects is therefore equal to that caused by a single axle load passing. Consider, for example, the third Eurocode traffic mix (EC3). All heavy loads (for instance larger than 200 kN) are included through the prescription of reference train type 5 (of which one wagon is used in the right column of figure 6.6). Within this train, however, on the level of bogies, all axles are found in sets of three, with equal distance in between them. Taking into account the notion of a critical span for destructive interference, it is concluded that such trains are very susceptible to this phenomenon. Passing a simply supported beam, with perfectly triangular influence line, the critical interference distance was shown to be equal to twice the axle distance. In case of reference train 5, this amounts to $2 \times 1.8\,\mathrm{m} = 3.6\,\mathrm{m}$. This coincides with the significant dip in reliability which is observed for calibration cases. Expanding on this theory, one could superimpose influence lines with offsets to unravel more critical patterns.

Now, consider what the influence is on the damage number. For this, the bogie consisting of two axles is used (left column). The cycles are counted, after which some damage number is calculated (merely proportional to a damage number), by summing all ranges, individually raised to a power m. Some realistic values for m have been used to plot the results in figure 6.7. The vertical axis is scaled logarithmically to fit all values. Clearly, the damage number is constant at first (for large spans compared to the axle distances), then decreases with increasing interference (compare figure 6.6, first column, for $a/L = 1$, $a/L = 2/3$, and $a/L = 1/2$). The minimum is at $a/L = 1/2$ ($L/a = 2$), after which the damage number increases. This pattern resembles the drop in reliability observed in the calibration quite accurately.

Another interesting finding is that concrete is affected to a lesser extent than reinforcement steel. Arguing from the observed phenomenon of destructive interference; this only alters the number of cycles. Comparing the S-N curves for concrete and reinforcement (see figure 6.8), clearly the former is more sensitive with respect to changing cycle magnitudes (larger fatigue exponent). Inverting this statement, it can be said that reinforcement is more sensitive with respect to the number of cycles. Because destructive interference only alters the number of cycles, it could be

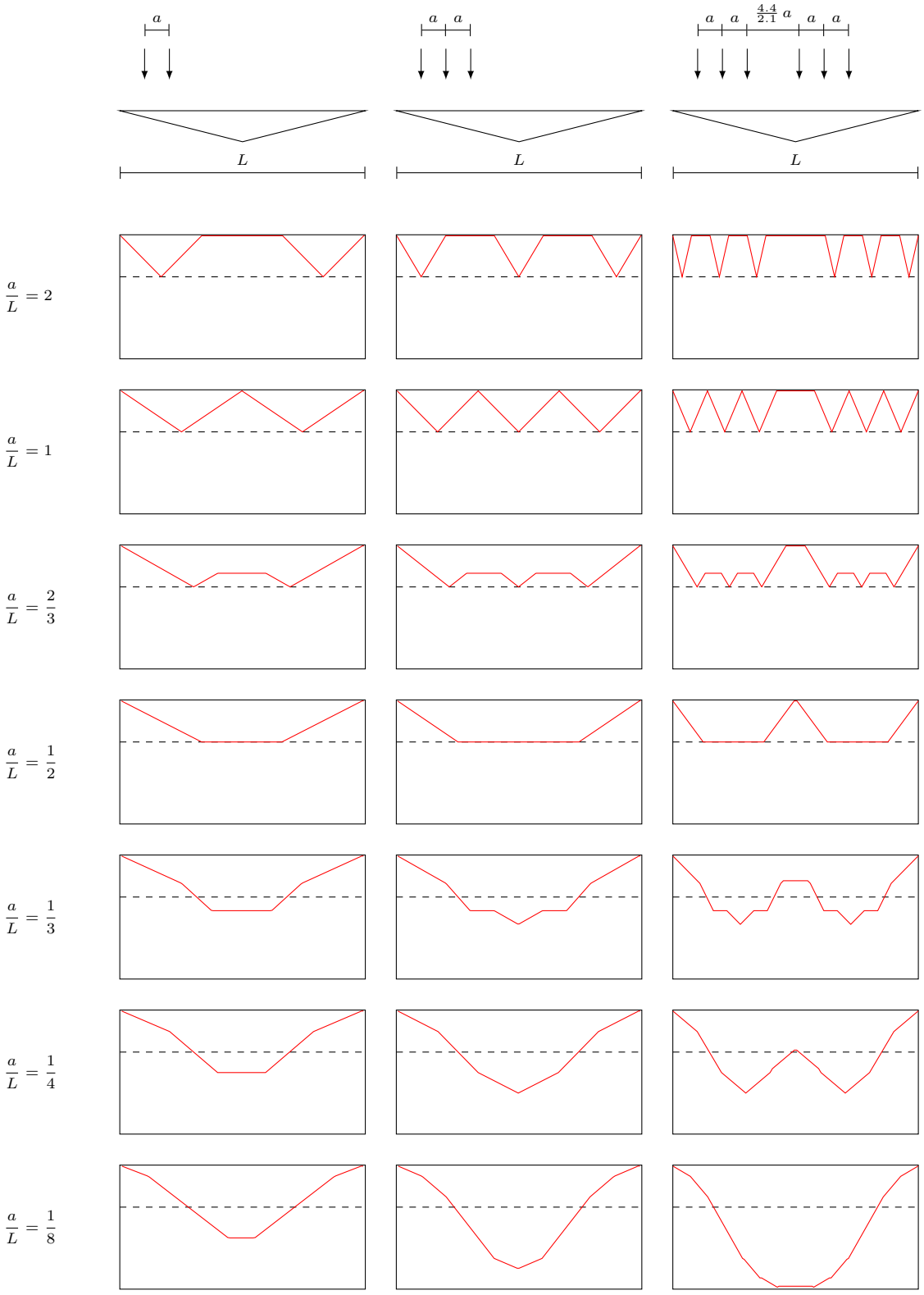

Figure 6.6: Stress-signals for passing of axle systems with various ratios of axle distance (a) to span length (L).

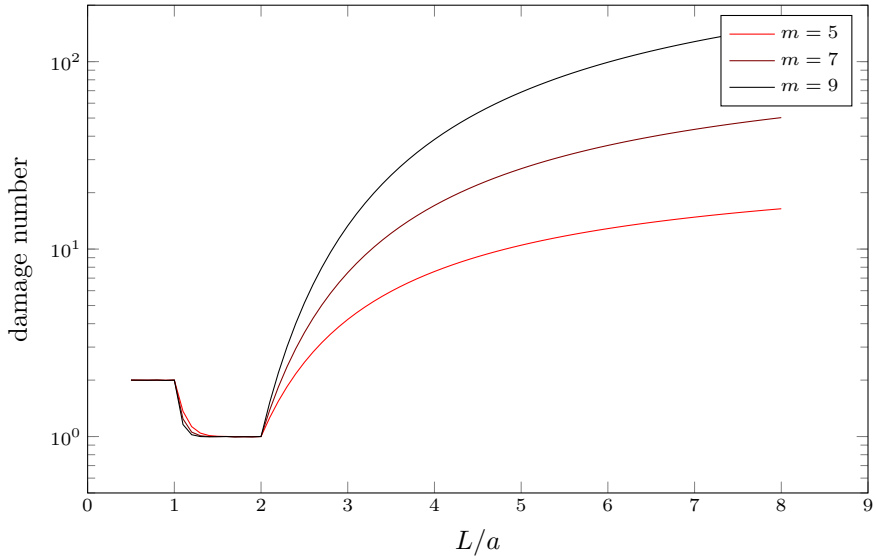

Figure 6.7: Relative damage numbers for different ratio's of span length (L) over axle distance (a). Note that this ratio is reciprocal to the ratio used in figure 6.6.

expected that reinforcement would be affected more, which corresponds to findings of this study.

Now, this destructive interference would not be problematic in case of equal behavior for real traffic. However, in real traffic the axle loads differ more, and a variety of axle distances presented itself. Therefore, the susceptibility of real traffic to destructive interference is only minor. This concludes the explanation of deviations in reliability caused by differences in traffic.

6.4.2 Non-linearity of the S-N curves

Ultimately, another cause of span-dependent reliabilities was identified as the being inherent to the S-N curve. In figure 6.9, spectra of stress ranges are portrayed for different span lengths. The spectra are given in the form of histograms, where the edges were chosen in such a way, that the bars are of equal width on logarithmic scale, as opposed to linear scale. In this way, anyone reading the graphs does not have to account for a different number of bars per unit length.

Furthermore, the design S-N curve for reinforcement steel is drawn. The dashed lines mark constant distance offsets from this S-N curve. Note that on logarithmic scale, these constant offsets correspond to constant multiplication factors: in this case, each dashed line signifies a division by 10, compared to the previous line. Also, as derived in appendix D, the dashed lines connect all points corresponding to an equal damage number. Taking the aforementioned into account, one can use these graphs to conclude which part of the spectra is responsible for most of the damage. Starting from the red line, move to the left, one dashed line at a time. Then, the first time where a dashed line touches a histogram bar, signifies the most damaging bar. Well, technically also the number of bars is of importance. However, this method allows for a quick visual assessment, just what is required in this case. Doing so for all spectra, the following can be observed:

- for short(er) spans, the main part of the damage is done by those cycles that are somewhat below the kink in the S-N curve;

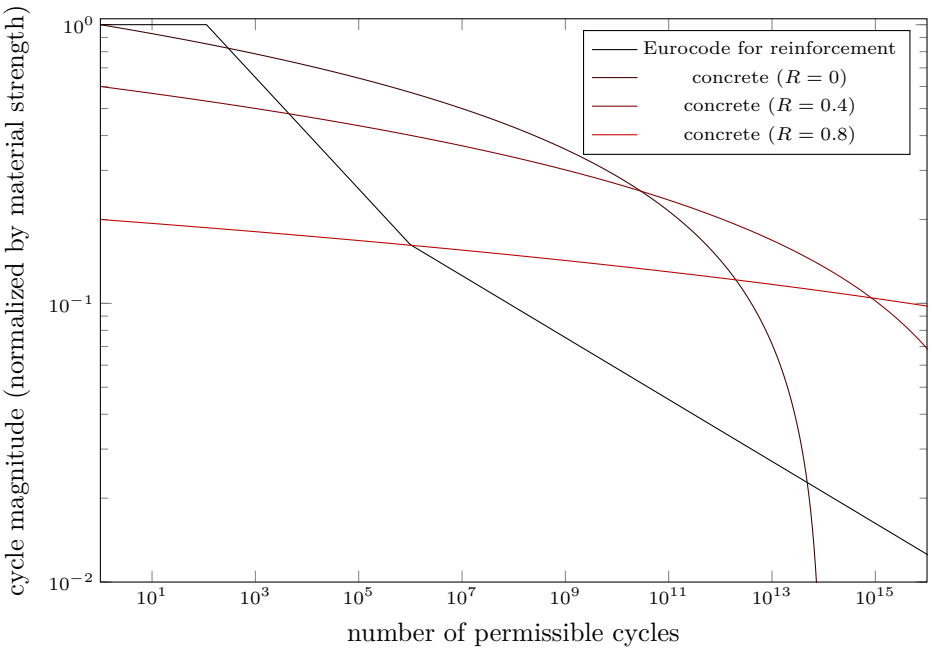

Figure 6.8: S-N curves for reinforcement and concrete (based on Lantsoght, 2014).

- for long(er) spans, the main part of the damage is done by a small portion of large stress ranges, which are near, or even at, the kink in the S-N curve.

Now, special attention should be paid to the kink in the S-N curves. The fatigue exponent, which changes here, is a measure of the sensitivity of the material with regard to changes in stress, given a fixed number of repetitions. The S-N curve therefore shows that the material is less sensitive to changes in stress above the kink, than below. Considering a reliability analysis, where for example modeling uncertainties could potentially cause the entire spectrum to shift upwards, it is now analyzed what consequences this has.

According to appendix D, the damage number will scale proportionally to changes in overall stress level, raised to a power equal to the slope of the S-N curve. Clearly, when taking into account the above observations, it can be concluded that the part that is mainly responsible for the damage number, shifts upwards in terms of stress range, for increasing spans. Thereby, the sensitivity with respect to changes in overall stress levels (e.g. modeling uncertainties), decreases significantly. This is therefore caused purely by the shape of the spectrum interacting with the shape of the S-N curve.

Its effect was assessed by using measured traffic as both the design constraint, and as the actual loading. In this way, all differences in traffic are eliminated. The resulting reliabilities are displayed in figure 6.10. The reliability is not constant for all spans. However, it can be concluded that the influence of the S-N curve non-linearity, interacting with the shape of the stress spectrum, is somewhat small.

6.5 Conclusions

- The reliability provided by design according to the Eurocode, given loading by the measured traffic, was determined and presented for all cases discussed in chapter 5.

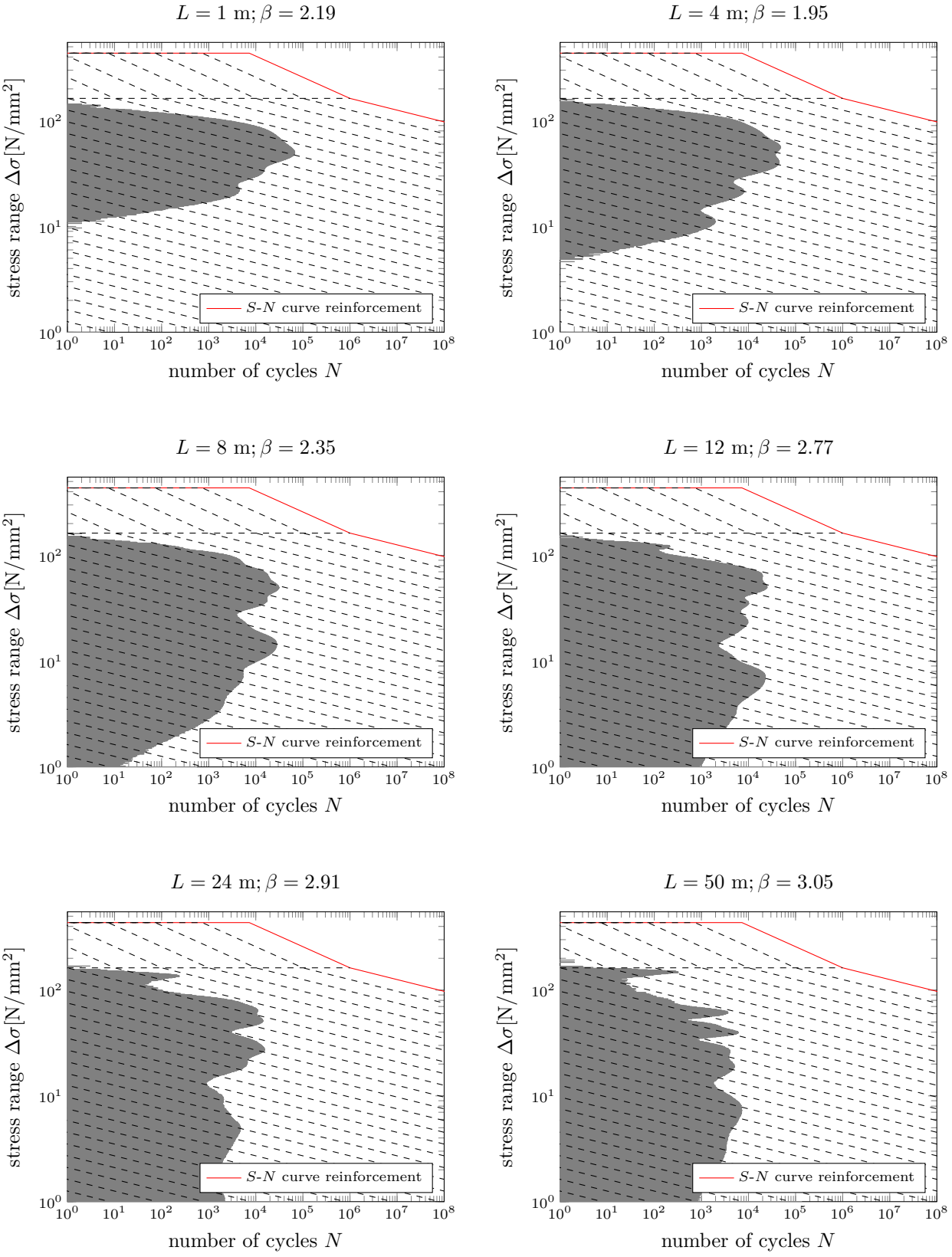

Figure 6.9: Spectra for different spans. Scheme 1, detector 111.

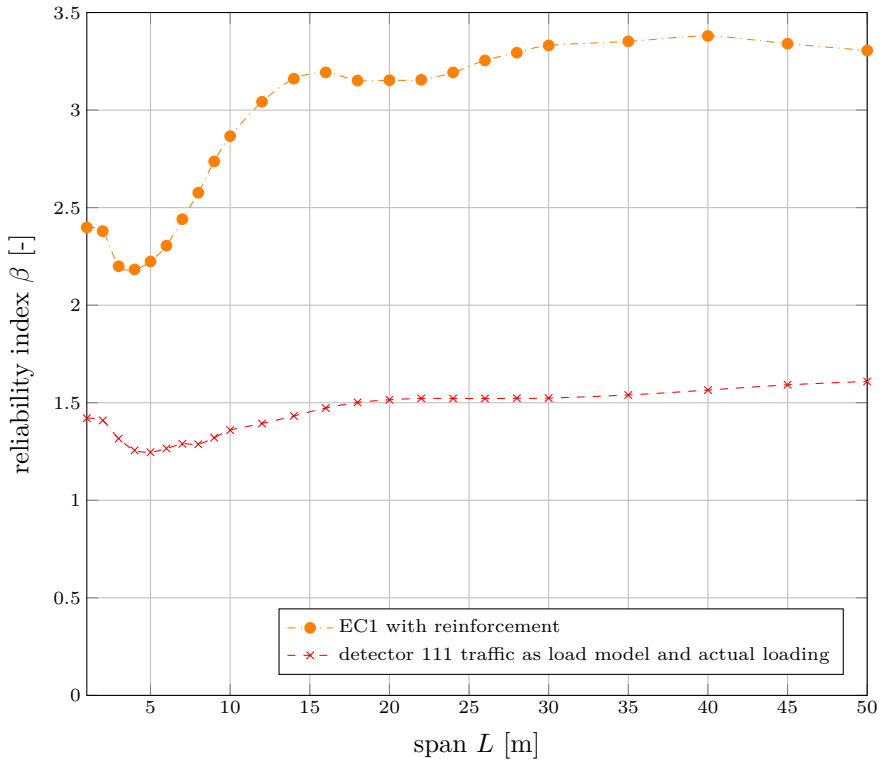

Figure 6.10: Reliability as a function of the span. Reinforcement, scheme 1, detector 111 traffic as both the load model as the design constraint (no Eurocode). For comparative reasons, the reliability obtained using the Eurocode traffic mix EC1 is added (which, therefore, **is** according to the Eurocode).

- Regarding the resulting reliabilities, two issues were identified. For both, the main cause was shown:
  - The overall reliability level is too low, compared to the target reliability set in chapter 3. Cause for this is the Eurocode's design fatigue load, which should be more severe. This, in turn, is caused by the partial factor for fatigue loading being equal to 1 (it is also possible to achieve the desired reliability using characteristic loads, granted that these are sufficiently aggressive). This value was justified by the notion that all uncertainties relating the fatigue loading itself would converge in time, which is generally true. However, the partial factor for loading also includes uncertainties in the modeling of loads and structures. These are systematic deviations, which do therefore not converge in time. The partial factor should include an appropriate margin of safety for these, or else the reliability suffers, as is currently the case.
  - There is a rather large spread in reliability, for different combinations of parameters. This is problematic, because the provided reliability should, ideally, be constant. The differences between the Eurocode traffic mixes and the measured traffic were shown to be dominant for the spread in reliability. The main issue with these, is that for certain spans and influence lines, a phenomenon was identified where cycles will vanish (coined as 'interference' in this thesis). In itself this is not a problem, if it would

also appear equally with measured traffic. However, measured traffic is much more diverse in its axle loads and distances, and therefore less prone to this interference, resulting in significant variations in the reliability for different spans.

- A sensitivity analysis has been performed, assessing the sensitivity of the calibration procedure with respect to the various parameters (all stochastic variables). Combining the conclusions with those drawn in chapter 5, it was concluded that the following items should be prioritized in further research:
  - dynamic amplification;
  - modeling uncertainties.

  For these it is also of significant importance to assess correlation between individual axles, between passages of trains, and between designs of structures (modeling uncertainties).

7 | Conclusions

In the introduction it was stated that both the required and provided reliabilities are needed for a comparison. This comparison corresponds to design according to the Eurocode, while being loaded by measured traffic. Also, other uncertainties in the design were incorporated in analyses, in order to calculate the reliabilities of structures.

For the fatigue limit state of reinforced concrete, the target reliability for ultimate limit states corresponding to consequence class 3 is adopted for this work, i.e. $\beta_{target} = 4.3$ ($P_{F;target} = 10^{-5}$) corresponding to the design life. Future differentiation in target reliability levels with respect to conditions of inspectability and detectability of fatigue in (reinforced) concrete may however allow lower reliabilities for some components.

The provided reliability was determined for a large variety of cases, for both concrete and reinforcement steel. Numerical figures can be found in chapter 6, summarized in figure 6.2. The reliability is far from constant for all cases, and was shown to depend quite heavily on the structure its span length. The most important reason was identified as the difference between the load model traffic, and the measured traffic records. Also, the non-linear nature of the S-N curves, interacting with the shape of the span-dependent spectra, contributes.

In the Eurocode load model for fatigue, heavy axle loads occur at constant axle distances, and are mainly of constant magnitude. For certain structures, at specific lengths, the structure will not be unloaded in between axle loads passing over it. Therefore, the number of stress changes is reduced, a phenomenon coined 'interference' in this thesis. Real traffic is far less constant in its axle distances and magnitudes, and therefore suffers from this phenomenon to a lesser degree. Important to note is that this phenomenon mainly seems affects the reliability of short(er) spans, order of magnitude 1-10 m.

Furthermore, the converging behavior of variations and uncertainties of fatigue loads does not occur for all aspects (not for model uncertainties, and possibly not for dynamic amplification; it was argued that these are somehow correlated between passages). Such behavior should be covered by the Eurocode. In practice, this should be done by increasing the design loads for fatigue.

The provided reliabilities, as calculated in this thesis, were generally below the determined target reliability, thereby answering the research question. For these analyses, traffic records from Tricht, Schiedam, and Zeist were used, which seemed the most aggressive available. It is especially the uncertainties or variations that are correlated over the design life of a single structure, which are responsible for not meeting the desired reliability.

Overall, it is concluded that the requirement regarding reliability is currently not met by appliance of the load models in NEN-EN 1991-2.

7.1 Recommendations

First and foremost, there are some recommendations regarding a new load model:

- In order to satisfy the demand set by the target reliability, it is highly recommended to increase the design loads (with the current partial factor being equal to 1, the design loads are also the characteristic loads). Such an increase can be achieved either through raising the characteristic loads, or by raising the partial factor on fatigue loads. To enable compatibility with measured loads, which were clearly lower than the loads prescribed in the Eurocode, it might be wise to introduce a format with a partial factor larger than 1, which is also valid for measured loads. This would also mean that the current characteristic Eurocode load model should be adjusted to resemble measured traffic to a greater extent. Until further investigations provide additional insights, no recommendation in terms of a numerical figure can be given for the partial factor for fatigue loading.
- A novel load model (traffic mix) should be created, with an emphasis on variation in spacing between **heavy** axle loads, using the insight that these are responsible for practically the entire fatigue load effect. The variations between axle distances should be sufficient to correspond to measured traffic, by preventing certain span lengths for which the phenomenon coined 'destructive interference' occurs. In practice this implies a traffic mix with similar distances between heavy axle loads, as measured traffic. Using this novel traffic mix, which should contain characteristic loads of similar magnitude as measured loads (see previous point), a numerical value for the partial factor on fatigue loading can then be determined.

Regarding the analyses, the following aspects were both of significant importance for the determination of provided reliability, and hard to quantify:

- Model uncertainties, i.e. the accuracy with which, ultimately, the stresses/strains in a cross-section are determined. Difficulties in quantifying were in both the accuracy of individual calculations and in correlation between the results of subsequent calculations.
- Dynamic amplification, with the same remarks as for model uncertainties.

This was caused by a lack of information. Overall, it is recommended to invest in future investigations for the aspects mentioned above.

For existing structures, designed using the current Eurocode fatigue verification procedure: it has been shown that their reliability is insufficient. Within all railway structures, three categories can be distinguished with regards to this aspect:

1. Structures for which the fatigue limit state proved governing in design. These are of primary importance.
2. Structures for which the fatigue limit state was of similar importance as ultimate strength. One should consider that, using a modified verification procedure which provides the target reliability, the fatigue limit state could prove governing subsequently.
3. Structures for which the fatigue limit state proved to be of minor importance, can be addressed with lesser priority.

For structures in categories 1 and 2, it should be checked whether the structure is actually subjected to heavy loading (such as at Tricht, Schiedam, or Zeist). If so, one could try to obtain measurements of local stresses/strains at fatigue-critical details in order to eliminate modeling uncertainties and uncertainties in dynamic amplification.

This can then be used to prove their reliability, or at least allow a much more accurate judgment.

As a final remark it is added that, in this thesis, the focus was only on fatigue effects caused by fluctuating stresses due to bending moments. It is recommended to repeat this approach for fatigue due to shear and torsional effects as well.

7.2 Discussion

Redistribution of stresses in concrete can be expected to mitigate fatigue problems considerably. However, this is not the case for reinforcement. It is therefore important to investigate the failure of sections by fatigue of concrete in compression, to determine to which extent it can actually occur. Also, the mechanism by which fatigue of reinforced concrete section works is not quite clear. Inclusion of aspects such as debonding or spalling in the calculation may alter the damage model which is used for these calculations, and thereby the resulting reliability. Another interesting fact is the increase of concrete compressive strength in time. As it is currently not clear to which extent this phenomenon is included in the resistance model and verification format, the reliability may very well benefit from future developments, especially because fatigue is such a time-related failure mechanism.

Also, in determining the reliability for concrete in compression, the resistance model proposed for the new Dutch national annex was used (according to Lantsoght, 2014). This model was stated to be less conservative than the current Eurocode resistance model (also with the modifications from the current national annex). Therefore, the reliabilities which were calculated for concrete in compression do not completely correspond to structures designed according to the current Eurocode (i.e. existing structures). Notably, in case the current Dutch national annex model was used, which was said to be conservative, the reliabilities of existing structures with respect to fatigue of concrete in compression will be higher than calculated in this thesis. In the authors opinion, it seems that fatigue of reinforcement poses the greatest risk. The more conservative material models used for concrete, combined with the possibility of redistribution within the concrete and the increasing concrete strength with time, are expected to increase the reliability significantly. For the reinforcement, redistribution is not really an option.

Regarding the target reliability: currently, the EN 1992 does not include differentiation with respect to inspectability and detectability of fatigue in concrete and reinforcement. Therefore, the target reliability for fatigue was chosen equal to that of ultimate limit states. However, if the aforementioned aspects differ for a certain section, a lower reliability might be more appropriate.

Finally, the identified voids in current knowledge, especially regarding model uncertainties and dynamic amplification, have their impact on the accuracy of the provided reliability. At least their workings and importance were demonstrated in this report, but future endeavors would greatly benefit from additional insight, which can only be gained by further investigations.

References

American Society for Materials. (1985). *Metallography and microstructures* (9th).

American Society for Materials. (2008). Fatigue. In *Elements of metallurgy and engineering alloys*.

Amzallag, C., Gerey, J. P., Robert, J. L., & Bahuaud, J. (1994). Standardization of the rainflow counting method for fatigue analysis. *Fatigue*, *16*, 287–293.

Baker, M. J. & Descamps, B. (1999). Reliability-based methods in the inspection planning of fixed offshore steel structures. *Journal of Construction Steel Reserach*, *52*, 117–131.

Bakker, J. J. (2009). *Strukton rail 303002 Willy G 1206*. Retrieved from https://commons.wikimedia.org/wiki/File:Strukton_Rail_303002_Willy_G_1206.jpg

Bakker, J. J. (2011). *Railion 1612*. Retrieved from https://commons.wikimedia.org/wiki/File:Railion_1612_(2).jpg

Bath, S. & Patibandla, R. (2011). Metal fatigue and basic theoretical models: a review. In E. V. Morales (Ed.), *Alloy steel – properties and use* (Chap. 9, pp. 203–236). Retrieved from http://www.intechopen.com/books/alloy-steel-properties-and-use/metal-fatigue-and-basic-theoretical-models-a-review

Bensalah, Y. (2000). *Steps in applying extreme value theory to finance: a review*. Bank of Canada.

Buar, T., Nagode, M., & Fajdiga, M. (2004). Reliability approximation using finite Weibull mixture distributions. *Reliability Engineering and System Safety*, *84*, 241–251.

CEB. (1988). *Fatigue of concrete structures: State of the art report* (Bulletin d'information No. 188). Comite Euro-International du Beton.

CEN. (2002a). NEN-EN 1990: Basis of Structural Design.

CEN. (2002b). NEN-EN 1991-2: Actions on structures - Part 2: Traffic loads on bridges.

CEN. (2005a). NEN-EN 1992-1: Design of concrete structures - Part 1.1: General rules and rules for buildings.

CEN. (2005b). NEN-EN 1992-2: Design of concrete structures - Concrete bridges - Design and detailing rules.

CEN. (2005c). NEN-EN 1993-1-9: Design of steel structures - Part 1-9: Fatigue.

CEN. (2006). NEN-EN 1993-2: Design of steel structures - Part 2: Steel bridges.

CEN. (2007). NEN-EN 1999-1-3: Design of aluminium structures - Part 1-3: Structures susceptible to fatigue.

CUR-committee E10. (1997). *Probabilities in Civil Engineering* [Part 1: probabilistic design in theory](No. CUR-publiction 190).

Dekking, F., Kraaikamp, C., Lopuhaä, H., & Meester, L. (2005). *A modern introduction to probability and statistics*. Springer-Verlag London Limited.

Fitzwater, L. M. (2004). *Estimation of fatigue and extreme load distributions from limited data with application to wind energy systems*. SANDIA.

Frýba, L. (2001). A rough assessment of railway bridges for high speed trains. *Engineering Structures*, *23*.

Ghosh, S. & Resnick, S. (2010). A discussion on mean excess plots. *Stochastic Processes and their Applications*, *120*, 1492–1517.

Gillet, G. (2010). *Simply supported composite railway bridge: a comparison of ballasted and ballastless track alternatives* (Master's Thesis, KTH Architecture and the Built Environment).

Hasofer, A. M. & Lind, N. (1974). An exact and invariant first order reliability format. *Journal of Engineering Mechanics Division*.

Haukaas, T. (n.d.). The first-order reliability method (FORM). University of British Columbia.

Helgason, T. & Hanson, J. M. (1974). Investigation of design factors affecting fatigue strengths of reinforcing bars — statistical analysis. American Concrete Institute.

Hemkes, R. (2014). *DBS 189 050-8, Amersfoort*. Retrieved November 12, 2015, from https://www.flickr.com/photos/rhemkes/15093361730/

Inspectie Leefomgeving en Transport. (2014). *Ontsporing goederentrein bij Borne*. Ministerie van Infrastructuur en Milieu.

Jacob, B. & Kretz, T. (1996). Calibration of bridge fatigue loads under real traffic conditions. *IABSE reports*, 479–487. band 74.

James, G. (2003). *Analysis of traffic load effects on railway bridges* (Doctoral Thesis, Royal Institute of Technology, Stocholm, Sweden).

Johannesson, P. (2006). Extrapolation of load histories and spectra. *Fatigue & Fracture of Engineering Materials & Structures*, *29*, 209–217.

Johannesson, P. & Thomas, J.-J. (2001). Extrapolation of rainflow matrices. *Extremes*, (3), 241–262.

Joint Committee on Structural Safety. (2000a). Probabilistic Model Code: Part 1 – basis of design.

Joint Committee on Structural Safety. (2000b). Probabilistic Model Code: Part 3 – material properties.

Joint Committee on Structural Safety. (2013). Probabilistic Model Code: Part 3.12 – material properties – fatigue.

Lantsoght, E. O. L. (2014). *Fatigue of concrete under compression*. Delft University of Technology – Universidad San Francisco de Quito.

Leon, D. D. & Pérez, F. (2000). Optimal inspection schedule for fatigue cracks in offshore structures.

Levine, D. (2009). Modeling tail behavior with extreme value theory. *Risk Management*, 14–18.

Ligaj, B. (2011). An analysis of the influence of cycle counting methods on fatigue life calculations of steel. *Scientific Problems of Machines Operation and Maintenance*, *168*, 25–43.

MAINLINE. (2013). *Assesment methods for elderly rail infrastructure*. MAINtenance, renewaL and Improvement of rail transport INfrastructure to reduce Economic and Environmental impacts.

Maljaars, J., Luki, M., & Soetens, F. (2013). Comparison between the Eurocode for fatigue of steel structures, EN 1993-1-9, and the Eurocode for fatigue of aluminium structures, EN 1999-1-3. *Procedia Engineering*, *66*, 34–48.

Matsuishi, M. & Endo, T. (1968). Fatigue of metals subjected to varying stress. *Japan Society of Mechanical Engineers*, 37–40.

Miner, M. A. (1945). Cumulative damage in fatigue. *Journal of Applied Mechanics*, *12*(3), A159–A164.

Motavalli, M., Havranek, B., & Saqan, E. (Eds.). (2011). First application on the detection of fatigue breaks in bridges with the magnetic flux method, 1–8.

Nagode, M. & Fajdiga, M. (1998). A general multi-modal probability density function suitable for the rainflow ranges of stationary random processes. *International Journal of Fatigue*, *20*(3), 211–223.

Naik, T. R., Singh, S. S., & Ye, C. (1993). *Fatigue behavior of plain concrete made with or without fly ash*. University of Wisconsin-Milwaukee.

Olagnon, M. (1994). Practical computation of statistical properties of rainflow counts. *Fatigue*, *16*, 306–314.

Pandey, M. D., Van Gelder, P. H. A. J. M., & Vrijling, J. K. (2001). The estimation of extreme quantiles of wind velocity using L-moments in the peaks-over-threshold approach. *Structural Safety*, *23*, 179–192.

Paris, P. & Erdogan, F. (1963). A critical analysis of crack propagation laws. *Journal of Basic Engineering*, 528–534.

Plos, M., Lundgren, K., Rempling, R., Gylloft, K., Cervenka, J., S., T., ... Gillesén, C. (2007). *Sustainable Bridges — Assessment for Future Demands and Longer Lives* (Technical report No. TIP3-CT-2003-001653). C.

Roylance, D. (2001, May). Fatigue.

Rylander, E. P. (2006). *Dynamic effects generated by trains on railway bridges* (Master's Thesis, Lund University of Technology).

Scholz, F. W. (n.d.). Nonparametric tail extrapolation. Boeing Information & Support Services.

Simiu, E. & Heckert, N. A. (1996). Extreme wind distribution tails: a "peak over threshold" approach. *Journal of Structural Engineering*, *122*(5), 539–547.

Singh, K. L. & Ranganath, V. R. (2010). Cycle counting using rainflow algorithm for fatigue analysis. In *National seminar on aerospace structures* (pp. 301–306).

Socie, D. F. & Pompetzki, M. A. (2004). Modeling variability in service loading spectra. *Journal of ASTM International*, *1*(2), 46–57.

Steel Construction Institute. (1993). European Steel Design Education Programme (ESDEP). Retrieved from http://www.fgg.uni-lj.si/~/pmoze/ESDEP/master/toc.htm

Sutherland, H. J. & Veers, P. S. (1995). Effects of cyclic stress distribution models on fatigue life predictions. *Wind Energy*, *16*, 89–90.

Tammer, M. & Kaminski, M. L. (2013). Fatigue oriented risk based inspection and structural health moitoring of FPSOs. *Proceedings of the 23rd International Offshore and Polar Engineering*, 438–449.

Tilly, G. P. (1979). Fatigue of steel reinforcement bars in concrete: a review. *Fatigue of Engineering Materials and Structures*, *2*, 251–268.

Tilly, G. P. (1984). Fatigue testing and performance of steel reinforcement bars. *Materials and Structures*, *17*, 43–49.

Tovo, R. (2001). On the fatigue reliability evaluation of structural components under service loading. *International Journal of Fatigue*, *23*, 587–598.

van der Veen, C. & den Uijl, J. A. (2015). Fatigue — CIE5126: Part on concrete and concrete structures. Lecture at Delft University of Technology.

van Beem, A. (2005). *General motors electro motive diesel class 66 pb017*. Retrieved from https://commons.wikimedia.org/wiki/File:General_Motors_Electro_Motive_Diesel_Class_66_PB017.jpg

Vrouwenvelder, T. (1996). Eurocode 1, basis of design, background information. *IABSE reports*, 25–32.

Weibull, W. (1949). *A statistical representation of fatigue in solids* (No. UDC 539. 431.). Royal Institute of Technology Stockholm, Sweden.

Wight, J. K. & MacGregor, J. G. (2012). *Reinforced concrete mechanics and design*.

Wikipedia. (2015a). Central limit theorem. Retrieved from https://en.wikipedia.org/w/index.php?title=Central_limit_theorem

Wikipedia. (2015b). Rainflow-counting algorithm. Retrieved from https://en.wikipedia.org/w/index.php?title=Rainflow-counting_algorithm

Wikipedia. (2015c). Standard error. Retrieved from https://en.wikipedia.org/w/index.php?title=Standard_error

Wikipedia. (2016a). Expected value. Retrieved from https://en.wikipedia.org/w/index.php?title=Expected_value

Wikipedia. (2016b). Log-normal distribution. Retrieved from https://en.wikipedia.org/w/index.php?title=Log-normal_distribution

Wikipedia. (2016c). Normal distribution. Retrieved from https://en.wikipedia.org/w/index.php?title=Normal_distribution

Wikipedia. (2016d). Triangular distribution. Retrieved from https://en.wikipedia.org/w/index.php?title=Triangular_distribution

Wikipedia. (2016e). Variance. Retrieved from https://en.wikipedia.org/w/index.php?title=Variance

Wirsching, P. H. (1984). Fatigue reliability of offshore structures. *Journal of Structural Engineering*, *108*, 2340–2356.

Zilch, K. & Bagayoko, L. (1997). *Fatigue design of concrete railway bridges: Loading, Resistance, Verification Formulae for ENV 1992-2* (No. ERRI D 183/DT 346). European Rail Research Institute (ERRI).

Appendices

A | Basic Reliability Theory

In this chapter, general aspects of reliability, of which explanations were deliberately omitted in the main report, are treated. Within the field of probabilistic calculations, four levels are normally distinguished:

Level 0 Formally, this is used to denote a deterministic calculation methodology, where uncertainties and variations are not taken into account.

Level I Semi-probabilistic calculations: uncertainties are taken into account by means of safety factors (for example the partial safety factors in the Eurocode).

Level II Fully probabilistic, i.e. all uncertainties are quantified or estimated, and taken into account. The reliability however is obtained by approximation techniques (in this report: FORM, see section A.5).

Level III Fully probabilistic, where the reliability is determined using exact methods or methods which are exact in nature (in this report: Monte Carlo analysis, see section A.4).

A.1 General concepts

Random variable

Random variables are variables, which can, with a certain probability, take on a set of possible values. They are also denoted as stochastic variables. Random variables can be either continuous or discrete: the former can take on any number in an interval (can be unbounded), while the latter is limited to only a finite set of distinct values. In this thesis, all stochastic variables are continuous.

Probability density functions (abbreviated with 'pdf') assign a certain chance to each value a random variable can take on. Because, in the continuous case, the number of possible realizations of a random variable is infinite, the probability of taking on one single value is zero. Probability distribution functions therefore define the chance of taking on a value in a relative way. The probability of taking on a value within an interval however, is determined by integrating the pdf over this interval.

Closely related to this, is the cumulative distribution function ('cdf'). It expresses the probability of non-exceedance as a function of a 'dummy variable' expressing the range. The cdf can therefore be expressed in terms of the pdf:

$$F_X(x) = P(X < x) = \int_{-\infty}^{x} f_X(x)dx \tag{A.1}$$

where

X = random variable
x = dummy variable, used for describing the range of possible outcomes
$F_X(x)$ = cumulative distribution function (cdf) of X
$f_X(x)$ = probability density function (pdf) of X
$P(X < x)$ = probability of X being smaller than x, i.e. the probability of non-exceedance

Therefore, the pdf can also be defined as the derivative of the cdf:

$$f_X(x) = \frac{dF_X(x)}{dx} \tag{A.2}$$

Expectation

The expectation of a random variable is the best estimator for it's outcome, and is determined by weighing possible realizations of this random variable with corresponding probabilities of attainment (Wikipedia, 2016a). For discrete random variables, this is a summation over all possible outcomes:

$$E[X] = \sum x_i \, P(X = x_i) \tag{A.3}$$

where

$E[\bullet]$ = expected value
X = random variable, in this case discrete
x_i = the i'th possible outcome of X
$P(X = x_i)$ = probability of X being equal to x_i

Analogously, for continuous distributions the expectation is defined as the first moment (commonly denoted by μ_X):

$$E[X] = \int_{-\infty}^{\infty} x \; f_X(x) \, dx = \mu_X \tag{A.4}$$

Variance

The variance of a random variable is a measure of its spread around its expectation (Wikipedia, 2016e). Numerically, the variance is equal to the expected squared distance between its possible outcomes and its mean, weighed by the outcome's probabilities. For discrete random variables:

$$\mathrm{Var}(X) = E[(X - \mu_X)^2] = \sum_{i=1}^{n} (x_i - \mu_X)^2 \, P(X = x_i) \tag{A.5}$$

For continuous random variables:

$$\mathrm{Var}(X) = \int_{-\infty}^{\infty} (x - \mu_X)^2 \, f_X(x) \, dx = \int_{-\infty}^{\infty} x^2 \, f_X(x) \, dx - \mu_X^2 = {\sigma_X}^2 \tag{A.6}$$

From these, the coefficient of variation is defined as a measure of variations relative to the mean value:

$$c_{v,X} = \frac{\sigma_X}{\mu_X} \tag{A.7}$$

Risk

Risk is defined as the product of expected consequences and their associated probability of occurrence:

$$\text{risk} = P\,C \tag{A.8}$$

where

P = probability of event occurring
C = consequences associated to this event

It is thus closely related to the expectation. In other words, risk may be interpreted as the expected costs from an adverse event (e.g. structural failure). In case of multiple possible events, risks should be summed, as is the case with expectations. As explained in chapter 3, risk can be used to objectively weigh the probability that some adverse event may occur, against e.g. the costs of improving strength.

Probability of failure

The probability of failure is denoted with P_F, and quantifies the likelihood of failure occurring. It should always be related to a time-frame, for example the probability that a bridge will fail during the coming 50 years. The reliability (L) is the complement of the failure probability, i.e.:

$$L = 1 - P_F \tag{A.9}$$

where

P_F = probability of failure
L = reliability

Therefore, one does not offer more information than the other.

Reliability index

The reliability index, denoted with β, is frequently used to express the reliability of, among others, structures. It is defined as:

$$\beta = \Phi^{-1}(1 - P_F) = \Phi^{-1}(L) \tag{A.10}$$

where

β = reliability index
$\Phi(\bullet)$ = standard normal distribution cdf ($\mu = 0$; $\sigma = 1$)
$\Phi(\bullet)^{-1}$ = inverse standard normal distribution cdf

and therefore

$$P_F = \Phi(-\beta) \tag{A.11}$$

A stated reliability index is fully replaceable by its corresponding probability of failure.

A.2 Probability distributions used in work

Some of the probability distributions which were deemed as 'generally known', were not elaborated in the main text. To provide all the information necessary for the reader, however, these have been included in this chapter.

Triangular distribution[1]

Probability density function (pdf):

$$f_X(x) = \begin{cases} 0 & \text{for } x < a \\ \frac{2(x-a)}{(c-a)(b-a)} & \text{for } a \le x < b \\ \frac{2}{c-a} & \text{for } x = b \\ \frac{2(c-x)}{(c-a)(c-b)} & \text{for } b < x < c \\ 0 & \text{for } c \le x \end{cases} \tag{A.12}$$

Cumulative distribution function (cdf):

$$F_X(x) = \begin{cases} 0 & \text{for } x < a \\ \frac{(x-a)^2}{(c-a)(b-a)} & \text{for } a < x < b \\ 1 - \frac{(c-x)^2}{(c-a)(c-b)} & \text{for } b < x < c \\ 1 & \text{for } c \le x \end{cases} \tag{A.13}$$

Mean value (expectation):

$$\mu_X = \frac{a+b+c}{3} \tag{A.14}$$

Variance:

$${\sigma_X}^2 = \frac{a^2+b^2+c^2-a\,b-a\,c-b\,c}{18} \tag{A.15}$$

Normal distribution[2]

Probability density function (pdf):

$$f_X(x) = \frac{1}{\sigma\sqrt{2\,\pi}}\, e^{-\frac{(x-\mu)^2}{2\,\sigma^2}} \tag{A.16}$$

Cumulative distribution function (cdf):

$$F_X(x) = \int_{-\infty}^{x} f_X(x)\,dx \tag{A.17}$$

Mean value (expectation):

$$\mu_X = \mu \tag{A.18}$$

Variance:

$${\sigma_X}^2 = \sigma^2 \tag{A.19}$$

Stochasts which are normally distributed are symbolized by 'X~$N(\mu_X, \sigma_X)$'.

[1] Based on Wikipedia (2016d)
[2] Based on Wikipedia (2016c)

Lognormal distribution[3]

Probability density function (pdf):

$$f_X(x) = \frac{1}{x\,\sigma\,\sqrt{2\,\pi}}\,e^{-\frac{(\ln x-\mu)^2}{2\,\sigma^2}} \tag{A.20}$$

Cumulative distribution function (cdf):

$$F_X(x) = \int_{-\infty}^{x} f_X(x)\,dx \tag{A.21}$$

Mean value (expectation):

$$\mu_X = e^{\mu+\sigma^2/2} \tag{A.22}$$

Variance:

$${\sigma_X}^2 = \left(e^{\sigma^2}-1\right)\,e^{2\,\mu+\sigma^2} \tag{A.23}$$

Stochasts which are lognormally distributed are symbolized by 'X~$LN(\mu_X, \sigma_X)$'.

A.3 Solving the reliability integral

This section, along with sections A.4 and A.5, is based on *Probabilities in Civil Engineering* (CUR-committee E10, 1997). The 'reliability equation' or 'limit state function' is written in such a way, that negative values of the safety margin Z correspond to failure. The reliability equation has the general form[4]

$$Z = R - S \tag{A.24}$$

where

Z = safety margin
R = resistance to failure
S = load or more generally: that what causes failure (from the word 'solicitation')

The probability of failure can then be expressed in terms of the reliability equation as

$$P_F = P(Z \leq 0) = P(R \leq S) \tag{A.25}$$

where P_F is the probability of failure. Calculating the failure probability comes down to determining the probability of Z being smaller than zero. This probability is calculated by integration of the probability density function of Z over the (hyper)space of variables, for those combinations where $Z \leq 0$.

This may seem more clear if 'integration' is replaced with 'summation'. First, imagine a n-dimensional hyperspace (for $n > 3$), where n is the number of (random) variables. Assume now that the probability density functions are known for each variable, and that variables are independent. The probability density at any point in the hyperspace, can then be determined from the product of probabilities that each variable attains the value corresponding to this point in the hyperspace. The probability of failure is determined from the probability density function defined on the hyperspace, only

[3] Based on Wikipedia (2016b)
[4] Any form is possible, as long as it is accompanied by a clear definition failure and survival.

concerning those points where $Z = g(X_1, X_2, \ldots, X_n)$ is less than or equal to zero, and is obtained from summation of probabilities related to all those possible combinations which lead to failure.

Back to the formulation using the integrals: the failure probability is expressed as

$$P_F = \iint\limits_{Z \leq 0} f_{R,S}\, dR\, dS \tag{A.26}$$

with

$$Z = g\left(X_1, X_2, \ldots, X_n\right) \tag{A.27}$$

This means that the failure probability can be calculated with the integral

$$P_F = \iint\limits_{Z \leq 0} \ldots \int f_{X_1, X_2, \ldots, X_n}\, dX_1\, dX_2 \ldots dX_n \tag{A.28}$$

from which it is clear that integration is performed over all variables, thus representing the aforementioned hyperspace. The integral in equation A.28 proves quite hard to solve for the failure probability, even to the extent that analytical solutions are an exception. Therefore, the integration is generally done using numerical routines (section A.4) or the reliability is determined using approximation techniques (section A.5).

A.4 Level III: Monte Carlo method

The Monte Carlo method is a 'brute force' approach to the solution of the reliability-integral. Starting from known distributions for all stochastic variables, a random realization of each variable is drawn. From this, the safety margin (Z) is determined by substitution in the reliability equation. Then it is checked whether $Z \leq 0$ (failure) or $Z > 0$ (survival). This process is repeated a large number of times, from which the failure frequency is calculated. This serves as an estimate for the failure probability, i.e.

$$P_F \approx \frac{n_F}{n} \tag{A.29}$$

where

n_F = number of simulated failures ($Z_i \leq 0$)
n = number of simulations

Equation A.29 converges to the true solution of the integral (equation A.28) for increasing n. The accuracy of the Monte Carlo is dictated by the number of simulations. Usually, the number of simulations required for acceptable accuracy is rather high which can make the method computationally expensive. As a general rule, for *crude* Monte Carlo, the number of simulations for 95 % accuracy is in the order of $^{400}/_{P_F}$, which shows that it it increasingly difficult to achieve a stable and accurate solution for a decreasing failure probability.

A.5 Level II: first order reliability method

In this section an approximate method for solving the reliability integral using first order linearization is explained. In case all variables in the reliability equation are normally distributed, and the reliability equation is some linear function of these

variables, then the reliability function itself will also be normally distributed. If so, the probability that of Z being equal to or smaller than zero can be directly calculated from

$$P_F = P(Z \leq 0) = \Phi\left(-\frac{\mu_Z}{\sigma_Z}\right) \tag{A.30}$$

to which the reliability index β owes its alternate definition:

$$\beta = \frac{\mu_Z}{\sigma_Z} \tag{A.31}$$

In this thesis the emphasis is on nonlinear reliability functions, due to the many nonlinearities in the fatigue verification. Such a nonlinear reliability function can be approximated by the first two terms of its Taylor-expansion (in this case at $\mathbf{x} = \mathbf{x}^*$):

$$Z = g(\mathbf{x}) \approx g(\mathbf{x}^*) + \sum_{i=1}^{n} \left.\frac{\partial g}{\partial X_i}\right|_{\mathbf{x}^*} (X_i - X_i^*) \tag{A.32}$$

with

$$\mathbf{x}^* = [X_1^* \; X_2^* \; \cdots \; X_n^* \;]^T \tag{A.33}$$

The mean and standard deviation of Z can then be approximated by

$$\mu_Z \approx g(\mathbf{x}^*) + \sum_{i=1}^{n} \left.\frac{\partial g}{\partial X_i}\right|_{\mathbf{x}^*} (\mu_{X_i} - X_i^*) \tag{A.34}$$

$$\sigma_Z \approx \sqrt{\sum_{i=1}^{n} \left(\left.\frac{\partial g}{\partial X_i}\right|_{\mathbf{x}^*} \sigma_{X_i} \right)^2} \tag{A.35}$$

from which the reliability index is approximated by substitution of equations A.34 and A.35 into equation A.31:

$$\beta = \frac{\mu_Z}{\sigma_Z} \approx \frac{g(\mathbf{x}^*) + \sum_{i=1}^{n} \left.\frac{\partial g}{\partial X_i}\right|_{\mathbf{x}^*} (\mu_{X_i} - X_i^*)}{\sqrt{\sum_{i=1}^{n} \left(\left.\frac{\partial g}{\partial X_i}\right|_{\mathbf{x}^*} \sigma_{X_i} \right)^2}} \tag{A.36}$$

According to equation A.36 the reliability index depends on the point in which the reliability equation is linearized ($\mathbf{x}^*$ in this case). Therefore Hasofer and Lind (1974) defined a reliability index which is invariant to the point of linearization, and can be visualized as the minimum distance between the origin of the variable hyperspace and the failure boundary, i.e. the set of points for which Z is equal to zero. This definition demands that all variables are transformed to standard normal variables ($\mu_{X_i} = 0$; $\sigma_{X_i} = 1$), so that the hyperspace of variables is a so-called 'standardized space'. The point which minimizes β is defined as the *design point*, with coordinates $\mathbf{x}^*$. The design point can be obtained by solving the following set of equations in an iterative manner:

$$\alpha_i = -\frac{\left.\frac{\partial g}{\partial X_i}\right|_{\mathbf{x}^*} \sigma_{X_i}}{\sqrt{\sum_{i=1}^{n} \left(\left.\frac{\partial g}{\partial X_i}\right|_{\mathbf{x}^*} \sigma_{X_i} \right)^2}} \approx -\frac{\left.\frac{\partial g}{\partial X_i}\right|_{\mathbf{x}^*} \sigma_{X_i}}{\sigma_Z} \tag{A.37}$$

$$g(\mathbf{x}^*) = g\left([X_1^* \; X_2^* \; \cdots \; X_n^* \;]^T\right) = 0 \tag{A.38}$$

with

$$X_i^* = \mu_{X_i} + \alpha_i \, \beta \, \sigma_{X_i} \tag{A.39}$$

so that

$$g(\mathbf{x}^*) = g\left(\begin{bmatrix} \mu_{X_1} + \alpha_1 \, \beta \, \sigma_{X_1} \\ \mu_{X_2} + \alpha_2 \, \beta \, \sigma_{X_2} \\ \vdots \\ \mu_{X_n} + \alpha_n \, \beta \, \sigma_{X_n} \end{bmatrix}\right) = 0 \tag{A.40}$$

The α-factors quantify the sensitivity of the reliability function with respect to each of the variables. Equation A.37 reveals that the magnitude of the sensitivity is dictated by the product of the partial derivative with respect to the variable of interest, and the variability of this variable (quantified by its standard deviation). This makes sense, as the partial derivative shows the change in safety margin for a change in the variable of interest.

The method explained in this section assumes normally distributed variables. In the case of variables with other probability distributions, these should be transformed to some approximate normal distribution. This can be done, based on the notion that, at the point of approximation, the cdf and its derivative (pdf), of the equivalent normal distribution, are equal to those of the original cdf. This results in convenient formulations for the transformed distribution's parameters:

$$\hat{\sigma}_X = \frac{\phi\left(\Phi^{-1}\left(F_X\left(X^*\right)\right)\right)}{f_X\left(X^*\right)} \tag{A.41}$$

$$\hat{\mu}_X = X^* - \Phi^{-1}\left(F_X\left(X^*\right)\right) \, \hat{\sigma}_X \tag{A.42}$$

where

$\hat{\sigma}_X$ = equivalent normal distribution's standard deviation
$\hat{\mu}_X$ = equivalent normal distribution's mean
f_X = actual probability density function of X
F_X = actual cumulative distribution function of X

Using the theory presented in this section, nonlinear reliability functions with non-normal distributions can be linearized to an approximate form which allows solution for the reliability index, and therefore also for the probability of failure.

B | Cases Concrete Fatigue

The most relevant cases were already listed in chapter 2. The remaining cases are (CEB, 1988):

1. Cantilevered bridge deck, New York City: the principle cause of failure was the repetitive deflection of a cantilevered floor beam, which caused secondary tensile and fatigue stresses in the concrete's upper surface. Other factors included insufficient reinforcement for distribution of loads, de-icing salt in relation to corrosion of reinforcement, and loss of concrete cover on the running surface.

3. Fatigue fracture of connecting joints is a prestressed bridge, Germany: cracking of concrete led to an increase in stress in prestressing tendons, from $16\,\mathrm{N/mm^2}$ to $196\,\mathrm{N/mm^2}$ (measured). This led to fractures of tendons, which were caused by fatigue.

5. Expansion joints in bridges, Sweden: very localized damage to expansion joints was observed, in which it was believed that fatigue played a role.

7. Traveling crane track, Sweden: crane tracks, connected to concrete elements by hold down bolts, were locally separated from each other. Repetitive loading is said to have caused spalling of concrete and cracking of mortar, resulting in shearing of bolts.

8. Viaduct over railway, Ashammar, Sweden: damage to a continuous slab supported by steel beams was observed. The damage consisted mainly of lost cover, which was related to corrosion of fatigue, in turn aided by carbonation of concrete. The sizes of cracks were too wide to be caused by solely static loading, and therefore fatigue is suspected;

9. Reconstruction of a concrete pavement, The Netherlands: cracks were observed in unreinforced concrete pavement slabs. One of the factors identified responsible was fatigue.

11. Demolition of prestressed concrete, Germany: during demolitions of prestressed structures it became clear that the fatigue resistance of prestressing steel in incorrectly grouted ducts was smaller than its original values. These losses were caused by corrosion. It is noted that corrosion pits of 150 to 250 microns can cause losses of fatigue strength of up to 50 %.

12. Collapse of the south peripheral arch, Kongresshalle, Germany: tendons were severely affected by corrosion, also aided by chlorides and carbonation. Ultimately, some wires broke because of fatigue loading by wind, snow and temperature.

13. Slab supporting presses, Sweden: a factory floor slab was designed to support two presses. When tested prior to installation, it was found that unacceptable

vibrations resulted, which also caused cracking of the concrete. Engineers concluded that if vibrations were unacceptable for men to work in, there potentially was a fatigue problem.

15. Wood chip processor, Kornasverken, Sweden: case of vibrations induced by machinery, which caused excessive cracking of the concrete structure. No detailed analysis was made, but it was considered that fatigue caused the cracks;

16. Papermill in Finland: the supporting structure, made of rather low strength concrete, was subject to long-term loads, vibrations and penetrating oil. Cracks were observed, but their cause is not given. It was reported, however, that the structure was not designed for fatigue.

17. Pile driving, Sweden: it is said that 6 % of concrete piles is damaged during driving. There are multiple causes and mechanisms, but fatigue is believed to contribute.

C | Measured Traffic

The data used in this thesis was provided by Ricardo Rail (formerly known as Lloyd's Register Rail). The measurements correspond to four locations, for all tracks at these sites. Information regarding the available data is summarized in table C.1, while overviews of the corresponding measured sites are given in figure C.1 – C.4.

DetectorID	km	GeoCode	GeoDetailDescription	TrackName	Latitude	Longtitude
11	51.72	104	Voorschoten I	LF	52.12324	4.42896
12	51.72	104	Voorschoten I	KF	52.12324	4.42896
18	51.72	104	Voorschoten II	MF	52.12291	4.42958
19	51.72	104	Voorschoten II	NF	52.12291	4.42958
111	24.801	513	Tricht	GU	51.89117	5.26765
114	24.801	513	Tricht	GJ	51.89117	5.26765
163	75.059	112	Schiedam	CF	51.95656	4.38279
164	75.059	112	Schiedam	DF	51.95656	4.38279
363	50.759	035	Zeist	AF	52.06595	5.31602
364	50.759	035	Zeist	AT	52.06595	5.31602

Table C.1: Information regarding measured locations.

C.1 Data acquisition[1]

The measurements are recorded using the 'Gotcha / Quo Vadis' system. This system was initially developed by NedTrain, which is the organization responsible for maintaining the trains for NS. The goal was to monitor the quality of wheels, with the aim of realizing more efficient maintenance. ProRail, Ricardo Rail and Baas R&D were also involved. ProRail collaborated in the development to enable the acquisition of information which can be used as a basis for the compensation which is paid by railway operators for the usage of infrastructure. All measurement systems were replaced in 2010/2011. Measurements which are available for this work, are post-replacement.

The system classifies as 'weigh-in-motion' (WIM), as measurements are obtained from moving trains. The installations consist of four glass-fiber sensors mounted on the underside of the tracks (two on each side). Also, an antenna is placed which reads RF-tags on trains, which can be used for identification. The system produces optic signals, i.e. when a train passes the sensors, the tracks bend slightly. This causes a disturbance in the optic signal, which is translated to a static weight and

[1]The information regarding the measurement system is based on: Inspectie Leefomgeving en Transport (2014)

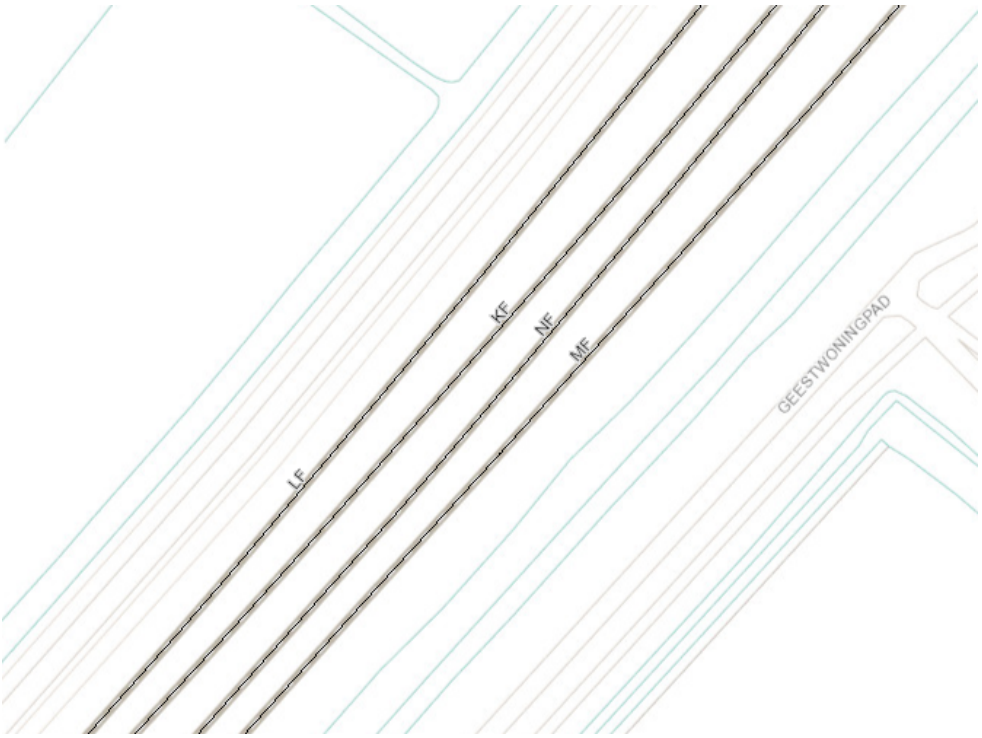

Figure C.1: Overview of tracks near Voorschoten (GeoCode 104).

Figure C.2: Overview of tracks near Tricht (GeoCode 513).

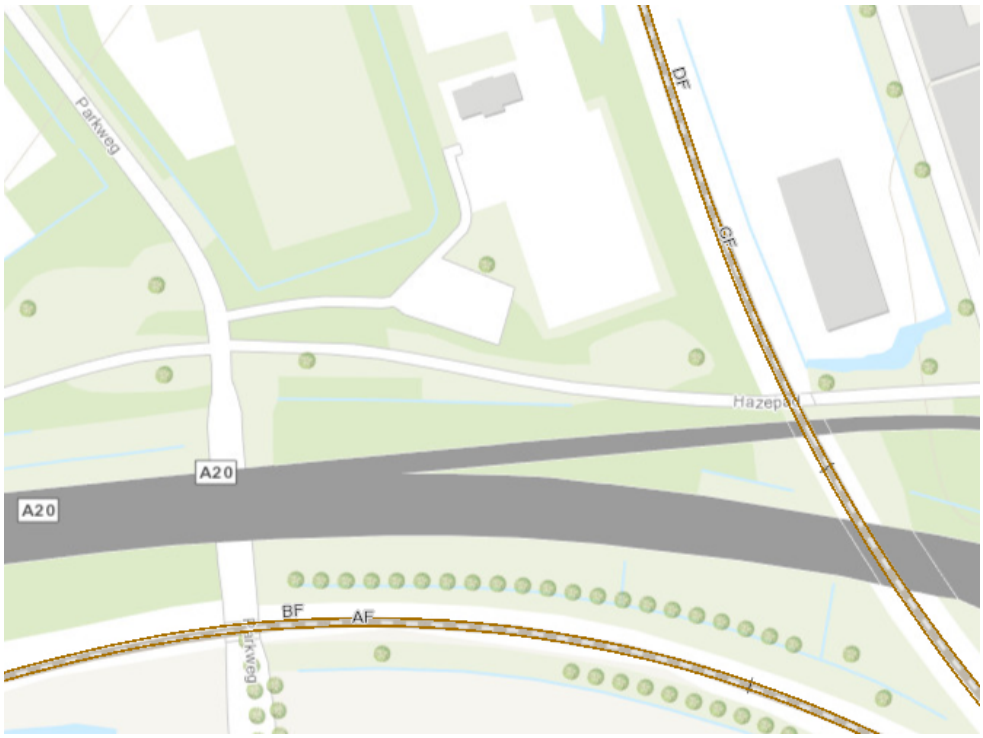

Figure C.3: Overview of tracks near Schiedam (GeoCode 112).

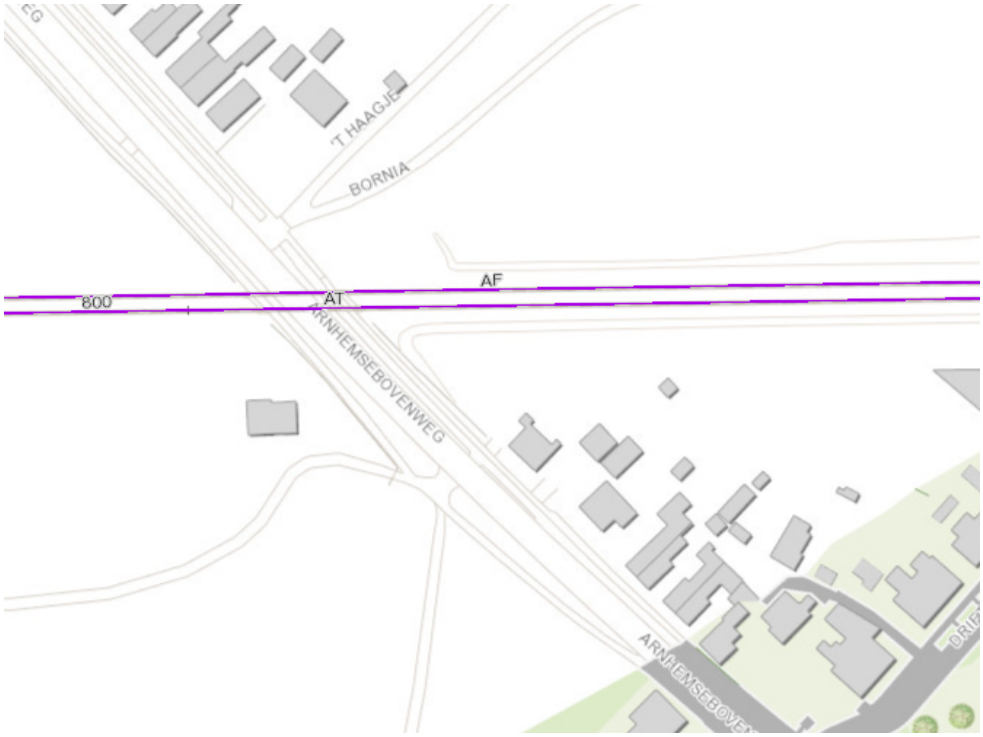

Figure C.4: Overview of tracks near Zeist (GeoCode 035).

dynamic forces. The system is calibrated frequently (order of magnitude is daily), using vehicles with known weights (preferably dedicated locomotives).

C.2 Data format

The data was supplied in the form of `.mat`-files, split in 63 files per track, named `Detector_xxx_1.mat` through `Detector_xxx_63.mat` (with `xxx` containing the ID of the detector). The data in these files is in chronological order. Two exceptions, where files are missing, were noticed. The missing files are:

- `Detector_11_46.mat` → The missing file contains a part of the trains that is enclosed chronologically, meaning that it cannot just be left untreated. Therefore the following method was used: all trains with time-stamps later than the missing file, had their time-stamps modified to succeed the last train from `Detector_11_45.mat`, in such a way that the time difference between the last train from `Detector_11_45.mat` and the first train from `Detector_11_47.mat` equals the average time between passages (approx. 15 minutes for this location).
- `Detector_114_61.mat` – `Detector_114_63.mat` → This was solved by merging the history up to `Detector_114_60.mat`. Because only the last part of the data is missing, there is no need for time correction of the remaining data.

Each `.mat`-file contains a structure `Data`. This struct contains several fields, of which the relevant ones are presented in table C.2 including a short description of their meaning. The quality of each measurement is determined automatically (criteria

`Data` =	
`WheelDamageID`	Unique ID for each passing wheel or axle
`TimeOfAxle`	String containing the time of passing per axle
`DetectorID`	ID of the detector, corresponding to table C.1
`TrainpassageInformationID`	Unique ID for each passage
`Axle`	Numbering of axles per train, chronologically and starting at 1
`Distance2PreviousAxle`	The distance between the current axle and the previous axle. Note that this is zero for the first axle of each train
`SpeedOfAxle`	Velocity at which each axle passed the detector
`AxleLoad`	The weight of each axle in metric tonnes
`ValidWIM`	Validity of the measurement as judged by the system
`VehicleType`	Type(s) in train passage

Table C.2: Explanation of the relevant fields in *structure array* 'Data', in which the measured data is provided.

not available), and expressed as a value `'ValidWIM'` between 0 and 1. According to Ricardo Rail, the threshold for a reliable measurement is at 0.75; all values with a ValidWIM-score which is larger than or equal to 0.75 can be trusted. Measurements with lower scores are to be discarded. For this analysis, the ValidWIM-score of a passage was defined as the minimum of scores corresponding to the train's axles. The 'validity' in table C.3 is defined as the fraction of trains with ValidWIM-scores larger than 0.75.

Now, for a fatigue load model, where the number of trains is an essential component, these trains cannot just be discarded. Therefore an alternate procedure is thought of. Under the assumption that the quality of measured loading is independent of the load itself, implying that the discarded measurements are purely random, these

inadequate measurements can be replaced by randomly sampled trains from the rest of the population. The population is, in this case, defined as all the trains that pass a certain measured location. In the process of sampling, some information belonging to the original (faulty) measurement was kept: the ID of the passage (`Data.TrainPassageInformationID`) and the time-stamp (`Data.TimeOfAxle`). After performing this procedure, some characteristics from the measured traffic were determined, being the cumulative annual tonnage, the maximum axle load, and the number of trains, see table C.3. Clearly, the annual cumulative tonnages prescribed in the Eurocode, set to 25×10^6 tonnes per year, are not exceeded in any of the cases.

`DetectorID`	validity	cumulative tonnage [10×10^6 ton/year]	maximum axle load [ton]	number of trains
11	0.9085	9.92	25.53	151052
12	0.9821	15.21	26.90	160538
18	0.5907	8.01	24.80	136727
19	0.9492	16.45	26.99	178031
111	0.8947	23.12	31.07	307762
114	0.9717	18.53	28.59	201047
163	0.9745	21.81	28.62	268493
164	0.9711	22.16	28.33	269374
363	0.9790	14.46	31.00	181064
364	0.9659	15.53	32.80	182739

Table C.3: Averaged yearly cumulative tonnage and validity of the data.

The measurements are merged into a structure `LH`, where only the data required for the rest of the analyses is kept. This is mainly done to limit the computational demands. The fields of `LH`, with their respective descriptions, are given in table C.4.

`LH` =	
`load(:,1)`	Vector of axle loads in [kN], obtained from multiplication of the original measurement in tons with the gravitational constant (9.81).
`load(:,2)`	Vector of cumulative axle distances in [m], with the first axle as reference.
`freq`	Number of passages of this train, equal to 1 for all measured trains.
`velo`	Velocity of the train at passage, calculated by averaging the velocities of all axles.
`time`	Time at which the train passed, defined as the value of `Data.TimeOfAxle` for the train's first axle.
`tpID`	The unique ID belonging to the passage of the train, i.e. `Data.TrainPassageInformationID`
`vWIM`	Minimum of all axle's `Data.ValidWIM`-scores.
`type`	Train types as present in the original measurements. Only unique entries are included.

Table C.4: Explanation of the fields in *structure array* `LH` (LoadingHistory), in which the measured data is stored.

C.3 Empirical distributions

The first analysis of the data is the extraction of empirical distributions for the magnitude of axle loads. Histograms are plotted for pairs of detectors, see figure C.5. Note that Voorschoten (4 tracks) is therefore represented by two plots. Results are analyzed per location.

Voorschoten Clearly, detectors 12 and 19 were subjected to axle loads of larger magnitudes than detectors 11 and 18. Also, the cumulative tonnages over these detectors is almost twice as large as that measured at the adjacent detectors.

Tricht The tracks near Tricht are used extensively for freight transports. Interestingly, the most frequent occurrence of large axle loads is measured at detector 111, i.e. track GU. Figure C.2 suggests that, given the assumption that most of the traffic on the Dutch railways is right-driving, this track is mainly used for inland transportation of freight, or export eastwards (e.g. Germany).

Schiedam Detector 163 and 164 measured similar loads in both directions. Axle loads from Rotterdam are slightly larger than those towards it.

Zeist Detector 363 shows a distinct peak near 70 kN axles, while detector 364 was passed far more frequently by large axle loads. It is assumed that this is the result of loaded freight trains in one direction (large axle loads), and unloaded trains in the other (smaller axle loads). This implies that freight is transported primarily from Utrecht towards the eastern part of the country. However, it is noted that the difference in average cumulative tonnages is small.

On a general note: the main bodies of all measured data-sets correspond quite well. These are formed by an accumulation of axle loads near 130 kN with a small left tail and a relatively wide right tail.

To compare all data-sets, the empirical cumulative density functions were plotted (figure C.6). The differences in especially the tails of the distributions are clear, as can be seen from the e.g. the 5th and 95th percentiles.

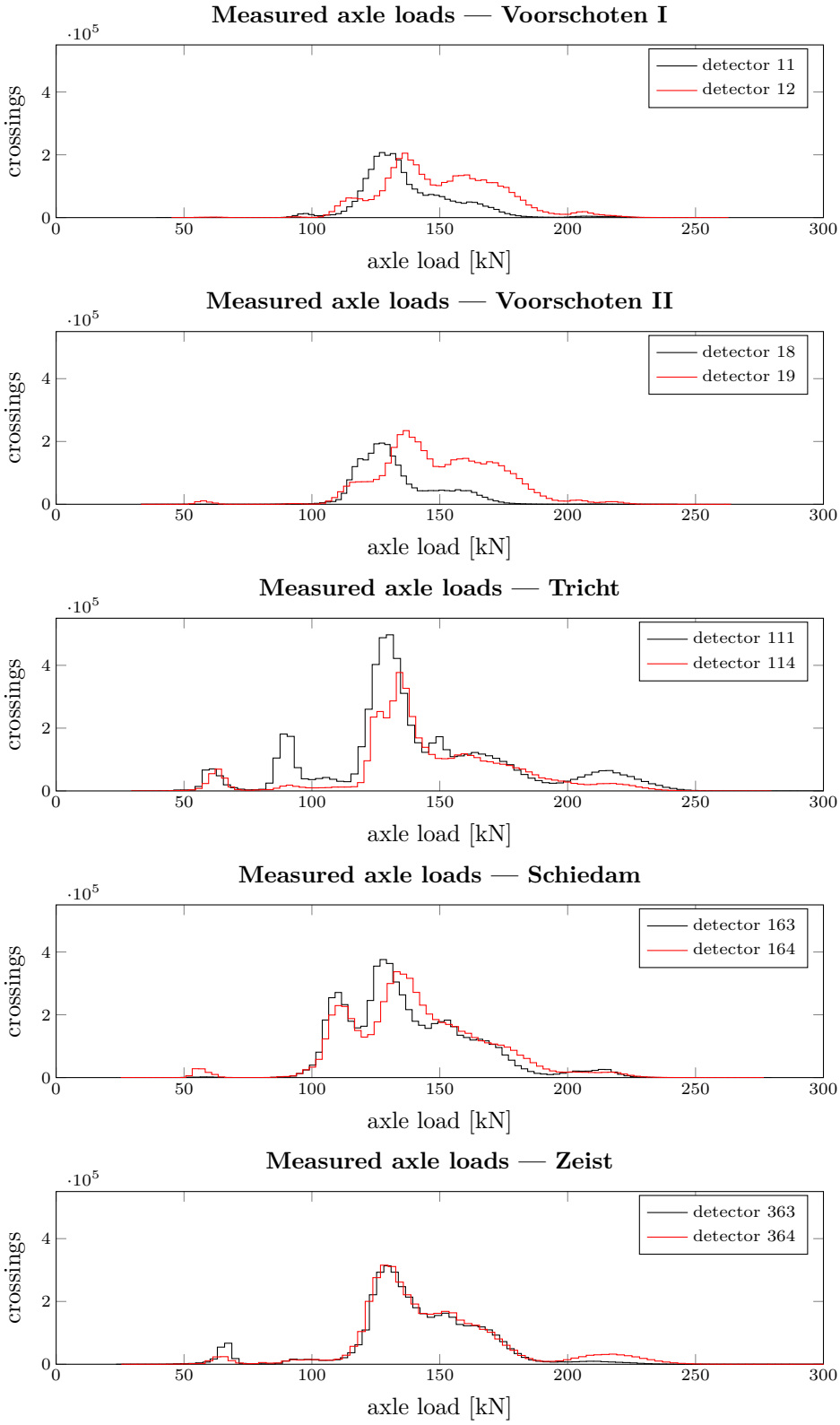

Figure C.5: Empirical density functions of measured axle loads, per location.

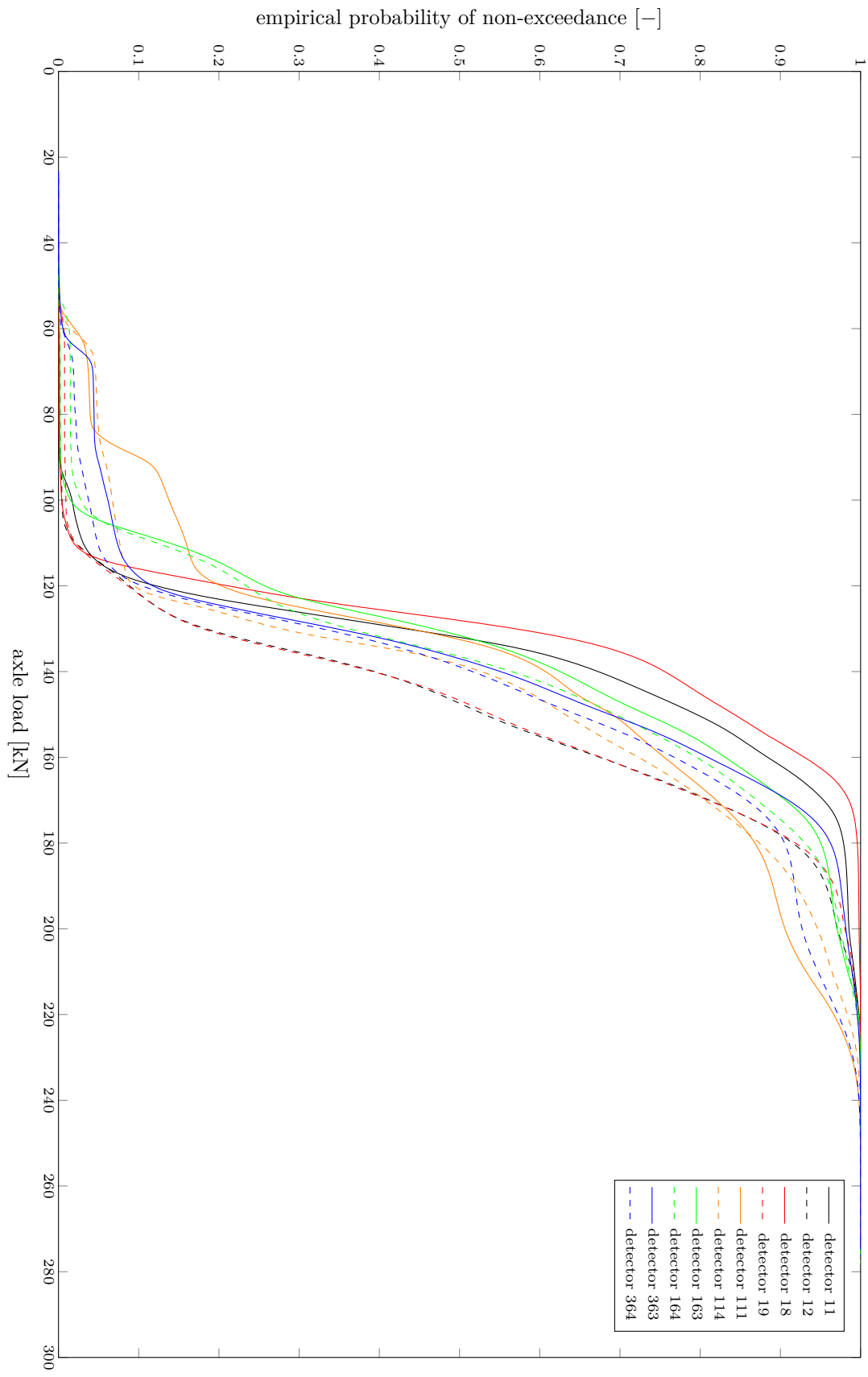

Figure C.6: Empirical cumulative density functions for all data-sets.

C.4 Assessment of historical trends

In order to use the data for extrapolation, it is important whether there is a long term *trend* in the measured loading histories. Also, the variability in time is an interesting characteristic. For such an analysis, the time-frame of measurements corresponding to each location was split into a number of sub-intervals. Using this, it was analyzed in which slot each train fits (based on the time at which the first axle was measured), and the tonnage was determined. Doing so for each train, the cumulative tonnage which passed during each time frame is determined through summation of axle loads. Graphs of the cumulative tonnage versus the time are given in figure C.7. In these plots, the averages are plotted with dashed lines. Below, some remarks concerning the time-dependence are given.

Voorschoten Different from the other locations, at Voorschoten there are 4 parallel tracks for all of which measurements are available. Voorschoten I is quite steady in cumulative tonnage, while data from Voorschoten II shows some large deviations. It seems as if part of the traffic which would normally pass detector 18 (track MF), was rerouted over detector 19 (track NF), during little over a year. This is concluded from the apparent dip in the former, which coincides time-wise with the peak in the latter. Observing the graphs, no significant trend can be spotted.

Tricht, Schiedam, Zeist The cumulative tonnages at the other locations appear steady and without a significant trend.

The only significant variation which was identified, possibly being a temporary rerouting of traffic, was at Voorschoten's MF and NF tracks. Although significant, it is also clearly a temporary distortion in a larger steady behavior. It is not expected that such variations are part of the large-scale behavior of the system. Therefore it would not be beneficial to include such a set of measurements in the calibration, as it could distort the results. However, the 2nd half of the measured time appears to show the normal situation at this location. This can thus be used for calibration.

There is also the possibility of other trends in the data. For example, axle loads might be increasing as parts of political decisions. Such a trend might not lead to a decrease in tonnage, because the number of trains could be reduced if larger loads are allowed. To spot such a trend, the mean axle loads have been analyzed for each sub-interval of the measured time-frame. This seems to be an appropriate marker, because it includes both the number of axles as the cumulative tonnage. Plots of the mean axle loads are displayed in figure C.8. Clearly, variations are minimal and no trend can be detected whatsoever. Therefore, the composition of axle loads as measured in this time-frame can be regarded as representative for longer time-frames as well.

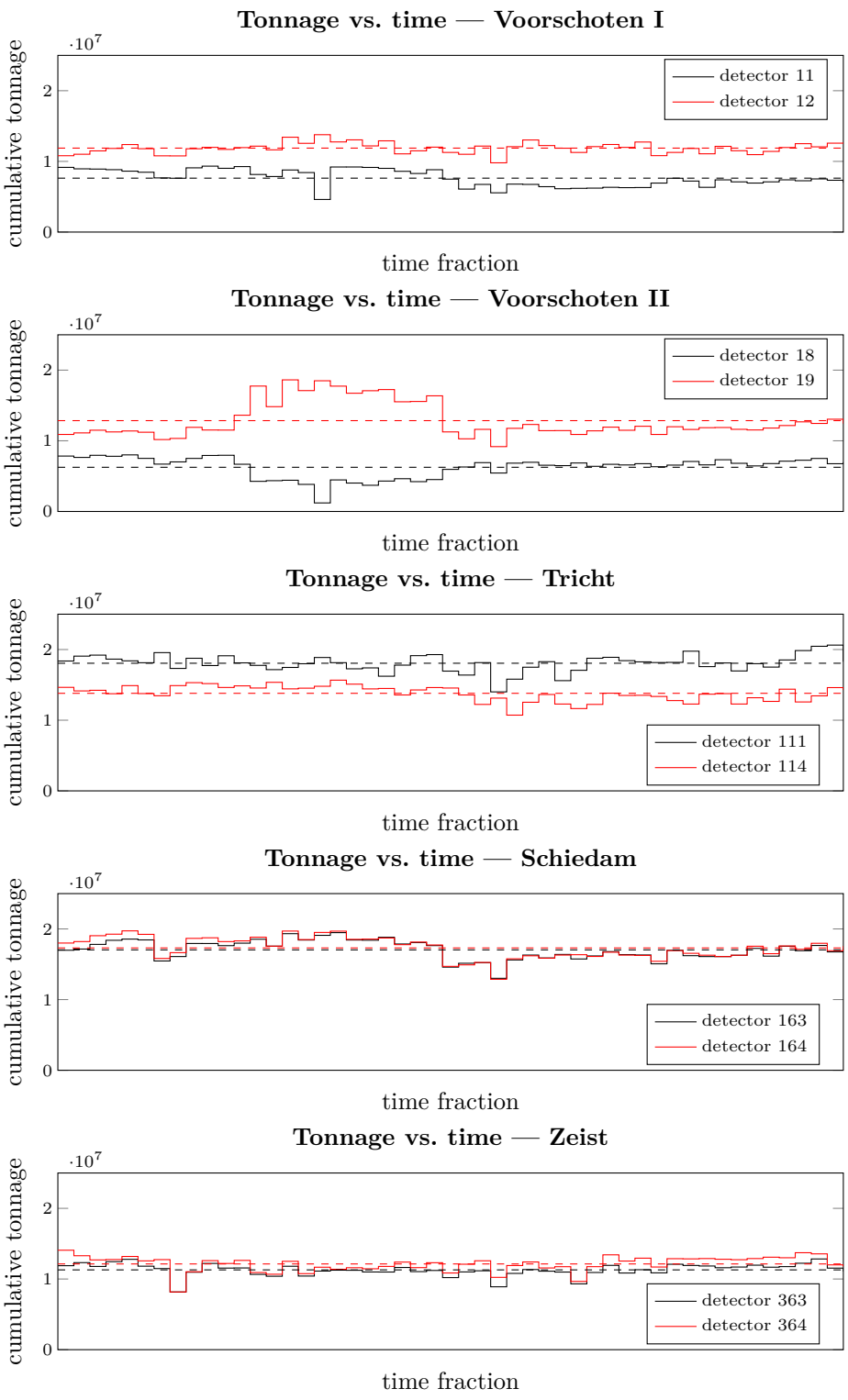

Figure C.7: Cumulative tonnage as a function of time. The measured time-frame was subdivided into 50 domains of equal time. Averages are plotted with dashed lines.

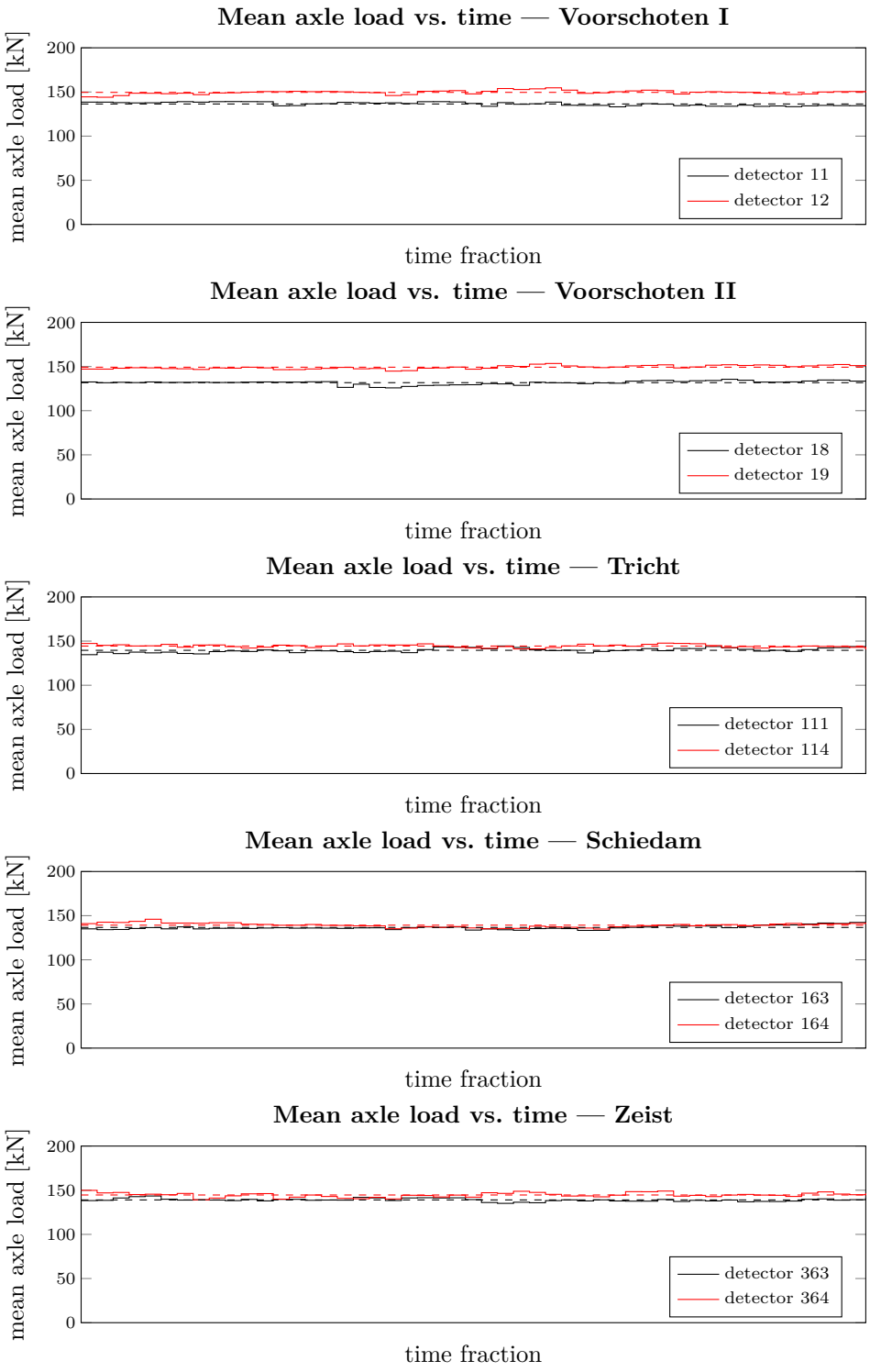

Figure C.8: Mean axle load as a function of time. The measured time-frame was subdivided into 50 domains of equal time. Averages are plotted with dashed lines.

D | Proportionality & Reliability

In this chapter some fundamental aspects of fatigue reliability are discussed. The main goal is to explore the relations between stress ranges, cycle counts and damage numbers. It is assumed here that the S-N curve can be simplified to a continuous line with a single slope m on a double-logarithmic scale, in order to allow for a simple mathematical description. At the end, concepts will be generalized to other S-N curves.

In addressing fatigue resistance, a key step is to transform loads to a spectrum of load cycles. Such a spectrum is a set which contains a description of cycles in terms of magnitudes and, when applicable, mean values. The frequency of occurrence is not included in this description, as recurring cycles can also be represented by including them repeatedly. Given a spectrum of load cycles, one can *transform* this into an equivalent number of load cycles, where transforming means: calculating the corresponding magnitude of the equivalent cycles. With this method, a spectrum is transformed into an equivalent spectrum consisting of constant amplitude cycles, and a number of repetitions. In the Eurocode approach the number of repetitions is fixed, and verification is done using an 'equivalent stress range'. If the cycles obey

$$N_e \, \Delta\sigma_e^m = \sum_{i=1}^{n} \Delta\sigma_i^m \tag{D.1}$$

where

N_e = equivalent number of cycles
$\Delta\sigma_e$ = equivalent stress cycle magnitude
$\Delta\sigma$ = stress range as part of the spectrum
m = fatigue exponent, as discussed in chapter 2
n = number of cycles

then the equivalent stress cycles will result in an equal damage number and can thus be seen as an adequate substitute for the spectrum. The magnitude of these equivalent cycles can be expressed directly by rewriting equation D.1:

$$\Delta\sigma_e = \left(\sum_{i=1}^{n} \frac{\Delta\sigma_i^m}{N_e} \right)^{\frac{1}{m}} \tag{D.2}$$

Focusing on the summation in equation D.2, this can be expanded into:

$$\sum_{i=1}^{n} \Delta\sigma_i^m = \Delta\sigma_1^m + \Delta\sigma_2^m + \ldots + \Delta\sigma_n^m \tag{D.3}$$

Now introducing two multiplication factors, for the stress level (η_σ) and the number of cycles (η_n), this summation can be written in terms of its proportionality to these

quantities[1]:

$$\sum_{i=1}^{\eta_n\, n} (\eta_\sigma\, \Delta\sigma_i)^m = (\eta_\sigma\, \Delta\sigma_1)^m + (\eta_\sigma\, \Delta\sigma_2)^m + \ldots + (\eta_\sigma\, \Delta\sigma_n)^m + \ldots + (\eta_\sigma\, \Delta\sigma_{\eta_n\, n})^m$$

$$= \eta_\sigma^m \left(\Delta\sigma_1^m + \Delta\sigma_2^m + \ldots + \Delta\sigma_n^m + \ldots + \Delta\sigma_{\eta_n\, n}^m\right)$$

$$\approx \eta_n\, \eta_\sigma^m \left(\Delta\sigma_1^m + \Delta\sigma_2^m + \ldots + \Delta\sigma_n^m\right)$$

$$= \eta_n\, \eta_\sigma^m \sum_{i=1}^{n} \Delta\sigma_i^m \tag{D.4}$$

This is only valid under the assumption that an increase in the number of cycles does not affect the intensity of the cycles, which can be assumed valid for small increases or spectra with little variation. Therefore the approximation-sign was used in the above derivation. One can imagine that a larger number of cycles with a random nature inherently increases the chances of a maximum occurring. This effect is neglected here by assuming that an approximation by repeating the same load model suffices. This will later be addressed as *extrapolation*, see appendix G.

Combining equations D.2 and D.4, the proportionalities (symbolized using $\propto$) of the equivalent stress range to alterations of either the stresses or the number of cycles, can be determined (assuming the equivalent number of cycles N_e as fixed):

$$\Delta\sigma_e = \left(\sum_{i=1}^{n} \frac{\Delta\sigma_i^m}{N_e}\right)^{\frac{1}{m}} \propto \left(\sum_{i=1}^{\eta_n\, \underline{n}} \left(\eta_\sigma\, \underline{\Delta\sigma_i}\right)^m\right)^{\frac{1}{m}} \approx \left(\eta_n\, \eta_\sigma^m \sum_{i=1}^{\underline{n}} \underline{\Delta\sigma_i^m}\right)^{\frac{1}{m}} \propto \eta_n^{\frac{1}{m}}\, \eta_\sigma\, \underline{\Delta\sigma_e} \tag{D.5}$$

where *underlined* ($\underline{\bullet}$) symbols represent some original values, while 'normally' printed symbols represent the outcome given an alteration of n and $\Delta\sigma$ by their respective factor η (i.e. $n = \eta_n\, \underline{n}$ and $\Delta\sigma = \eta_\sigma\, \underline{\Delta\sigma}$). For the damage number an equivalent proportionality would be:

$$D \propto \Delta\sigma_e^m \approx \left(\eta_n^{\frac{1}{m}}\, \eta_\sigma\, \underline{\Delta\sigma_e}\right)^m = \eta_n\, \eta_\sigma^m\, \underline{\Delta\sigma_e^m} \tag{D.6}$$

This shows that there is a large difference between safety factors used for the stress and for the damage number (which is proportional to the number of cycles), namely an exponent m. This explains why some codes prescribe very large safety factors (up to 10 in offshore engineering) compared to the factors used in the Eurocode (which clearly uses verification in the stress-domain, by using equivalent stresses).

Another interesting finding can be obtained from the above result. Consider that both the magnitude of stress ranges as the number of cycles is subject to variations or uncertainties, described by probability distributions. Let these be represented by their respective multiplication-factors, η_n and η_σ. Then, the proportionalities presented in equations D.5 and D.6 can be used to express equivalent probability distributions

[1] It is assumed here that the product $\eta_n\, n$ is an integer. This leads to a rounding error, which vanishes for an increasing number of cycles.

including variations or uncertainties in both, **thereby allowing for the variations in the number of cycles, to be incorporated into a safety factor on the stress range, alongside a safety factor on the stress range itself**. This is graphically depicted in figure D.1. In the figure, all variations are *lumped* onto the stress level, which implies that the corresponding number of equivalent cycles remains fixed at N_e.

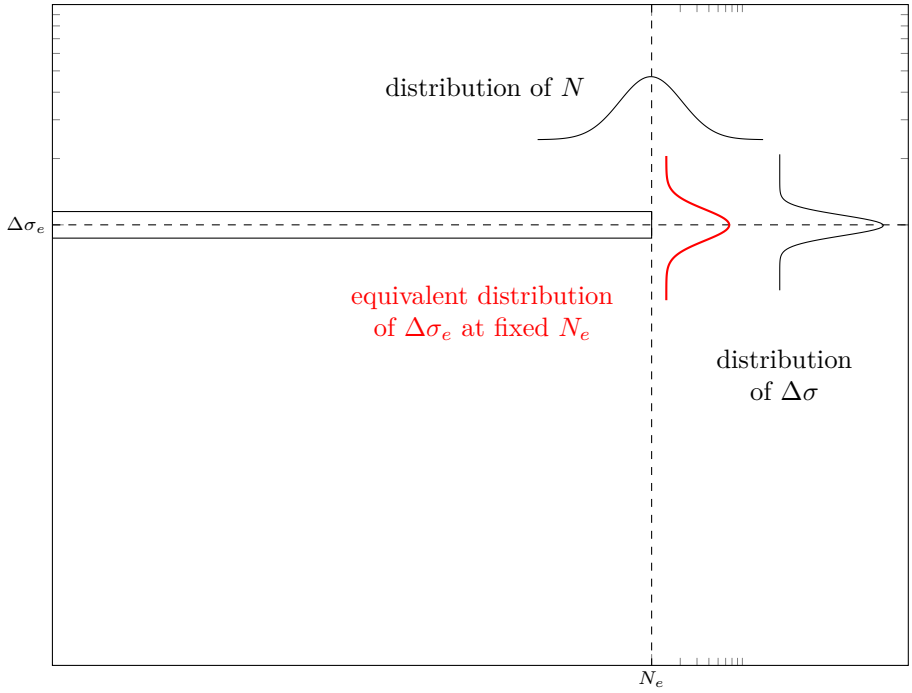

Figure D.1: Equivalent distribution of the equivalent stress with inclusion of uncertainties in cycle count. Here all spread is lumped in the stress-domain, while fixing the number of equivalent cycles.

The next point of interest concerns the number of equivalent cycles N_e. For this the proportionalities are examined once more. The equivalent stress can be determined using

$$\Delta\sigma_e = \left(\sum_{i=1}^{n} \frac{\Delta\sigma_i^m}{N_e} \right)^{\frac{1}{m}} \tag{D.2}$$

Therefore the equivalent stress clearly obeys

$$\Delta\sigma_e \propto \left(\frac{1}{N_e} \right)^{\frac{1}{m}} \tag{D.7}$$

which can be represented on logarithmic paper as

$$\log \Delta\sigma_e \propto \log \left(\frac{1}{N_e} \right)^{\frac{1}{m}} = \frac{1}{m} \left(\log 1 - \log N_e \right) = -\frac{1}{m} \log N_e \tag{D.8}$$

This shows that the equivalent stress is not so much a single point in the S-N plane, but rather a line following a slope of $^{-1}/_{m}$, connecting all combinations (points) which result in an equal damage number. This is also true for the reliability corresponding to this damage, causing these lines to represent a constant reliability.

In case of differently shaped S-N relations, this theory does not hold in its current mathematical form. However, the conclusions which were drawn are generally valid.

Conclusions

- In fatigue loading analysis, both the number of cycles as their magnitudes are important. Therefore this is also true for their uncertainties.
- The uncertainties have been shown to be interchangeable between domains (stress range and number of cycles), using the concept of an equivalent stress range. This also proves that verification is possible in both the domains of intensity and cycle count, both incorporating all uncertainties.
- The relative importance of the uncertainties has been shown for the case of a continuous and linear S-N curve on double-logarithmic scale. Compared to the linear impact of the number of cycles on the damage number, variations of the stress range are amplified by the fatigue exponent. Similar behavior will be observed for S-N curves of other shapes.
- The probability distribution of the equivalent stress follows the shape of the S-N curve. Therefore this should be visualized as a field of lines parallel to the S-N curve, each representing equal reliability (only valid for double-logarithmic scale).

The theory which has been presented in this chapter, mainly serves to provide insight in the nature of typical S-N relations, damage number, and its corresponding cycle count and stress ranges. The actual techniques are not relevant from a practical points of view, and for the probabilistic analyses other methods will be employed, which are more suited to a wider range of S-N curves.

E | Influence Lines & Cycles

In this chapter the use of influence lines to generate signals is explained and illustrated. Subsequently, methods for cycle counting from these signals are treated. These operations correspond to the influence-operator and the rainflow-operator, as introduced in chapter 4.

E.1 Influence lines

An *influence line* is a graphical representation of a certain effect at a given position (shear or axial force, bending moment, rotation, deflection, ...) in terms of magnitude, caused by an action with a varying location. In essence it is a plot of an influence factor for a varying position of the action along the span of the structure.

Influence lines are used extensively in fatigue design and engineering. Their role is to aid the transformation from a system of axle distances and loads to a stress history at the detail of interest. This is achieved by employing the influence line to calculate the effect of each axle load, at its current distance (by using the corresponding value of the influence line at this position). The total effect is then determined using the principle of superposition (assuming linear elastic calculations, as prescribed in the Eurocode). The entire system of axle loads is then shifted along the span, mimicking the actual passing of a train. Mathematically, this is expressed as

$$E_i(x) = \sum_{j=1}^{m} c_{i,j}\, F_j \tag{E.1}$$

where:

$E_i(x) = i$'th effect
$c_{i,j}$ = influence factor relating the i'th effects and the j'th action
F_j = j'th action

Because the *influence-operator* can be seen as a nonlinear transformation (from a system of axle loads and distances to a signal), it has to be included in the calibration. It's importance will be shown by a simple example for a simply supported beam as displayed in figure E.1. This is done by calculating the signal resulting from the passing of a single train (reference train 1 from appendix J) for varying spans L.

The different signals plotted in figure E.2 show a clear difference for increasing spans. The effects have been normalized by division by L because of the proportionality as given by the influence factors. However, a clear increase in magnitude is visible for increasing spans. This increase is caused by the summation in equation E.1, from which it is clear that a larger span will carry more axles resulting in a higher magnitude in total effects. The load thus acts in a more distributed manner when the span increases, so one might consider normalizing with $^1/_{L^2}$.

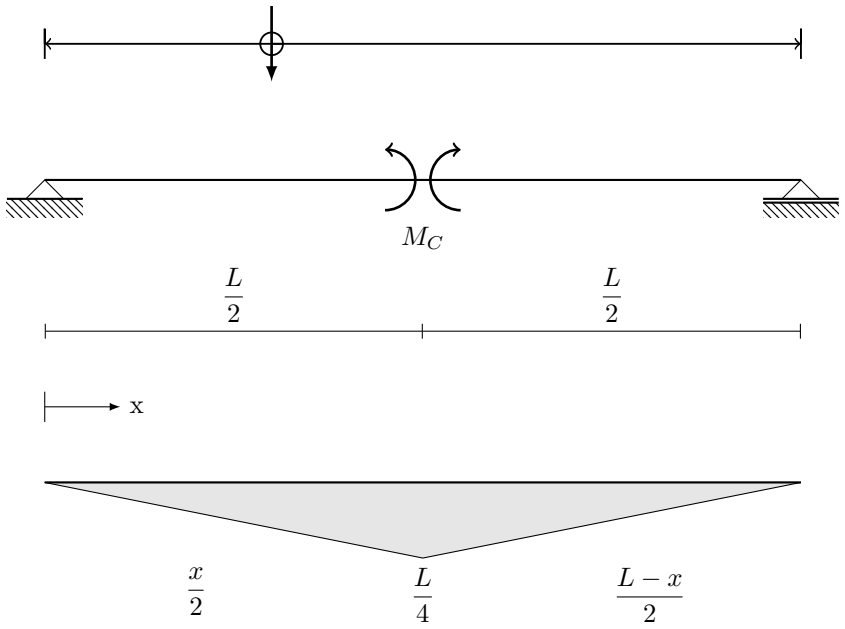

Figure E.1: Influence line for the mid-span bending moment M_C.

Apart from the aforementioned increase in magnitude, the shape of the signal is also very different. Smaller spans, in the same order of magnitude as the axle distances, result in more *spikes* in the signal, resembling pulses of loading. Because of the large number of repetitions in loading for small spans, the relative importance of the fatigue limit state with respect to the strength limit state increases, as is always the case for loading of a highly repetitive nature. This is caused by the fact that the resistance required for the strength is proportional to the amplitude of the loading. For larger spans the number of repetitions at full loading is much smaller: compare passing of trains to passing of bogies or even individual axles.

E.1.1 Effect of multiple tracks

Now that it is clear what influence lines are and how they are employed in fatigue analysis, their use is expanded slightly. When calibration is done for a structure with multiple tracks, it may be clear that the presence of multiple tracks contributes to the fatigue damage. To incorporate such an effect, an influence line is needed to express the behavior in the transverse direction (where the influence lines as treated before are labeled the longitudinal influence lines).

Combination of these influence lines results in an *influence field*. Especially for statically indeterminate structures, the determination of such a two-dimensional influence surface can be quite elaborate. These influence fields can also be generated using finite element calculations, where the loads are simply applied on each point of a grid, and the relevant effect is monitored for each application. A plot of the effect vs. the coordinate of force application yields the influence line.

A main problem that arises however, is the fact that the Eurocode traffic mixes (see section 2.1.4.2) are supplied without further information regarding application to multiple tracks. Therefore it is not possible to compare structures with multiple tracks, without the use of significant assumptions. **This has led to the decision to focus on comparing the load effects for traffic on a single track in this**

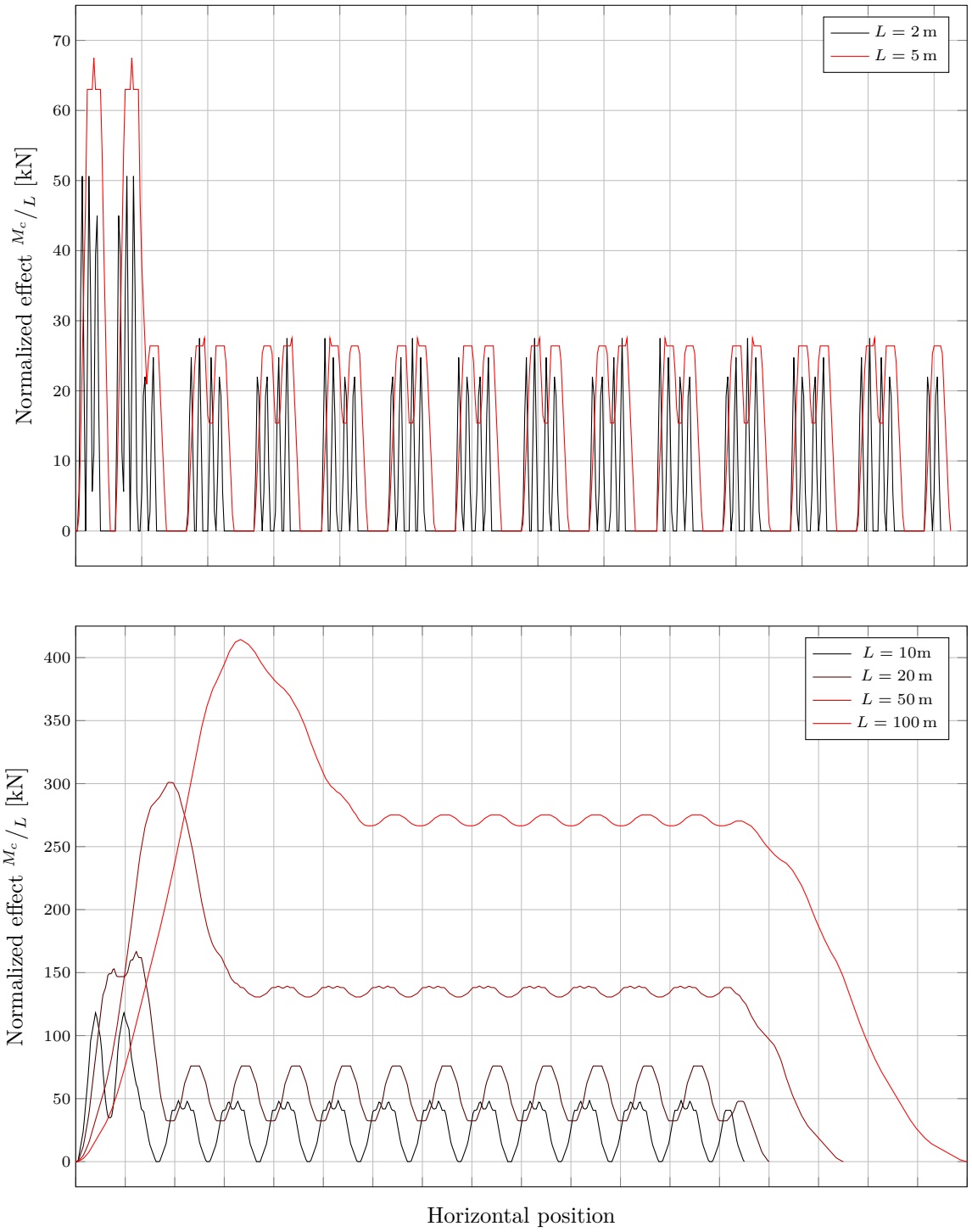

Figure E.2: Effect *signals* for different span lengths. Effects have been normalized, i.e. divided by the span L.

thesis. Important to note is, that there is no solution to this lack of specification. One could not, for instance, let trains pass over tracks at random intervals or times, as a load model is deterministic by definition. Without knowing in which way the model is meant to be applied for multiple tracks, which could be anywhere between no simultaneous passings and all passings coinciding, it can not be applied.

E.1.2 Creating structures

Logically, the influence fields are to be determined for finite element models which correspond to real structures. A straightforward approach for load application to FEM-models, is to the nodes directly, although this poses demands on their position in the mesh. The strategy will be to create the mesh in such a manner that direct application of loads is possible for each step.

Running the analysis, axles composed of two 0.5 [−] loads are passed over the mesh, together representing a unit axle load. For each time-step, the effects are recorded. To create a mesh that complies with the above criterion of direct nodal application, it is essential to know:

- The distance between the wheel in transverse direction, i.e. the width of the tracks.
- It was chosen to work with increments in the coordinate instead of time, therefore basically replacing time with pseudotime. This requires choosing the length of increments.

In reality, tracks are often positioned on a ballast bed on the structure. If this is the case, then some spreading through this medium is generally taken into account. For this work however, such spread of axle loads through ballast beds is not considered. The same is true for spread by rails and sleepers, which were also not considered. Note that this assumption is off far less importance because it concerns a comparison of loads, instead of a real design.

An example of a simple slab with two tracks is shown in figure E.3. Here, also the corresponding finite element mesh is given, with node numbering. It is emphasized again, that even though there are two tracks on the slab in figure E.3, the analyses will only employ one.

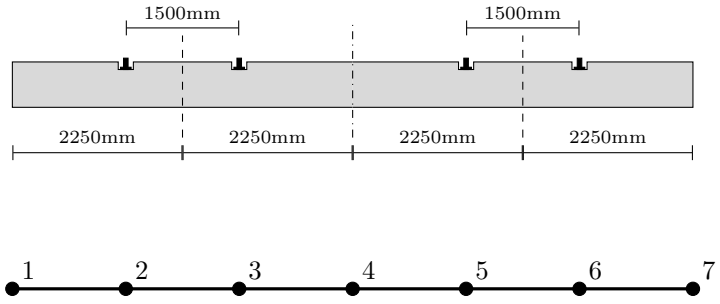

Figure E.3: Cross-section of a slab with two tracks, with its finite element discretization.

E.1.3 MATLAB and OpenSees implementation

Several MATLAB scripts were written to automate the procedure of mesh-generation and subsequent analysis for each pseudotime-step. Finite element analyses are done using OpenSees, which is an open source FEM package developed at the University of California, Berkeley. Firstly, the script `createMesh.m` is used to create a FE mesh from input. The input is in the form of nodal coordinates for each transverse section

(specified by y and z coordinates), as well as a connectivity table to span elements between the nodes of each incremental section. This saves one of performing this cumbersome task manually, and therefore reduces the error rate significantly.

`createMesh.m` was set up to write text-files with `.tcl`-extension, which is the default for OpenSEES. Output consists of:

- table with nodal coordinates → `nodalcoords.tcl`
- table with element connectivity → `connectivity.tcl`
- table with constraints → `constraints.tcl`
- table with sequence of loaded nodes for each time-step → `loadsequence.tcl`

These files serve as input files for the next step, which is controlled by `analysis.m`. The analysis-script loops over all steps, and steers the FEM-package, OpenSees, to do its analysis. OpenSees was set up to record the forces in the elements to a file named `element.out` which is filled with a string of generalized forces per element. These can then be retrieved and coupled with the original elements using MATLAB and the script `ele_stress_rec.m`, which also records the forces for each timestep to a cell-array `Rec_element`.

For each step, MATLAB, which is running `analysis.m`, calls OpenSees using a `.tcl`-file which defines what kind of FE analysis is requested: in this case linear static. The analysis is then performed using the input files, in turn modified by MATLAB for each step. The overall result is a record of all cross-sectional forces for each time step.

E.1.4 Creating influence lines

Influence lines can now be obtained using the method described in the foregoing section. As an example, this is demonstrated for the cross-section shown in figure E.3. Here, it was chosen to apply boundary conditions corresponding to clamped supports, along with a span of 10 m. Furthermore, the exact location where the bending moment is obtained from, is under the track over which the train passes (mid-span). The resulting influence line is shown in figure E.4. Most analyses were of course done using a more refined grid. It is noted that the exact location, chosen from the

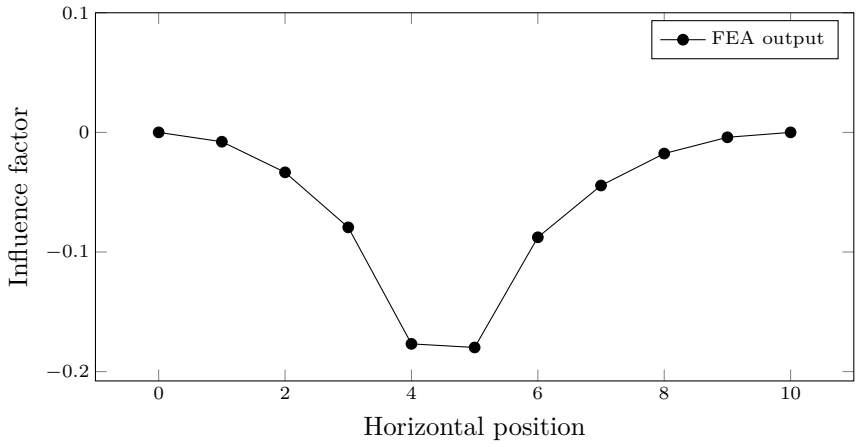

Figure E.4: Influence line for the mid-span bending moment for a concentrated load. Cross-section is taken from figure E.3, combined with a span length of 10 m.

finite set of integration points which are available, is not that important. Of main

importance is the **shape** of the influence line, rather than for instance the maximum bending moment. With reference to chapter 4, it is remarked that differences in pure scaling of the influence line (in magnitude, that is), are compensated by an appropriate proportionality factor u. Such a scaling does therefore not change results of a comparison, as opposed to a design situation, where the absolute magnitudes are of course of considerable importance.

The actual structural schemes chosen for the calibration procedure, and therefore the influence lines as well, are presented in chapter 5. Inclusion of all influence lines was ommitted in this report, in order to save some paper (about 30 pages). An overview of available influence lines, however, is presented in table E.1. The definition of structural schemes 1–7 can be found in chapter 5. Anyone interested in these influence lines is encouraged to contact the author for a copy.

span [m]	scheme 1	scheme 2	scheme 3	scheme 4	scheme 5	scheme 6	scheme 7
1	✓	✓	✓	✓	✓		
2	✓	✓	✓	✓	✓		
3	✓	✓	✓	✓	✓		
4	✓	✓	✓	✓	✓		
5	✓	✓	✓	✓	✓	✓	✓
6	✓	✓	✓	✓	✓	✓	✓
7	✓	✓	✓	✓	✓	✓	✓
8	✓	✓	✓	✓	✓	✓	✓
9	✓	✓	✓	✓	✓	✓	✓
10	✓	✓	✓	✓	✓	✓	✓
12	✓	✓	✓	✓	✓	✓	✓
14	✓	✓	✓	✓	✓	✓	✓
16	✓	✓	✓	✓	✓	✓	✓
18	✓	✓	✓	✓	✓	✓	✓
20	✓	✓	✓	✓	✓	✓	✓
22	✓	✓	✓	✓	✓	✓	✓
24	✓	✓	✓	✓	✓	✓	✓
26	✓	✓	✓	✓	✓		
28	✓	✓	✓	✓	✓		
30	✓	✓	✓	✓	✓		
35	✓	✓	✓	✓	✓		
40	✓	✓	✓	✓	✓		
45	✓	✓	✓	✓	✓		
50	✓	✓	✓	✓	✓		

Table E.1: Overview of influence lines.

E.2 Cycle Counting

To obtain the stress-cycles from a stress-signal, a so-called *counting method* is employed. Input is a signal, reduced to its extrema (minima and maxima) or turning points. Several methods are available, i.a.:

- level cross counting;

- peak counting;
- simple-range counting;
- rainflow counting.

The methods are not investigated into further detail, as several authors recommend the rainflow cycle algorithm for fatigue analysis, yielding the highest accuracy among the methods available (Ligaj, 2011; Singh & Ranganath, 2010; Olagnon, 1994). Therefore it is used in many different industries, among which the automotive, aircraft, energy, and steel industry (Amzallag, Gerey, Robert, & Bahuaud, 1994). This justifies the choice for the rainflow cycle counting algorithm for this work, which is also prescribed in the Eurocode.

E.2.1 Rainflow cycle counting algorithm

The Rainflow cycle counting algorithm, first introduced by Matsuishi and Endo (1968), is based on an analogy between a stress-history and the flow of water from a *pagoda*-roof (Wikipedia, 2015b). Basically, eight steps can be distinguished:

1. The stress history is reduced to its extrema, i.e. peaks and troughs. These are also known as *turning points*.
2. The time-history is imagined as a 'pagoda'[1].
3. The time-history is turned 90 degree in the clockwise direction. This means that the time-axis is now vertical with the starting time at the top.
4. It is imagined that a source of water emerges from each tensile peak. This water then 'drips down the pagoda'.
5. The number of half-cycles are counted by considering that the flow is terminated when:
   (a) the end of the time-history is reached, or
   (b) the flow merges with a flow which has started at an earlier tensile peak, or
   (c) a trough of greater magnitude is encountered.
6. Step 5 is repeated for compressive troughs.
7. Each half-cycle gets assigned a magnitude, which is equal to the difference between its start and termination.
8. Half-cycles are paired up with half-cycles of equal amplitude to form complete cycles (this step is optional).

The steps listed above form the algorithm, resulting in a spectrum of cycles. Such a spectrum contains all the information necessary for the determination of the damage number according to the methodology (assumptions) followed in this report. The order of cycles is not important because of the linear damage accumulation rule of Miner, while the duration of loading is neglected in the Eurocode's S-N curves.

E.2.2 The algorithm in action

To provide some insight into the rainflow cycle counting algorithm, an example is presented in this section. Starting points is the first part of a Eurocode reference train passing over a 5 meter long beam. For this the signal corresponding to the mid

[1] Pagoda: traditional Eastern-Asian tower with characteristic stepped roof.

span bending moment is determined and reduced to its turning points. Duplicate points were removed (two or more consecutive points in time with zero difference).

Using the algorithm described above, the signal is decomposed into cycles. The graphical representation of this process is displayed in figure E.5. Each half-cycle is visualized with a black line (original signal is drawn in red), ending with a short perpendicular dash. To finalize the process, the cycles are counted and combined to produce the spectrum, given in table E.2.

E.2.3 MATLAB implementation

The algorithm has been implemented in MATLAB by Adam Nieslony in 2009, written in C and compiled accordingly. This has resulted in a very fast algorithm for rainflow cycle counting. The results are verified according to the example presented in section E.2.2, which resulted in perfect agreement.

Input for the algorithm consists of a (time) signal, in the form of a $1 \times n$ vector. Optionally, the time can be included, but this is not required for this work and therefore omitted. The output is a rainflow table comparable to table E.2, without the cycle's number, start value, and stop value. Only the essential information is thus kept, i.e. the amplitude (= half the range), the mean, and the count. The output is a $3 \times m$ matrix of counted rainflow cycles.

E.3 Conclusions

- The influence field/line is of critical importance to the fatigue damage. In comparing different traffic for damage, it is therefore unavoidable to consider different influence lines, and thus actually structures.
- It was decided to compare structures solely based on the passage of trains over a single track. Reason for this, is that the Eurocode traffic mixes are given without guidelines on appliance to multiple tracks (e.g. simultaneous or subsequent passages).
- It was concluded that, for the purpose of comparing effects from traffic, only the shape of the influence line is of importance. The magnitude, or scale, is thus not of importance at all. Note that this is of course not true for an actual fatigue verification.
- To convert signals to stress ranges or cycles, the rainlow cycle counting method will be used. An example, which was used to verify the implementation of the algorithm, was presented.

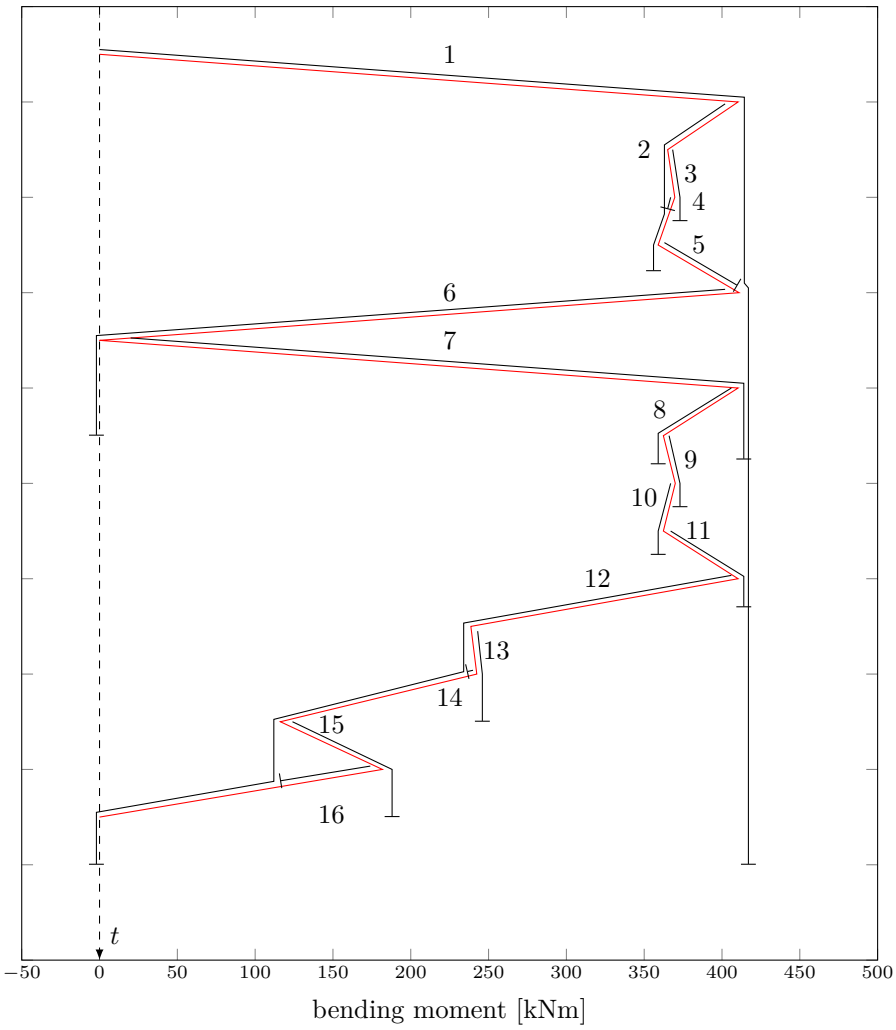

Figure E.5: Effect *signals* for different span lengths.

#	start	end	amplitude	mean	count
1 + 6	0	411	205.5	205.5	1
2	410	359	25.5	384.5	0.5
3 + 4	365	369	2	367	1
5	359	410	26	386	0.5
7 + 12	0	410	205	205	1
8 + 11	410	362	24	386	1
9 + 10	362	370	4	366	1
13 + 14	239	242	1.5	240.5	1
15 + 16	116	182	33	149	1

Table E.2: Result of Rainflow algorithm applied to the signal from figure E.5. Start, end, amplitude, and mean values are all in kNm.

F | Traffic Decomposition

Using the measured traffic, as discussed in appendix 2, it is interesting to perform some preliminary analyses. In this chapter, two question are addressed:

1. What is the relative importance of **cycles** with respect to the damage number?
2. What is the relative importance of **trains** with respect to the damage number?

It is thus investigated whether fatigue damage is mainly accumulated through many repetitions (cycles), or mainly through a few large loads (say 1 % of cycles). This is, among others, interesting in dealing with the extrapolation of measured load histories (treated in section 5.2.3 and appendix G).

This analysis is based on a reference case, which was chosen for this purpose:

- All data is processed in a fully deterministic manner, thus without taking account of e.g. model, material, and measurement uncertainties.
- The traffic from detector 111 (Tricht) will be used because of its versatility in axle loads. This will be compared to a 'gentler' traffic record: detector 11 (Voorschoten).
- The influence line used in this example is based on a doubly clamped slab, span length 10 m (see also chapter E). The effect of interest is the mid-span bending moment in longitudinal direction. The width of the slab is sufficient to accommodate two tracks, but one track of traffic is applied.
- The comparison is done for concrete in compression, using the resistance model presented in the Dutch national annex of the Eurocode. The assumed characteristic concrete strength is $45\,\mathrm{N/mm^2}$, the ratio of permanent load over design strength was set to 0.3.
- The proportionality-factor u (see chapter 4) is determined based on the Eurocode standard traffic mix (EC1), thereby yielding a design according to the Eurocode.

Using the above assumptions, the analyses in this chapter were performed. Throughout the report, these assumptions are denoted as forming the 'reference case'.

F.1 Relative importance of cycles

For both traffic records (detector 11 and 111), the damage-increments are determined. Here, a damage-increment is defined as the damage resulting from either a half or a full cycle, as contained in the rainflow matrix. From this, the damage is plotted as a function of the cumulative number of cycles, see figure F.1.

The figure is constructed as follows: first of all, the damage increments were sorted in magnitude, largest first. Starting from the total damage number done by the detector

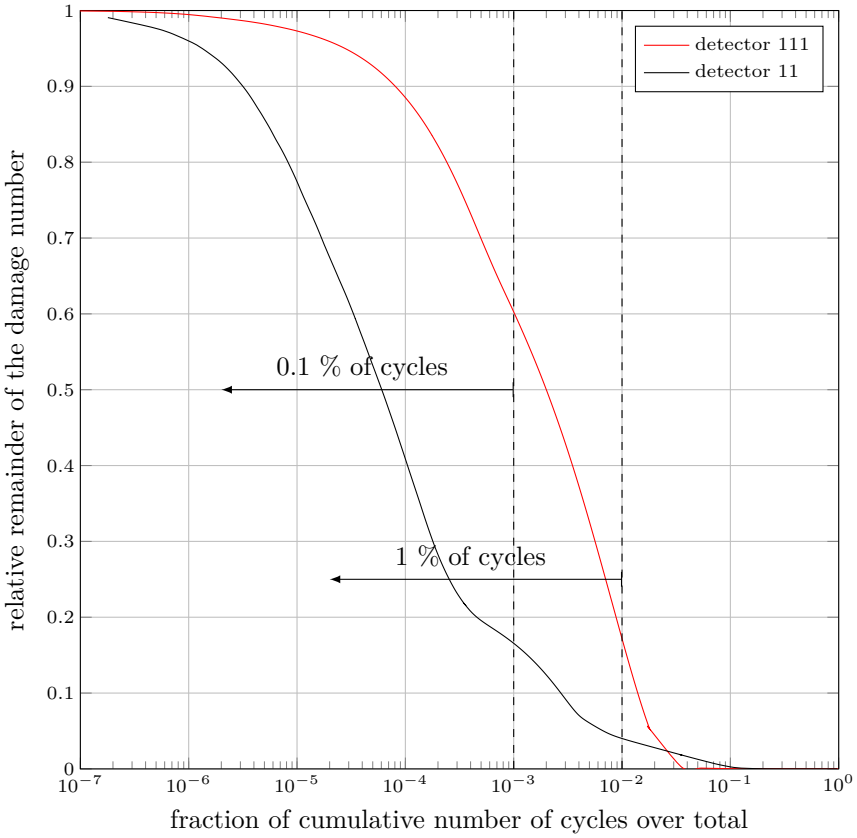

Figure F.1: Importance of cycles, characterized by their relative fraction of the damage number. The gap in the graphs near a relative cumulative damage of 1 is caused by the fact that a remainder of damage which is equal to 1, corresponds to zero cycles. This zero cannot be represented on the logarithmic scale. Cycles are sorted in descending order, based on their individual damage number.

traffic, the cumulative sum of damage increments from the sorted set is determined, starting from zero damage increments. These are substracted from the total damage number, thus for zero cycles, the remainder of damage number is 1, for a single cycle, the remaining is the total damage number minus the largest increment, and so on. Finally, both axes are normalized.

This figure provides a lot of insight into the real accumulation of fatigue damage. Clearly, one percent of the cycles does practically all damage. It was expected that the traffic recorded by detector 111 would do its damage mainly by a few aggressive events, as there is large variation in the axle loads. Detector 11, with its gentler axle loads, was expected to have a larger parts of the cycles contribute to the damage number. Apparently, this is not the case. The question remains, what causes this behavior. The following theory is proposed: the more severe loading events occur less frequently at detector 11, while doing practically all damage. Therefore, their **relative** importance is larger than at detector 111 where these loads occur more frequently.

If this procedure is repeated for reinforcement steel, where it is assumed that it is welded (fatigue exponents 3 and 5), a different picture emerges. Now, 90 % of damage is done by approximately 8 % (detector 111) to 15 % (detector 11) of cycles. In

practice however, welded reinforcement is used seldom. With 'regular' reinforcement steel, with fatigue exponents 5 and 9, the results resemble those found for concrete to a greater degree (for detector 111, 1 % of cycles is responsible for 50 % of the damage).

F.2 Relative importance of trains

In the previous section, it has been shown that for the reference case, 1 % of the cycles was practically responsible for the entire damage number. In this section, the goal is to obtain insight into the exact traffic which does this damage. For this, the procedure to calculate damage numbers was adjusted, in order to process one train at a time. Subsequently, the trains can be grouped according to type to see whether a specific type of traffic does excessive damage.

Important is that, even if it is known that a small fraction of all cycles does all damage, this does not automatically imply anything about the number of trains that cause them. If each train results in 100 cycles, and one of these is of far larger amplitude than the others, the result would still be as obtained in the previous chapter.

The decomposition of damage into fractions, caused by individual trains, can be tricky. Attention should be paid to the cycle counting algorithm (rainflow cycle counting). The method of calculating damage per train is implemented by looping over all trains in a traffic record, and for each determining the signal using the relevant influence line and parameters, counting the cycles, from which the damage number is determined. Now, this is only valid for signals that are strictly positive or negative with inclusion of zero (and axle loads which are all positive, which is an assumption that it satisfied with greater ease). Otherwise, negative peaks (troughs) caused by some trains, may form large cycles with peaks in other train's signals (characteristic of rainflow cycle counting). Then, the damage calculation over parts of the signal is no longer valid, because it would neglect these larger cycles (which are the largest cycles overall, so the error would be significant).

In case all values of the influence line share the same sign, this problem does not occur. Then each peak is matched against the points of zero effect in the signal, which is present in between trains. An exception can be made for concrete in compression, where tensile peaks are set equal to zero anyway because cracked concrete is assumed.

In figure F.2 the results of this analysis (damage per train) are shown for the traffic from detector 11 and detector 111. It is clear that not only about 1 % of the cycles is responsible for practically the entire damage number, but the same is shown to be true on the scale of train passages. In other words, 1 % of trains does practically all damage.

Damage fractions corresponding to the most damaging 1, 10, and 100 trains are summarized in table F.1. Clearly, results correspond to those in figure F.2. For detector 11, the 100 most aggressive trains are even responsible for 70 % of the damage number, while a milder 10 % results with detector 111.

number of trains	damage fraction	
	detector 111	detector 11
1	0.0048	0.027
10	0.026	0.172
100	0.09	0.695

Table F.1: Damage fraction caused by most aggressive number of trains.

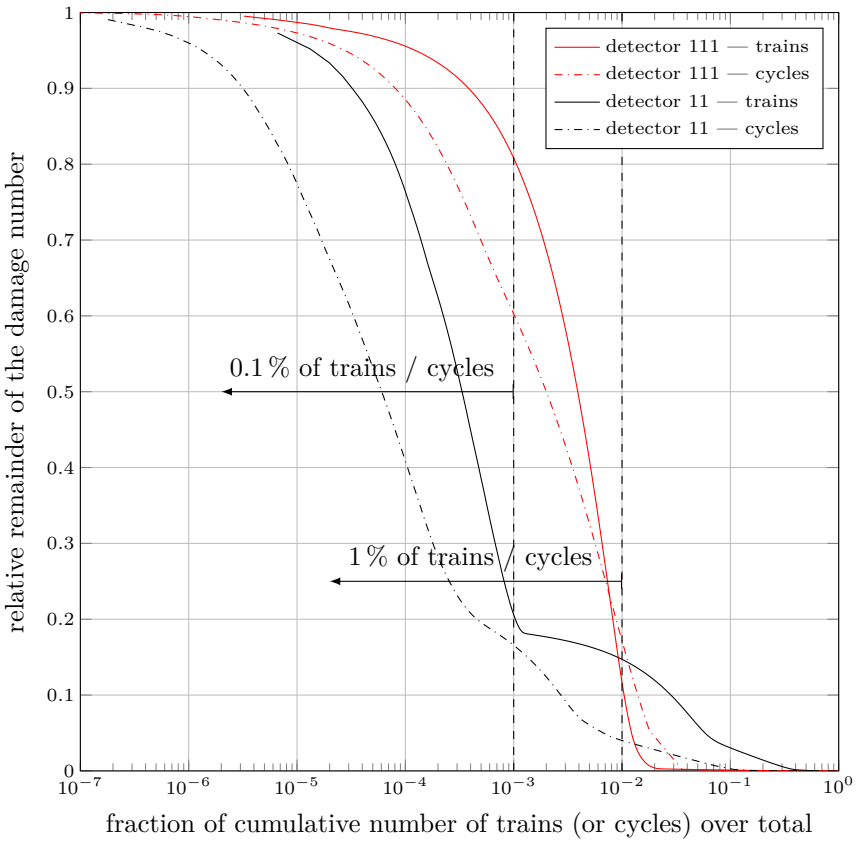

Figure F.2: Relative remainder of the damage number as function of the cumulative number of trains / cycles. Train and cycles are sorted in descending order, based on their individual damage number.

Next, it is of interest which trains cause the most damage. Most frequently (72 out of first 100 at detector 111, 62 out of first 100 at detector 11), the most aggressive trains were identified as (`LH(i).type` corresponding to the entry as explained in appendix C):

```
LH(i).type =
    'EL BR189'
    'Unknown Vehicle'
```

Furthermore, occurrences of

```
LH(i).type =
    'EL Lok 1600/1700/1800'
    'Unknown Vehicle'

LH(i).type =
    'DL G1206'
    'Unknown Vehicle'

LH(i).type =
    'DL JT42CWR (Class 66)'
    'Unknown Vehicle'
```

were frequently observed in the top of most aggressive trains. In figure F.3 some examples of the locomotives of these most aggressive trains are shown.

The 'Class 66'-locomotives were exclusively found in the top 100 records of detector 111 (not in detector 11). Note that in structure `LH`, only the unique types found in each train are present. This means that the `type`-field including duplicate train types would for instance look like:

```
LH(i).type =
    'EL BR189'
    'EL BR189'
    'EL BR189'
    'EL BR189'
    'EL BR189'
    'EL BR189'
    'EL BR189'
    'EL BR189'
    'Unknown Vehicle'
    'Unknown Vehicle'
    ...
    ...
    'Unknown Vehicle'
```

(a)

(b)

(c)

(d)

Figure F.3: Locomotives which were frequently identified as part of the most damaging trains at detector 111: (a) BR 189 (image by Hemkes, 2014); (b) JT42CWR Class 66 (image by Van Beem, 2005); (c) G 1206 (image by Bakker, 2009); (d) Lok 1600/1700/1800 (image by Bakker, 2011)

`'Unknown Vehicle'`

where each `'Unknown Vechicle'` represents a freigt car's axle. The eight entries of `'EL BR189'` represent the axles of two locomotives. This information was however not included in `LH` to reduce the data size.

Upon further inspection, the types identified above are lengthy freight trains with double locomotives. The most damaging train at detector 11 was found to be 202 m in length (between first and last axle). This train consisted of 64 axles, with an average load of 184 kN. For detector 111 the most damaging train had a length of 575 m, 224 axles, and an average axle load of 216 kN.

Further analysis concentrated on the occurrence of several types of trains, and their damage increments. To this extent, all `LH(i).type` entries were filtered according to containing a predefined string. The output which was generated, consisted of:

- the number of entries which contain the pre-defined string, i.e. the pre-defined vehicle.
- the relative number of occurrences defined as the number of trains with the entry, divided by the number of trains.
- the relative damage number done by trains for which the `type`-field contains this string.
- the first occurrence in a list of trains, where the list was sorted by damage number increment per train in descending order (sorted on aggressiveness).

Results for detector 111 are summarized in table F.2. It is clear that most of the damage ($> 99\,\%$) is caused by passages of trains containing the entry `'Unknown Vehicle'`, which is assumed to be freight transport. Another interesting conclusion can be drawn. Regarding the plans of increased passenger transport[1], where a number of intercity-trains ('VIRM') are added to the train table, it can be concluded that, in this analysis, these trains cause negligible damage compared to the transportation of freight. **Overall, the damage caused by passenger transportation is concluded to be insignificant for this track.**

The analyses presented in this chapter show that the a small fraction of the traffic is indeed responsible for the main part of the damage number. It was already clear from section F.1 that this was true for a small fraction of cycles, however, now these most damaging cycles have been linked to specific trains. It can be concluded that practically the entire damage number is the result of (heavy) freight trains passing (`'Unknown Vehicle'`).

F.3 Conclusions

- The relative importance of cycles, in terms of fatigue damage to concrete in compression, was assessed for real traffic. It was concluded that, for a reference case, about 1 % of cycles is practically responsible for the entire damage number. Further investigation should point out whether this is also true for other cases. If so, such a finding may be used to justify proportional charges for users operating on the tracks, thereby especially targeting these overloads.
- The same experiment was performed for individual trains, as opposed to cycles. Using this, it has been shown that the same conclusion can be drawn for the relative importance of trains with respect to fatigue damage.

[1] Program known as 'PHS', or 'Programma Hoogfrequent Spoorvervoer'.

string	number	fraction	rel. damage	1st occurrence
'Unknown Vehicle'	15530	0.0505	0.991	1
'BR189'	4155	0.0135	0.851	1
'JT42CWR'	763	0.0025	0.053	8
'G1206'	2245	0.0073	0.023	62
'Lok 1600/1700/1800'	4831	0.0157	0.044	68
'EL BR186 (Traxx)'	2372	0.0078	0.017	339
'G2000'	155	0.0001	0.012	17
'BR203'	1002	0.0033	0.002	22
'Lok 6400'	34	0.0001	0.000	2908
'VIRM'	93377	0.3034	0.002	6652
'EMU DDAR'	496	0.0016	0.000	8523
'EMU Mat 64'	726	0.0024	0.000	9035
'EMU ICM'	1213	0.0004	0.000	9942
'EMU SLT'	107065	0.3479	0.000	22565
'EMU ICE'	987	0.0032	0.000	34601
'Thalys'	20	0.0000	0.000	64255
'EMU SGM'	762	0.0025	0.000	109949

Table F.2: Data analysis using the type-field of detector 111. Note that damage number fractions do not add up to unity because of the presence of multiple train types (strings) in one train, e.g. a 'BR189' locomotive with 'Unknown Vehicle' freight cars.

- It has been investigated which **type** of traffic is mainly responsible for the damage. Results show that freight traffic is of main importance. Furthermore, the transportation of passengers was shown not to be significant in terms of its contribution to the damage number.

G | Extrapolation

In this work, the term 'extrapolation' is used for the activity in which one tries to gain insight into loads which can be expected in the future, based on measured traffic loads. Extrapolation should provide an answer to the question: "Which loads can be expected in the future, and should thus be incorporated into the design of structures?". In chapter 3, it was stated that railway bridges are designed for 100 years. Therefore, it is important to gain insight into the loads which can be expected during such a 100 year period. Clearly, these may differ from those loads which were observed. Also, the interest is not solely on one single extrapolated set of loads or load effects, but rather on some description of all possible sets of loads or load effects which may occur, each with a probability of occurrence.

A general introduction to extrapolation of traffic histories was given in chapter 5, with reference to this chapter. As stated there, four methods were identified:

1. Extrapolation of traffic, i.e. extrapolation 'on the level of traffic' as opposed to the other methods.
2. Time-extrapolation using extreme value theory, in this case the 'peak over threshold' method.
3. Spectrum fitting, both uni- and bivariate.
4. Extrapolation of the damage number (increments).

In this chapter each of these methods will be discussed first, after which a choice will be presented with justification. A selection of methods is then compared so that an extrapolation method can be picked.

G.1 Extrapolation of traffic

The first method for extrapolation which is discussed, is the extrapolation of traffic, thus the actual loads. It is possible to analyze the traffic and to generate distributions for its various characteristics, including correlation matrices. These can then be used to simulate future traffic, allowing for more extreme loads than those that occurred during the measured period. Basically, the relevant characteristics would be:

- axle loads;
- axle distances;
- velocities.

Apart from distributions for the above characteristics, also information regarding their correlation is required. Problems might be in the fact that correlation is not necessarily linear, which further complicates the analysis. Then some kind of model is needed to make sure that when new traffic is simulated, the vehicles are actually sensible trains.

One can imagine that it is quite difficult to come to sensible vehicles through sampling from the above, as there are only specific combinations that are observed in reality. Bounding some vehicle creation model to these combinations is expected to be a tedious task. Considering the result: because of the difficulty in modeling sensible traffic, the vast set of rules which lie at the basis of such a model will limit the output to 'something like the measured history'. Viewed skeptically: it is anywhere from very cumbersome to impossible to get better output from such a model, than the traffic that was recorded, especially if the time over which measurements are done is large, as is the case for this thesis. Fortunately, other methods are available which are believed to produce better results.

Also note that, if the damage is mainly accumulated through few cycles, that this is equivalent to stating that fatigue damage is a result of the exceptions in traffic. In a model for random traffic generation, bound by the need for sensible traffic, it is hard to include such extremely infrequent loading events. In other words, extremely infrequent events clearly are exceptional, and therefore not necessarily well represented by the observed traffic.

G.2 Time-extrapolation using EVT

Time extrapolation using extreme value theory (EVT) works in the time-domain, i.e. one step further (after appliance of the influence-operator, see chapter 4) in the fatigue assessment than describing the traffic using a statistical method. First the measured traffic is used to obtain a time-signal for an effect under consideration. As described by Johannesson (2006, 3), one could then focus on the highest peaks (and lowest valleys, analogously), and their distribution. In the cited work, an exponential distribution function is employed to approximate the peaks over a certain *threshold*-value (hence the name: *Peak over Threshold* or PoT).

This technique is quite promising for the extrapolation of time series, as it results in an actual signal instead of a set of cycle's ranges (as with fitting a distribution function over stress ranges, described in the coming section). In this way, cycles in the extrapolated signal are realistic, and include information required to determine their mean values, essential for the fatigue verification of concrete.

The threshold plays a central role in the peak-over-threshold method (from now on: PoT). It is this threshold, above which all peaks (analogously, this is valid for valleys below a threshold) are used in the inference-step, i.e. the 'function fitting'. Note that below the threshold, the peaks remain unaltered by this method of extrapolation. The signal itself is repeated to the desired length (hence the term 'time-extrapolation'), where only peaks surpassing the threshold are replaced by realizations of the fitted function.

Referring to the beginning of this chapter, where it was mentioned that the **importance** and the **uncertainties** are essential, the following can be noted. Applying the PoT-method for extrapolation, one assumes that the main body of the data is certain and/or unimportant enough to be assumed *as is*, and thus not meeting the demand for requiring extrapolation. The tail of the distribution however, is both important (i.e. causes the most damage per cycle) and quite uncertain because of its limited appearance in the measurements. For the tails both conditions are thus met.

In his article, Johannesson proposed to use an exponential distribution to model the exceedances. Other sources claim successful application of the generalized Pareto distribution (GPD), which is actually mentioned in most literature on the peak-over-threshold method. Actually, the GPD possesses some interesting characteristics which make it "*a natural choice for modeling peaks over a threshold*" (Ghosh & Resnick,

2010). Namely, for a large number of distributions, the distribution of excesses is asymptotically equivalent to the GPD with some parameters. This means that, for excesses over a threshold, the tails of these distributions actually converge to the GPD in an asymptotic sense, i.e. for increasing threshold values.

Some information on the GPD: the cumulative distribution function is given in equation G.1 (Ghosh & Resnick, 2010):

$$G_{\xi,\beta}(x) = \begin{cases} 1 - (1 + \xi\, x\,/\beta)^{-1/\xi} & \text{if } \xi \neq 0 \\ 1 - \exp\left(-x/\beta\right) & \text{if } \xi = 0 \end{cases} \tag{G.1}$$

with conditions on the distribution parameters (ξ and β)

$$\beta > 0, x \geq 0, \text{ when } \xi \geq 0$$
$$0 \leq x \leq -\beta/\xi, \text{ when } \xi < 0$$

For $\xi = 0$, the GPD is equal to the exponential distribution. Thereby, the link with Johannesson and Thomas, who use an exponential distribution, becomes clear. The GPD is fitted on the exceedances over a certain threshold (more on this level will follow). After choosing this threshold value, denoted with r, the distribution of excesses over this level is defined as (Ghosh & Resnick, 2010):

$$F_r(x) = P\left[X - r \leq x | X > r\right] \tag{G.2}$$

and analogously for valleys under a (different) threshold. The threshold is difficult to determine, and not uniquely defined as 'the right value'. Actually, the way this is frequently done, is by varying the threshold level, fitting a GPD to the excesses, and observing the parameter estimates for the distribution corresponding to each threshold-level. Then one searches for regions of r which result in stable parameter estimates.

Several authors state that the choice of a threshold can be difficult, and problematic in the sense that results depend heavily on it (Simiu & Heckert, 1996; Bensalah, 2000; Pandey, Van Gelder, & Vrijling, 2001). Part of the problem lies in the duality of the threshold choice: it should be large enough to satisfy the conditions which permit its application, while at the same time leaving sufficient observations for the estimation. Inclusion of a larger number of observations does not necessarily improve the accuracy:

> "*The choice of the threshold is subject to a trade-off between variance and bias. By increasing the number of observations for the series of maxima (a lower threshold), some observations from the centre of the distributions are introduced in the series, and the index of tail is more precise (less variance) but biased. On the other hand, choosing a high threshold reduces the bias but makes the estimator more volatile (fewer observations).*" — Bensalah, 2000

One way to obtain a suitable threshold, is by examining the *mean excess* function. In case of an independent and identically distributed sample $X_1, X_2, \ldots, X_n$, the estimator for the mean excess function is defined as (Ghosh & Resnick, 2010):

$$\hat{M}_e(r) = \frac{\sum_{i=1}^{n} (X_i - r)\, I_{[X_i > r]}}{\sum_{i=1}^{n} I_{[Xi > r]}} \tag{G.3}$$

Ghosh and Resnick continue by stating that for a random variable which follows a generalized Pareto distribution, the expected value is finite only if $\xi < 1$. If this

condition is satisfied, the mean excess function corresponding to this distribution is

$$M_e(r) = \frac{\beta}{1-\xi} + \frac{\xi}{1-\xi} r \tag{G.4}$$

and therefore linear in r. One can use this property of the GPD to find regions of stability from parameter estimations for different thresholds as was also stated by Levine (2009, 17). Basically, this is done by determining the mean excess estimator for various thresholds. Using the knowledge that it should be linear for the GPD, a suitable threshold is chosen. This linearity of the mean excess function was also noted by Bensalah (2000), who proposes a two step procedure:

1. The threshold is chosen from a stable region (i.e. approximately linear) of the mean excess graph.
2. The GPD parameters β and ξ, given the chosen threshold, are estimated using the maximum likelihood procedure.

Depending on the importance of the peaks for the determination of damage, this technique can be employed. If the importance of the medium-range cycles is dominant, then for the determination of the damage number, the high-range cycles may be of little importance and it would be unnecessary to extrapolate those. This is a drawback of the peak over threshold method, as it only considers the peaks. Medium-range cycles are thus not extrapolated, even if there is little data which implies the need for extrapolation due to uncertainty.

G.3 Spectrum fitting

With this technique, a probability density function is fitted over a spectrum of cycles. Multiple techniques are possible, here the two main ideas will be discussed: *fitting to ranges* and *fitting to rainflow matrices*.

G.3.1 Density function for ranges

The concept of range fitting is understood quite easily. Given a signal, the cycle's ranges are extracted and plotted in a histogram. Now, this histogram can be used as an estimate for the probability density function of cycle's ranges. This histogram can be used as the basis for a probability density function, for which multi-modal Weibull distributions are frequently employed (Sutherland & Veers, 1995; Nagode & Fajdiga, 1998; Tovo, 2001; Buar, Nagode, & Fajdiga, 2004). The choice for a parametric distribution function has the advantage that it automatically includes an upper tail. In the cited studies, a number of 3-parameter Weibull distributions are used, with pdf (Nagode & Fajdiga, 1998)

$$f_X(x) = \sum_{l=1}^{m} w_l \frac{\beta_l}{\theta_l} \left(\frac{\beta_l}{\theta_l}\right)^{\beta-1} \exp\left(-\left(\frac{x}{\theta_l}\right)^{\beta_l}\right) \tag{G.5}$$

where m is the number of Weibull distributions (each with distribution parameters β_l and θ_l). These are said to be very versatile and therefore suited for fitting a wide range of spectra. By fitting such a distribution, it is assumed that the cycles may come from a broader spectrum, than the spectrum which was measured. The fitted pdf can then be used to describe longterm loading, including variations.

Considering this method for concrete in fatigue, information is missing for an adequate assessment. Apart from the range information, the mean of cycles plays a crucial role in the current fatigue damage model. Therefore it is insufficient to generate only a set of (extrapolated) cycle ranges.

G.3.2 Rainflow matrix density

An alternative method which allows for this sort of extrapolation, is the extrapolation of rainflow matrices as described by, among others, Socie and Pompetzki (2004). A 'rainflow matrix' is a bivariate histogram which shows both the cycle means and amplitudes, each along their own axis. In some cases this matrix is presented in a *to–from* format, which basically contains the same information. On such a 'histogram-grid', one could perform similar techniques as with fitting to the cycle ranges. One major obstacle, however, is the availability of density functions with multiple variables (mean and amplitude). Given the irregular shapes of most rainflow matrices, no sensible parametric density function will be able to produce a fit of any quality.

There is another technique available for nonparametric fitting, known as *kernel density estimation*, which can produce better results. An excellent and intuitive explanation of kernel density estimation is given by Dekking, Kraaikamp, Lopuhaä, and Meester (2005). Consider a number of measured values, forming a data-set. For now the univariate case will do. Now, put a 'pile of sand' around each of the measured values. Where multiple measurements are close to each other, the sand will pile up. The resulting plot will be smoother than a histogram.

The *kernel* is a function which is used to describe the shape of individual piles, generally defined on the interval $[-1, 1]$. This shape can be mapped to a certain width, as defined by the *bandwidth* or *smoothing parameter*. The kernel density estimate is then obtained from summation of each kernel and subsequent normalization to ensure that the density function integrates to unity over $< -\infty, \infty >$, generally dividing by the number of observations.

For the bivariate case, this technique is applied in two dimensions. The piles of sand are 3-dimensional and a landscape is formed. In this way, bivariate density functions can be fitted to e.g. measurements using the technique of kernel density estimation.

Socie and Pompetzki (2004) proposed an approach for the extrapolation of rainflow matrices which is fully based on kernel density estimation. However, contrary to standard kernel density estimation with a fixed bandwidth, they argue that the bandwidth should be based on the *local variability*. Basically, this is measured by the number of values which are near a point. If, for instance, one outlying point is considered, significant variability can be expected. This translates to a wide kernel for this specific point. Analogously, for points where more data is available, the variations are expected to be less, or actually: better represented by the available data. This method is known as *kernel density estimation with adaptive bandwidth*.

The procedure will be explained next (based on Socie and Pompetzki, 2004). Overall, the kernel density estimate is obtained by summation of all kernels which are placed centrally on measured points x_i and y_i. In the case of a rainflow matrix, x_i and y_i represent a cycle's amplitude and mean. Note that the kernel is scaled using two parameters: h depends on the variability of the entire data-set, while λ_i corresponds to the local variation as mentioned above. The result is divided by the number of points in order to normalize the density function, which reads:

$$f_{X,Y}(x,y) = \frac{1}{n} \sum_{i=1}^{n} \left[\frac{1}{(h\,\lambda_i)^2} K\left(\frac{x - x_i}{h\,\lambda_i} \, \frac{y - y_i}{h\,\lambda_i} \right) \right] \tag{G.6}$$

where

$f_{X,Y}(x,y)$ = bivariate kernel density estimate, i.e. the resulting bivariate pdf
$K(x,y)$ = bivariate kernel function
x_i, y_i = coordinates of i'th data-point, i.e. the amplitude and mean of cycle i
n = number of data-points used for the estimate
h = bandwidth-parameter, depends on variability of entire data-set
λ_i = bandwidth-parameter which depends of the local variability of measurement i

It is proposed to use the bivariate Epanechnikov-kernel[1], i.e. truncated quadratic kernel, described by

$$K(x,y) = \frac{9}{16}(1-x^2)(1-y^2) \qquad \text{if } x^2 < 1 \text{ and } y^2 < 1 \tag{G.7}$$

$$K(x,y) = 0 \qquad \text{otherwise} \tag{G.8}$$

The method of kernel density estimation is a two-step process. First, using **one overall value** for λ, a first estimate of the density is determined. Then, using the local densities obtained in the first step, the final density estimation is performed. For both steps, h is determined as

$$h = 2.4\,\sigma\, n^{-\frac{1}{6}} \tag{G.9}$$

where σ is the standard deviation of the data in the rainflow matrix. From this, the first kernel density estimate is constructed. Subsequently, this density is used to estimate the adaptive bandwidth λ_i for each point in the histogram using[2]:

$$\lambda_i = \sqrt{\frac{\left(\prod_{i=1}^{n} f(X_i,Y_i)\right)^{\frac{1}{n}}}{f(X_i,Y_i)}} \tag{G.10}$$

With the λ_i's based on the first run, a second run is performed. The result is a density estimate for the cycles's amplitudes and mean values, similar to a pdf expressing the density for a single variable, only now expressing the density in terms of two variables.

To create a *random spectrum*, the desired number of cycles are drawn from the extrapolated joint probability density function in a random manner. This produces a unique spectrum (thus, a unique rainflow matrix) each time it is done, while allowing slightly different cycles than measured. Basically, the 'extrapolated rainflow matrix' is used as the parent distribution from which the measured sample could have been a realization.

Using this joint pdf, load sequences for 100 years can be generated, or actually for an arbitrary design life. If the variables would be independent, drawing would be easy as the univariate case. However, the variables are dependent, which will be directly clear considering the example later in this chapter. Because of this dependence, one drawn value for the mean, for instance, influences the corresponding pdf for the amplitude. In other words: for each randomly drawn mean value, there exists a pdf for corresponding amplitudes. Analogously, this is true for the reverse. Therefore,

[1] In Socie and Pompetzki (2004) a normalizing constant of 0.785 was used. Integration of the kernel over the ubounded surface, however, yields a constant of $^9/_{16}$, which was also found in other literature. Therefore, this value is used in this work.

[2] Again, Socie and Pompetzki (2004) propose a different formula (although with significant similarity), which yielded ridiculous results. This led to the conclusion that this must be a mistake. Other sources propose the formula based on the geometric mean which is printed here.

drawing randomly from a joint pdf is quite a cumbersome process. Starting from the joint cdf:

$$F_{X,Y}(x,y) = P(X \leq x, Y \leq y) = \int_{-\infty}^{x} \int_{-\infty}^{y} f_{X,Y}(x,y)\, dy\, dx \tag{G.11}$$

This cdf can be determined by integration of the joint pdf, i.e. the kernel density estimate. The way to draw random samples from the joint pdf, is by first drawing a sample for one of the stochastic variables from the marginal pdf, defined as (expressed in terms of X and Y, which where used here to denote the cycle's mean and amplitude, respectively):

$$f_X(x) = \int_{-\infty}^{\infty} f_{X,Y}(x,y)\, dy \tag{G.12}$$

The marginal pdf of X simply disregards all dependence of X on Y. Integration of this marginal distribution over x results in the marginal cdf, which is used for drawing the sample for X:

$$F_X(x) = \int_{-\infty}^{x} f_X(x)\, dx \tag{G.13}$$

Next, it is required to determine the conditional cdf for Y, given the value for X which was just sampled. The conditional pdf is defined as

$$f_Y(y|X=x) = \frac{f_{X,Y}(x,y)}{f_X(x)} \tag{G.14}$$

and can be interpreted as 'slicing' the joint pdf at the previously drawn X sample. The conditional cdf for Y is determined by integration of equation G.14:

$$F_Y(y|X=x) = \int_{-\infty}^{y} f_Y(y|X=x)\, dy \tag{G.15}$$

and it is used for drawing a sample for Y, which pairs with the previously drawn X. With the equations presented here, it is possible to draw random samples (cycles) that obey the bivariate kernel density estimate. This means that a full random spectrum (equivalently: rainflow matrix) of arbitrary length can be generated from a given spectrum determined from measured loads.

G.4 Extrapolation of damage numbers

The approach presented here is based on a suggestion by Fitzwater (2004). The S-N relations are very sensitive to changes in stress range. Using an extrapolation method for these stress ranges (described as 'spectrum fitting'), one endeavors to obtain the right tail of extrema which lie outside of the measured data. Such a process is sensitive to the measurement's maxima, small errors in distribution fitting (which is never exact) can thus be amplified by the S-N relations.

To omit this sensitive step, it is argued that it might be more appropriate to extrapolate in the domain of damage numbers. Basically this would be done by first determining the damage increment per (half) cycle, and subsequently fitting a probability distribution function to either the resulting spectrum of damage increments,

or only its upper tail. Then, instead of drawing cycles in a random manner, the actual 'damage increment per cycle' is drawn directly. Summation then yields the damage number. The end-result is expected to be less sensitive to the upper tail of the fitted distribution, because the inevitable inaccuracies which will always be present in an extrapolation of this kind, are not magnified by the S-N relations. The main drawback of this method is that it requires pdf fitting to (at least the tail of) the distribution of damage increments, which can, for the reason mentioned above, be far from smooth and thus hard to fit. Taking this into consideration, the same errors are probably made using both approaches (extrapolation of stress ranges vs. extrapolation of damage increment per load cycle). Therefore it was decided not to take this method into further consideration.

G.5 Comparison of selected methods

In appendix F, it was concluded that practically the entire damage number is the result of extreme cycles, i.e. the top 1 %. This forms the basis for the choice of the extrapolation strategy. Two of the mentioned methods, i.e. both the spectrum fitting methods (density function for stress ranges and rainflow matrix density), were proposed to include variations in **all** the cycles as opposed to focusing on the extreme events. Now that is has become clear that practically all damage is done by these extremes, and under the assumption that these extremes coincide with the peaks in the signal, the lower events are of less importance. Therefore, it has been shown that extrapolation of these lower, more frequent, events is **not important** for the distribution of the damage number. One method remains: time-extrapolation using peak-over-threshold.

Following the logic as laid out in the foregoing paragraph, only the peak-over-threshold approach has to be applied. To verify this theory, a comparison of the PoT to another technique was deemed appropriate, because of the unusualness of such methods. The proposed verification technique is spectrum fitting of the rainflow matrix using kernel density estimation, which incorporates variations in the entire spectrum of cycles, as opposed to the PoT only extrapolating the fairly infrequent events.

The two methods, peak-over-threshold and rainflow matrix kernel density estimation, will be demonstrated in this section. Both have been implemented in MATLAB for this thesis[3], and were applied to extrapolate the signal which was obtained in the example of section F.1. The signal corresponds to the measured time frame of circa 4 years, and it is to be extrapolated to a design life of 100 years. This section is concluded with a comparison of the methods. Only the magnitudes are extrapolated, i.e. the number of cycles corresponding to the design life is taken as constant, according to the extrapolation factor of 25 ($\frac{100}{4}$).

G.5.1 Demonstration of PoT

In this section the peak-over-threshold method is demonstrated using the traffic from detector 111 and the reference structure. This method uses the signal for the generalized force of interest, and alters this directly. Part of the signal (chosen randomly) is plotted in figure G.1. The label of the horizontal axis denotes 'pseudo-time', caused by the fact that time was not considered in creating this signal. Furthermore, the signal is passed through an algorithm to extract its turning points, so the horizontal axle's scale is not constant (non-turning points have been removed).

[3]Most computations were done using an Intel® Core™i7-4610M @ 3 GHz (dual core, 4 threads) with 16 GB of DDR3 memory. Others using an Intel® Core™2 Duo E8400 @ 3.6 GHz (dual core, 2 threads) with 4 GB of DDR2 memory.

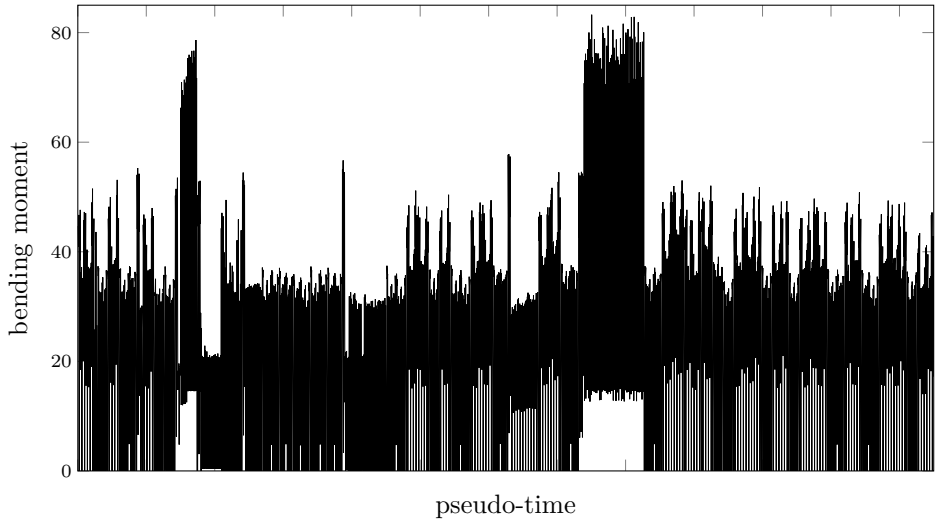

Figure G.1: Part of the bending moment signal for the passing of detector 111 traffic over the reference structure introduced in section F.1. Here, 2500 turning points are displayed, from a total of 11763588.

As described in section G.2, a generalized Pareto distribution is fitted to the peaks over a threshold. It is noted that peaks are defined as the maximum value between two *upcrossings*[4] of the threshold. Obtaining the threshold is the most difficult part of this technique. For this, it was chosen to vary the threshold, r, from 75 to the maximum of the signal, ± 97. For each threshold a GPD is fitted, with parameter estimates $\hat{\xi}$ and $\hat{\beta}$. Also, the mean excess estimator is determined (equation G.3). The parameters for each plot are displayed in figure G.2.

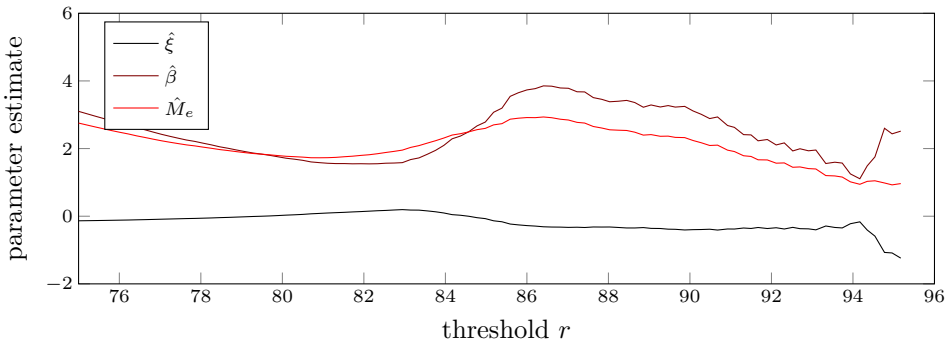

Figure G.2: GPD-parameter estimates for varying threshold-values.

According to theory, the threshold should be chosen in either a stable region of the mean excess function (Bensalah, 2000), or a region which returns stable parameter estimates (Levine, 2009, 17). From trial and error it has become clear that 'low thresholds' (lower than 85) are not even influenced by the tail, and are dominated by the more frequent lower observations (severe bias). Higher thresholds seem to produce better results, i.e. actually following the tail nicely, which is in perfect accordance with theory. The best obtained fit was achieved by a threshold of 91, for which the probability plot is displayed in figure G.3. Now, first the original signal is repeated

[4] An *upcrossing* is where the signal crosses the threshold with positive slope.

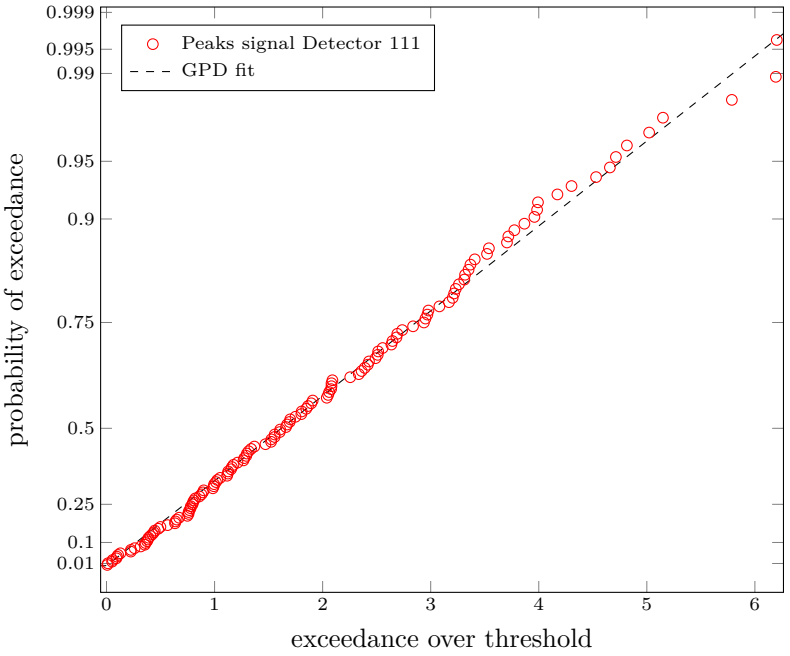

Figure G.3: GPD fit for peaks over threshold, $r = 91$.

(without alterations) to the desired length. In this case 25 times the measured period. Subsequently, peaks are replaced by randomly generated values from the fitted GPD distribution. Note that each time this is done, in principle a unique signal is obtained. The resulting cycles are counted using the rainflow algorithm, after which the damage number can be determined using the S-N curves. To gain some insight into the results obtained using the method, this process was repeated 1000 times sequentially[5]. Results are shown in figure G.4. Clearly, variations are very small and could therefore very well be neglected.

In this example, the S-N curves from the Dutch national annex were used. These include a vertical jump at $N = 10^6$, which influences the most damaging cycles in this example, which are on near this region. Therefore, the vertical jump effectively truncates the damage increment per cycle. This may be different for i.a. other loading histories, other concrete classes, other structures and so on. However, manual variation of u, which shifts the spectrum relative to the S-N curve, showed that variations in damage numbers remain negligibly small for other values of u. In figure G.5 the amplitudes gained through the kernel density estimate are compared to linear extrapolation in a so-called *cumulative exceedance diagram*. The amplitudes are sorted first. The vertical axis gives an amplitude, which is exceeded by the number of cycles given on the horizontal axis.

Figure G.5 reveals a reason for the small variation in resulting damages. Only a small part of the cycles is altered with this technique, and variations caused by the alteration are also quite small. The cumulative exceedance diagram also shows that the data has several 'bulges', of which only the largest one is extrapolated.

[5]Each repetition takes about 45 s.

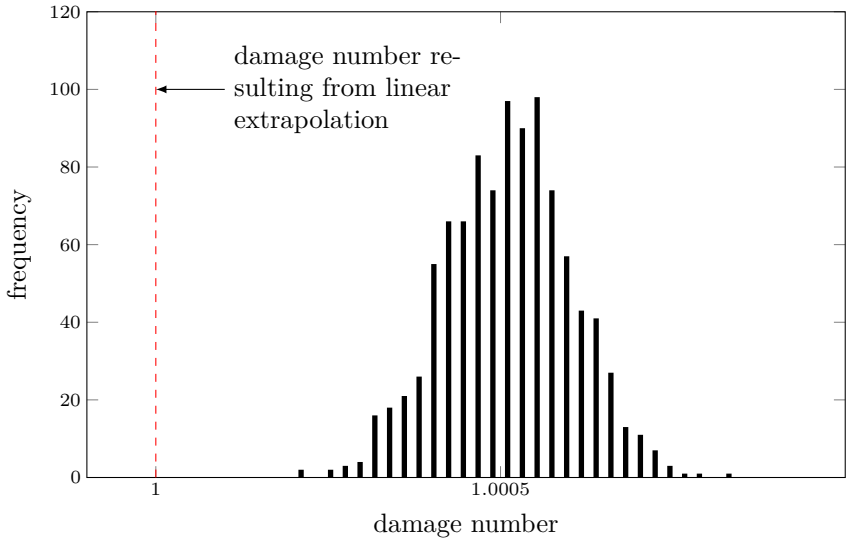

Figure G.4: Distribution of damage numbers corresponding to randomly generated load histories (1000 repetitions) using the peak-over-threshold method.

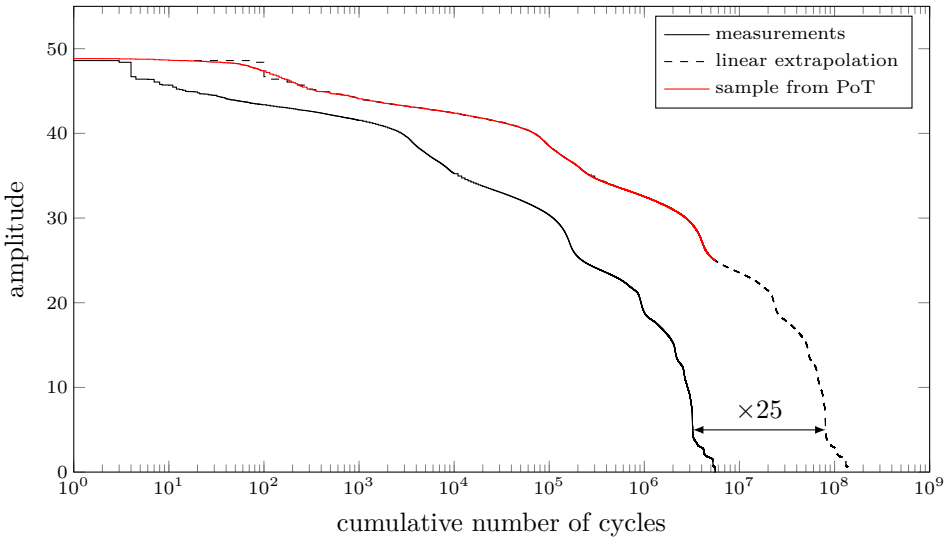

Figure G.5: Cumulative exceedance diagram, comparing the result of extrapolation using the peak-over-threshold method to the measured response.

G.5.2 Demonstration of bivariate KDE

In this section, the kernel density estimation is demonstrated for the reference structure. First of all, it has become clear that this method is very expensive in a computational manner, which may very well be a problem if a large number of samples is requested. Creation of a kernel density estimate for the detector 111 traffic, evaluated on a 500-by-500 mesh, takes ±11 hours. This time is closely related to the number of cycles, 5.7 million in this case, and almost linear scaling of computational time with this number was observed. Drawing random samples is also quite time-consuming: sampling 50 million half-cycles takes ±5 hours, and this is only simulates about 20 years of traffic (so a single sample of 100 years of traffic would take about 1.2 days, which is definitely unfeasible if multiple samples are requested).

Initial endeavors in the application of this technique would not lead to a satisfactory result. Due to a large bandwidth, the spectrum was extrapolated over a large area in the rainflow matrix, allowing for example amplitudes of twice the observed maximum. Clearly, this is not the desired result, as such an amplitude would lead to an overload, thereby implying direct failure. This is very unrealistic, as the PoT already showed that the increase in maximum amplitudes can be expected as minimal. The KDE was mainly proposed to investigate its effects on everything except these peaks.

After numerous tries, with different parameters, the input was reconsidered. Attention was drawn to the estimate for the smoothing parameter h, as given in equation G.9. With its dependence on the variance of data, it basically quantifies the amount of variability to be expected. Up to this point, the entire range of amplitudes was used to determine the standard deviation, σ, used in the expression. Considering a rainflow matrix as formed by the load on the reference case, there clearly are distinct peaks (will become clear in the remainder of this section). Now, calculating the standard deviation for the entire spectrum gives rather large values, implying enormous spreading, as if all data is clustered around one peak. It is therefore argued that a better measure of the variability in the data would be some sort of 'local variance' around the peaks.

This raises the question, whether it is possible to define such a measure. Useful information on the subject could not be found in literature, and therefore a pragmatic solution is proposed. Starting with a histogram of half-cycle amplitudes, displayed in figure G.6 for the reference case, a clear number of modes (bulges or peaks) can be distinguished. Six modes are identified in this case. This may seem rather abstract at first, but it is important to consider that the modes which are described, do not occur at the same mean stress. This means that they are not continuously connected in the landscape formed by the mean and amplitude axes. One might mistakenly identify the portion from 6 to 27 as one mode, while in reality this portion does not form a continuous shape in the aforementioned plane.

As the identified modes appear approximately normally distributed, it is proposed to asses the variability through a mixture of normal distributions. Such a multimodal distribution is fitted to the data in the histogram. For each component, its weighing factor, mean, and standard deviation are obtained. Subsequently, the *average* standard deviation is determined through weighing:

$$\sigma_k = \sqrt{\sum_{i=1}^{k} (w_i \, \sigma_i)^2} \tag{G.16}$$

where

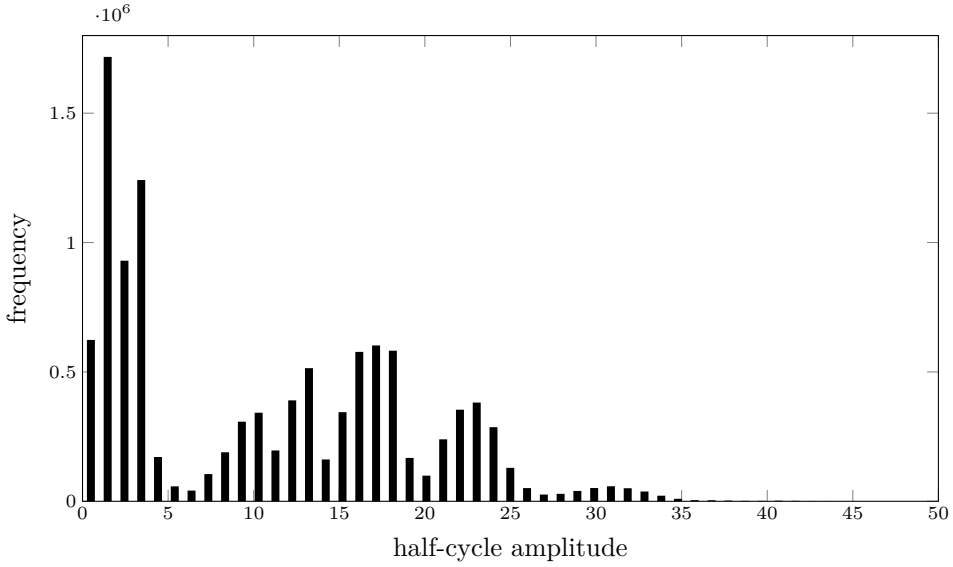

Figure G.6: Histogram of half-cycle amplitudes, obtained from detector 111 traffic passing over the reference structure.

σ_k = weighted average standard deviation
k = number of modes
w_i = weight-factor for mode i
σ_i = standard deviation for mode i

Using the weighted average standard deviation as a measure of the local variance yields results which are closer to what is expected and shown using PoT: a rather small increase of maximum amplitude, while the rest of the spectrum remains practically unaltered. The data from figure G.6 is split up at amplitudes 6, 11, 16, 19, and 26. Using MATLAB, a mixture of normal distributions is fitted to the data. The result is plotted in figure G.7, while the component-distributions and their properties are listed in table G.1. Applying equation G.16 to the data from table G.1, a weighted

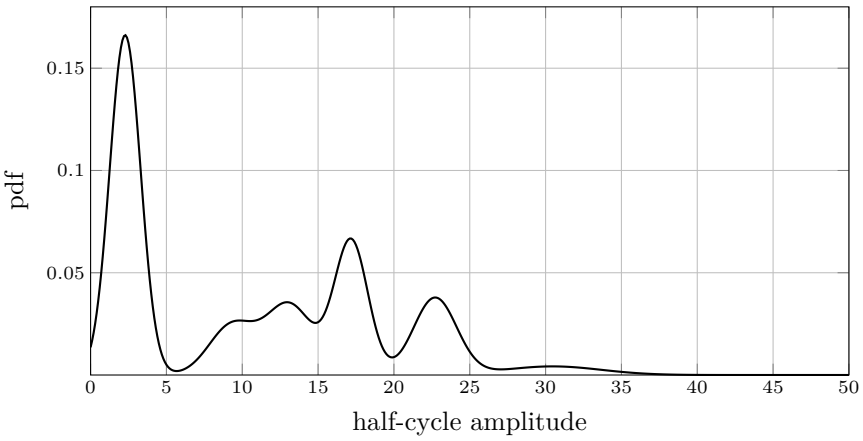

Figure G.7: Multimodal distribution of half-cycle amplitudes, obtained from detector 111 traffic passing over the reference structure.

component	w_i	μ	σ
1	0.42	2.27	1.03
2	0.09	9.32	2.27
3	0.13	13.09	2.42
4	0.18	17.17	1.23
5	0.13	22.71	2.03
6	0.03	30.46	10.23

Table G.1: Mixture of normal distributions fitted to amplitudes of figure G.6, as displayed in figure G.7.

standard deviation of 0.76 is found. When the standard deviation is determined over the entire data-set, a value of 8.55 is found. Using the standard deviation from the normal mixture, the procedure for kernel density estimation is continued. It is noted that the overall objectivity of this method is somewhat impeded by this sensitivity with respect to the standard deviation or kernel width, because no proper proof can be given. Therefore, subjectivity is introduced.

A further adaptation of the method will be to focus on the relevant part of loadings. As shown in section F.1, this constitutes only focusing on the 1 % of cycles that is most damaging. The remaining 99 % of the spectrum can be used in a deterministic fashion, or could even be neglected for extrapolation. Results may however be less accurate for reinforcement steel (due to the smaller fatigue exponent, showing that concrete is more sensitive to increasing stresses). A solution for reinforcement steel is straightforward: incorporate a larger portion of the cycles, e.g. corresponding to 99 % of damage for reinforcement steel, into the extrapolation.

The first kernel density estimate, with constant bandwidth parameters, is performed for all the measured cycles. A rather coarse mesh is used, to save some time. The second and final run is done using only a portion of the measured cycles (most relevant part in terms of damage). For this, a finer mesh is used to prevent measured cycles with narrow kernels to be skipped because no grid point is in their vicinity.

An actual example will be presented now, based on the reference structure from section F.1 in combination with detector 111 traffic. First the (deterministic) rainflow matrix is determined, see figure G.8. This is done by simulating the crossing of measured traffic over the bridge (influence-operator), and using the rainflow cycle counting algorithm to extract the cycles (each described by their mean value and amplitude). A total of 5.7 million cycles was obtained from the passing of traffic. As described above, the first kernel density estimate will be based on all these cycles. The relevant part, chosen as those cycles which cause 99 % of damage[6], is used for the final run while the remaining cycles are treated deterministically. The rainflow matrix corresponding to these, in this case 141000 cycles, is presented in figure G.10. The kernel density estimate, based on this rainflow matrix, is given in figure G.9 (3D) and figure G.11 (top view).

The rectangular shape of the kernel is clearly visible in these figures. Furthermore, the adaptive bandwidth causes great variation in the local bandwidth. For isolated cycles, i.e. *outliers*, the kernel is visible as a large patch. If cycles are generated from such a patch, the variability is therefore relatively large.

[6]This may seem a lot, but it is argued that cycles which cause negligible damage in deterministic context, might be more damaging when extrapolated. Therefore a margin is built in by choosing more cycles for the extrapolation.

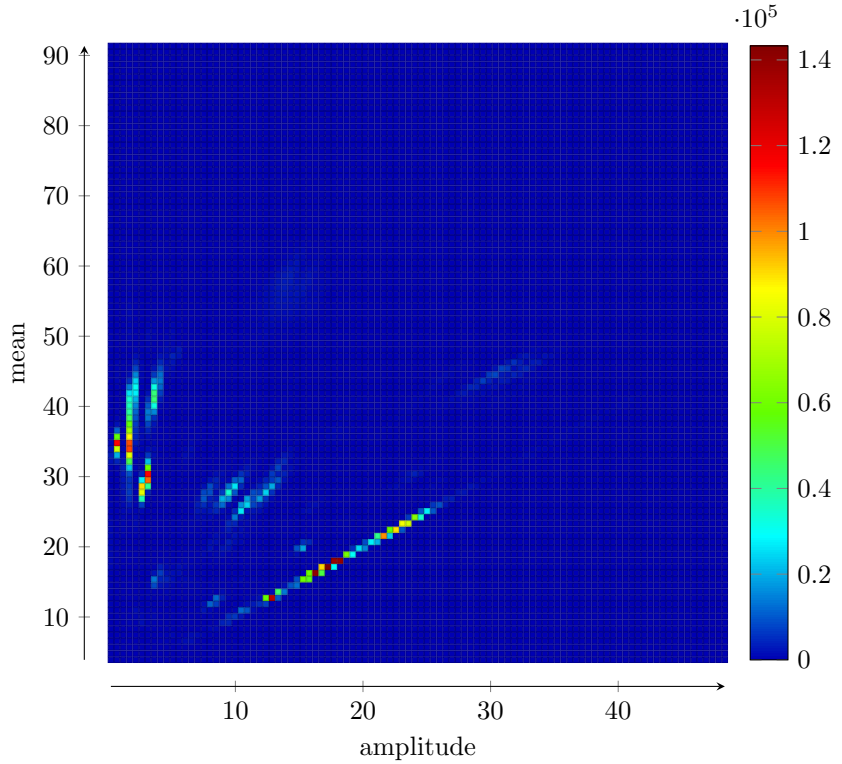

Figure G.8: Rainflow matrix for detector 111 over the reference structure introduced in section F.1.

The obtained kernel density estimate was then used to generate a large number of random cycles, over 25 million in this case (based on the KDE for the most damaging 141 thousand cycles). Consecutively, the damage increment for each cycles was determined, resulting in a large database of possible damage increments per cycle. The fraction of cycles generated from measurements totals 141044 full cycles (taking into account half-cycles). Because the number of cycles is treated deterministically in this section, possible damage numbers corresponding to a design life can be constructed by summation of $25 \times 141044 = 3526100$ randomly generated damage events (resulting from generated cycles). In this way, an arbitrary number of possible damage numbers can be generated, although limited by the diversity of the database of generated cycles.

Results from the procedure described are shown in figure G.12. Here, the damage numbers resulting from the KDE are normalized using the damage number obtained from linear extrapolation. The spread in damage numbers clearly surpasses that which was found using the peak-over-threshold method. However, variations are still negligibly small. Apart from this, the same remark as given with results from the PoT method is valid, that is, regarding the truncation by the S-N curve. Also, the mean damage number surpasses unity. Considering symmetrical variation around each measurement, all cycles which are higher than expected will do exponentially more damage compared to the lower cycles, resulting in a shift of the mean value towards more damage. Mathematically this is expressed as $E[X^n] \neq E[X]^n$, which is generally valid for the nonlinear case (i.e. $n \neq 1$).

A normal distribution was fitted to the damage numbers, with parameter estimates

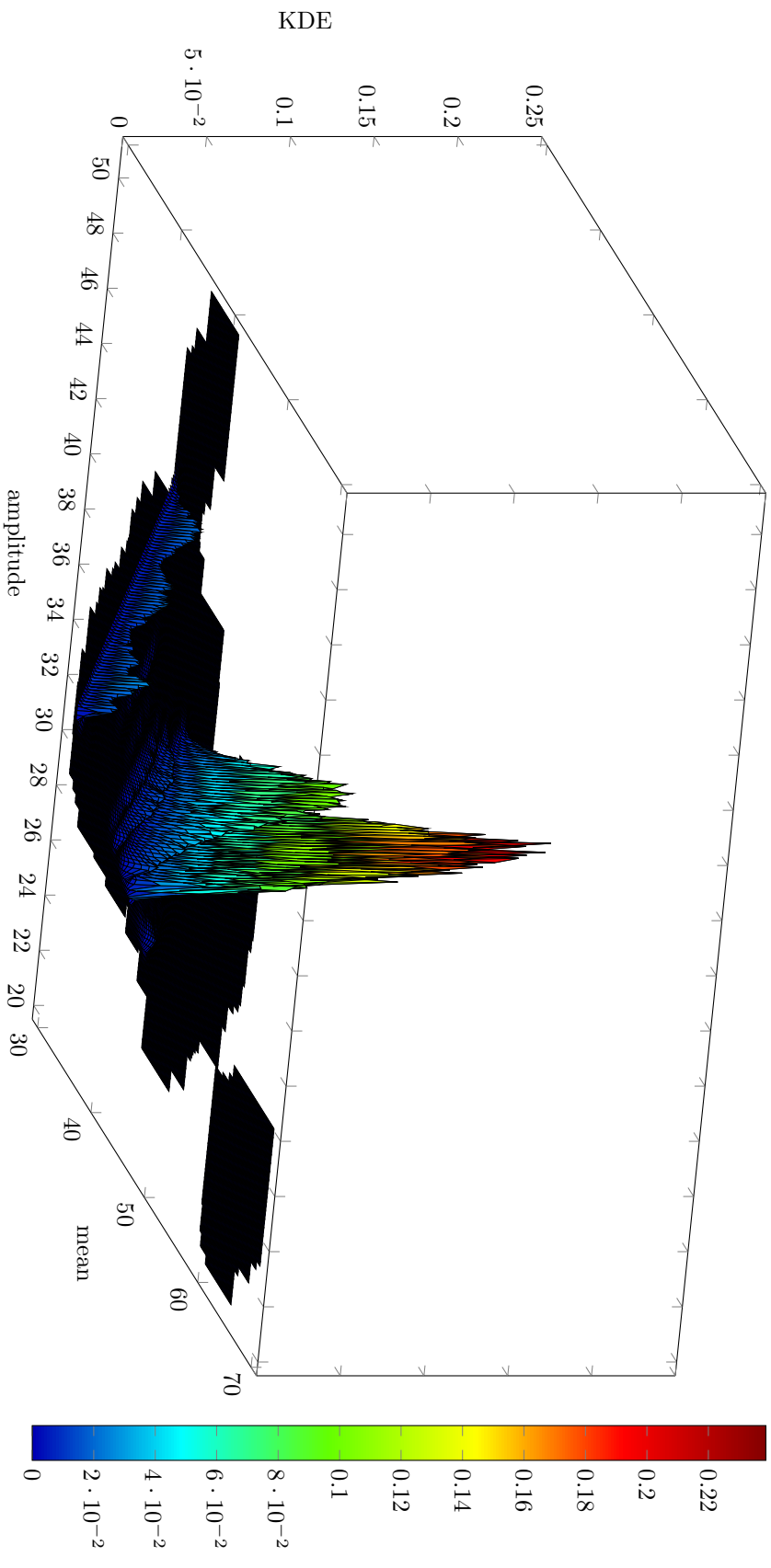

Figure G.9: 3D-view showing the joint probability function, obtained from kernel density estimation, for the detector 111 traffic on the reference structure introduced in section F.1. Only the fraction of cycles which causes 99 % of damage are included (144000). Points where the function equals 0 have been skipped for clarity.

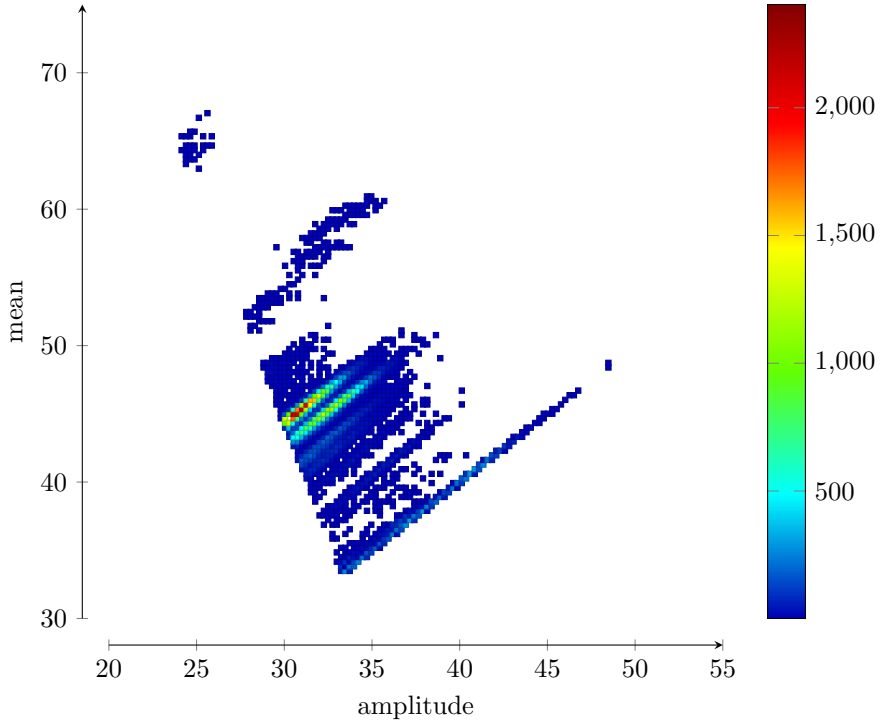

Figure G.10: Rainflow matrix, only displaying the 141000 most damaging cycles for detector 111 on the reference structure introduced in section F.1.

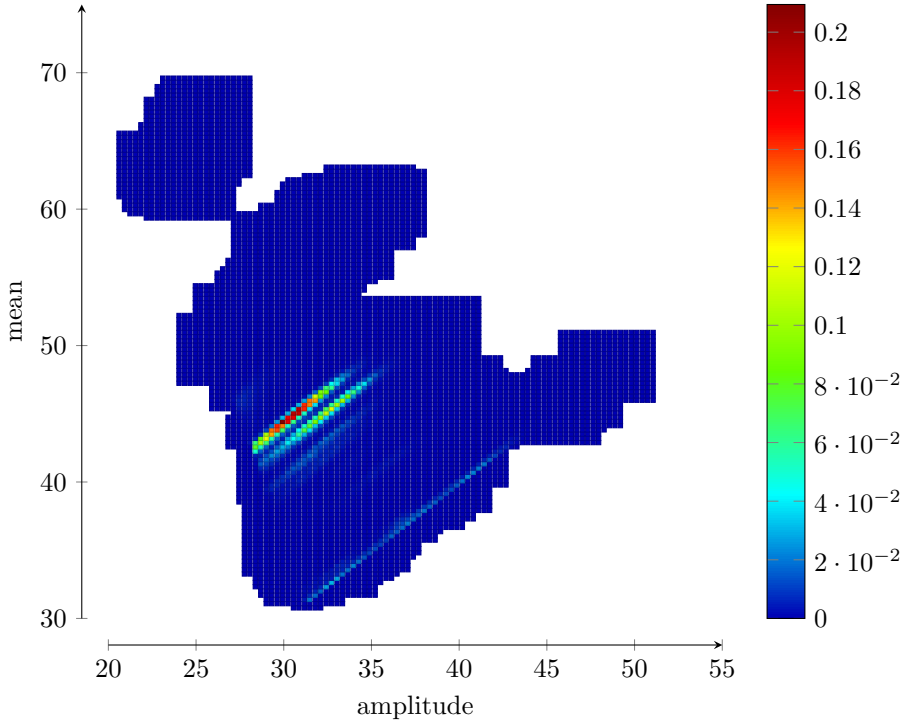

Figure G.11: Bivariate kernel density estimate based on the 141000 most damaging cycles for detector 111 on the reference structure introduced in section F.1.

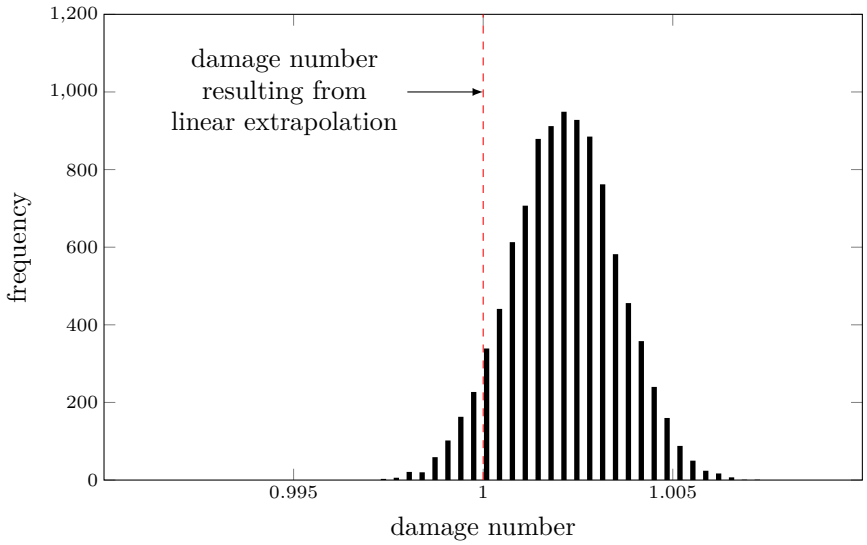

Figure G.12: Distribution of damage number corresponding to randomly generated load histories using the bivariate kernel density estimate.

$\mu = 1.00213$, $\sigma = 0.001386$. This means that variations are negligibly small (probability of normalized damage number surpassing 1.01 equals 6.8×10^{-9}).

Figure G.13 displays the amplitudes gained through the kernel density estimate, compared to linear extrapolation a cumulative exceedance diagram (explained in section G.5.1). Clearly, when comparing the result from the KDE with a linear extrapolation, the differences are quite small. The maximum amplitudes are increased, which was to be expected. Also, the magnitude of amplitudes is clearly limited, which is the result of the kernel shape, which is also limited. In other words, using this method with the prescribed kernel, there always exists an upper bound for extrapolated amplitudes. The remainder of the spectrum, however, shows excellent correspondence to the linear extrapolation, implying that the extrapolation of these lower cycles is not quite necessary.

G.5.3 PoT and KDE side-by-side

The results obtained from the demonstration of both methods can now be compared. For this, the cumulative exceedance diagrams are compared, see figure G.14. Note that the kernel density estimation was only done for the *important cycles*, i.e the part responsible for 99 % of the damage number. Therefore, the lower part of the KDE-sample is vertical. Also, results from the PoT were truncated at an amplitude of 25. The most interesting part is that of large amplitudes, for example the largest 1000. This is where the differences between methods of extrapolation can be observed. Most notably is that the KDE results in larger amplitudes than PoT. Also, the top is shaped differently. The top's shape is dominated by the shape of the kernel (KDE) or the fitted GPD (PoT), and therefore this explains the difference.

The remaining part of the cycles corresponds quite perfectly to the linear extrapolation. Furthermore, differences between the methods are rather small, although the variations in damage numbers clearly are larger when the KDE is applied. Fundamentally the KDE seems more appropriate, because it also allows variations in the rest of the spectrum, while the PoT only alters the part above the threshold which does clearly not cover the entire range of *important* cycles. It is however concluded that

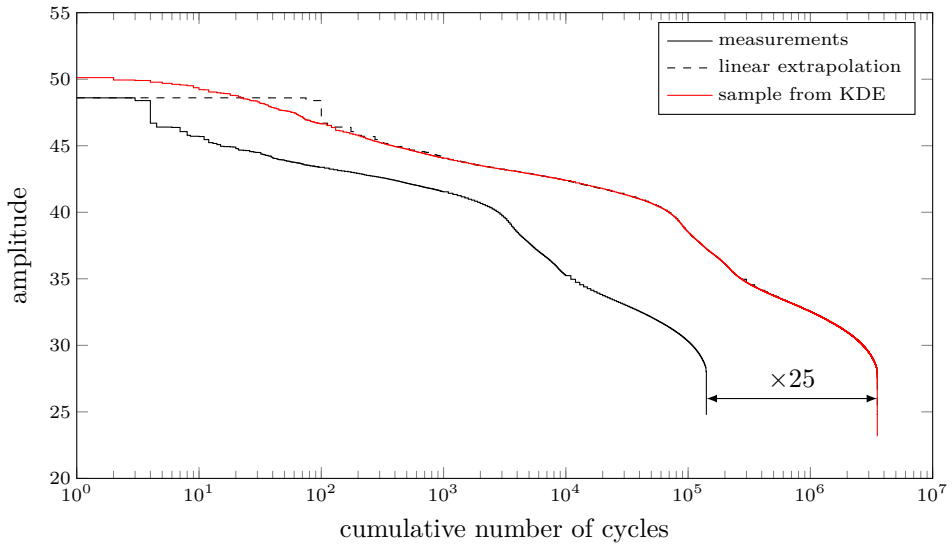

Figure G.13: Cumulative exceedance diagram, comparing the result of extrapolation using the kernel density estimate to the measured response.

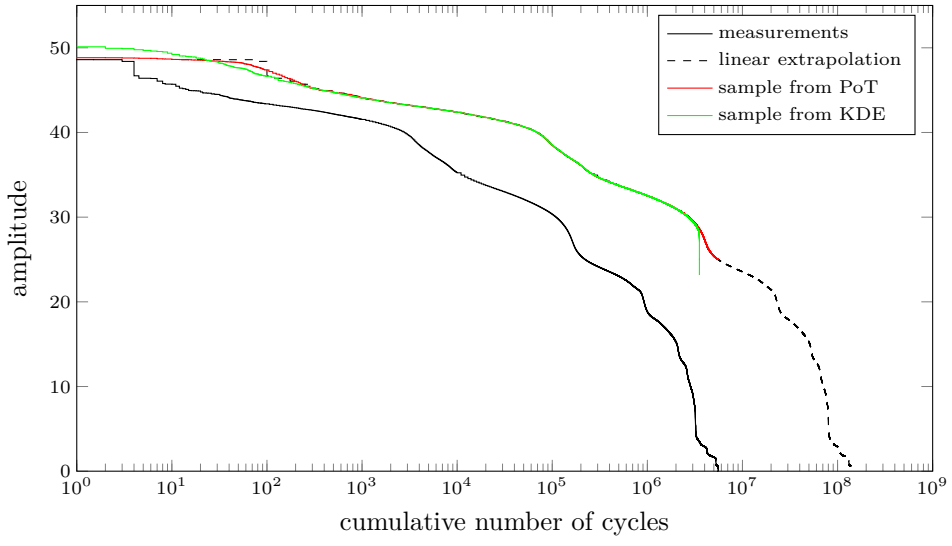

Figure G.14: Cumulative exceedance diagram, comparing the result of extrapolation using the peak-over-threshold method and the kernel density estimate to the measured response.

the larger variations in damage numbers found by using KDE compared to PoT, are a direct consequence of the kernel shape, and not by the fact that the entire spectrum is extrapolated compared to only the top part. Exactly this kernel shape and width are quite subjective matters which should be kept in mind when judging results.

Computationally, there are some differences as well. The extrapolation using PoT requires significantly more time than KDE for a large number of samples. With the KDE, one is forced to construct the estimate first (taking approximately 12 hours for the example used in this section), after which the sampling of cycles, and thus the damage numbers, can be done relatively fast. For the PoT however, this is not the case. Each sample then takes significant time ($\pm 45\,\mathrm{s}$ per history), which adds up to more than the KDE for a large number of sampled histories. Reason for this is that a signal for the entire design life needs to be processed within each repetition.

As a concluding remark it can be said that the extrapolations of magnitudes were shown to produce negligible variations (between methods as well as in resulting damage numbers), and can therefore be neglected in the remaining analyses of this thesis.

G.6 Number of cycles

So far only uncertainties in the magnitude of loadings were treated. As shown in detail in appendix D, uncertainties in the number of cycles are of importance as well, although less pronounced for equal spread. However, in case the uncertainties in the number of cycles are found to exceed those of magnitudes, the overall effect may very well be dominant. Therefore it is studied in this section.

In appendix 2 the dependence of loading on time was already briefly studied, although in another context. It is noted that the cumulative tonnage, as studied before, is not necessarily a valid marker for variations in the number of cycles. It seems more appropriate to investigate the number of cycles using a more direct approach.

The procedure to assess the variability in cycles was chosen as follows. The measured time-frame is divided into equal intervals. Subsequently, trains are coupled to their corresponding interval, and cycles are determined **per train**. The total number of cycles per interval is calculated as the sum of all counted cycles resulting from each interval's trains. Results of this procedure for the detector 111 traffic are plotted in figure G.15 (left). For this, the measured time-frame was divided into 100 intervals of equal duration (ca. 14 days per interval). Variation between intervals is definitely visible (coefficient of variation: 0.09). The data does not follow a normal distribution very well because of the large centered portion.

This data is extrapolated as follows: a single design life is assumed to be composed of intervals as measured (treated discretely). The corresponding number of cycles per interval is sampled and summed to obtain an estimate for the number of cycles to be expected during the design life. In doing so, it is implicitly assumed that the number of cycles per unit time follows the discrete distribution as displayed in figure G.15 (left). This procedure was repeated 10000 times[7] to obtain the histogram from figure G.15 (right), in which the results are normalized by the mean number of expected cycles in a design life. Using the central limit theorem, which states that

> "*The arithmetic mean of a sufficiently large number of iterates of independent random variables, each with a well-defined expected value and well-defined variance, will be approximately normally distributed, regardless of the underlying distribution.*" — Wikipedia, 2015a.

[7] The same result could be predicted from the distribution on the level of an interval, but it was chosen to include this step as a visual aid.

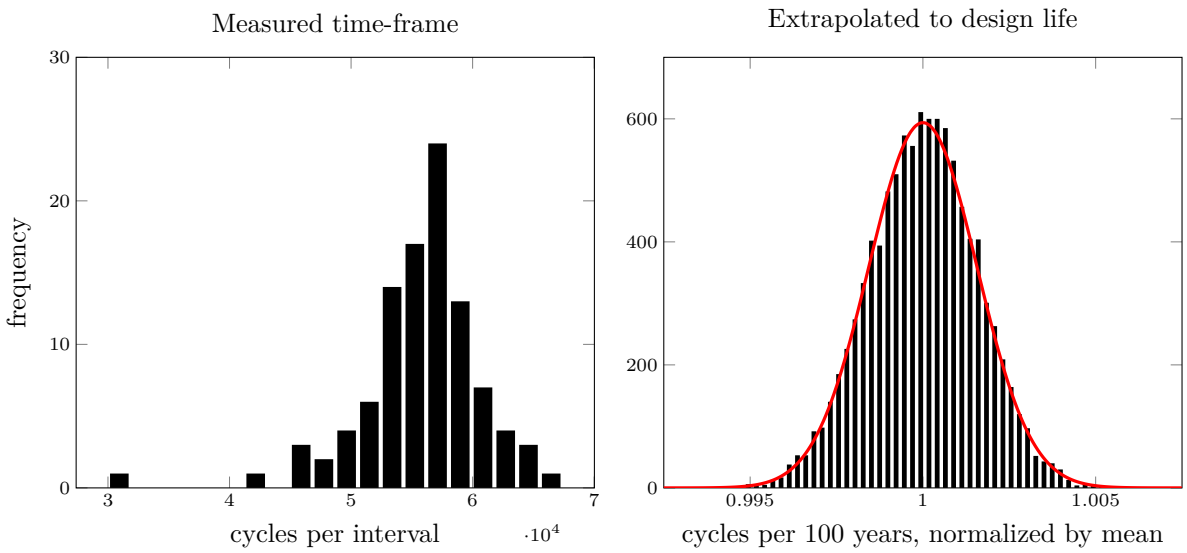

Figure G.15: Number of cycles per time-interval (division of measured time-frame into 100 time-intervals).

this result should follow a normal distribution. Therefore this has been fitted (red line in figure). With MATLAB's maximum likelihood procedure, a mean of 1 (normalized) and a standard deviation of 0.0018 were found, the latter being equal to the coefficient of variation due to the normalization.

Clearly, variations on this level are very small. Reason for this, is that the coefficient of variation is proportional to $\frac{1}{\sqrt{n}}$. The obtained mean number of cycles is equal to the extrapolation factor multiplied by the mean number of cycles per interval.

This procedure was repeated for the detector 11 traffic record. Similar results were obtained, i.e. an overall coefficient of variation equal to 0.0035 for the normalized design life cycle count. This is used as a justification for neglecting the variations in number of cycles around its mean value.

What was basically shown here, is that the sum of realizations from a process which follows a distribution with bounded variance, will converge to its mean. This behavior is commonly known as the *law of large numbers*, generally formulated by relating the average to the expected value, which is equivalent to the statement regarding the sum. A logical next move, now that it is known that the number of cycles will converge to its mean with negligible variance, is to consider the uncertainty which is introduced by estimation of the mean value.

When a mean value is estimated from samples, it is generally said that it will follow a normal distribution for cases with more than 30 samples. It's standard deviation is denoted as the 'standard error of the mean' ($\mathrm{SE}_{\bar{X}}$), and can be determined by (Wikipedia, 2015c):

$$\mathrm{SE}_{\bar{x}} = \frac{s_x}{\sqrt{n}} \tag{G.17}$$

where

$\mathrm{SE}_{\bar{x}}$ = standard error of the mean
s_x = sample standard deviation
n = number of samples

Because the standard deviation of the samples is estimated, as opposed to known, the student t-distribution should be used. However, in case of a large number of samples, the normal distribution offers an adequate approximation, and was therefore used here.

The sample standard deviation is influenced by the number of time-intervals. Division of the measured time into a larger number of intervals, yields a smaller standard deviation. Using this method, however, it is assumed that the number of cycles in each interval is *independent*. This assumption is voided by an increase of the number of intervals, although the exact optimum is not known. For this work, it was assumed that 100 intervals result in a fair approximation in terms of both the standard deviation as the requirement for independence. This procedure was repeated for all detectors, after which the standard error of the mean was determined for each. Results have been summarized in table G.2.

	$\bar{x}$	$\mathrm{SE}_{\bar{x}}$	CoV
detector 11	27863	485	0.0174
detector 12	39012	306	0.0078
detector 18	23675	554	0.0234
detector 19	42911	900	0.0210
detector 111	55740	496	0.0089
detector 114	44686	393	0.0088
detector 163	61633	564	0.0091
detector 164	61588	571	0.0093
detector 363	39242	330	0.0084
detector 364	39819	351	0.0088

Table G.2: Standard error for the mean per detector (100 time-intervals).

For this thesis a practical approach is proposed, namely using the variations obtained from the reference structure for all subsequent cases, and equal for traffic records from all detectors. This means that the results from table G.2 are used to account for variations in the number of cycles from here on, where a coefficient of variation of 0.01 is deemed an appropriate generalization for all detectors. This was mainly done to show the influence of such uncertainties (by inclusion in the sensitivity analysis), and not so much because of the magnitude of variations, which clearly is quite small.

G.7 Conclusions[8].

- Multiple techniques for extrapolation were considered, namely: extrapolation of traffic, time-extrapolation using extreme value theory, uni- and bivariate spectrum fitting and extrapolation of damage increments.
- Two methods, time-extrapolation using EVT and the bivariate spectrum fitting using kernel density estimation, have been implemented and demonstrated. Comparison has shown that the KDE results in a larger spread in damage numbers than the PoT. Notably, the maximum amplitudes were obtained by appliance of the KDE method. It was argued that the latter is fundamentally more powerful because it allows variations in the entire spectrum, although differences in damage numbers were mainly attributed to differing extrapolations

[8] Also presented in chapter 5

of the largest load cycles. Also, the KDE involves estimating the kernel width, which turned out to be both essential and somewhat subjective.

- Variations in damage obtained by the extrapolation of the load histories were negligibly small. Therefore it was decided to omit this entire step in subsequent analysis, as this saves a considerable amount of time while maintaining practically all accuracy in determining the damage numbers.
- Variations in the number of cycles have been quantified. The main source of uncertainties was shown to be in the determination of the mean value. For this, standard errors were determined. Furthermore, the assumption has been made to use an average coefficient of variation obtained for traffic from all detectors (0.01) over the reference structure, for all future analyses, regardless of the exact structure or detector.

The most interesting conclusions, however, might be the resulting variations in damage numbers obtained from the extrapolation. It has been shown that these are very small, even negligible, and therefore it seems that 4 years of measurements seems enough to draw conclusions about design life fatigue loading. At least, the measurements have converged, thereby not implying an expected occurrence of much larger loads. Also, even more useful than determination of expected variability through extrapolation, may be the *feeling* one gains for the data, yielding the confidence required to proceed with result of extrapolation methods such as those described in this thesis.

H | Solving for the Reliability

In this chapter, methods to solve the reliability equation (limit state function) for the resulting failure probability, or equivalently the reliability index, are discussed. For this, a practical example (reference case from appendix F) is used to demonstrate all steps.

H.1 Practicalities

To solve for the failure probability, $P_F = P(Z \leq 0)$, a few steps are required (corresponding specifically to the format and methodology used in this thesis). The first step in obtaining P_F is determining u_{limit} from the combination of a structure (influence line), a traffic mix (Eurocode), and, in case of concrete in compression, the ratio of permanent stresses ζ_{perm}. Using this information, and the fatigue damage formulations for concrete of reinforcement, the value of u_{limit} is obtained by optimization with the constraint that the damage should be equal to unity. Note that this includes partial factors, or actually only for the material because that for fatigue loading is not included as it is equal to 1.

With the value for u_{limit} which is obtained, the reliability functions (eq. 5.20 and 5.22) are fully defined in terms of their variables. Using this, the safety margin, expressed with Z, can be calculated, this time without applying partial factors. The remainder of this chapter is dedicated to solving for P_F using the Monte Carlo method (section H.2) and the first order reliability method (FORM, see section H.3). An explanation of both methods can be found in appendix A. The Monte Carlo analysis is used to verify the results obtained using FORM. After this, an optimization-strategy regarding the generation of signals is presented, in order to save some computational expense.

H.2 Solving using Monte Carlo method

The first approach to obtain the failure probability from equations 5.20 and 5.22 is using the Monte Carlo method. As stated in appendix A, the accuracy of this method is dictated by the number of iterations. Technically, it can only be checked *a posteriori* whether the number of iterations was sufficient, as it depends on the outcome of the analysis itself (reciprocal of the failure probability). Therefore this is more or less a process of trial and error. Ultimately the convergence was studied as a function of the number of iterations.

First a case was chosen, of course the 'reference case' was picked again for this purpose. The signal resulting from the measured traffic is also probabilistic, caused by the inclusion of measurement uncertainties (axle loads and velocity), and uncertainties in dynamic amplification. Therefore, upon repetition of the procedure for generating signals, each time a unique signal is obtained. More on this influence can be found in section H.4.

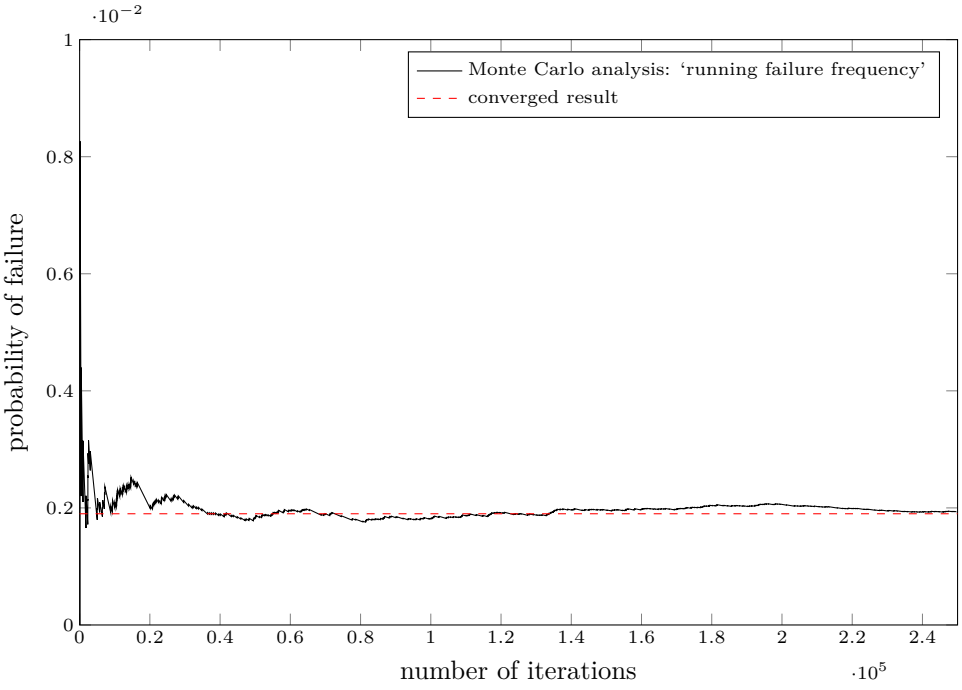

Figure H.1: Running failure frequency resulting from the Monte Carlo analysis.

It was certainly not practical to determine a unique signal for each iteration, as this would require far too much time for the calculation (generation of signals, i.e. applying the influence-operator, forms a relatively large portion of the overall computational expense). Therefore it was decided to use a single signal for 1000 iterations, which made the analysis achievable within a reasonable amount of time.

The result of the Monte Carlo Analysis, which included the generation of 250 random signals, with 1000 iterations done for each signal (250000 iterations in total), were[1]:

Resulting probability of failure (failure frequency)	$P_F = 484/250000 = 0.0019$
Resulting estimate of reliability index	$\beta \approx 2.888$

The number of iterations was large enough to obtain convergence, so it seems. A plot of the *running failure frequency*, that is, the number of failures up until and including iteration i divided by the current iteration i, is plotted in figure H.1.

Overall the results may look satisfying, but there is one huge drawback: the time it took. This analysis in itself required circa 100 hours of calculations. This makes it infeasible for a large number of analyses, as this would simply require too much time. Therefore it was attempted to solve for the reliability index using FORM, which should be able to save a considerable portion of this time.

H.3 Approximate solution using FORM

Because of the computational expensiveness of the Monte Carlo method, a logical next step was to try and see if an approximation using the first order reliability method would prove itself sufficiently accurate, and how much time can be saved in

[1] After performing this analysis and the approximation using FORM as demonstrated in the upcoming section, one of the distributions was altered. Therefore, these β's do not correspond exactly to the value in the final report.

using this method instead of Monte Carlo. The theoretical background of FORM was explained in appendix A.

The FORM-implementation was written in MATLAB, following the guidelines laid out in *Probabilities in Civil Engineering* (CUR-committee E10, 1997). The first estimate for the design point is taken as the mean of each variable. At this point, the reliability is linearized, and a first estimate of the reliability index (β) is obtained. This value for β is combined with the α-values for each variable, yielding a new estimate for the design point.

The partial derivatives, which are required when using FORM, where determined using numerical differentiation, as an analytical formulation clearly was not possible due to the operators in the limit state function. It was chosen to apply central differentiation, thus, for each stochastic variable, in the form of

$$\mathbf{X} = \begin{bmatrix} X_1 \\ X_2 \\ \vdots \\ X_i \\ \vdots \\ X_n \end{bmatrix} \quad \mathbf{x}_i^- = \begin{bmatrix} X_1 \\ X_2 \\ \vdots \\ X_i - \Delta X_i \\ \vdots \\ X_n \end{bmatrix} \quad \mathbf{x}_i^+ = \begin{bmatrix} X_1 \\ X_2 \\ \vdots \\ X_i + \Delta X_i \\ \vdots \\ X_n \end{bmatrix} \tag{H.1}$$

where the partial derivative with respect to x_i is approximated by

$$\frac{\partial g}{\partial X_i} \approx \frac{g(\mathbf{x}_i^+) - g(\mathbf{x}_i^-)}{2\ \Delta X_i} \quad \text{for } i = 1, 2, \ldots n \tag{H.2}$$

thus requiring the reliability function to be evaluated twice for each variable.

The first order reliability method allows for iterative solving, and some criteria is required to judge convergence. Here it was chosen to check two criteria (based on Haukaas (n.d.)), namely the value of the limit state function at the design point, and whether the hyperplane (from linearization) at the design point is perpendicular to the vector between the design point and the origin of the **normalized** variable space (which should be the case in order to obtain the smallest distance between these points). In formulae:

$$Z|_{\mathbf{x}^*} \leq \epsilon \tag{H.3}$$

for the value of the limit state function, and

$$1 - \frac{\alpha^T \mathbf{x}^*}{||\mathbf{x}^*||} \leq \epsilon \tag{H.4}$$

as a measure of the difference between a perpendicular vector and the actual vector, where the numerator is found by taking the dot-product, and the vertical bars in the denominator symbolize the vector norm. For the FORM-analyses performed in this work, ϵ was set equal to 10^{-3} (this results in an accuracy of the reliability index in the order of 10^{-2}).

Using the described method, the reliability was determined using FORM. For this it was chosen to generate 1000 signals and determine the resulting reliability indices. The overall resulting reliability index is then the average (averaged using the equivalent probabilities of failure, not reliability indices). Of great importance is the comparison to the Monte Carlo analysis, which serves the role of reference. The resulting failure probability and reliability index using FORM were:

Resulting estimate probability of failure	$\hat{P}_F = 0.0019$
Resulting reliability index	$\beta = 2.894$

It may be clear that differences are well within the margins of error, and that FORM can therefore be used to determine the reliability for subsequent cases.

H.4 Influence of signal

A major component of the time required for the determination of reliability is spent on creating signals, which is an intensive activity, also caused by the large number of trains of which passings are simulated. The question now arises whether different signals actually result in a different reliability, or that the probabilistic components in the signal are averaged enough, so that the reliability is practically invariant to the actual signal.

The most pragmatic way to assess such a preposition, is by actually trying. Therefore, the reliability which was determined using FORM, for a total of 1000 times (thus from 1000 signals, required time approx. 70 hours), was studied. Each signal thus result in a unique reliability index, all of which are plotted in figure H.2.

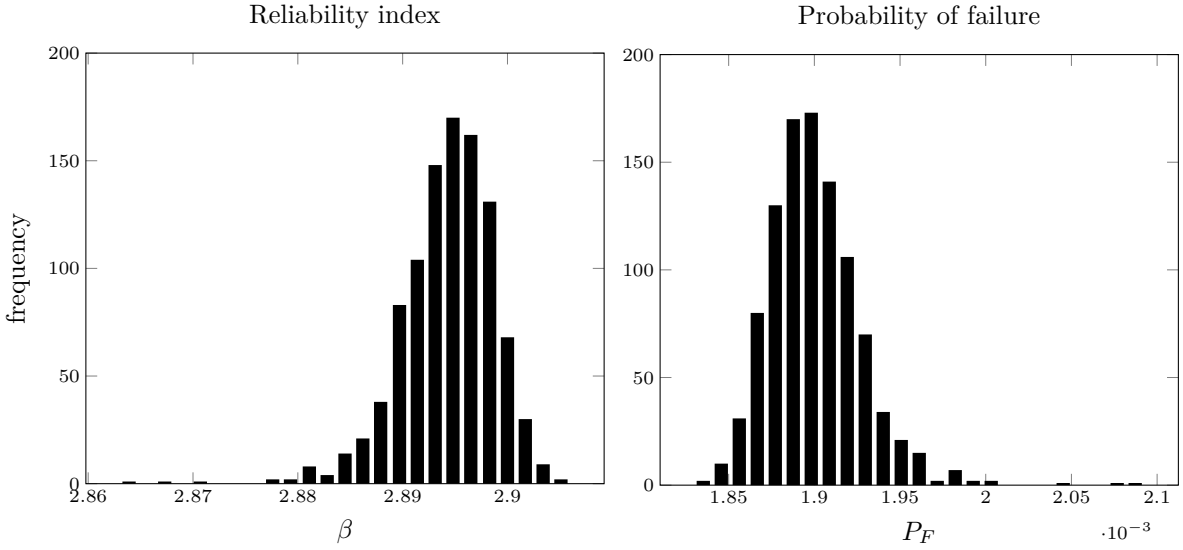

Figure H.2: Reliability index and probability of failure for different signals. All results correspond to a design life of 100 years.

From figure H.2 it can be concluded that the differences between reliability indices are, although present, quite small. Also, it is very important to realize that for this, it is **not the lowest value of the reliability index that is governing**. In essence the reliability index should incorporate these differences between signals. Analogously to a Monte Carlo analysis, the overall failure probability is actually the mean of all resulting failure probabilities.

This, the differences being quite small, is a positive result as is it allows the reliability to be determined using only one signal as input, speeding up the analysis considerably, while maintaining sufficient accuracy. Fundamentally speaking, it is of course preferable to include a larger number of signals, but to limit the overall computational expense, taking into account the small influence on the reliability and the large number of calibration cases, it was chosen to only use a single signal for each calibration. Also, the magnitude of the error is deemed smaller than the accuracy of the entire methodology used.

H.5 Verification result FORM analysis

One case which resulted in a low β-value was examined in detail. This concerns structural scheme 1, 4 meter span, detector 111 traffic, and a design based on load model EC1. In this section, a calculation closest to a hand calculation is demonstrated for reinforcement. Due to the large amount of data and steps in the analysis, some parts are not verifiable by hand (influence operator, cycle counting and summation to obtain damage number).

First of all, the limit value of u was determined, as well as the difference between the obtained damage and unity (included to confirm convergence):

$$u_{\text{lim}} = 2.5489, \;\; \Delta_D = 1.19 \times 10^{-8}$$

The FORM algorithm then ran 8 iterations until convergence was reached. The resulting value of Z at the design point was:

$$Z^* = g(\mathbf{x}^*) = 6.93 \times 10^{-4}$$

The final β was 2.1835, corresponding to the design point

$$\mathbf{x}^* = \begin{bmatrix} \xi_{\text{ext}} \\ \theta_S \\ N^* \\ \Delta \end{bmatrix}^* = \begin{bmatrix} 25.1285 \\ 1.4606 \\ 6.3692 \\ 0.8676 \end{bmatrix}$$

The damage number can be calculated with the values corresponding to the design point (see figure H.3) and table H.1):

$$D = \sum \mathcal{D}\left(\mathcal{R}\left(u_{\text{lim}}\, \mathcal{I}\left(\mathbf{H}\right)\right)\right) = 0.0346$$

Note that this damage number corresponds to ca. 4 years of measurements, and thus needs to be multiplied with the extrapolation factor. Filling in the limit state function yields:

$$Z^* = g(\mathbf{x}^*) = \frac{\Delta}{\xi_{\text{ext}}\, D} - 1 = \frac{0.8676}{25.1285 \times 0.0346} - 1 \approx 0$$

At the design point, the lognormal distributions are approximated by an equivalent normal distribution. At the final design point, these are:

$\theta_S \sim N(0.8783,\, 0.2893)$
$\Delta \sim N(0.9526,\, 0.2547)$

The α-factors in the final iteration are part of the output (and can be derived from the partial derivatives at the design point combined with the standard deviation of each variable):

$$\boldsymbol{\alpha} = \begin{bmatrix} 0.0052 \\ 0.9219 \\ -0.3560 \\ -0.1529 \end{bmatrix}$$

using which it is possible to check the design point, as $X_i = \mu_{X_i} + \beta\, \alpha_i\, \sigma_{X_i}$:

$$\mathbf{x}^* = \begin{bmatrix} 25.1256 \\ 0.8783 \\ 6.6 \\ 0.9526 \end{bmatrix} + 2.1835 \begin{bmatrix} 0.0052 \times 0.2513 \\ 0.9219 \times 0.2893 \\ -0.3560 \times 0.2969 \\ -0.1529 \times 0.2547 \end{bmatrix} = \begin{bmatrix} 25.1285 \\ 1.4606 \\ 6.3692 \\ 0.8676 \end{bmatrix}$$

The partial derivatives at the design point are:

$$\left.\frac{\partial g}{\partial \xi_{\text{ext}}}\right|_{\mathbf{x}^*} = -0.0398 \qquad \left.\frac{\partial g}{\partial \theta_S}\right|_{\mathbf{x}^*} = -6.1240$$
$$\left.\frac{\partial g}{\partial N^*}\right|_{\mathbf{x}^*} = 2.3042 \qquad \left.\frac{\partial g}{\partial \Delta}\right|_{\mathbf{x}^*} = 1.1532$$

From the above, the mean value and standard deviation of Z are approximated using linearization:

$$\begin{aligned}
\mu_Z &\approx g(\mathbf{x}^*) + \sum_{i=1}^{n} \left.\frac{\partial g}{\partial X_i}\right|_{\mathbf{x}^*} (\mu_{X_i} - X_i^*) \\
&= 0 + (-0.0398\,(25.1256 - 25.1285)) + (-6.1240\,(0.8783 - 1.4606)) + \ldots \\
&\quad (2.3042\,(6.600 - 6.3692)) + (1.1532\,(0.9526 - 0.8676)) \\
&= 0 + 1.15 \times 10^{-4} + 3.566 + 0.5318 + 0.098 = 4.1959 \\
\sigma_Z &\approx \sqrt{\sum_{i=1}^{n} \left(\left.\frac{\partial g}{\partial X_i}\right|_{\mathbf{x}^*} \sigma_{X_i} \right)^2} \\
&= \sqrt{(-0.0398 \times 0.2513)^2 + (6.1240 \times 0.2893)^2 + (2.3042 \times 0.2969)^2 + \ldots} \\
&\quad \overline{(1.1532 \times 0.2547)^2} \\
&= \sqrt{1.0 \times 10^{-4} + 3.1379 + 0.4680 + 0.0863} = 1.9215
\end{aligned}$$

Using this, the final value of β can be validated:

$$\beta = \frac{\mu_Z}{\sigma_Z} \approx \frac{4.1959}{1.9216} = 2.1835$$

With this, it has been shown that a valid solution for FORM its set of equations has been obtained, which satisfies the constraint of $Z \approx 0$.

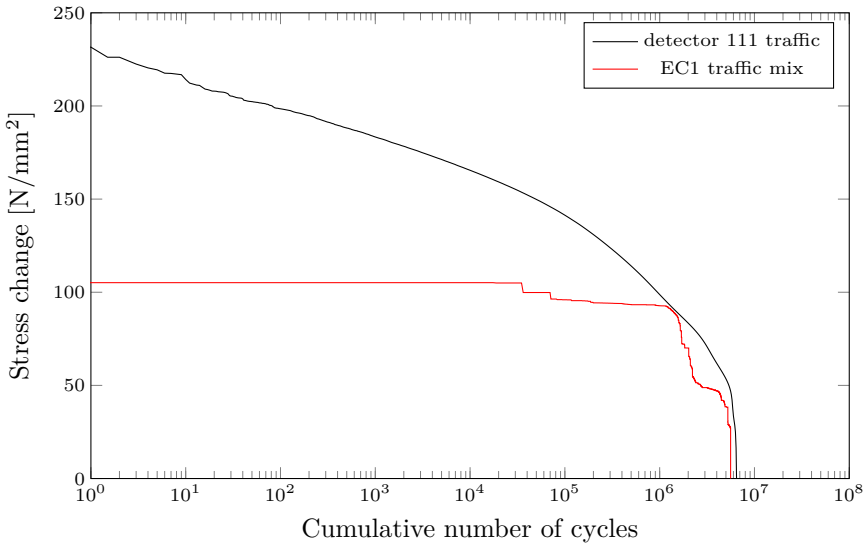

Figure H.3: Spectra at design point, expressed in stress changes (thus including u_{lim}). Note that these include dynamic amplification and all uncertainties, and therefore represent the situation at the design point.

from [N/mm^2]	to [N/mm^2]	N_i	incr. damage nr.	cum. damage nr.
0	10	116719	6.95×10^{-4}	0.00069504
10	20	213326	1.40×10^{-3}	0.002090482
20	30	287689	1.70×10^{-3}	0.003792333
30	40	482567	2.40×10^{-3}	0.006196929
40	50	1156137	0.006692178	0.012889107
50	60	989061	0.005174495	0.018063602
60	70	905980	0.005191742	0.023255344
70	80	844315	0.004481154	0.027736498
80	90	526082	2.72×10^{-3}	0.030452836
90	100	339079	1.59×10^{-3}	0.032044659
100	110	238735	1.10×10^{-3}	0.03314022
110	120	158684	5.99×10^{-4}	0.033739352
120	130	101386	4.49×10^{-4}	0.034188109
130	140	61083	1.74×10^{-4}	0.03436214
140	150	30889	1.10×10^{-4}	0.034472266
150	160	12537	3.92×10^{-5}	0.03451145
160	170	4262	8.46×10^{-6}	0.034519914
170	180	1209	2.12×10^{-6}	0.034522029
180	190	298	6.45×10^{-7}	0.034522674
190	200	68	1.28×10^{-7}	0.034522802
200	210	10	3.21×10^{-9}	0.034522805
210	220	4	9.55×10^{-11}	0.034522805
220	230	2	7.78×10^{-12}	0.034522805
230	240	0	0	0.034522805
				0.034522805

Table H.1: Table of stress ranges with incremental and cumulative damage numbers. These correspond to the detector 111 traffic spectrum at the design point, see figure H.3. Therefore, also the S-N curve corresponding to the design point was used to calculate these damage number increments.

From figure H.3 it may be clear that the spectrum corresponding to the actual loading exceeds that which is designed for (detector 111 spectrum results in a larger load effect than the EC1 traffic mix). Because these represent the situation at the design point, it can be concluded that the load at design point is larger than the characteristic value thereby formally corresponding to a partial factor greater than one. Apparently, the resistance at the design point, being equal to the solicitation by definition, surpasses the design resistance, the latter being based on the Eurocode spectrum. This shows that the current partial factors are not correctly distributed between load and resistance.

H.6 Conclusions

- Using a Monte Carlo analysis with 250000 iterations, an estimate of the reliability index of 2.888 was obtained. It was clear that, with its duration of 100 hours, this method is unfeasible for large scale calibration.
- The same case was solved using the first order reliability method (using 1000 signals), which resulted in a reliability index of 2.894, which is very close to the results obtained using the Monte Carlo. Therefore it was decided to use FORM for subsequent analyses. The requirement in terms of time, 70 hours, had still only improved marginally.
- The variability between signals (each randomly generated) was investigated, and found to be quite small. Because a large portion of time is spent on generating signals, elimination of iterations benefits the computational expenses significantly. This resulted in the choice to base the reliability in calibrations on a single signal, allowing for a runtime of about 5 minutes per analysis.

I | Results

scheme	detector	results plotted in
1	111	figure 6.1
	164	figure I.1
	364	figure I.2
2	111	figure I.3
	164	figure I.4
	364	figure I.5
3	111	figure I.6
	164	figure I.7
	364	figure I.8
4	111	figure I.9
	164	figure I.10
	364	figure I.11
5	111	figure I.12
	164	figure I.13
	364	figure I.14
6	111	figure I.15
	164	figure I.16
	364	figure I.17
7	111	figure I.18
	164	figure I.19
	364	figure I.20

Table 6.1: Overview of calibration results.

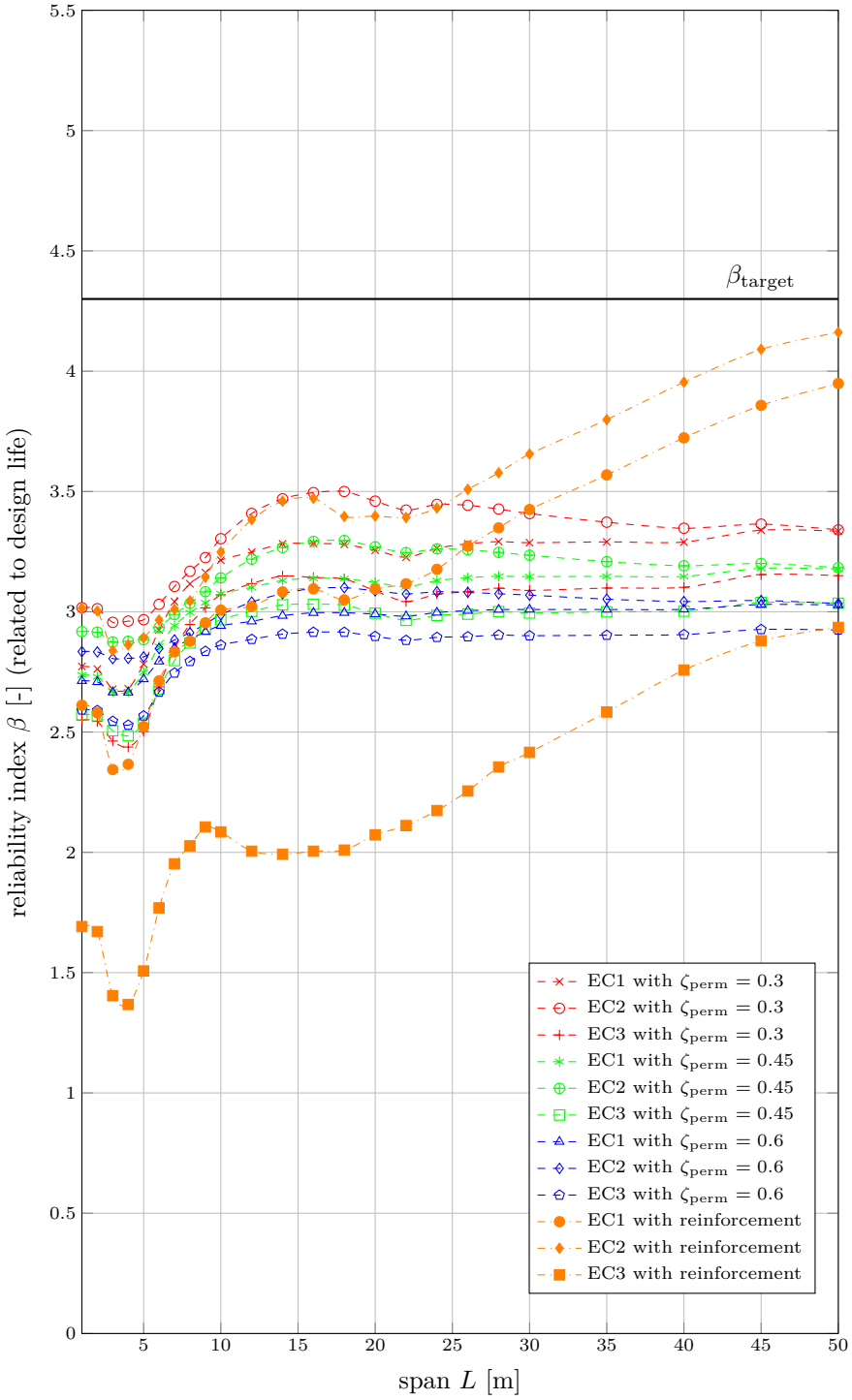

scheme	detector
1	164

Figure I.1: SC1-ECX-164

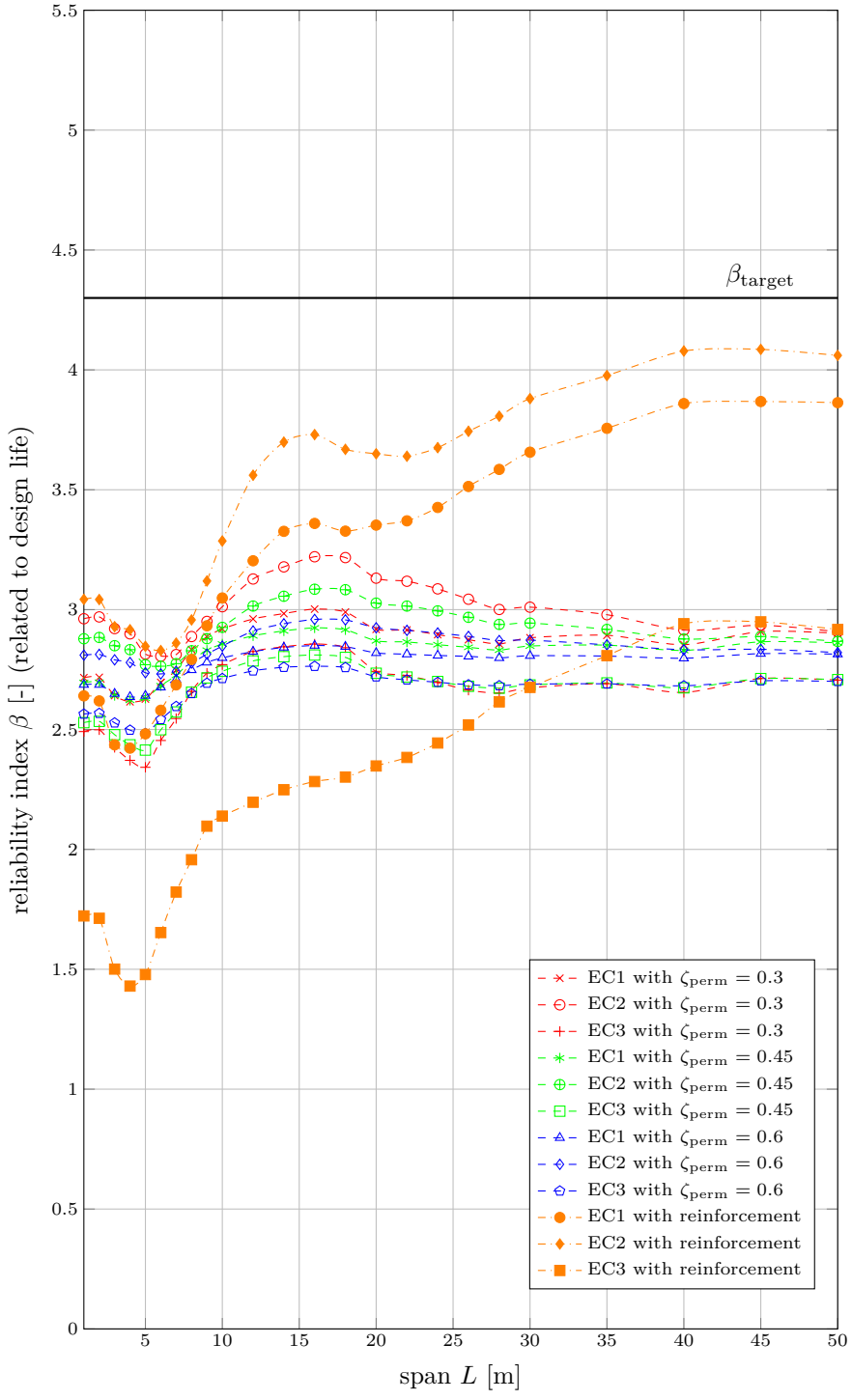

scheme	detector
1	364

Figure I.2: SC1-ECX-364

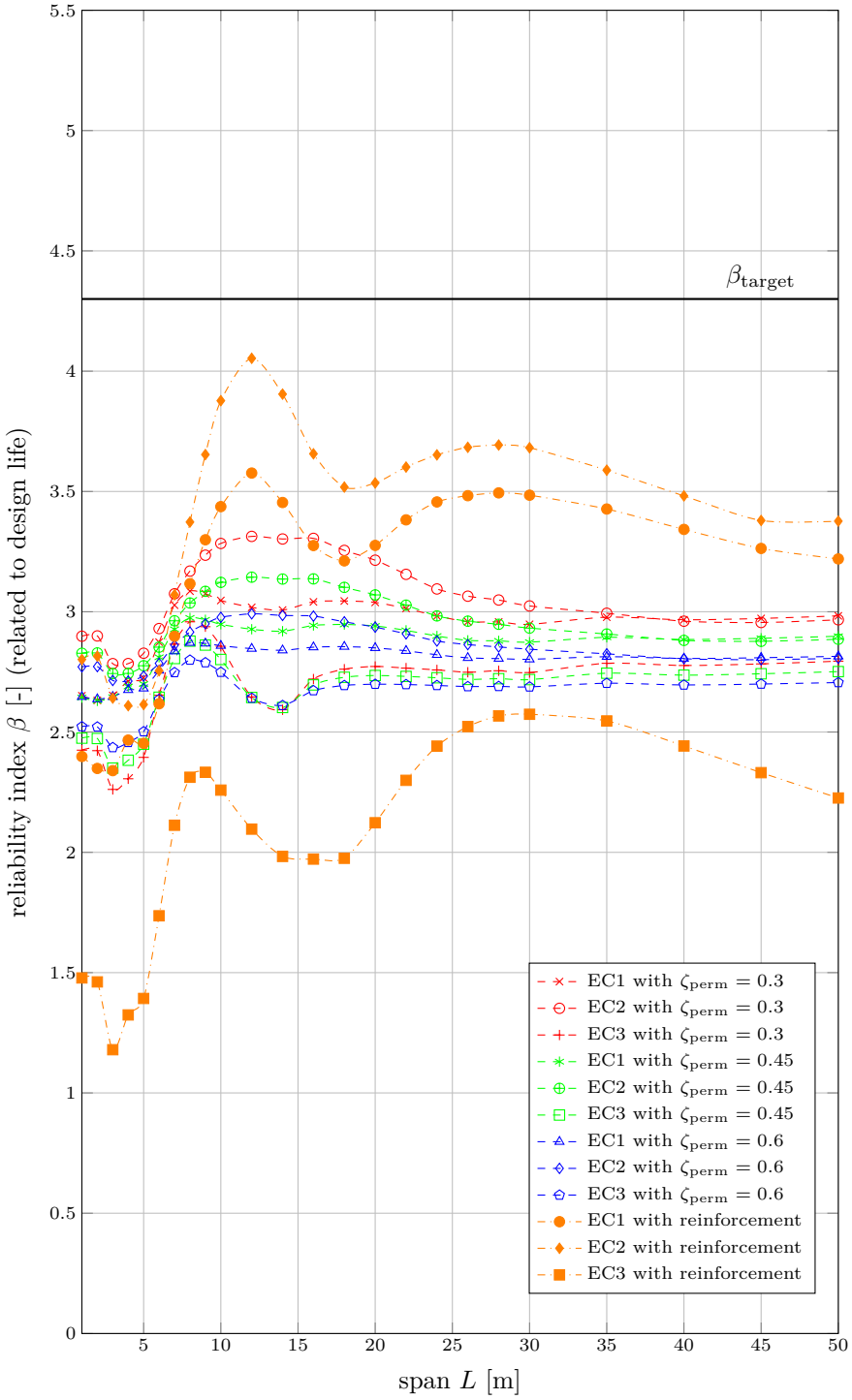

scheme	detector
2	111

Figure I.3: SC2-ECX-111

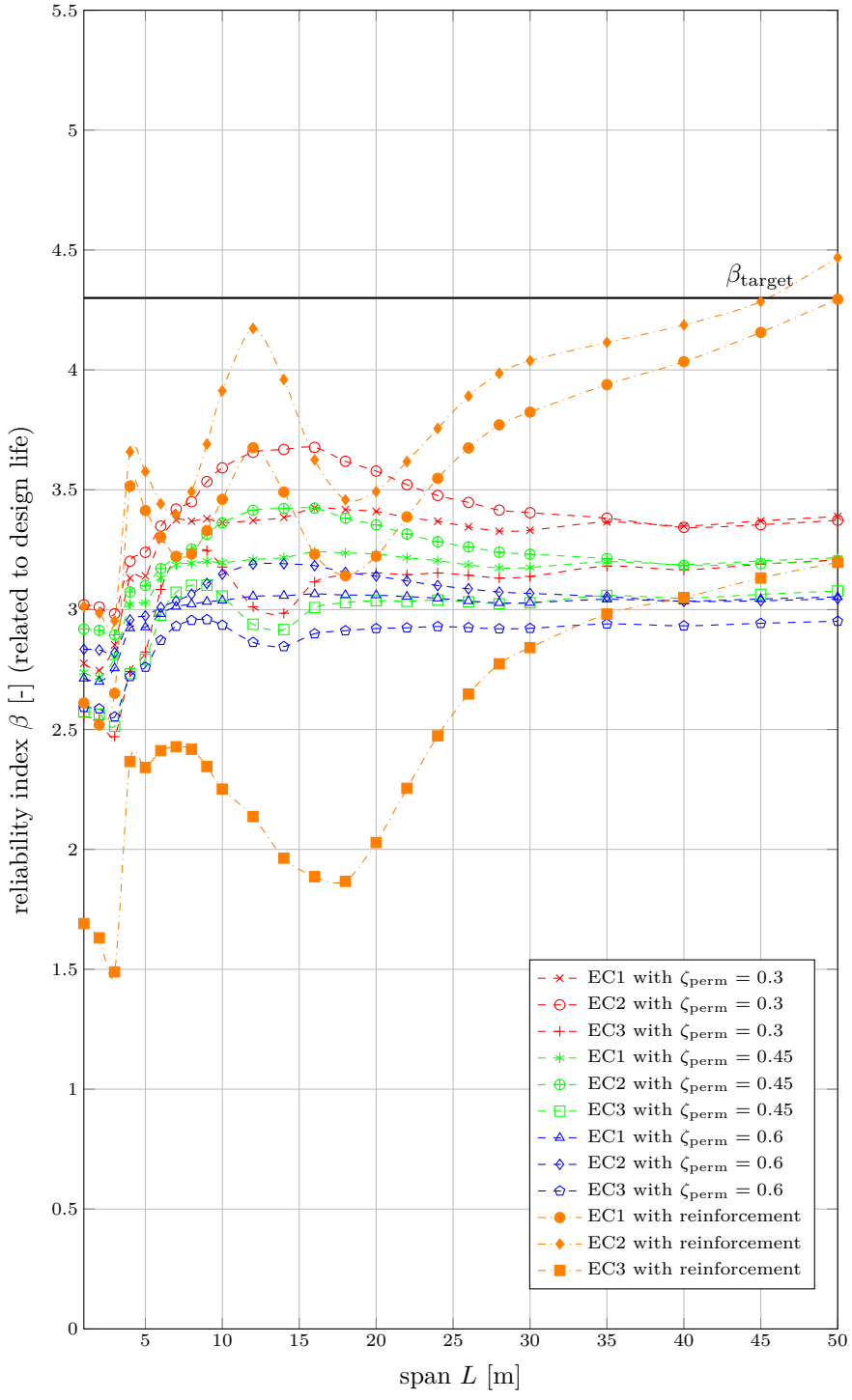

scheme	detector
2	164

Figure I.4: SC2-ECX-164

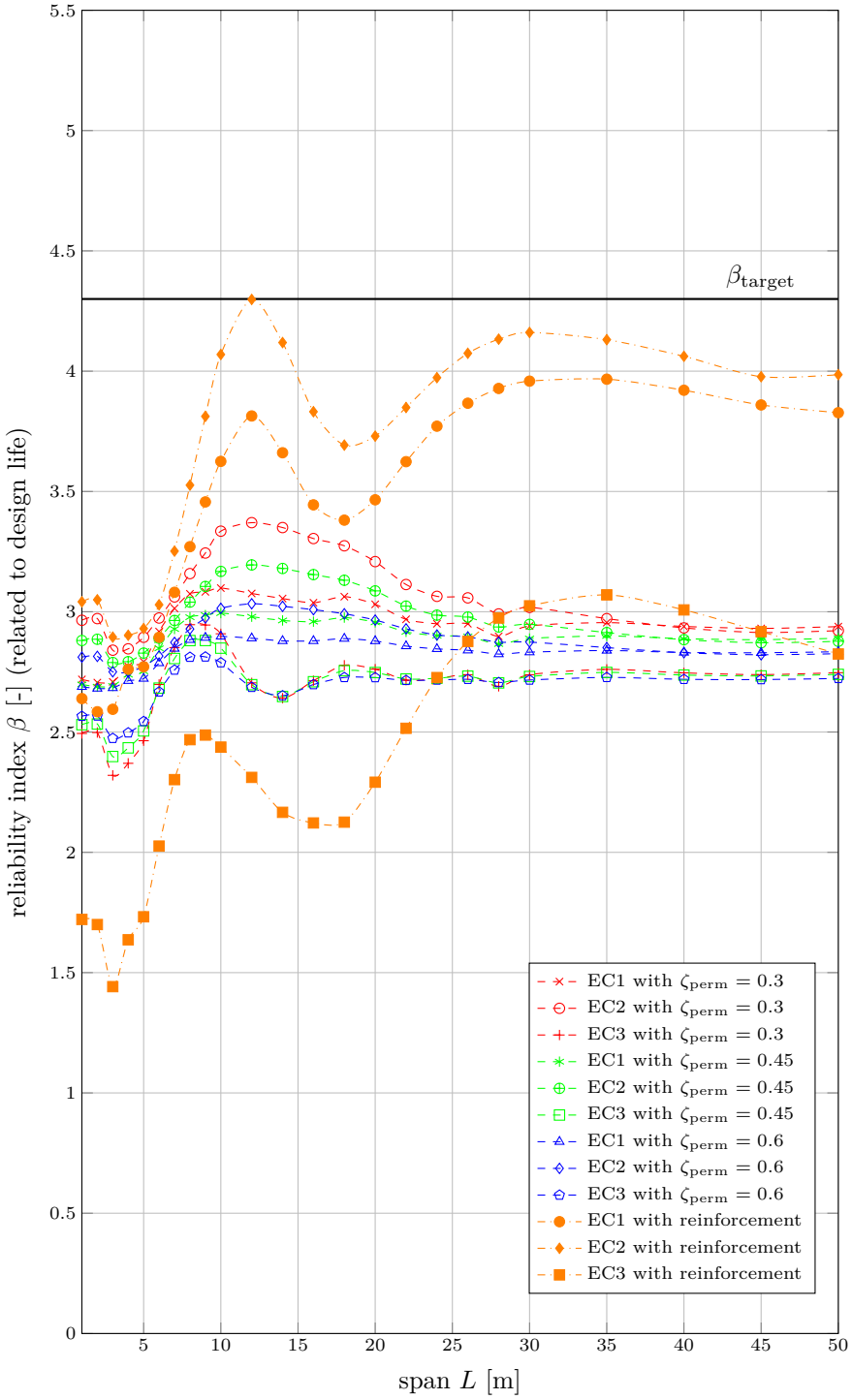

scheme	detector
2	364

Figure I.5: SC2-ECX-364

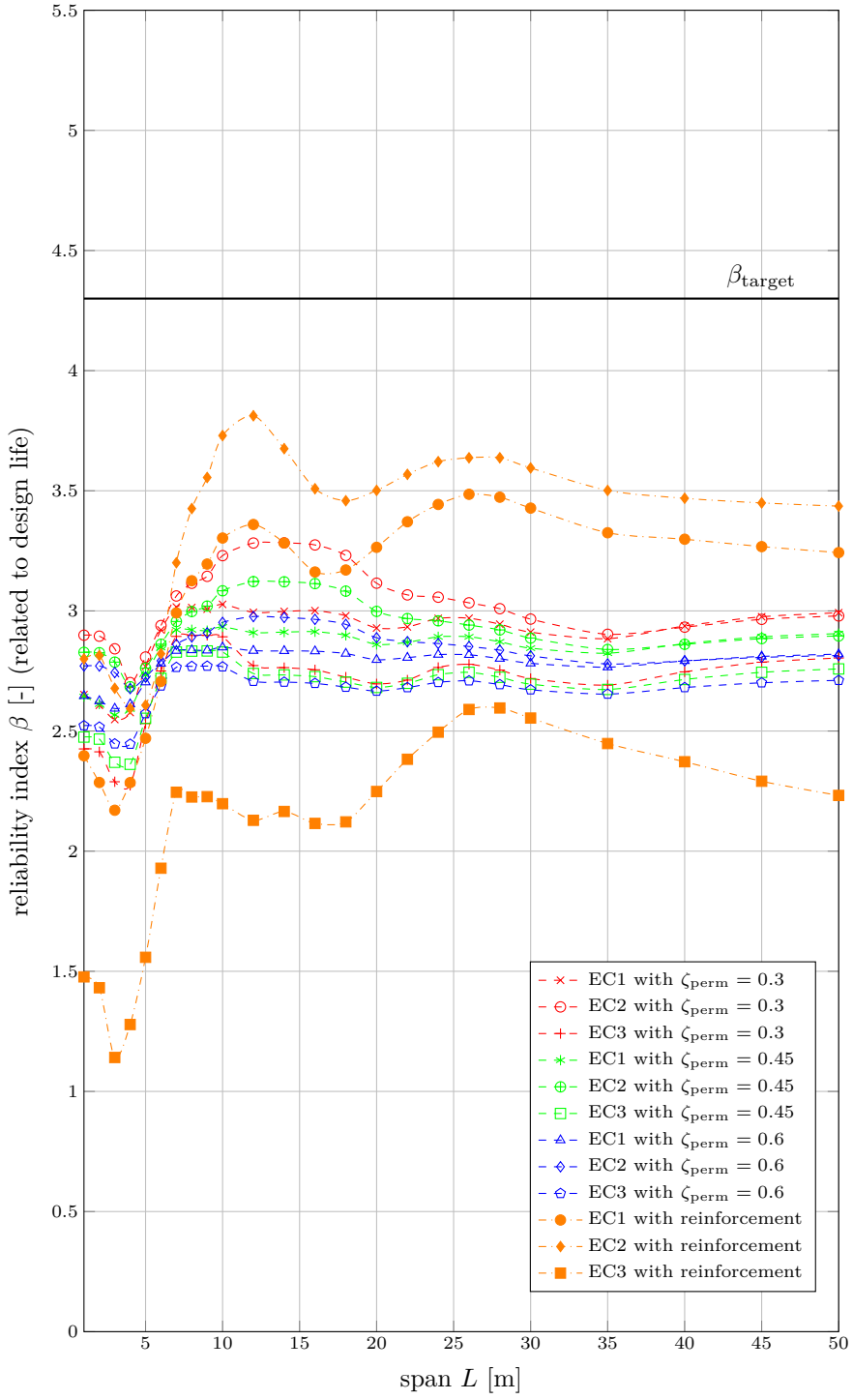

scheme	detector
3	111

Figure I.6: SC3-ECX-111

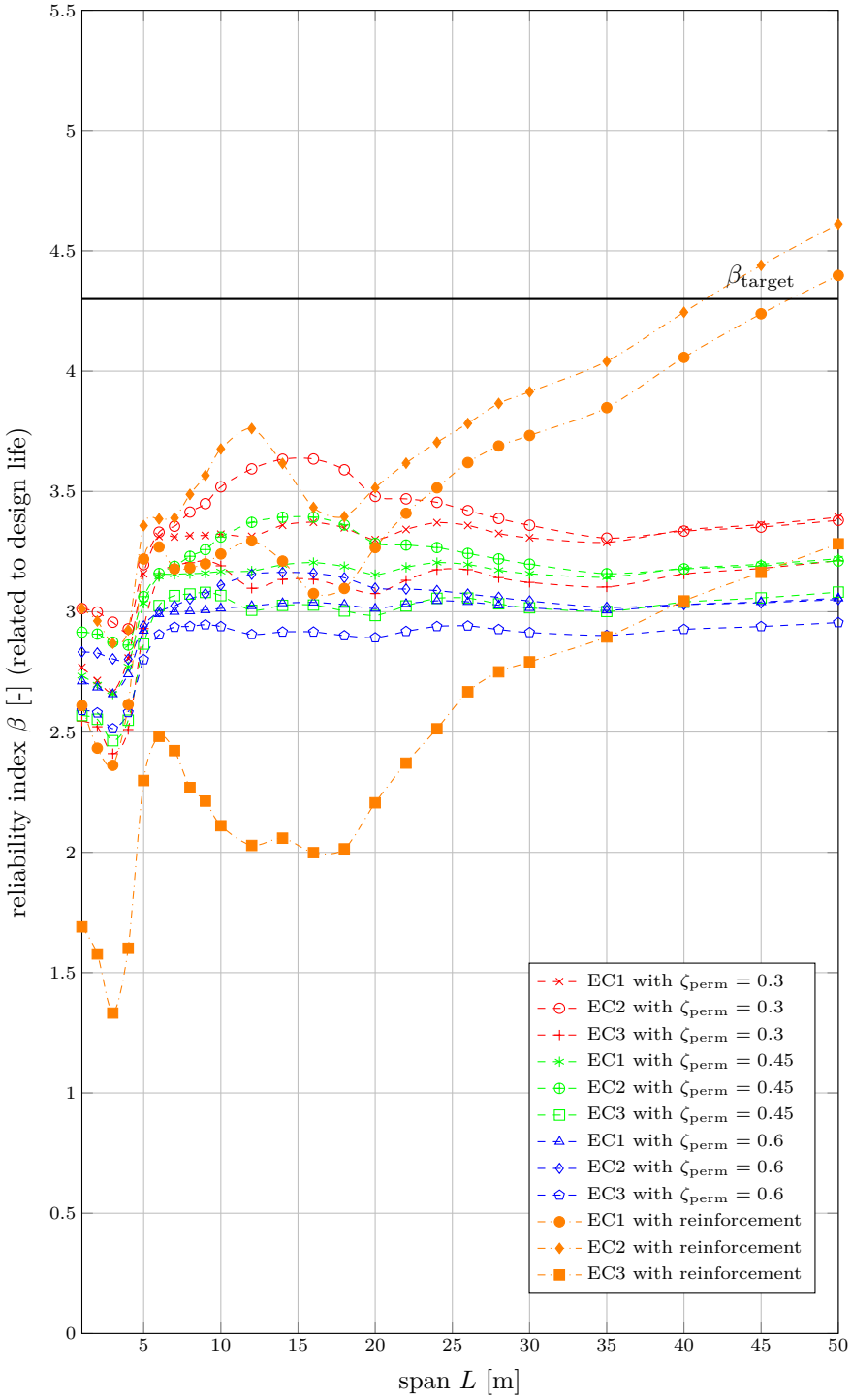

scheme	detector
3	164

Figure I.7: SC3-ECX-164

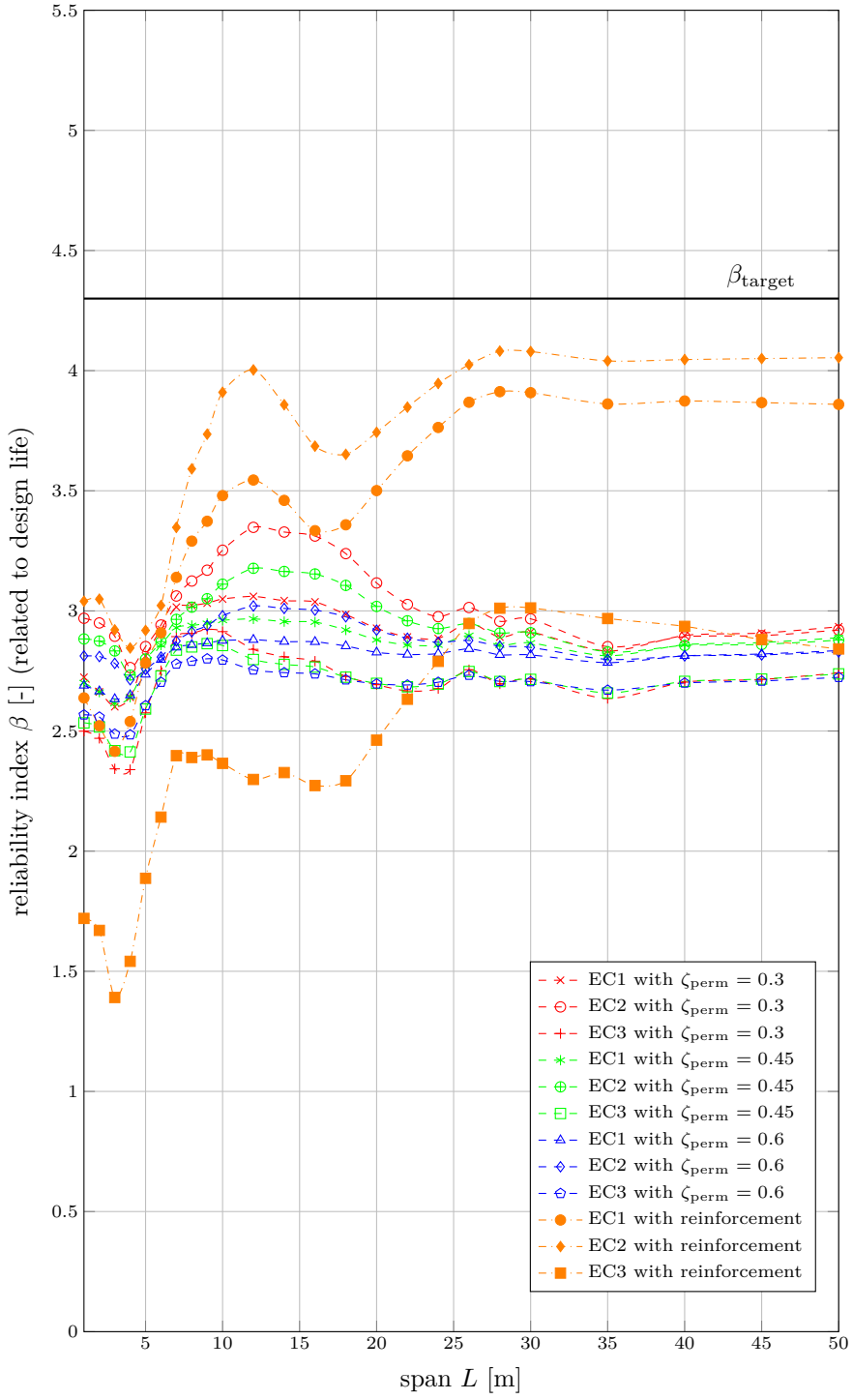

scheme	detector
3	364

Figure I.8: SC3-ECX-364

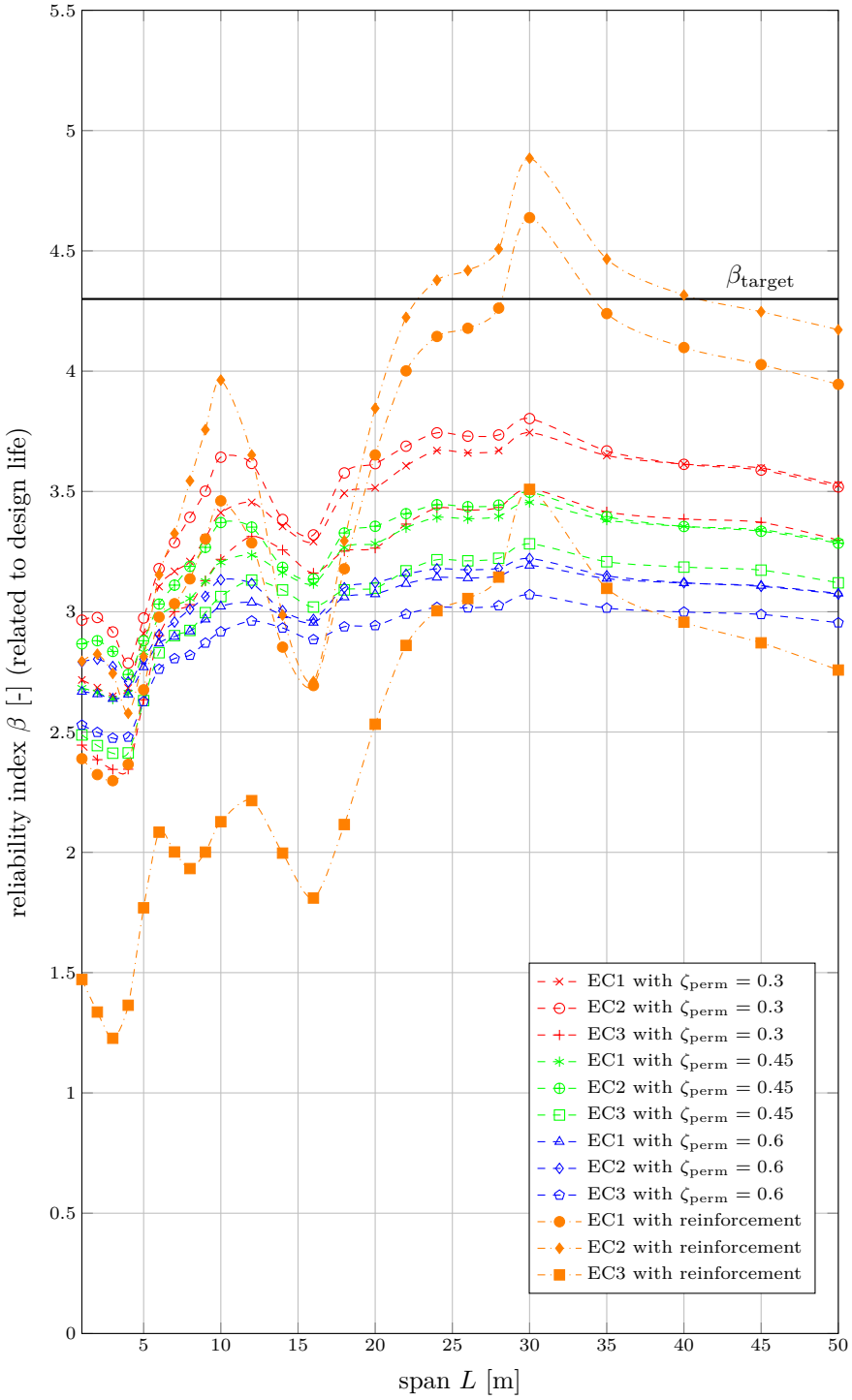

scheme	detector
4	111

Figure I.9: SC4-ECX-111

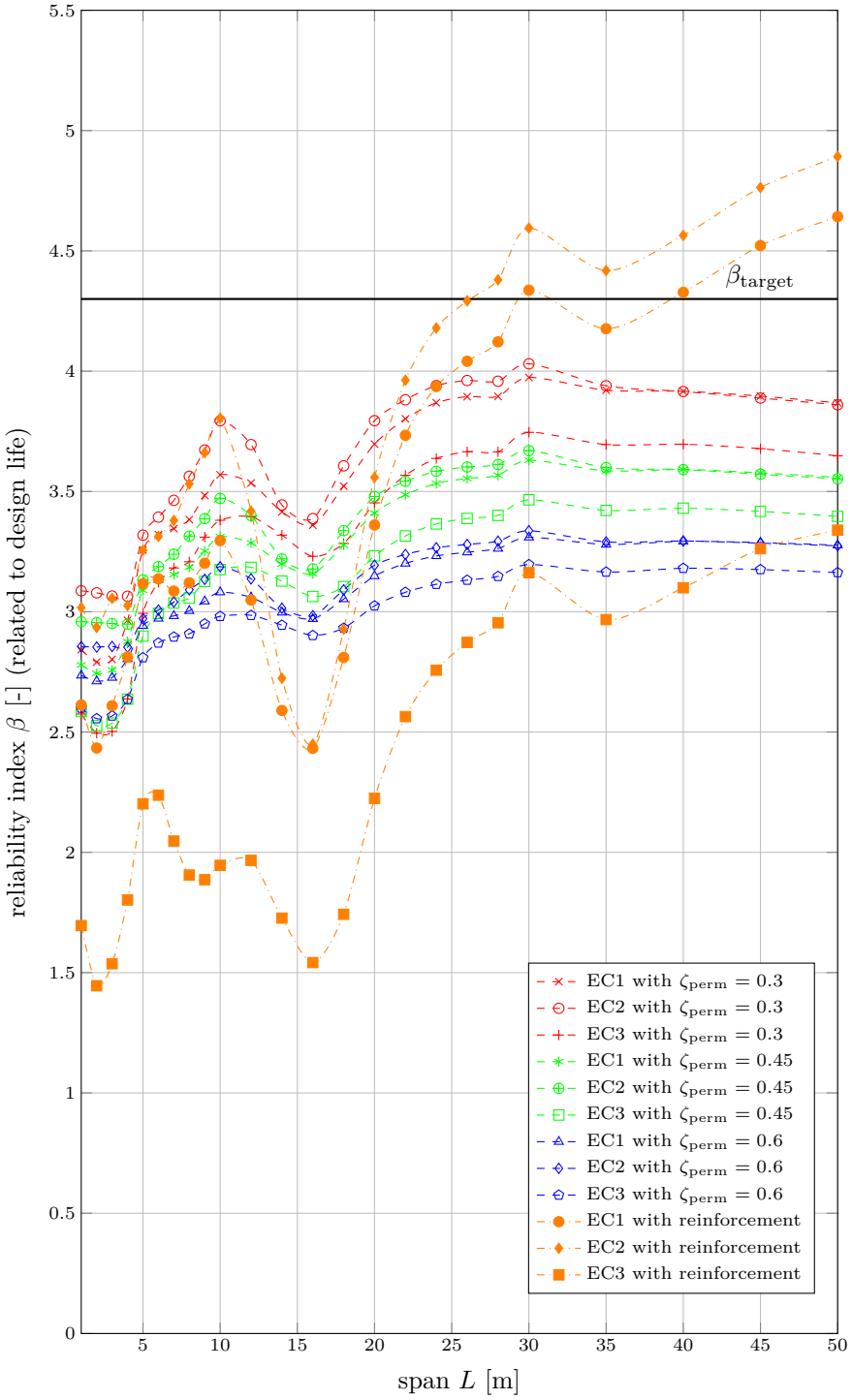

scheme	detector
4	164

Figure I.10: SC4-ECX-164

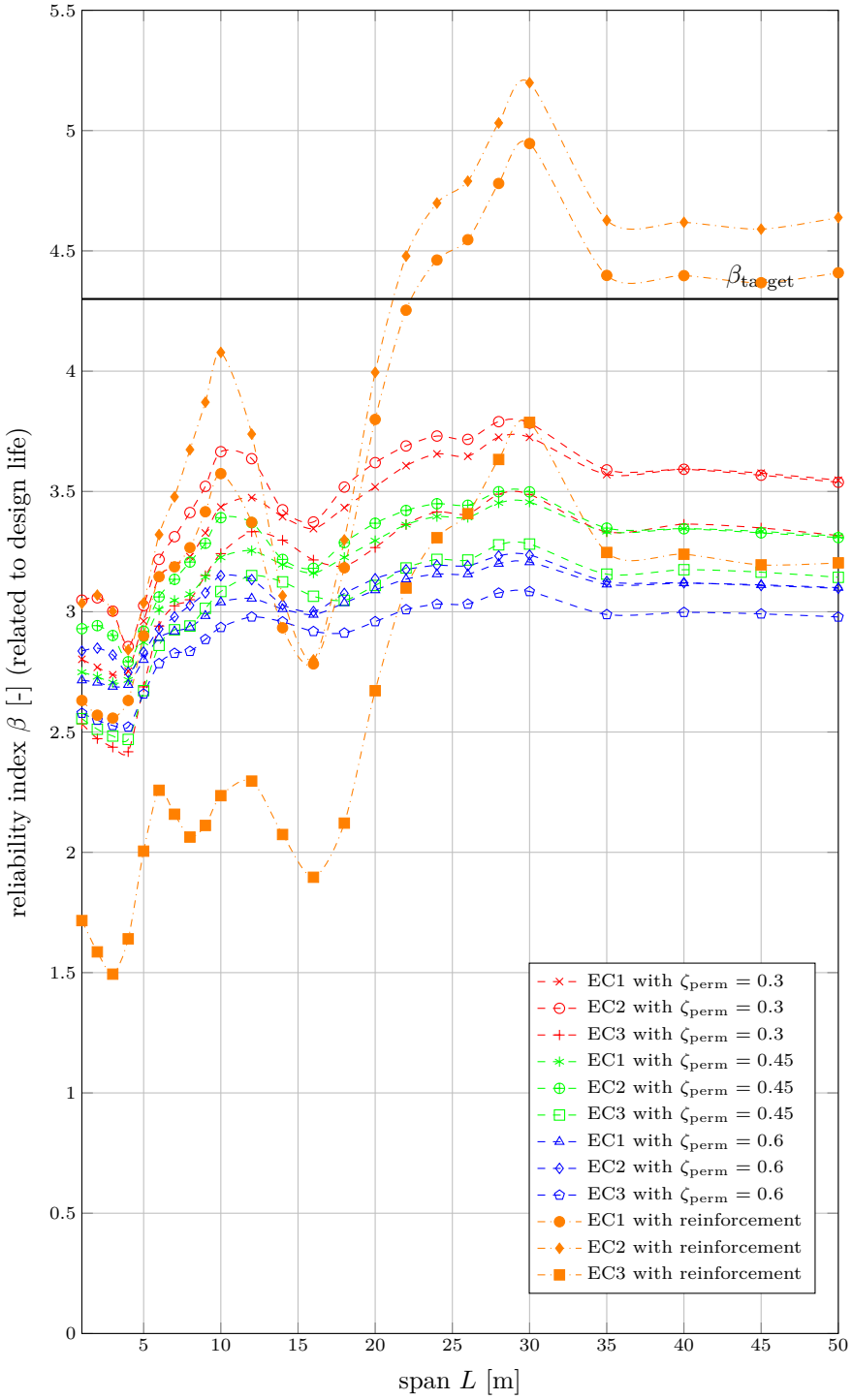

scheme	detector
4	364

Figure I.11: SC4-ECX-364

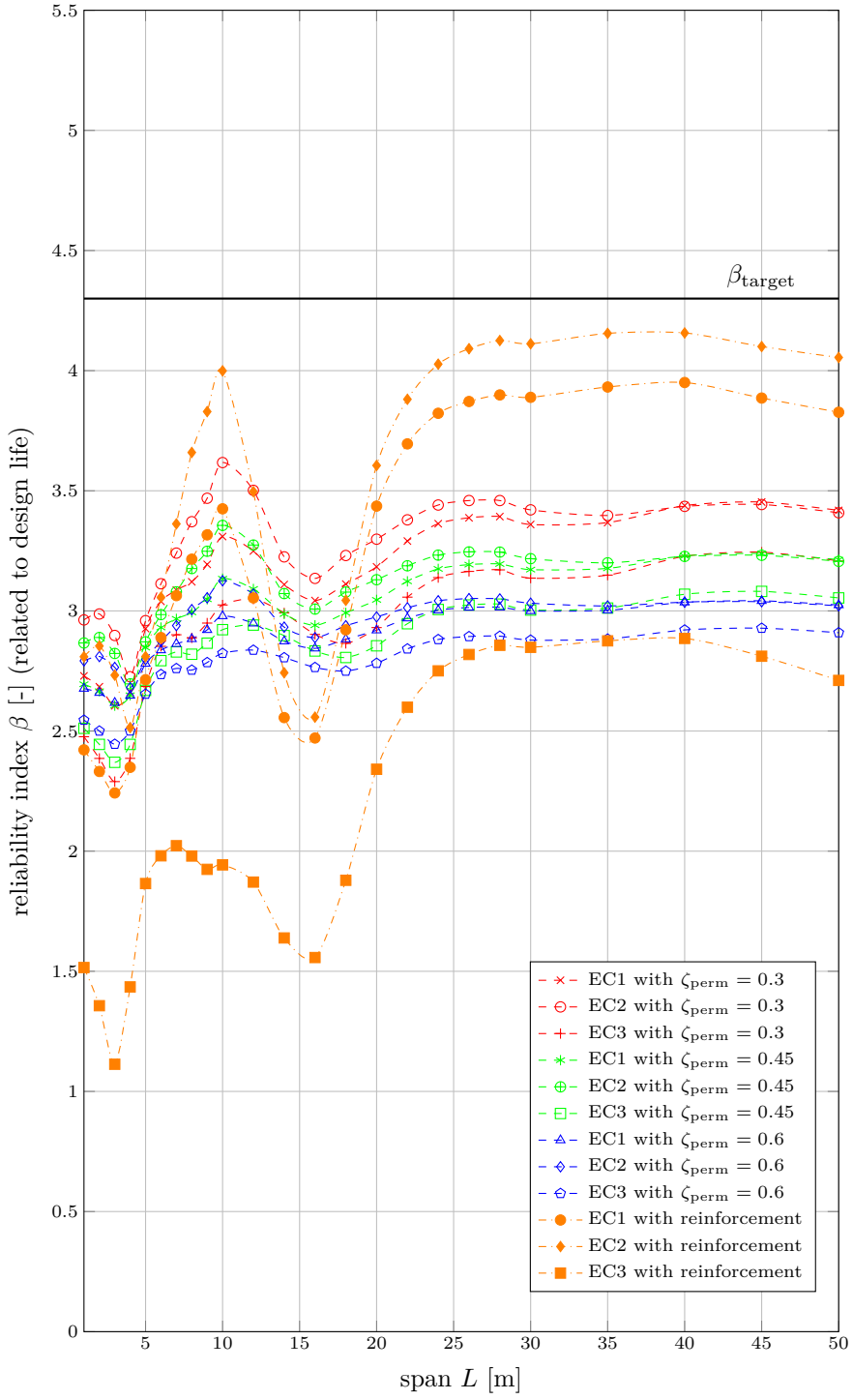

scheme	detector
5	111

Figure I.12: `SC5-ECX-111`

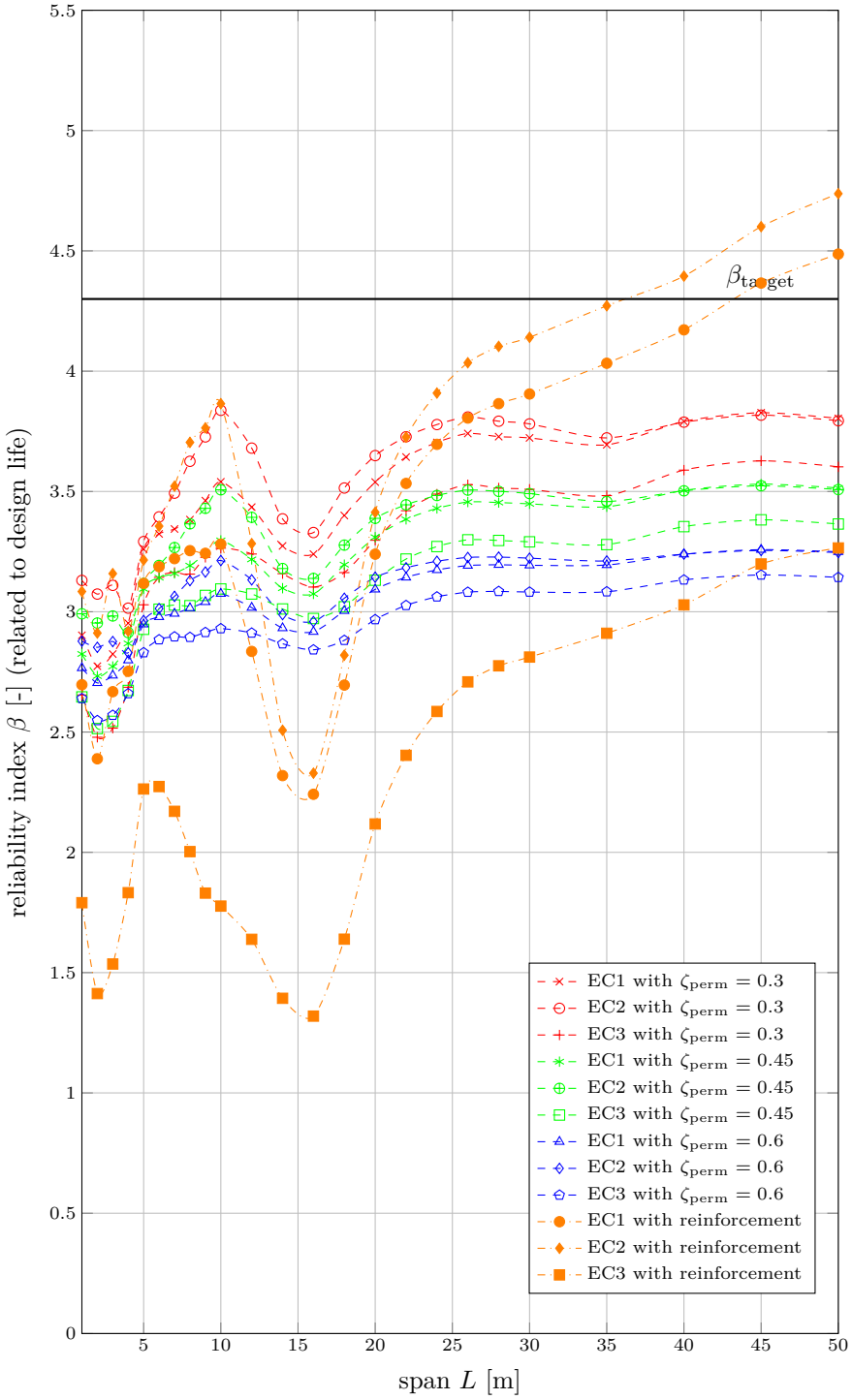

scheme	detector
5	164

Figure I.13: SC5-ECX-164

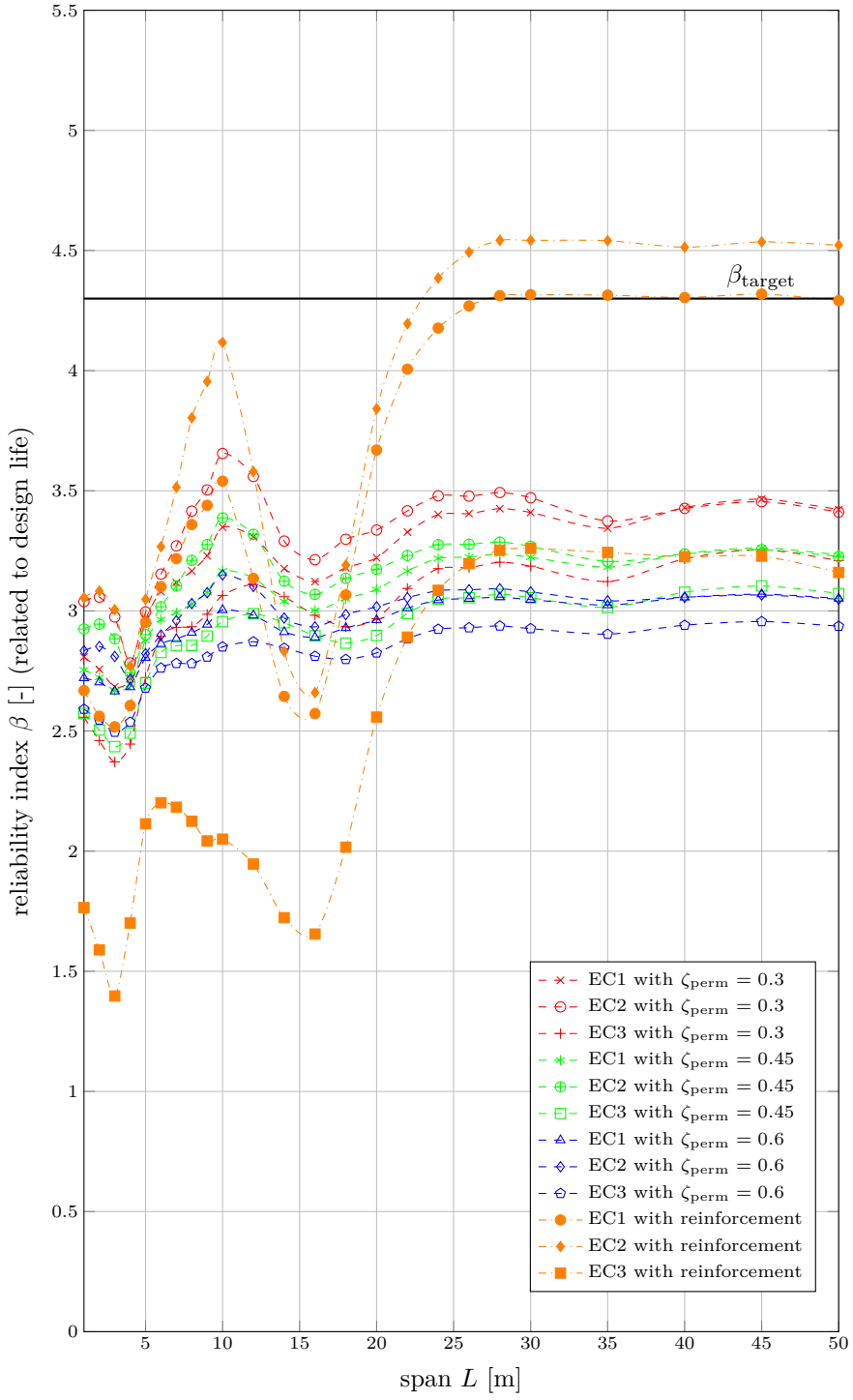

scheme	detector
5	364

Figure I.14: SC5-ECX-364

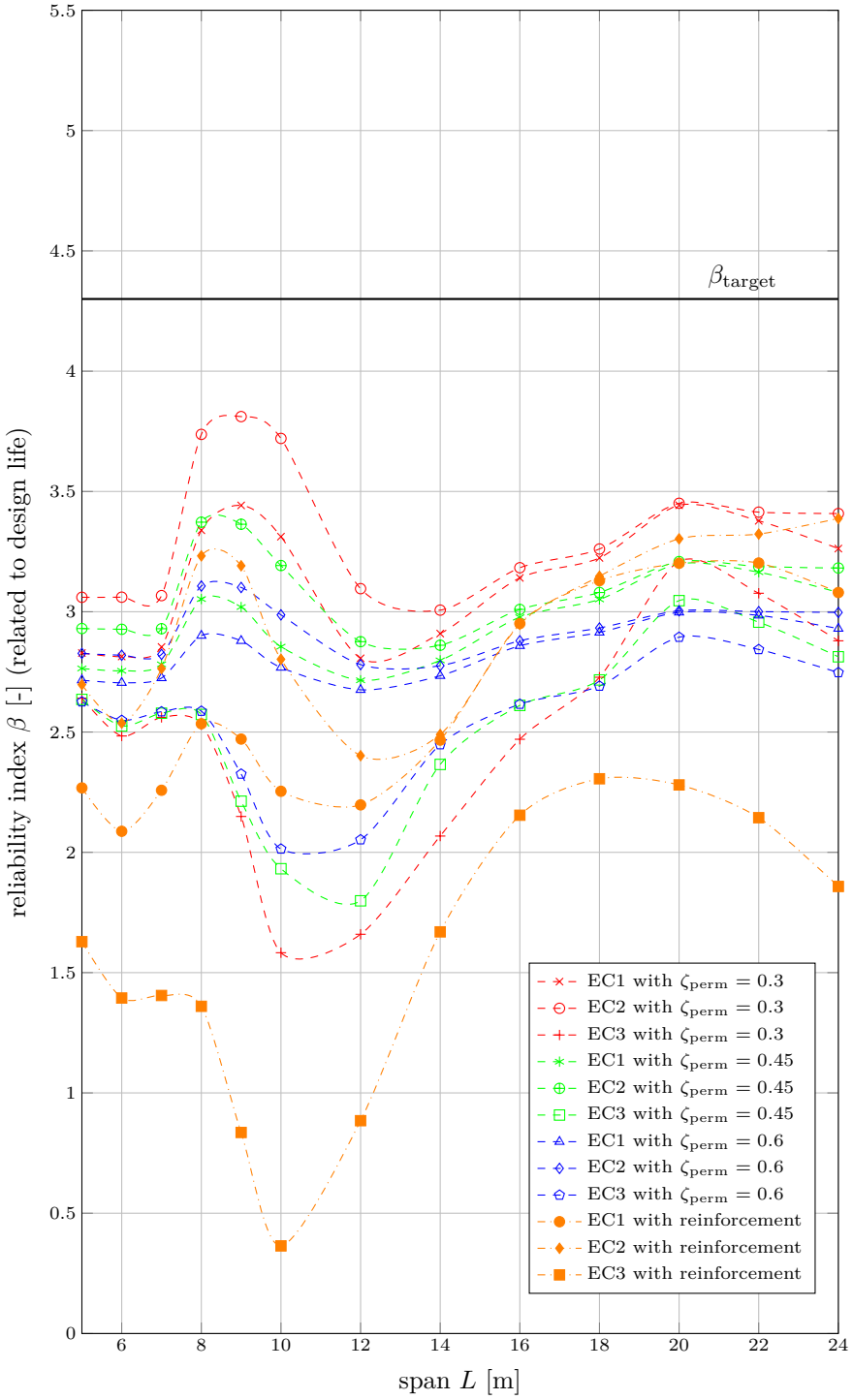

scheme	detector
6	111

Figure I.15: SC6-ECX-111

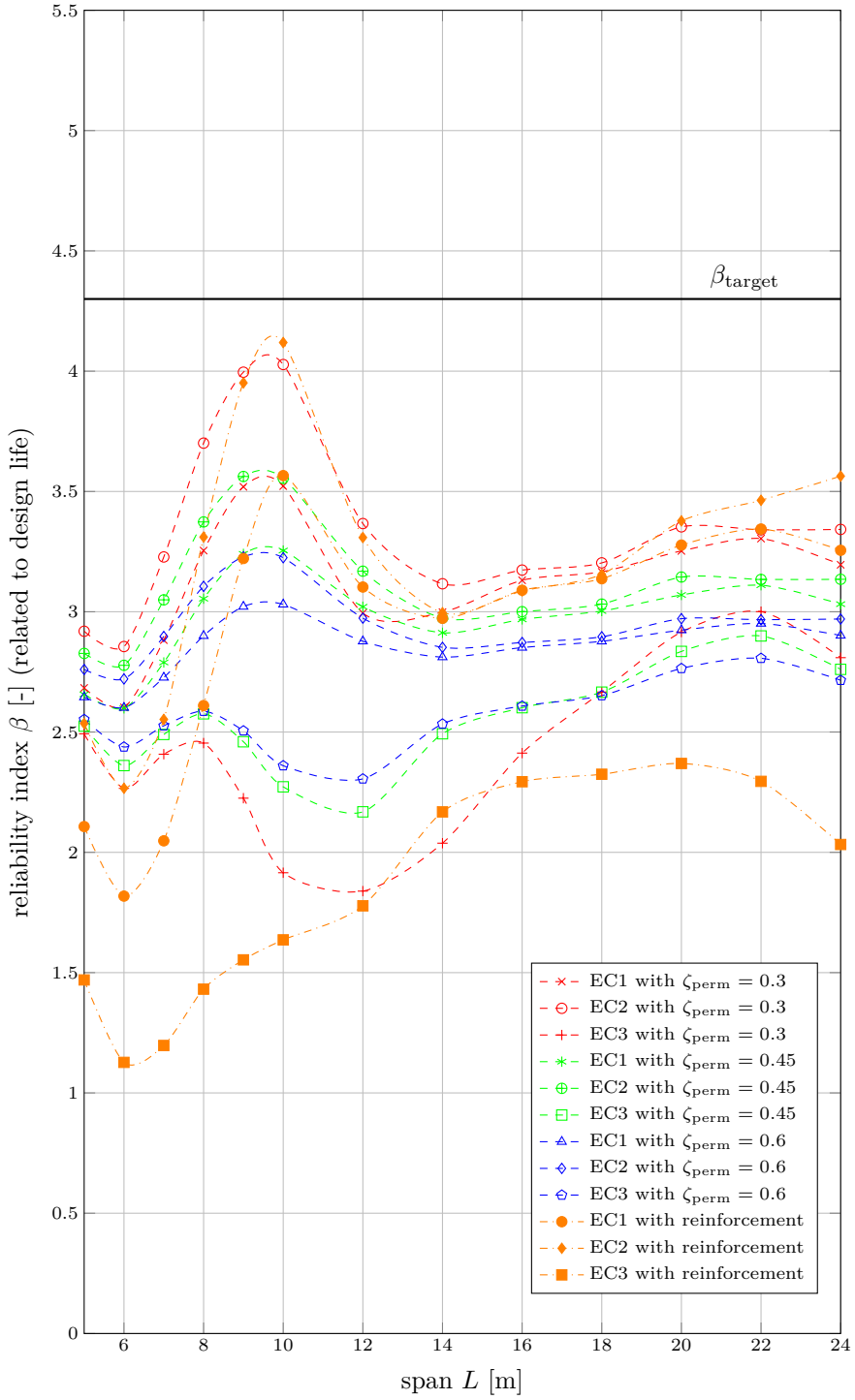

scheme	detector
6	164

Figure I.16: SC6-ECX-164

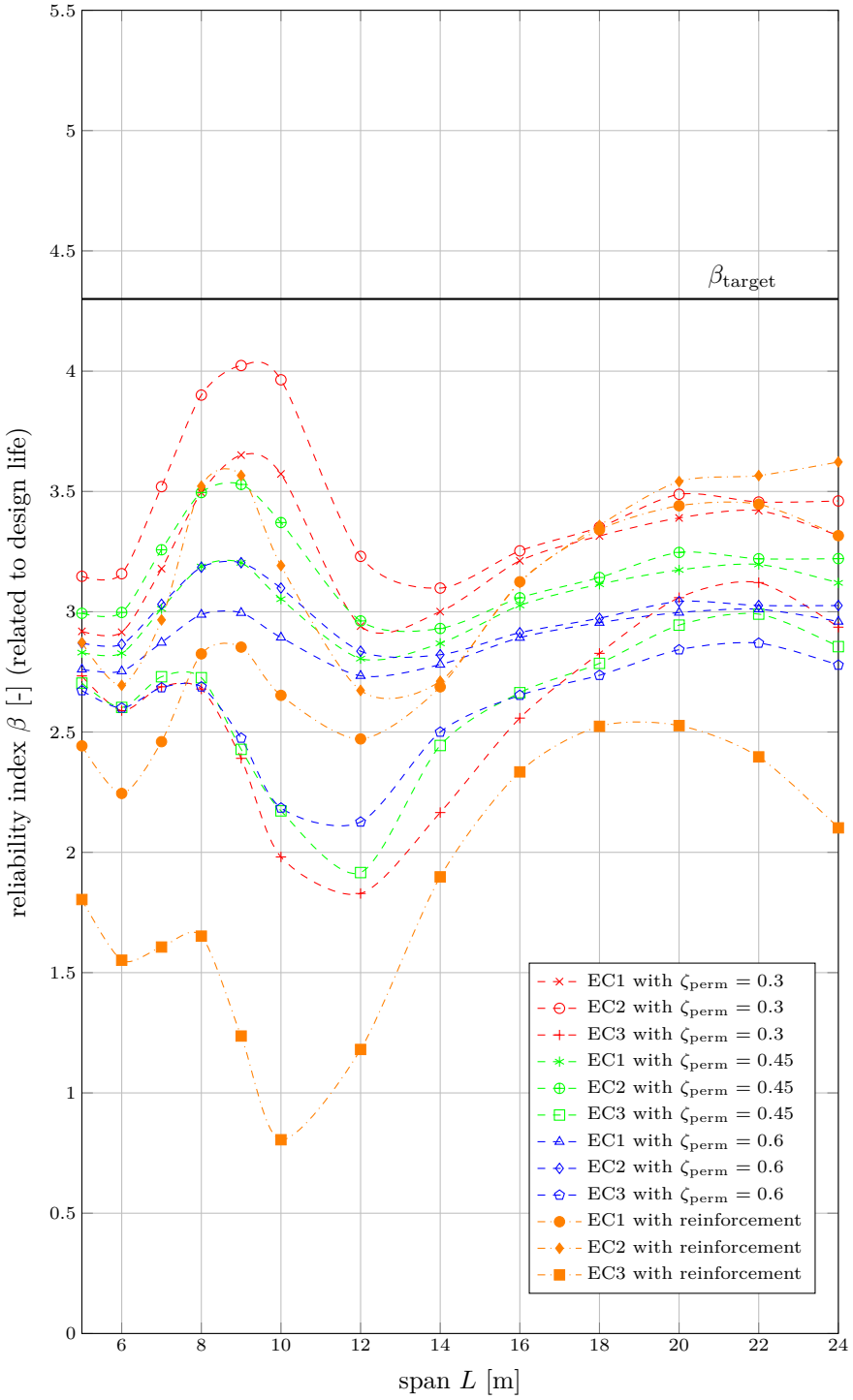

scheme	detector
6	364

Figure I.17: SC6-ECX-364

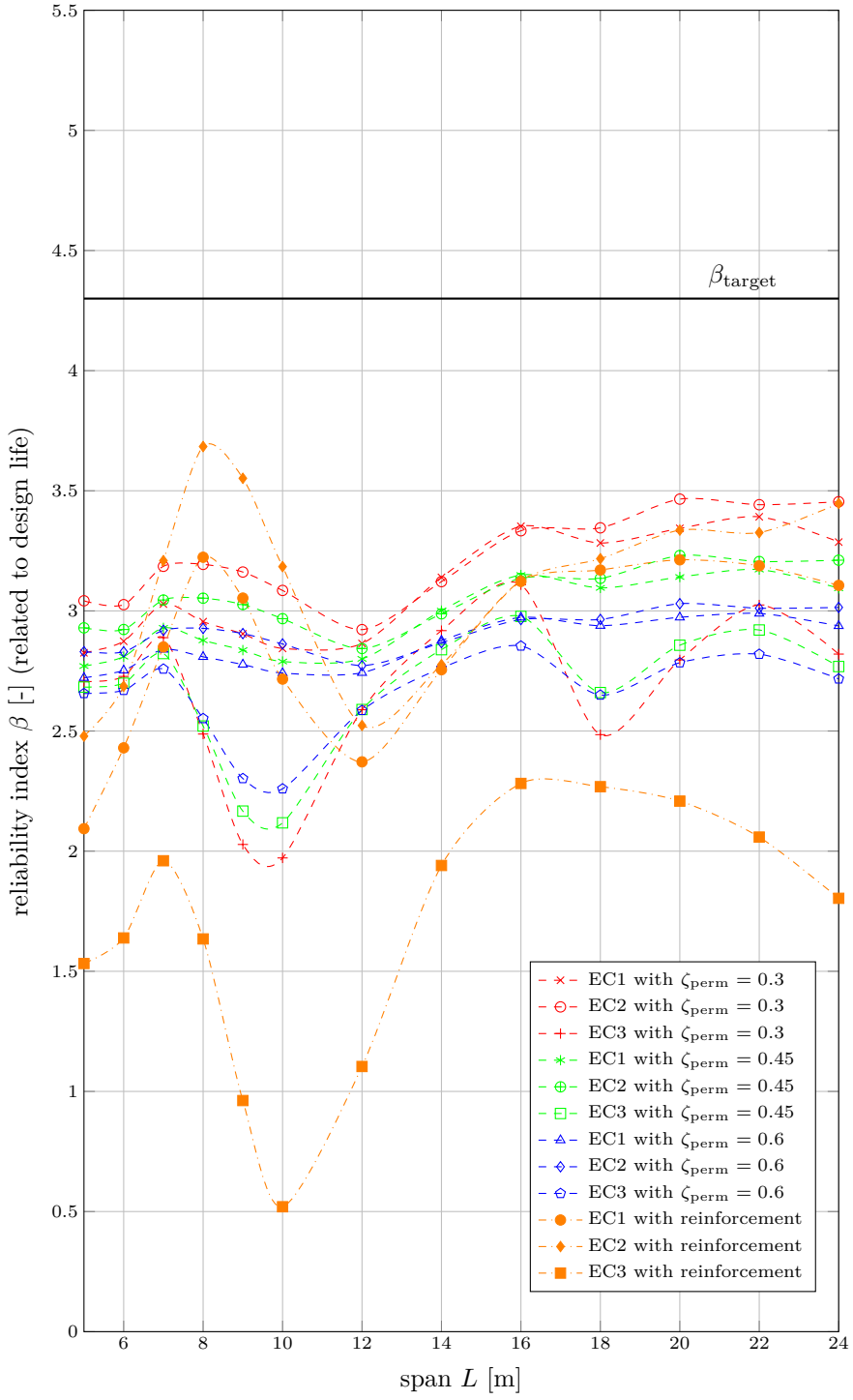

scheme	detector
7	111

Figure I.18: SC7-ECX-111

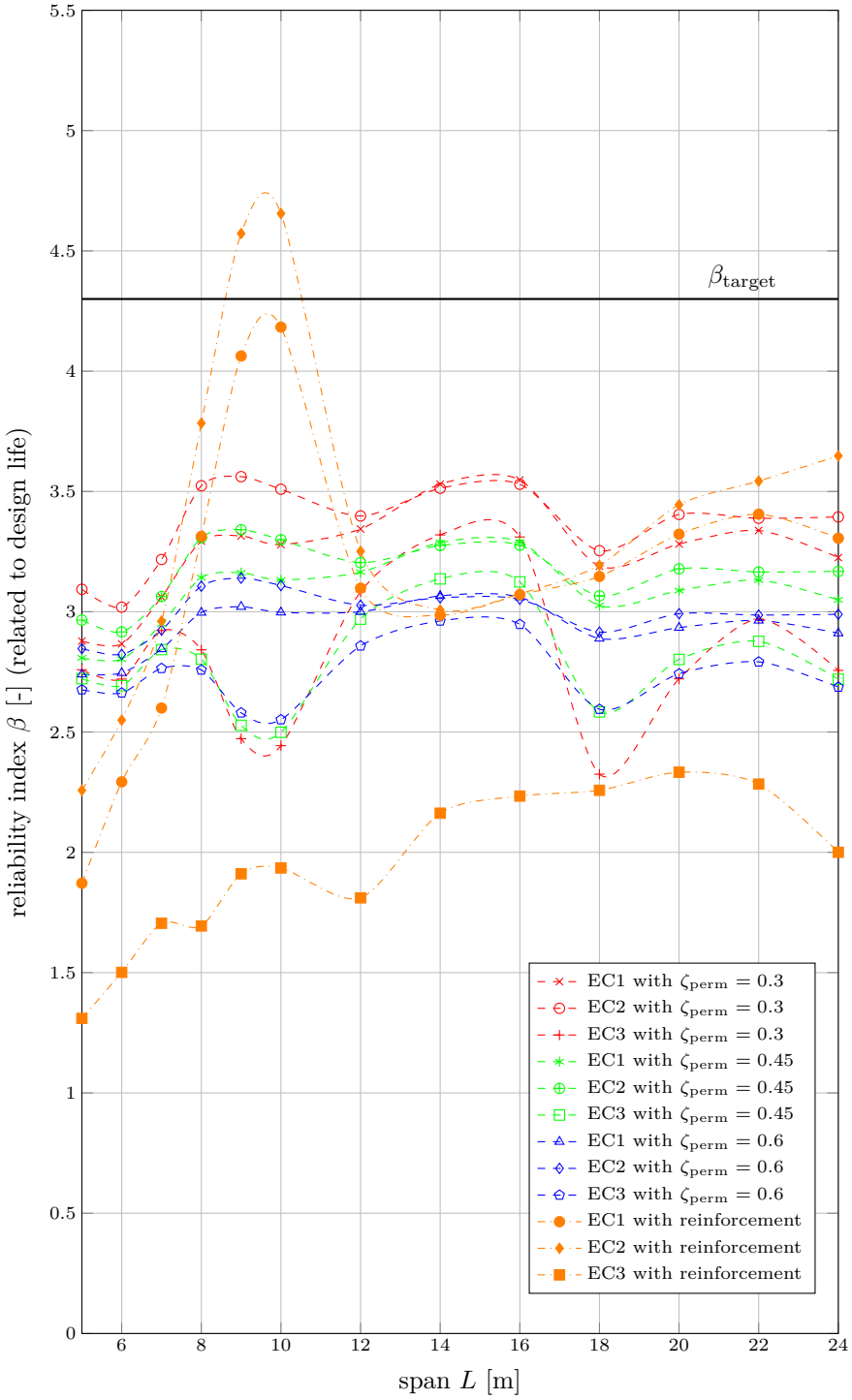

scheme	detector
7	164

Figure I.19: SC7-ECX-164

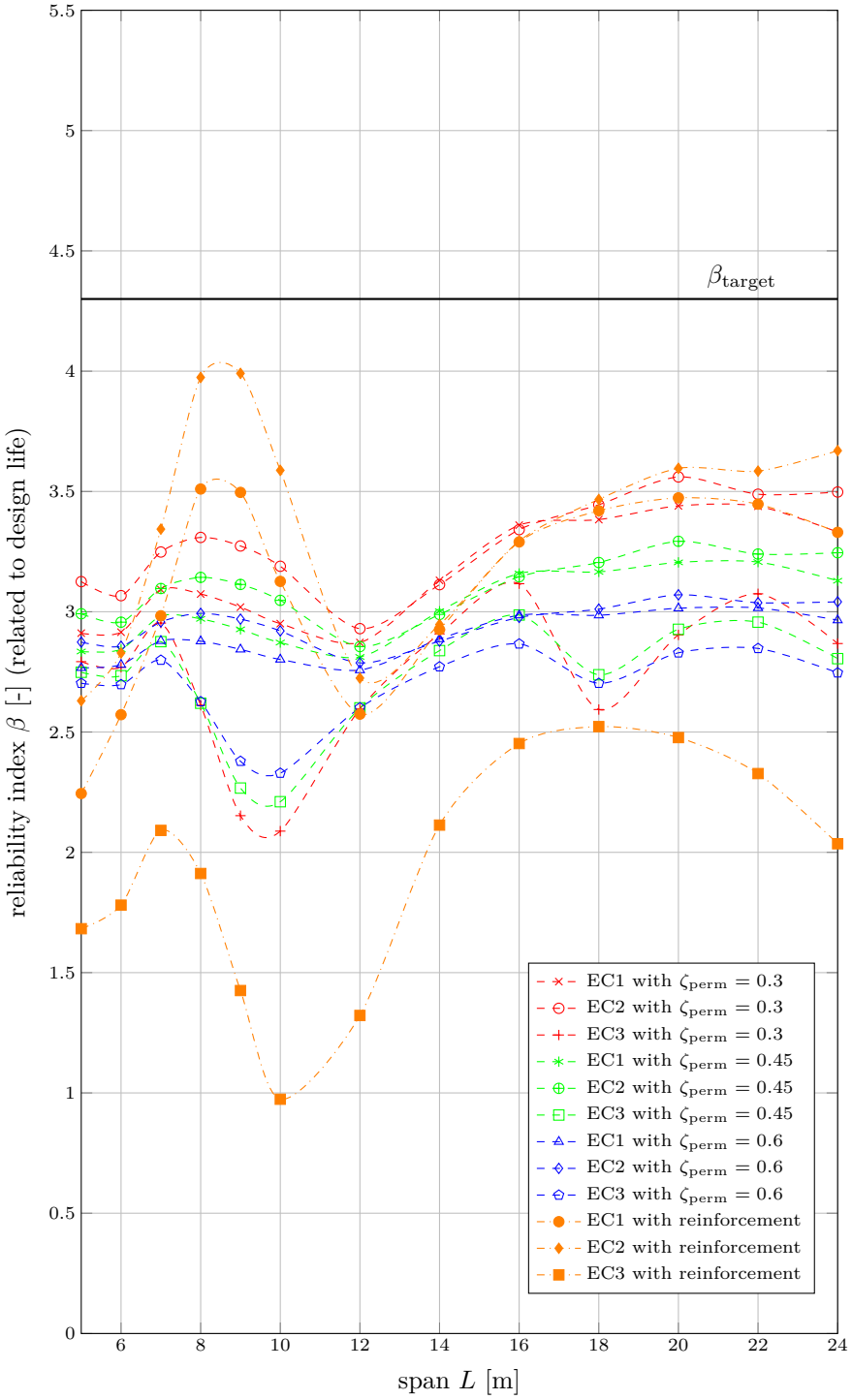

scheme	detector
7	364

Figure I.20: SC7-ECX-364

J | Reference Trains

In NEN-EN 1991-2 (CEN, 2002b) the following reference trains are given:

Type 1 Door een locomotief getrokken reizigerstrein

$\Sigma Q = 6630\text{kN}$ $V = 200\text{km/h}$ $L = 262{,}10\text{m}$ $q = 25{,}3\text{kN/m'}$

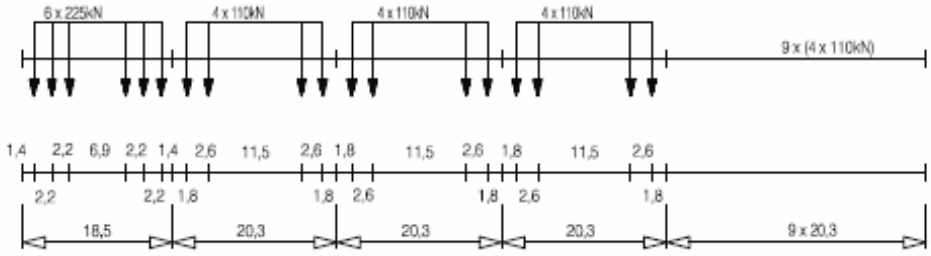

Type 2 Door een locomotief getrokken reizigerstrein

$\Sigma Q = 5300\text{kN}$ $V = 160\text{km/h}$ $L = 281{,}10\text{m}$ $q = 18{,}9\text{kN/m'}$

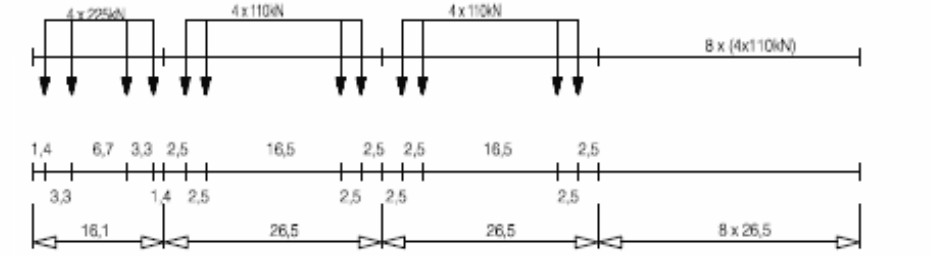

Type 3 Hogesnelheidsreizigerstrein

$\Sigma Q = 9400\text{kN}$ $V = 250\text{km/h}$ $L = 385{,}52\text{m}$ $q = 24{,}4\text{kN/m'}$

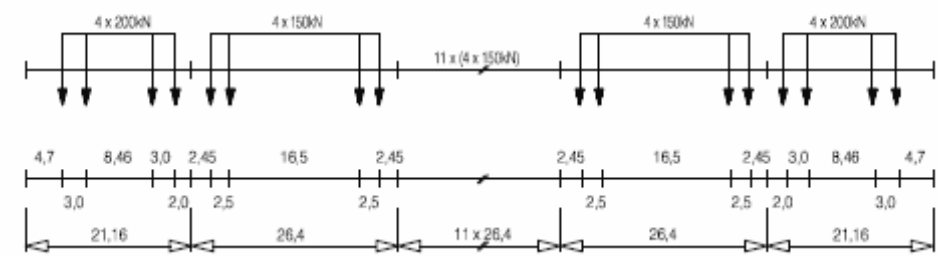

Type 4 Hogesnelheidsreizigerstrein

$\Sigma Q = 5100\text{kN}$ $V = 250\text{km/h}$ $L = 237{,}60\text{m}$ $q = 21{,}5\text{kN/m'}$

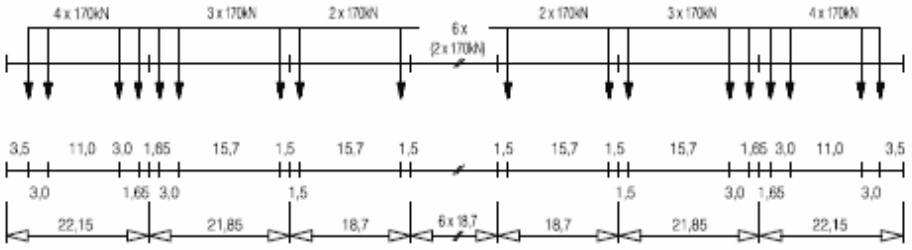

Type 5 Door een locomotief getrokken goederentrein

$\Sigma Q = 21600\text{kN}$ $V = 80\text{km/h}$ $L = 270{,}30\text{m}$ $q = 80{,}0\text{kN/m'}$

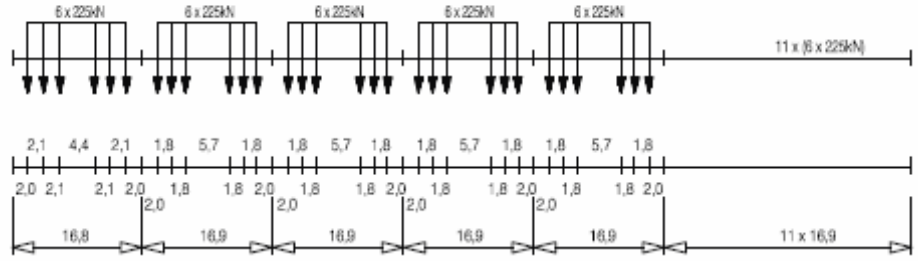

Type 6 Door een locomotief getrokken goederentrein

$\Sigma Q = 14310\text{kN}$ $V = 100\text{km/h}$ $L = 333{,}10\text{m}$ $q = 43{,}0\text{kN/m'}$

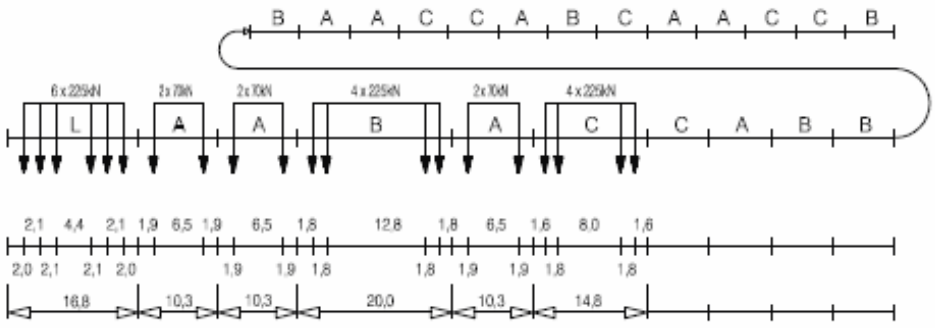

Type 7 Door een locomotief-getrokken goederentrein

$\Sigma Q = 10350\text{kN}$ $V = 120\text{km/h}$ $L = 196{,}50\text{m}$ $q = 52{,}7\text{kN/m'}$

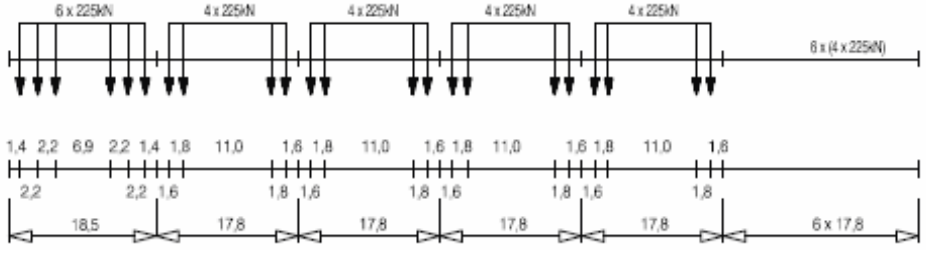

Type 8 Door een locomotief getrokken goederentrein

$\Sigma Q = 10350\text{kN}$ $V = 100\text{km/h}$ $L = 212{,}50\text{m}$ $q = 48{,}7\text{kN/m'}$

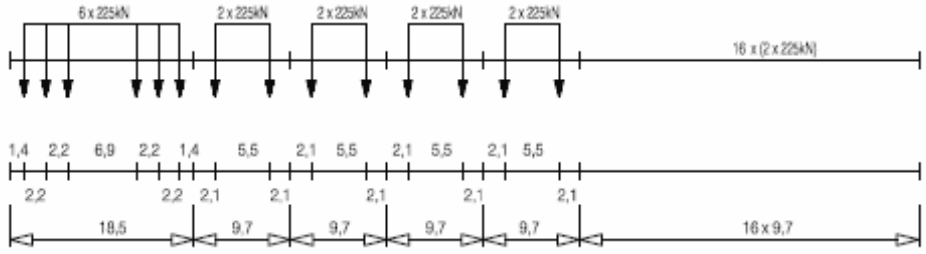

Type 9 Reizigerstrein met gelede wagens

$\Sigma Q = 2960\text{kN}$ $V = 120\text{km/h}$ $L = 134{,}80\text{m}$ $q = 22{,}0\text{kN/m'}$

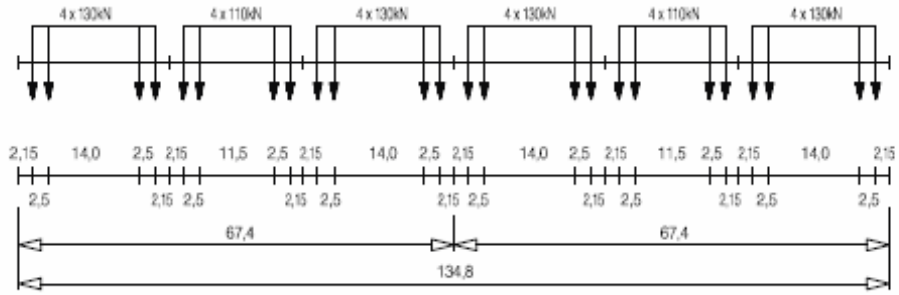

Type 10 Metrotrein

$\Sigma Q = 3600\text{kN}$ $V = 120\text{km/h}$ $L = 129{,}60\text{m}$ $q = 27{,}8\text{kN/m'}$

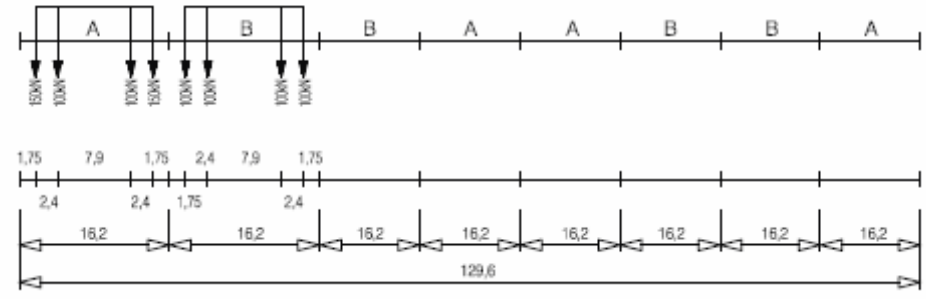

Type 11 Door een locomotief getrokken goederentrein

$\Sigma Q = 11350\text{kN}$ $V = 120\text{km/h}$ $L = 198{,}50\text{m}$ $q = 57{,}2\text{kN/m'}$

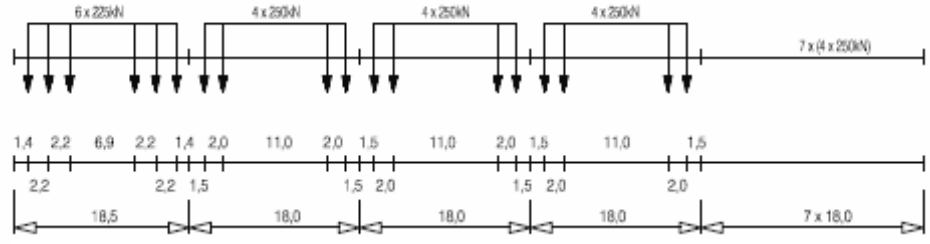

Type 12 Door een locomotief getrokken goederentrein

$\Sigma Q = 11350\text{kN}$ $V = 100\text{km/h}$ $L = 212{,}50\text{m}$ $q = 53{,}4\text{kN/m}'$